UNIVERSITÉ DE STRASBOURG

EDSC
École Doctorale des
Sciences Chimiques

ÉCOLE DOCTORALE DES SCIENCES CHIMIQUES

UMR 7509

THÈSE

présentée par

Xavier MARTIN BENLLOCH

soutenue le 09 janvier 2015

pour obtenir le grade de
Docteur de l'université de Strasbourg

Discipline/ Spécialité : Chimie

Synthesis and physico-chemical study
of a novel flavone antiviral lead

THÈSE dirigée par :
  Mme. DAVIOUD-CHARVET Elisabeth   Docteur, Université de Strasbourg
  M. ELHABIRI Mourad   Docteur, Université de Strasbourg

RAPPORTEURS :
  M. QUIDEAU Stéphane   Professeur, Université de Bordeaux
  M. TRABOLSI Ali   Professeur, NYU Abu Dhabi

AUTRES MEMBRES DU JURY :
  Mme. LOBSTEIN Annelise   Professeur, Université de Strasbourg
  Mme. MAHUTEAU-BETZER Florence   Docteur, Institut Curie

We are like dwarfs sitting on the shoulders of giants. We see more, and things that are more distant, than they did, not because our sight is superior or because we are taller than they, but because they raise us up, and their great stature add to ours.

John of Salisbury

Acknowledgements

First, I would like to thank the members of the jury for accepting to read and evaluate my PhD work: Pr. Stéphane Quideau, Pr. Ali Trabolsi, Pr. Annelise Lobstein and Dr. Florence Mahuteau-Betzer.

I am most grateful to Dr. Elisabeth Davioud-Charvet and Dr. Mourad Elhabiri for giving me the opportunity to work in such an interesting and challenging project as well as for their counseling and guidance during these three years. They have allowed me to become a better scientist and are a great inspiration for the scientist I want to become in the future.

Next, I would like to thank all the people with whom I have shared experiences during these three years at the Laboratory of Bioorganic and Medicinal Chemistry: Elena, Sabah, Parastoo, Katharina Li Wen, Didier and Karène, who made working at the laboratory a real pleasure. It is thanks to them that this laboratory is such a good place to work at. Special thanks go to Thibault, from whom I learnt a great deal and shared innumerable good moments and to Don Antoine, for his help and advices for the synthesis of the flavones. Last but no least, I would like to thank all the students I had the pleasure to supervise, Benjamin, Fabian and Saravanan, who helped me a lot with my project.

I also thank all the members of the UMR 7509, specially Mickael, Mathieu, Jérémy and Pierre-Antoine, with whom I have shared almost every meal during these three years. Thanks for the good times and the bizarre yet extremely entertaining discussions.

I am also grateful to Michel Schmitt for his help with NMR analyses, Mathieu Chessé for his help with the ESI-MS identification of the metal complexes and the whole Services Communs d'Analyses de l'Université de Strasbourg. I would also like to thank Patrick Gizzi for the pharmacokinetic studies and Prof. Pietschmann and his group for the help with the antiviral tests.

I would also like to thank my friends, either in Spain, England, Germany or France for their support during all these years as well as for changing my ideas when chemistry was not working as desired.

I would also like to express my gratitude to Marjorie, with whom I have shared the best four years of my life and hopefully will share many more to come. T'estime. Special thanks to her family who has welcomed me with open arms and made me feel like a part of it.

Last but most certainly not least I would like to thank my family, especially my parents. It is thanks to them and all their years of hard work that I have the privilege of writing these lines. Moltes gràcies.

Abbreviations

AcOH	Acetic acid
AIDS	Acquired immune deficiency syndrome
AM1	Austin Model 1
ALT	Alanine aminotransferase
apoE	Apoliprotein E
CAN	Ceric ammonium nitrate
CAPE	Caffeic acid phenethyl ester
CD81	Cluster of differentiation 81
CLDN-1	Claudin-1
CsA	Cyclosporine A
CSE	Copper-copper(II) sulfate electrode
CV	Cyclic voltammetry
DAA	Direct acting antiviral
DCM	Dichloromethane
DDQ	2,3-dichloro-5,6-dicyano-1,4-benzoquinone
DFO	Deferoxamine
DGAT-1	Diacylglycerol acyltransferase 1
DMAP	4-dimethylaminopyridine
DMF	Dimethylformamide
DMSO	Dimethyl sulfoxide
DNA	Deoxyribonucleic acid
ds	double stranded
E1	Envelope glycoprotein 1
E2	Envelope glycoprotein 2
EC_{50}	Half maximal effective concentration
EGC	Epigallocatechin
EGCG	Epigallocatechin gallate
EGFR	Epidermal growth factor receptor
EHF	Ebola hemorrhagic fever
equiv.	Equivalents
ER	Endoplasmic reticulum
ESI	Electrospray ionization
ESIPT	Excited state intramolecular proton transfer
EtOAc	Ethyl acetate

FDA	Food and drug administration
FP	Final precursor
g	gram(s)
GAG	Glycosaminoglycan
GC	Gallocatechin
GC	Gas chromatography
GCE	Glassy carbon electrode
h	hour(s)
HAV	Hepatitis A virus
HBV	Hepatitis B virus
HCC	Hepatocellular carcinoma
HCV	Hepatitis C virus
HCVcc	Hepatitis C virus cell culture
HCVpp	Hepatitis C virus pseudoparticles
HIV	Human immunodeficiency virus
HOMO	Highest occupied molecular orbital
HSPG	Heparan sulfate proteoglycan
HSV	Herpes simplex virus
HVR-1	Hypervariable region 1
ICP	Inductively coupled plasma
ICTV	International Committee on Taxonomy of Viruses
IFN	Interferon
IR	Infrared
IRES	Internal ribosome entry site
SG	Interferon-stimulated gene
kDa	Kilodalton
LC	Liquid chromatography
LDL	Low density lipoprotein
LDLR	Low density lipoprotein receptor
LiHMDS	Lithium hexamethyldisilazane
LUMO	Lowest unoccupied molecular orbital
M	Molarity
miRNA	Micro-RNA
mM	Millimolar
mp	Melting point
MS	Mass spectrometry
MW	Microwave
n-Buli	*n*-buthyllithium

NANBH	Non-A, Non-B hepatitis
NHE	Normal hydrogen electrode
nM	Nanomolar
NMR	Nuclear magnetic resonance
NPC1L1	Niemann-Pick C1-Like 1
NS	Non-structural protein
NTA	Nitrilotriacetic acid
NTR	Non-translated region
OCLN	Occludin
p7	Membrane protein
PBMC	Peripheral blood mononuclear cell
PEG	Polyethylene glycol
pH	potential hydrogen
PKA	Protein kinase A
pM	Picomolar
PTB	Polypyrimidine tract-binding protein
RBV	Ribavirin
RdRp	RNA-dependent RNA polymerase
RNA	Ribonucleic acid
ROS	Reactive oxygen species
RT	Room temperature
RT-PCR	Reverse transcription polymerase chain reaction
SARS	Severe acute respiratory syndrome
SCQ	Short chloroquine
SR-B1	Scavenger receptor class B member 1
ss	Single stranded
SVR	Sustained virological response
TfR1	Transferrin receptor 1
THF	Tetrahydrofuran
TLC	Thin layer chromatography
TRGO	Thermally reduced graphene oxide
UV	Ultraviolet
Vis	Visible
VLDL	Very low density lipoprotein
VSV	Vesicular stomatitis virus

Résumé en français

Les virus sont des entités biologiques ubiquitaires qui infectent les plantes, les animaux et les bactéries entre autres. En utilisant la machinerie métabolique de l'hôte pour sa réplication, ils peuvent causer des maladies souvent fatales. Parmi les maladies causées par des virus, le Syndrome d'Immunodéficience Acquise (SIDA) est sûrement le plus connu. D'autres maladies comme Ebola ou la grippe sont aussi causées par des virus.

Le Virus de l'Hépatite C (VHC) est l'un des virus le plus répandus sur la planète. En effet, il est estimé que plus de 150 millions de personnes sont infectées dans le monde et qu'il cause environ 500 000 morts par année dans le monde et près de 2 600 en France. Il appartient aux *Hepacivirus* et, plus précisément, à la famille des *Flaviviridae*. Il est composé d'une enveloppe qui entoure une capside contenant le matériel génétique (une molécule d'un seul brin d'ARN de sens positif).

Les personnes infectées par ce virus ont de fortes chances de développer une Hépatite C chronique, ce qui arrive à près de 75-80% des individus infectés. Une des principales raisons pour laquelle le VHC est si répandu, c'est qu'il possède un stade asymptomatique pendant lequel le virus se réplique mais le patient ne montre aucun symptôme, ce qui rend le dépistage très difficile. Parmi ces personnes infectées, 15 % d'entre elles vont développer une cirrhose,[1] qui peut conduire à terme à un cancer du foie. En effet, l'Hépatite C chronique est estimé être responsable de près de 25 % de tous les cas de cancers de foie au monde.[2]

Le cycle de vie du VHC consiste en trois étapes essentielles. Dans une première phase, l'entrée du virion se fait par un processus complexe où les glycoprotéines présentes à la surface de l'enveloppe virale (protéines structurales E1 et E2) interagissent avec différentes protéines exprimées à la surface des hépatocytes (protéines CD81, SR-B1, Claudin, Occludin, NPC1L1).[3]
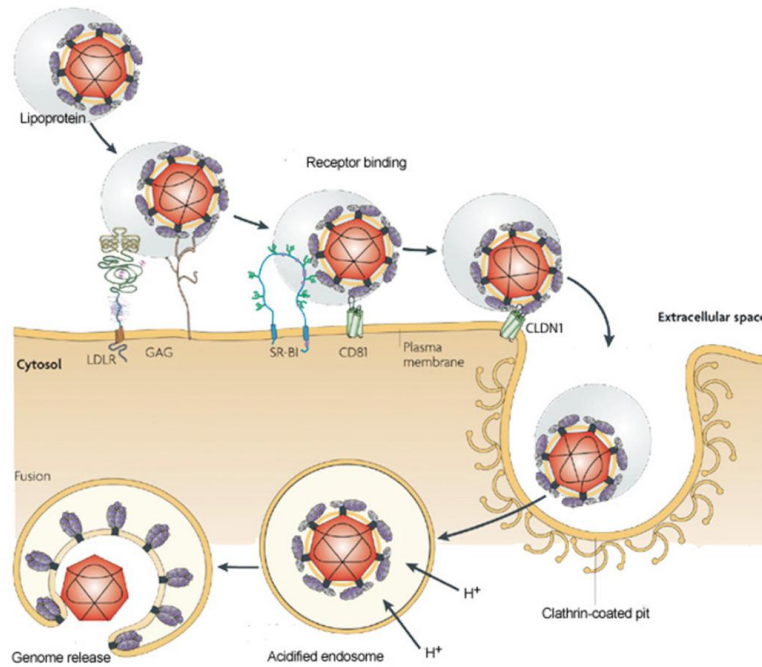
Figure 1. Entrée du Virus de l'Hépatite C dans les hépatocytes.[3]

Une fois que le matériel génétique se trouve à l'intérieur de la cellule cible, le virus utilise la machinerie de l'hôte pour sa réplication.[3] Pendant ce processus, une polyprotéine étendue est produite puis coupée en trois protéines structurales (C, E1 et E2), une protéine à canal ionique (p7) et six protéines non-structurales (NS2, NS3A, NS4A, NS4B, NS5A et NS5B). Dans la dernière étape, le virion est prêt à être assemblé et quitte la cellule hôte pour pouvoir infecter de nouvelles cellules.

Un arsenal important de molécules thérapeutiques ciblant les différentes étapes du cycle de vie du VHC peut être utilisé pour traiter cette infection. La thérapie anti-VHC s'est, en effet, beaucoup développée au cours de ces dernières 5 années. Il reste, cependant, encore beaucoup de défis à aborder.

La première thérapie utilisée consistait en l'utilisation d'IFN-α (IFN = interféron ; les interférons sont des glycoprotéines produites par les cellules du système immunitaire). L'utilisation d'un IFN exogène permet de produire un état d'alerte dans la cellule en activant le système immunitaire pour lutter contre l'infection. Cependant, cette thérapie ne conduisait pas à de très bons résultats jusqu'à l'introduction d'un deuxième composant (multithérapie), la ribavirine (RBV). En effet, la double thérapie de l'IFN-α avec la RBV a permis d'améliorer le taux de réponse virologique soutenue (RVS) de 16 % jusqu'à 42 %.[4] La bithérapie fût à la suite encore améliorée avec l'utilisation de PEG-IFN-α qui présente un meilleur profil pharmacocinétique.[5] Cependant, cette thérapie présentait d'importants

inconvénients tels que de nombreux effets secondaires. En outre, beaucoup de patients n'étaient pas éligibles à ce traitement.
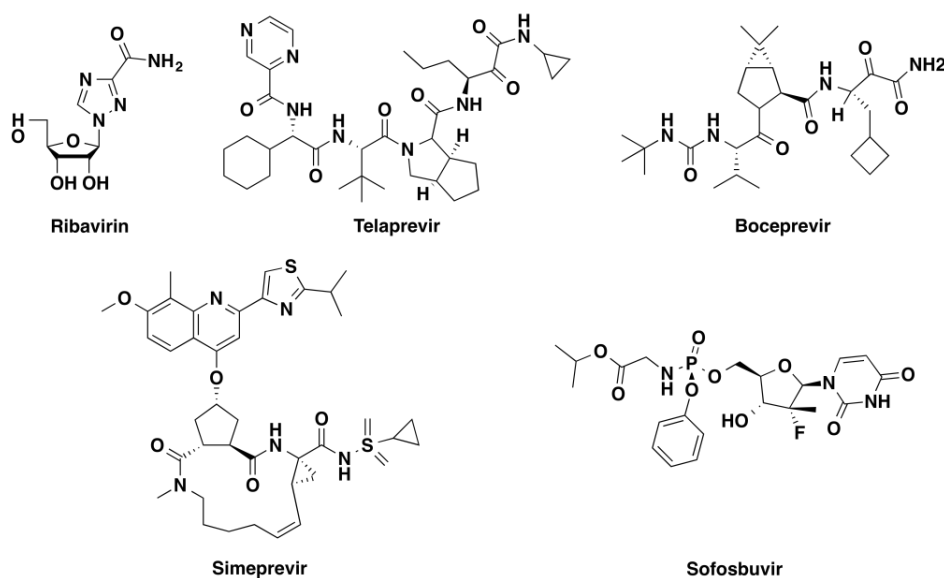

Figure 2. Structures chimiques de composés anti-VHC.

Ces dernières années, des composés qui attaquent directement le cycle de vie du virus (DAAs = Antiviraux Agissant Directement) ont commencé à être développé. Récemment, 4 composés ont été approuvés pour leur mise sur le marché Américain ou Européen (Telaprevir, Boceprevir, Simeprevir, et Sofosbuvir, Figure 2). Ces composés ciblent les protéase NS3/4A ou NS5B et permettent d'augmenter significativement les taux de RVS (jusqu'à 90 % pour le sofosbuvir en combinaison avec le PEG-IFN-α et la RBV)[6]. Beaucoup d'espoir est porté dans la possibilité que, dans un futur proche, l'IFN-α pourra être retiré de la thérapie anti-VHC.

Au-delà de l'efficacité de ces nouveaux composés, le plus grand inconvénient est leur prix extrêmement élevé. En effet, pour un traitement de 12 semaines avec le sofosbuvir, il faut compter environ 84 000 $ par patient et par traitement. Les pays pauvres ou en voie de développement sont cependant ceux qui sont le plus touchés par le VHC, ce qui conduit à ce que ces nouveaux composés ne seront certainement pas aisément accessibles à la majorité des individus infectés. C'est pour cela que le développement de nouveaux composés efficaces (DAAS), qui ne soient pas chers et facilement accessibles, reste un axe majeur de recherche pour le futur de la thérapie anti-VHC.

Les flavonoïdes sont des composés naturels qui sont présents de manière ubiquitaire dans le règne végétal (fruits, fleurs, légumes…). La structure de base des flavonoïdes est présentée à la Figure 3 et est constituée d'un motif C_6-C_3-C_6.
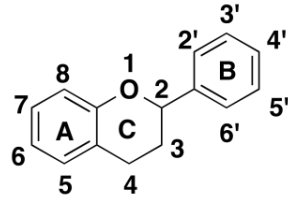
Figure 3. Structure de base des flavonoïdes.

Les flavonoïdes sont des métabolites secondaires synthétisés dans le cytosol à partir de la phénylalanine et du malonylCoA.[7] Ces composés sont utilisés par les plantes pour se protéger des rayonnements UV qui peuvent causer des espèces oxygénées réactives. Un autre rôle important des flavonoïdes est l'allélopathie (interactions biochimiques d'une plante vers une autre - incluant les micro-organismes). Enfin, parmi les autres fonctions importantes des flavonoïdes, nous pouvons également citer la pigmentation, la régulation de la croissance[8] et ou encore la défense de la plante.[9]

Les flavonoïdes exercent aussi nombreux bénéfices sur la santé humaine. Par exemple, des herbes médicinales contenant ce type de composés ont été utilisées pendant des siècles dans la médicine traditionnelle. L'activité la plus étudiée est leurs propriétés antioxydantes (piégeurs de radicaux).[10] Ainsi, ces dernières années, les flavonoïdes ont suscité beaucoup d'intérêt suite à la découverte de nombreuses activités biologiques : anticancéreux,[11] diminution du risque d'infarctus,[12] propriétés hépato-protectrices,[13] antibactériens,[14] ou antiviraux[15] entre autres.

Historiquement, notre projet de recherche a commencé lorsque des extraits aqueux de plantes de la famille des *Lamiaceae* (sauge, menthe, mélisse…) ont démontré une forte activité anti-VIH.[16] Une approche de fractionnement bio-guidé a ensuite permis l'identification du principal composé à action antivirale, la ladanéine (Figure 5).

En outre, ce composé a montré une forte activité antivirale contre le VHC. Il est intéressant de noter que le mode d'action original de la ladanéine ne touche pas au processus de réplication du virus mais qu'il bloque l'entrée du virion dans la cellule (inhibition de l'infectivité du VHC). Une première synthèse de la ladanéine a été proposée (BJ486K) et les propres propriétés antivirales du composé de synthèse ont été confirmées. Des études préliminaires ont montré que l'exposition de virions à enveloppe à BJ486K inhibait fortement leur infectivité dans une étape d'entrée (post-fixation), tandis que l'exposition à la ladanéine de virions liés à la surface des cellules cibles n'avait pratiquement aucun effet antiviral ou aucun rôle sur la réplication et l'assemblage de l'ARN. La cinétique de blocage d'entrée cellulaire du VHC induite par BJ486K est comparable avec celle d'anticorps spécifiques de la protéine CD81 ou avec le composé ITX5061 (composé en phase de tests cliniques qui empêche

l'infection virale par le VHC en inhibant l'interaction avec le récepteur SR-B1). Cette action semble large puisque l'entrée du VIH est également altérée après un traitement des particules virales avec BJ486K. En outre, BJ486K est efficace contre tous les génotypes du VHC, y compris une variante résistante à un inhibiteur d'entrée de référence. Parallèlement, une analyse ICP-MS a montré que les fractions les plus actives de ladanéine extraites étaient considérablement enrichies en Cu et Fe. La complexation au Fe(III) joue un rôle essentiel en empêchant la dégradation de la flavone par oxydation non spécifique à 2 électrons et la formation consécutive de quinones. La chélation du métal peut favoriser une oligomérisation à 1-électron et conduire à des réactions de couplage C,C ou C,O (couplage phénolique oxydant). Il est donc suspecté que l'activité antivirale de la ladanéine, qui a été démontré comme étant dépendante à la fois du Fe(III) et du pH, soit étroitement liée aux propriétés physico-chimiques de cette flavone. Enfin, la combinaison de ladanéine et de la cyclosporine A conduit à un effet synergique sur l'inhibition de l'infection par le VHC, tandis que la chloroquine (un médicament antiparasitaire) exerce un effet additif sur le VHC. Cette découverte a conduit au dépôt d'un brevet Européen en 2012.

Les inhibiteurs d'entrée sont, en effet, en phase de gagner une place prépondérante en recherche anti-VHC car ils peuvent être utilisés en combinaison avec d'autres composés (inhibiteurs de protéase ou autres) qui ciblent d'autres phases de développement du virus, augmentant ainsi l'efficacité du traitement (action pléiotropique).
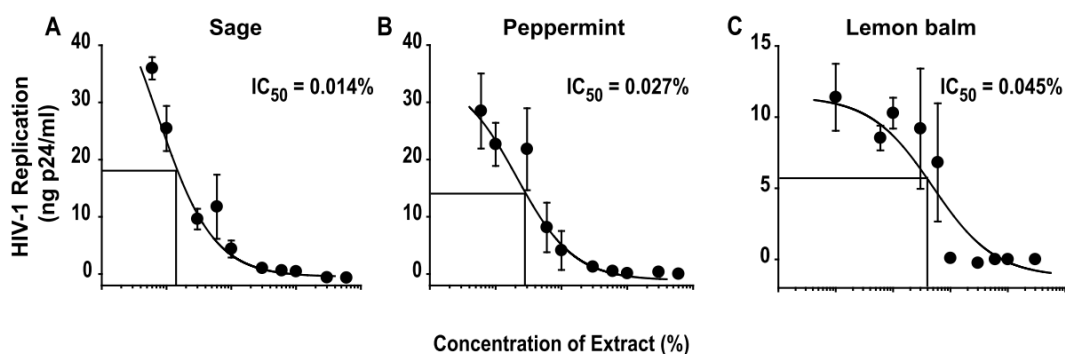

Figure 4. Activité anti-HCV des extraits de *Lamiaceae*.
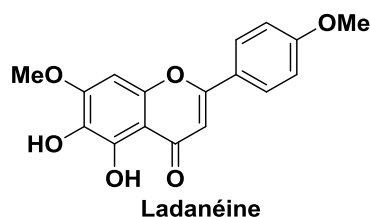

Figure 5. Structure chimique de la flavone ladanéine.

Dans ce contexte, les objectifs de ma thèse de Doctorat étaient:

- Développer une nouvelle synthèse avec de meilleurs rendements et plus rapide,
- Etudier les propriétés physico-chimiques de la ladanéine et de ses analogues,
- Améliorer le temps de demi-vie de la ladanéine par la formation d'un complexe métallique,
- Etudier la synthèse d'un complexe portant deux pharmacophores.

Synthèse

La synthèse des flavonoïdes a été très tôt un axe développé par les chimistes du fait des importantes activités biologiques démontrées par ces composés. Ainsi, les premières synthèses ont commencé à être décrites en 1901 par Kostanecki.[17] Peu de temps après, d'autres synthèses ont été aussi développées: la synthèse d'Auwers,[18] la synthèse d'Allan-Robinson,[19] la synthèse de Baker-Venkataraman[20] ou la synthèse d'Algar-Flynn-Oyamada.[21] Plus récemment, des synthèse modernes ont aussi été décrites, utilisant des réactions telles que la réaction de Heck,[22] le couplage de Suzuki-Miyaura[23] ou à partir d'*o*-alkynoylphenols.[24]

Au début de ce projet, une première synthèse avait été développée afin d'obtenir la version synthétique de ladanéine pour pouvoir continuer les tests biologiques. Ainsi, une stratégie robuste permettant d'obtenir le produit désiré avec 16 % de rendement totale avait été choisie. Cette synthèse est présentée dans le Schéma 1.
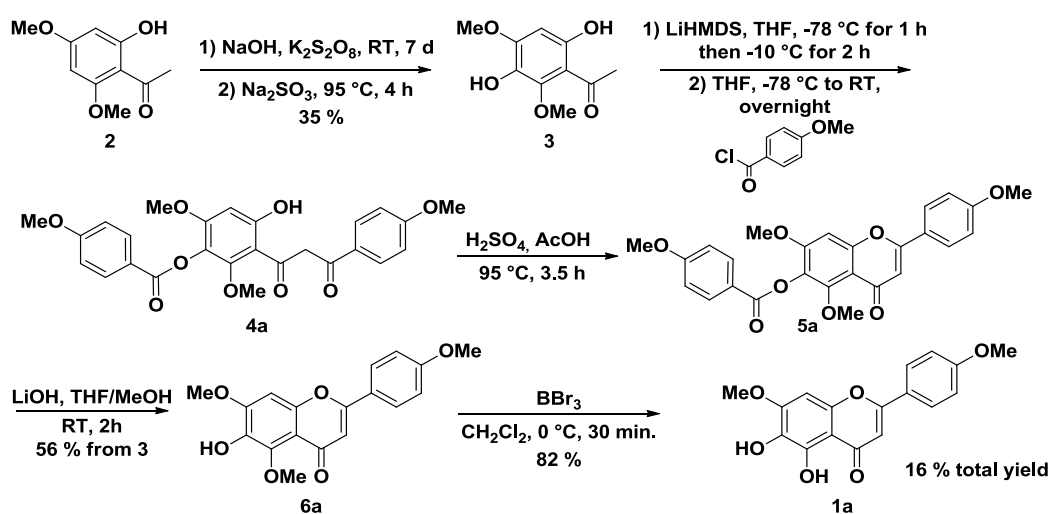

Schéma 1. Ancienne synthèse de la ladanéine (**1a**) développée au sein du laboratoire.

Cependant, cette voie synthétique présente plusieurs inconvénients à améliorer. La synthèse commence par une oxydation d'Elbs du composé **2** pour former l'acétophénone **3**. L'inconvénient de cette réaction est le temps nécessaire (7 jours) ainsi que le bas rendement obtenu (35 % en moyenne). De plus, si le produit **2** est commercial il est assez cher. D'autre part, si le réactif LiHMDS est un composé commercial, sa qualité n'est cependant pas consistante d'un lot à l'autre, ce qui limite la reproductibilité de la réaction. Enfin, ladanéine **1a** est obtenue après une étape de déméthylation avec BBr$_3$. Après cette étape, le produit doit être purifié par une colonne Sephadex LH-20, car le produit se dégrade s'il est purifié par colonne de silice. La Sephadex LH-20 est un produit cher et il faut en général plusieurs purifications par colonne pour obtenir le produit sous une forme pure. Les produits **3** et **6a** sont également obtenus après de longues colonnes de silice qui constituent une méthode de purification beaucoup plus lente que la recristallisation et moins adaptée à des grandes quantités.

Du fait de ces inconvénients, le premier objectif de ma thèse a été de développer une nouvelle synthèse donnant accès à la ladanéine et à ses analogues de manière plus rapide et efficace et sur de plus grandes quantités. La nouvelle synthèse démarre par une acétylation réductrice du produit **11** en présence de Zn et HCl avec un rendement quantitatif suivie d'une réaction de Fries en présence de BF$_3$·Et$_2$O pour donner les composés **3** et **12** après une filtration sur silice (Schéma 2). Les deux produits peuvent être séparés par colonne de silice ou recristallisation mais ce n'est pas nécessaire à ce stade car le mélange peut être utilisé tel quel pour la suite de la synthèse. Les deux réactions ont été effectuées sur des échelles de 30 g.
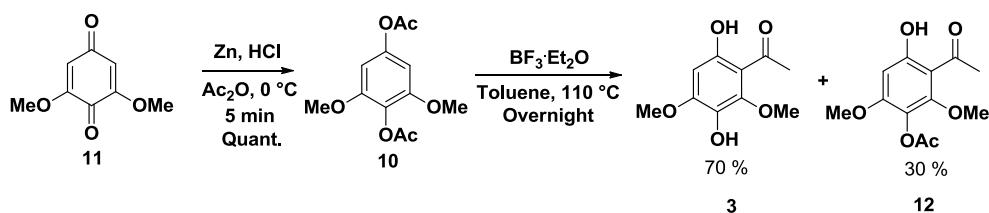

Schéma 2. Approche améliorée conduisant aux précurseurs initiaux **3** et **12**.

La synthèse continue ensuite comme l'ancienne avec une réaction de Baker-Venkataraman pour former la dicétone **4**. Afin d'avoir une base de meilleure qualité, le LiHMDS a été fraîchement préparé par réaction entre le HMDS et le *n*-BuLi. La dicétone est ensuite cyclisée grâce à l'utilisation d'acide acétique et d'acide sulfurique pour donner la flavone **5**. Une saponification avec LiOH permet d'obtenir le précurseur final **6a**. Un nouveau traitement (basé sur les propriétés physico-chimiques des produits) a été mis en place et permet l'obtention du produit **6a** pur par recristallisation dans l'eau/EtOAc (Figure 6). Ces trois réactions ont été effectuées à l'échelle de 5 g.
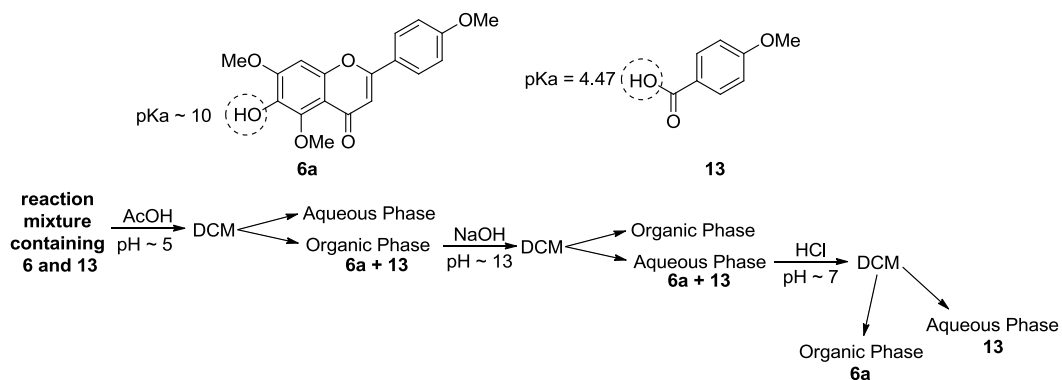
Figure 6. Constantes de protonation de la flavone **6a** et l'acide carboxylique **13** et nouvelle stratégie de work-up pour purifier **6a**.

La dernière amélioration concernait l'étape de déméthylation du précurseur final **6a** en présence de BBr$_3$. La nouvelle étape de déméthylation est faite avec du MgBr$_2$ etherate, qui peut être facilement synthétisé et permet d'obtenir ladanéine **1a** après recristallisation sans besoin de colonne Sephadex LH-20. Cette réaction a été effectuée à l'échelle de 5 g.

La synthèse finale est donnée au Schéma 3 et permet d'obtenir la ladanéine avec 54 % de rendement total après 6 étapes.
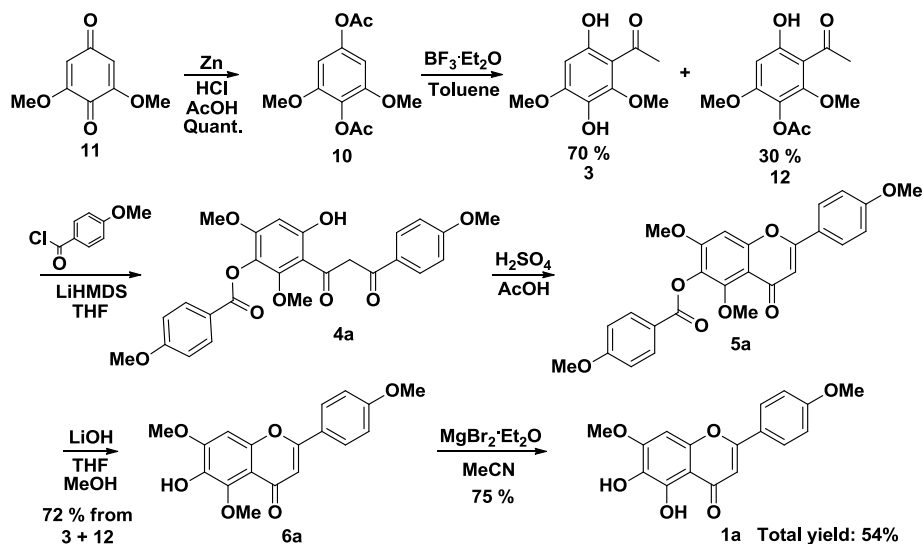
Schéma 3. Voie synthétique améliorée.

Au cours de mon travail de thèse, d'autres analogues de la ladanéine ont été aussi synthétisés avec cette nouvelle approche (Figure 7).
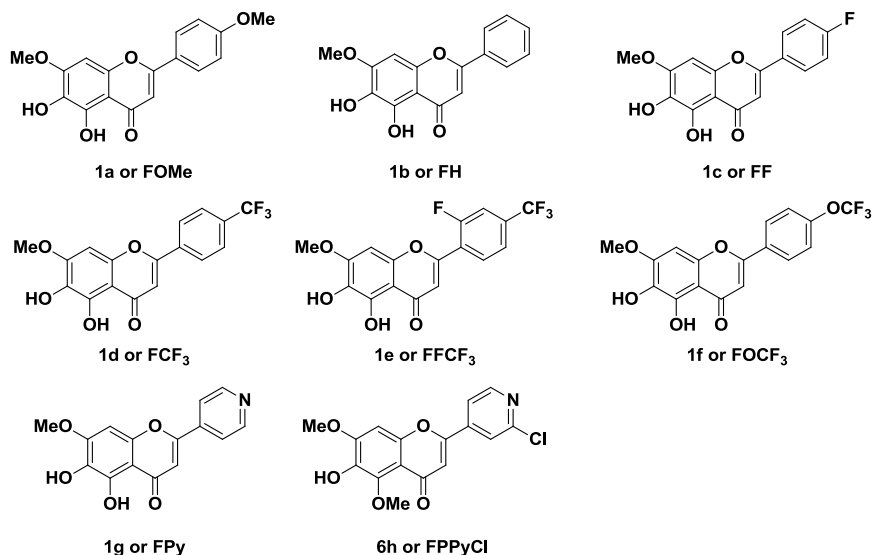
Figure 7. Différents analogues préparés avec la nouvelle approche synthétique.

Les activités anti-VHC pour ces nouveaux composés ont été déterminées et sont réunies dans le Tableau 1. On peut noter que les composés portant des atomes de F présentent les meilleures activités antivirales.

Tableau 1. Propriétés antivirales des flavones synthétisées.

Compounds	EC$_{50}$ (µM)
FOMe/1a	1,6^a / 2^b
FH/1b	2,4^a
FF/1c	1,4^a
FCF$_3$/1d	0,3^c / 0,2^c
FFCF$_3$/1e	0,36^a
FOCF$_3$/1f	0,3^d

Propriétés acido-basiques

De manière intéressante, il a été démontré que la ladanéine possédait une activité antivirale accrue lorsque le pH augmentait (Figure 8). Il a donc été décidé d'étudier les propriétés acido-basiques de ces composés car ces processus ont sûrement une influence sur leurs activités antivirales. Il est à noter que bien que de nombreux polyphénols aient été décrits dans la littérature, il existe peu d'approches physico-chimiques sur ce type de composés.
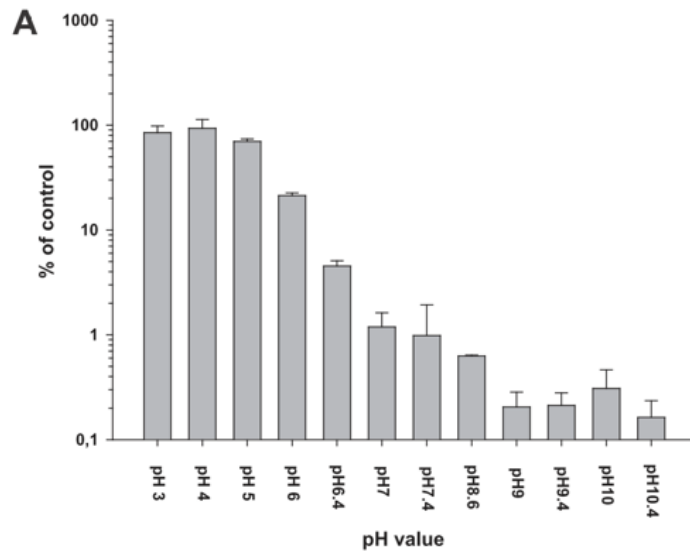
Figure 8. Activité pH dépendante de ladanéine.

Ainsi, nous avons évalué les propriétés acido-basiques de notre série de flavones synthétiques par des titrages spectrophotométrique (absorption) en fonction du pH dans un mélange MeOH/H_2O (80/20) pour assurer leur solubilité. Les spectres d'absorption des flavones se caractérisent par deux bandes d'absorption centrées dans la zone UV. La bande I est centrée entre 320 et 380 nm, tandis que la seconde, la bande II, est située à des énergies plus grandes. La bande I est généralement associée aux noyaux B et C (groupement cinnamoyl) pendant que la bande II est sûrement due au noyau A (acide benzoique, Figure 9).
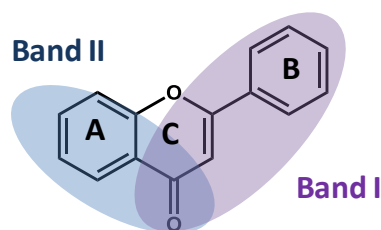
Figure 9. Chromophores majoritaires supposés être à l'origine des bandes d'absorption I et II.

A titre d'exemple, la **Figure 10** montre les variations spectrales en fonction du pH pour la ladanéine. La déprotonation suivie implique très probablement le groupement 6-OH présent sur le cycle A. Cette deprotonation induit un déplacement bathochrome de la bande II et un déplacement hypsochrome de la bande I. En conséquence, les deux bandes tendent à s'amalgamer pour conduire à une seule bande centrée autour de 300 nm.
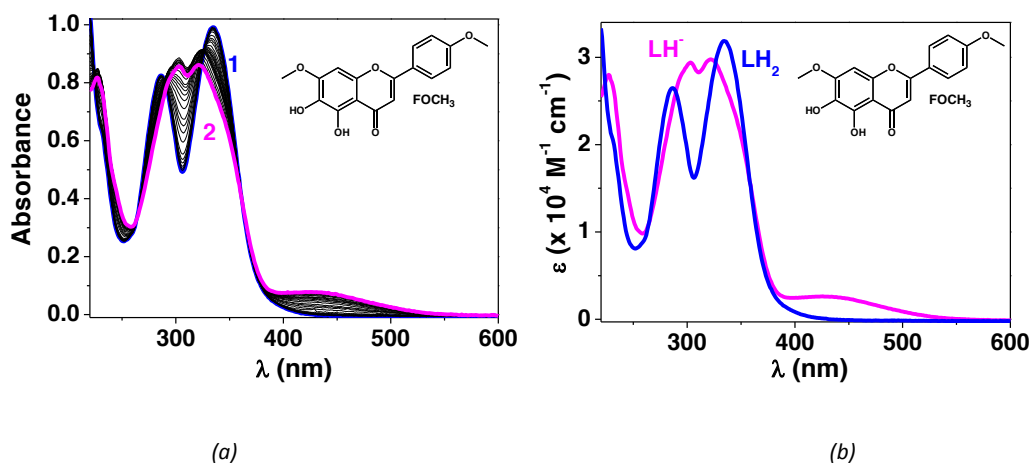
(a)   *(b)*

Figure 10. (a) Titrage spectrophotométrique de la ladanéine (**FOMe**) en fonction du pH et (b) spectres électroniques d'absorption des espèces protonées de ladanéine. Solvant : CH$_3$OH/H$_2$O (80/20 w/w) ; I = 0,1 M (NEt$_4$ClO$_4$); T = 25,0(2) °C ; l = 1 cm; [**FOMe**]$_{tot}$ = 3,12 x 10^{-5} M ; (1) pH = 6.99 ; (2) pH = 12.15.

Après avoir étudié l'ensemble de nos composés, nous pouvons suggérer que le(s) substituants portés par le cycle B avec un caractère –I ou –M (F, CF$_3$, OCF$_3$) ont peu d'influence sur les positions des bandes I et II. Cependant, de grands déplacements bathochromes ont été mesurés pour ladanéine qui porte un substituant methoxy (-I, +M). Des effets mésomères (résonance) pourraient donc avoir un rôle important sur les propriétés électroniques de la molécule (Schéma 4).
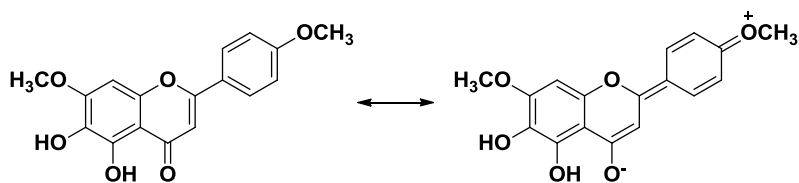

Schéma 4. Effets mésomères suggérés pour la ladanéine.

Les données spectrophotométriques et potentiométriques ont été traitées au moyen d'outils statistiques[25–28] et ont permis de calculer la constante de protonation du groupement 6-OH ainsi que les spectres électroniques des espèces protonées. Les valeurs de pK_a obtenues ont été rassemblées dans le Tableau 2. Il est important de noter que la valeur de pK_a pour le groupe 5-OH n'a pu être calculée dans nos conditions expérimentales et sa valeur est probablement >> 12 du fait d'une forte liaison hydrogène avec le carbonyle adjacent porté par le cycle C.

Tableau 2. Propriétés acido-basiques des flavones.

Composé	log K^H (6-OH) ($\pm\sigma$)
FH/Negléteine	9.75(9)

FOMe/Ladanéine	10.33(5)
FP	10.10(3)
FOCF$_3$	9.47(6)
FF	9.87(5)
FFCF$_3$	10.15(2)
FCF$_3$	10.08(3)
[a] Solvant : CH$_3$OH/H$_2$O (80/20 w/w) ; I = 0,1 M (NEt$_4$ClO$_4$) ; T = 25,0(2) °C. [b] Tampons phosphate. na = non applicable	

Comme nous pouvons l'observer, les valeurs de pK_a sont assez insensibles à la nature et la position du(des) substituant(s) présent(s) sur le cycle B, ce qui est en accord avec les observations faites à partir des propriétés d'absorption. De légères variations sont néanmoins obtenues pour la ladanéine ainsi que pour le précurseur final **FP** et le composé **FFCF$_3$,** qui sont plus basiques. Cependant, cela restent de petites différences qui ne devraient pas avoir une influence majeur dans un milieu biologique. Ces valeurs de pK_a sont assez proches de celles d'autres inhibiteurs d'entrée du VHC comme la curcumine ou l'épigallocatéchine gallate (EGCG) pour lesquelles des mécanismes d'action anti-VHC comparables à la ladanéine ont été démontrées. En outre, tous ces composés sont présents sous une forme protonée (neutre) dans le foie (Figure 11).
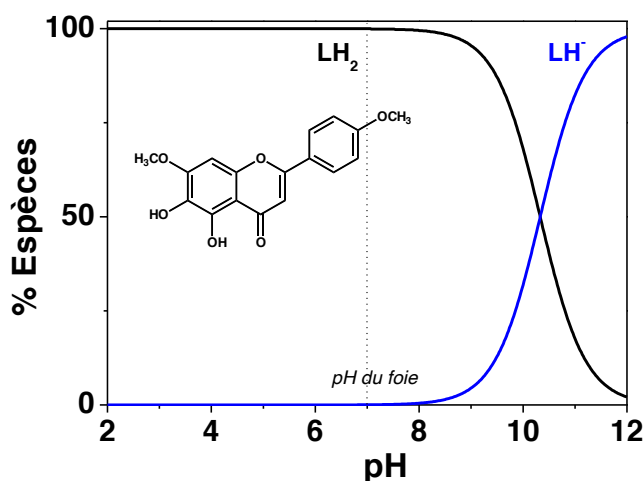

Figure 11. Diagrammes de distribution des espèces protonées de la ladanéine. [ligand] = 10^{-6} M ; I = 0,1 M ; T = 25°C.

Nous nous sommes ensuite intéressés à la stabilité de notre série de flavones en milieu basique et avons suivi leur cinétique d'oxydation/dégradation. Les polyphénols, et plus particulièrement les flavonoïdes, sont connus par leurs capacités à piéger des radicaux (propriétés antioxydantes). Le mécanisme d'oxydation des polyphénols et leur stabilité en solution est très dépendante de la valeur du pH et sont intimement liés aux propriétés acido-basiques. Afin de mieux comprendre le

mécanisme d'oxydation de nos composés, les cinétiques d'oxydation de la ladanéine et des analogues **FH** et **FCF₃** ont été étudiées en présence de quantités croissantes de base, l'hydroxyde de tétraéthylammonium NEt₄OH. En absence de base (milieu acide à milieu neutre), Les composés sont très stables. Cependant, dès l'ajout de base et la déprotonation de l'hydroxyle en position 6, nous pouvons clairement observer une oxydation/dégradation relativement lente, à l'origine de variations spectrales importantes (**Figure 12**).
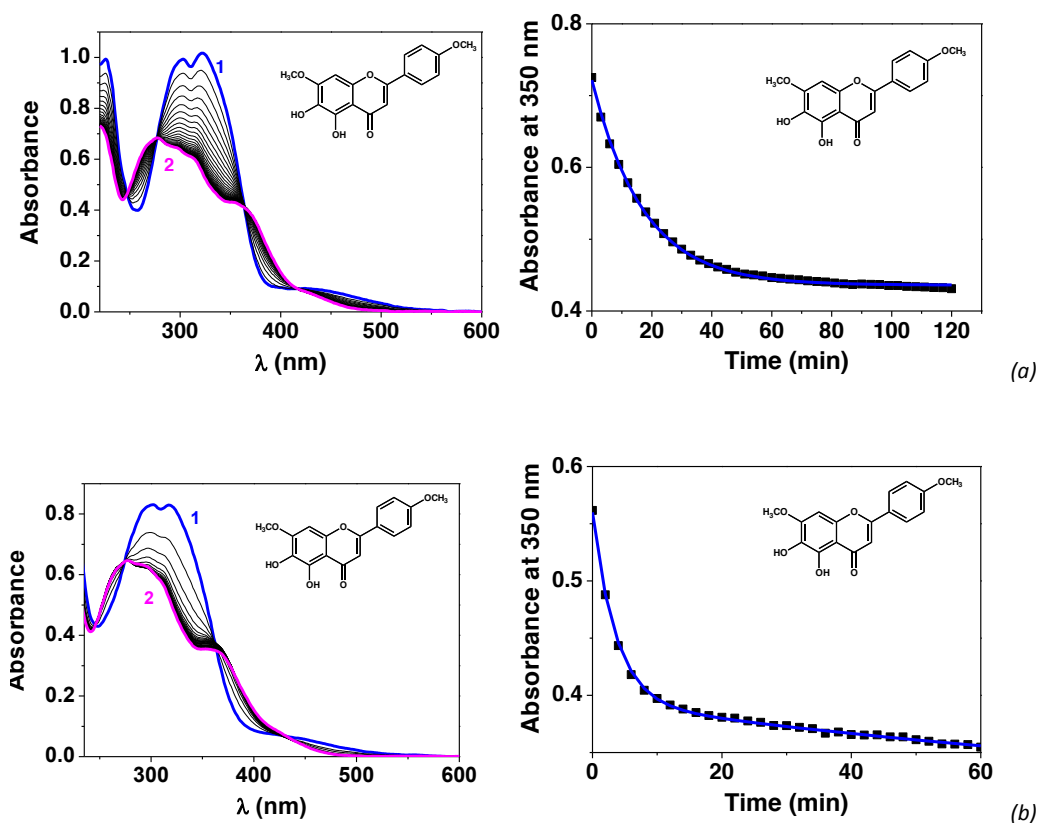
Figure 12. Spectres d'absorption de la ladanéine en fonction du temps (2h) et en présence de base. Solvant : CH_3OH/H_2O (80/20 *w/w*) ; l = 0,1 M NEt₄ClO₄; T = 25,0(2) °C. (*a*) [**FOMe**]$_{tot}$ = 4.83 x 10^{-5} M ; [NEt₄OH]$_{tot}$ = 9.63 x 10^{-4} M ; (*b*) [**FOMe**]$_{tot}$ = 4.27 x 10^{-5} M ; [NEt₄OH]$_{tot}$ = 8.75 x 10^{-3} M ; l = 1 cm.

Nous pouvons observer que les absorptions à 303 et 322 nm disparaissent tandis que de nouvelles bandes apparaissent à 277 et 354 nm. La présence de points isosbestiques montre la formation d'une espèce majoritaire. D'autres expériences, menées avec une plus grande concentration de base, donnent des résultats comparables avec, en outre, une diminution lente de l'absorption à 354 nm ce qui suggère la formation d'une troisième espèce minoritaire. Afin d'obtenir plus d'information sur la nature des produits d'oxydation, nous avons mené une étude par spectrométrie de masse en mode électrospray ESI-MS (Figure 13). Nous pouvons clairement observer l'apparition de nouveaux pics après l'ajout de base qui peuvent être attribués à l'oxydation de la ladanein en *ortho*-quinone.
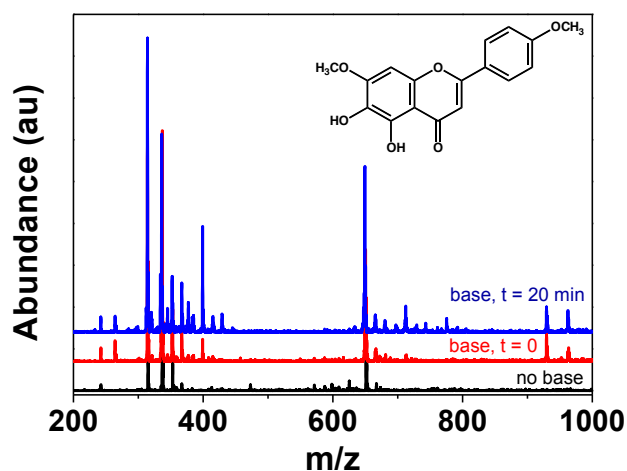
Figure 13. Spectre ESI-MS de la ladanéine en fonction du temps (0 et 20 min) et en présence de base (NH$_4$OH). Solvant : CH$_3$OH/H$_2$O (80/20 *w/w*). (*a*) [**FOMe**]$_{tot}$ = 5 x 10^{-5} M; NH$_4$OH (0,01 *v/v*). Fragmenteur = 100 V.

Cette oxydation n'a pas été observée pour le précurseur final **FP**, ce qui suggère l'importance du groupement 5-OH dans ce processus d'oxydation. Ces données suggèrent que la deprotonation du groupement 6-OH induit l'oxydation à 1 e$^-$ du phénolate, si et seulement si le groupement 5-OH est présent.

Electrochimie

Suite à ces premières données, nous avons examiné le comportement électrochimique de la ladanéine et des analogues synthétisés, car il est fort probable que leurs activités antivirales soient également liées aux propriétés redox de ces composés. Il est envisageable que le produit actif ne soit pas la flavone elle même mais l'un de ses produits de couplage formés *in vivo*. En général, le comportement redox des polyphénols est intimement lié avec d'autres propriétés physico-chimiques telles que les caractéristiques acido-basiques.

Pour des raisons de solubilité, l'étude électrochimique des flavones a été menée dans le DMSO par voltampérométrie cyclique (CV). Dans un premier temps, il a été décidé d'étudier le comportement des flavones entre -0,8 et +1,2 V. La Figure 14 montre le profil électrochimique de la ladanéine dans ces conditions expérimentales à différentes vitesses de balayage.
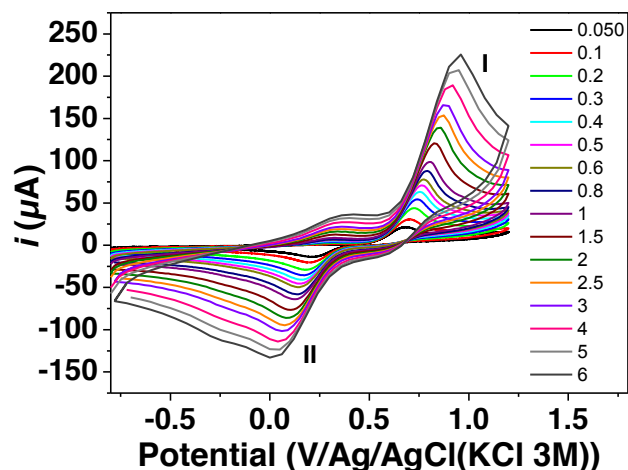
Figure 14. Profil électrochimique CV de la ladanéine (2,32 mM) en fonction de la vitesse de balayage mesuré dans le DMSO avec 0,1 M n-Bu$_4$NPF$_6$ comme électrolyte support à 25 ºC. Electrode de référence = KCl(3M)/Ag/AgCl; électrode de travail = disque de carbone vitreux de 0,07 cm^2 d'aire; contre-électrode = fil de Pt.

On peut observer deux pics anodiques et cathodiques I et II qui correspondent à une oxydation irréversible (I) et la réduction (II), typiques d'un mécanisme de type ECE (réaction Electronique-Chimique-Electronique) lié au catéchol. Si nous compare le voltampérogramme de la ladanéine avec ceux de la 2-phénylchromone (flavone sans substituants) et du DMSO (Figure 15A), nous pouvons conclure que ces processus sont très probablement dues aux groupements présent sur le cycle A. Nous pouvons aussi observer sur la Figure 15B que les différents substituants portés par le noyau B n'influence pas de façon importante le comportement rédox dans cette gamme de potentiel, ce qui confirme que le processus est centré sur le cycle A et que les substituants du cycle B ont une influence mineure.
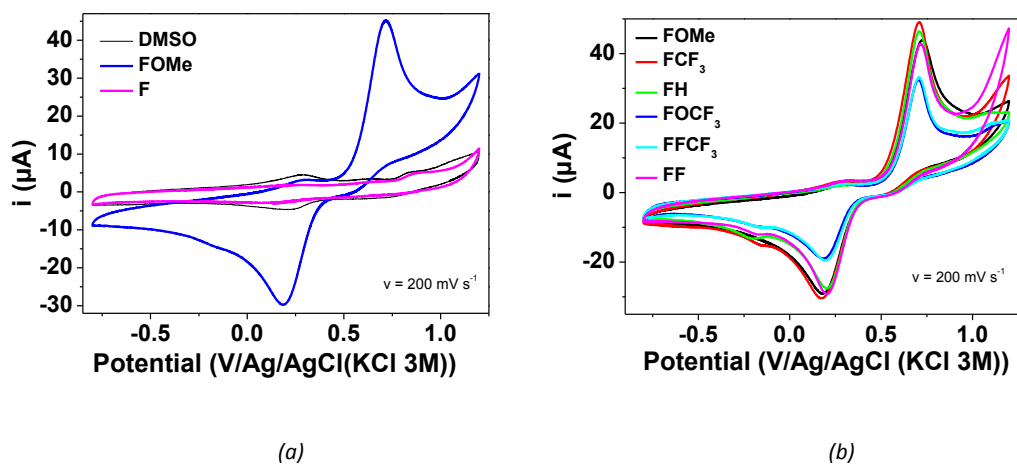

(a)

(b)

Figure 15. (a) Profils CV de la ladanéine (2,32 mM), du DMSO et de la 2-phénylchromone (2,97 mM) mesurés dans le DMSO à une vitesse de balayage de 200 mV/s. (b) Profils CV des différents flavones (concentration 2-2,5 mM) mesurés dans les

mêmes conditions expérimentales avec 0,1 M *n*-Bu$_4$NPF$_6$ comme électrolyte de support à 25 ºC. Electrode de référence = KCl(3M)/Ag/AgCl; électrode de travail = disque de carbone vitreux de 0,07 cm^2 d'aire; contre-électrode = fil de Pt.

Le traitement des donnés obtenues nous a permis de confirmer que les deux processus (oxydation et réduction) sont contrôlés par la diffusion dans nos conditions expérimentales (pente de log(i_p) = *f*(log(*v*) proche de 0,5). La séparation entre le pic cathodique et anodique (ΔE_p) obtenue pour les divers composés est de plusieurs centaines de mV et varie avec la vitesse de balayage, ce qui confirme qu'il s'agit bien de processus à caractère irréversible contrôlés par la diffusion. Nous avons aussi pu déterminer qu'il s'agit d'un processus à deux électrons (combinaison d'expériences DOSY pour la mesure des coefficients de diffusion et expériences électrochimiques). Il est donc suggéré que ces processus sont le fruit d'un transfert d'électron limité par une étape de déprotonation lente.

Les propriétés redox de ces composés ont ensuite été étudiées entre -2,35 et -1,2 V. Dans cette gamme de potentiel, nous pouvons observer un signal quasi-réversible qui peut être attribué à la fonction énone présente au sein du noyau C. La Figure 16 compare le profil électrochimique de la ladanéine à celui de la 2-phénylchromone dans cette gamme de potentiel, ce qui confirme que le processus est bien centré sur le cycle C.
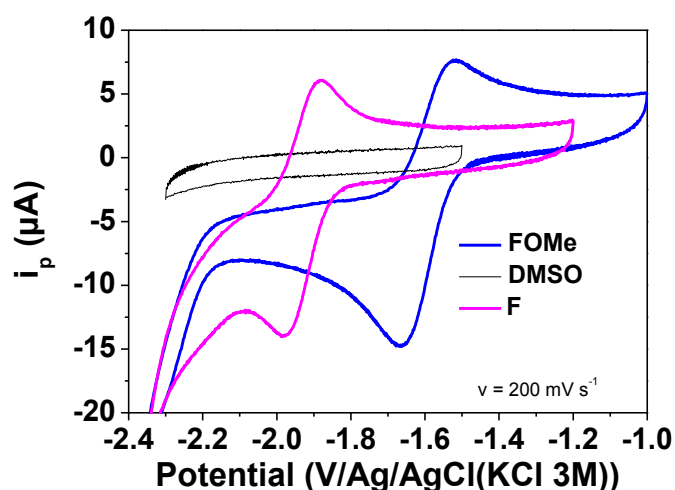

Figure 16. Profils CV de la ladanéine (2,32 mM), du DMSO et de la 2-phénylchromone (2,97 mM) mesurés dans le DMSO à une vitesse de balayage de 200 mV/s avec 0,1 M *n*-Bu$_4$NPF$_6$ comme électrolyte de support à 25 ºC. Electrode de référence = KCl(3M)/Ag/AgCl; électrode de travail = disque de carbone vitreux de 0,07 cm^2 d'aire; contre-électrode = fil de Pt.

Les valeurs de E_{pa} et E_{pc} augmentent légèrement avec la vitesse de balayage, ce qui confirme qu'il s'agit d'une réaction quasi-réversible. Ceci est également confirmé par les valeurs de ΔE_p et le ratio i_{pa} *vs.* i_{pc} (< 1, réaction quasi-réversible). Si ce processus est également contrôlé par la diffusion, il s'agit dans ce cas d'un processus à un électron et non pas à deux comme précédemment.

Contrairement au processus électrochimique centré sur le cycle A, les signaux liés à cette oxydation/réduction sont influencés par le substituant présent sur le cycle B (Figure 17). En effet, l'énone étant conjuguée avec le cycle B, elle devient sensible aux changements électroniques induite par ce noyau. Il est intéressant de noter que la substitution du cycle A (5,6-dihydroxy,7-methoxy) provoque un déplacement de plus de 280 mV (**FH** par rapport à la 2-phénylchromone **F**) par rapport à la flavone « nue ». Ceci peut être dû à des effets électroniques causés par cette substitution sur le noyau A mais également à la forte liaison hydrogène entre le 5-OH et le carbonyle de l'énone. La methoxylation de la position 4' (cycle B) cause un déplacement cathodique additionnel de 50 mV (ladanéine **FOMe**). Pour le précurseur final **FP** (5-methoxy), ce couple rédox est encore déplacée 150 mV vers les potentiels cathodiques.
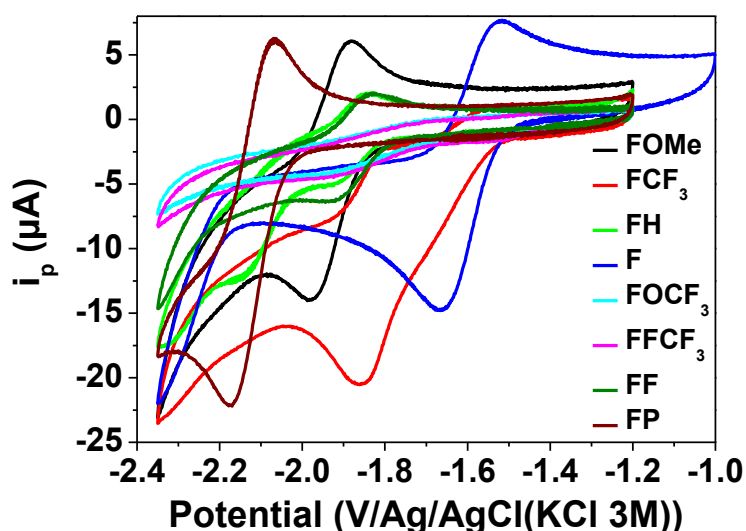

Figure 17. Profils CV des différentes flavones qui démontrent l'effet de la substitution sur le cycle B sur le signal quasi-réversible dû à l'énone. Spectres mesurés dans le DMSO à une vitesse de balayage de 200 mV/s avec 0,1 M n-Bu$_4$NPF$_6$ comme électrolyte de support à 25 ºC. Electrode de référence = KCl(3M)/Ag/AgCl ; électrode de travail = disque de carbone vitreux de 0,07 cm^2 d'aire ; contre-électrode = fil de Pt.

Le ratio i_{pc}/i_{pa} étant éloigné de la valeur idéale de 1, nous pouvons en déduire qu'il existe des réactions secondaires (dismutation, couplage) qui peuvent conduire à la formation de produits de dégradation. Lorsque le profil électrochimique est examiné sur une très large gamme de potentiel, la formation de produits (induite par la réduction de l'unité énone) est clairement mise en évidence par l'apparition de nouveaux pics (Figure 18).
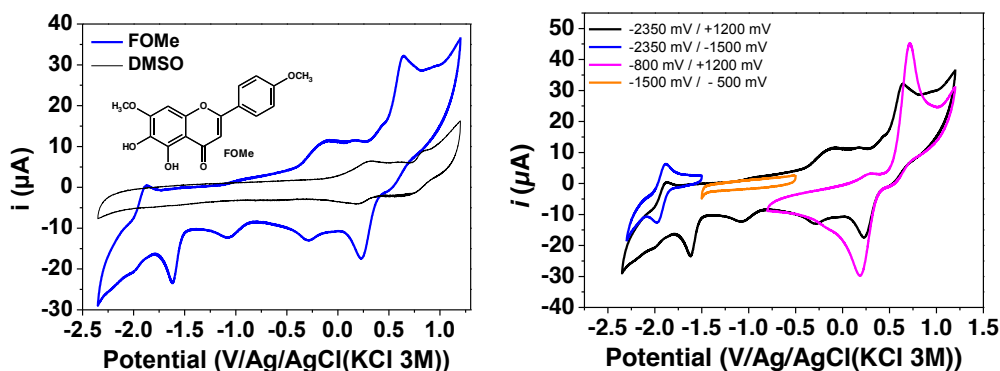
Figure 18. Profils CV de la ladanéine (2.32 mM) qui montrent l'apparition de nouveaux pics lorsque la gamme potentiel est élargie. Spectres mesurés dans le DMSO à une vitesse de balayage de 200 mV/s avec 0,1 M n-Bu$_4$NPF$_6$ comme électrolyte de support à 25 ºC. Electrode de référence = KCl(3M)/Ag/AgCl ; électrode de travail = disque de carbone vitreux de 0,07 cm^2 d'aire ; contre-électrode = fil de Pt.

Complexes de Fe(III)

Les flavonoïdes sont également connus comme étant de bons chélateurs de métaux. Dans de nombreux cas, leur activité biologique est liée à cette capacité de métaux prooxydants (Fe(III), Cu(II)). Au début de ce projet, une analyse ICP-MS sur les fractions les plus actives de ladanéine avait montré qu'elles étaient enrichies en Fe(III) et en Cu(II). D'autre part, lorsque qu'un chélateur puissant du Fe(III) est ajouté (ferrioxamine B), la ladanéine perd son activité biologique (Figure 19). Enfin, la complexation du Fe(III) est susceptible d'empêcher une dégradation non contrôlée de la flavone et peut diriger vers des produits de couplages issus de couplages *C,C* ou *C,O* à 1 électron. Ceci nous a donc amené à considérer plus en détail les capacités de complexation du Fe(III) par la ladanéine.
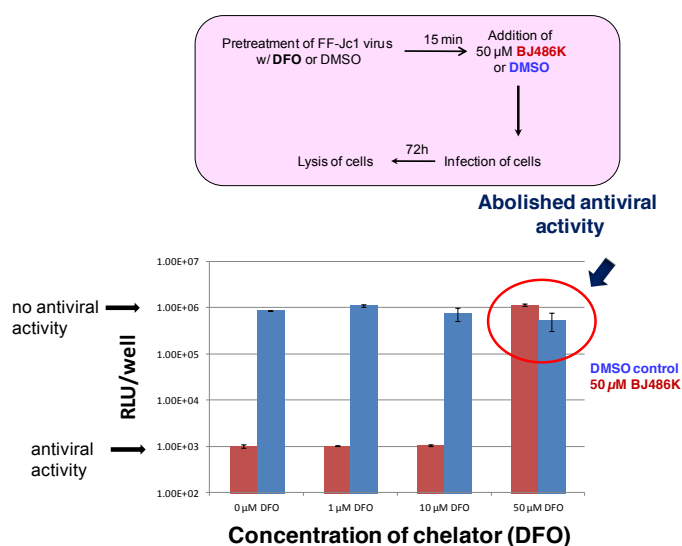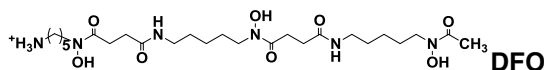
Figure 19. Influence du chélateur DFO très puissant et sélectif du Fe(III) sur l'activité antivirale de la ladanéine.

La complexation du fer(III) par la ladanéine et de la salvigénine (analogue de la ladanéine méthylée sur la position 6-OH) a été étudiée par spectrophotométrie d'absorption afin de caractériser le site de complexation métallique. La ladanéine possède en effet deux sites de chélation bidentés potentiels (5,6-OH et 5-OH-4-carbonyle). La Figure 20 montrent très clairement que ces deux composés peuvent se lier au Fe(III) selon des processus identiques démontrant que le site de complexation est l'unité 5-OH-4-carbonyle et non le catéchol (qui en fait ne possède pas un comportement typique de catéchol du à la forte liaison hydrogène entre le groupement 5-OH du cycle A et l'unité carbonyle en 4 du cycle C). Le précurseur final **FP** qui possède un groupement methoxy en 5 n'est pas capable de complexer le Fe(III), ce qui confirme nos premières hypothèses.
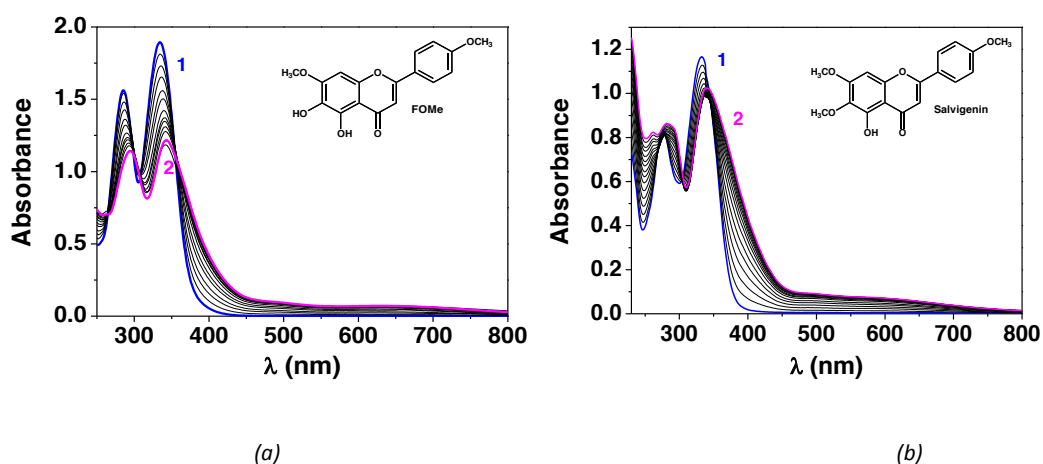

(a) *(b)*

Figure 20. Titrage par spectrophotométrie d'absorption de la ladanéine (a) et de la salvigénine (b). Solvant : CH_3OH/H_2O (80/20 par poids) ; I = 0,1 M (NEt_4ClO_4) ; T = 25,0(2) °C ; pH = 2,0 ; l = 1 cm ; (1) [**FOMe**]$_{tot}$ = 5,92 × 10^{-5} M ; (2) [Fe(III)]$_{tot}$/[**FOMe**]$_{tot}$ = 1,60 ; (1) [salvigénine]$_{tot}$ = 3,48 × 10^{-5} M ; (2) [Fe(III)]$_{tot}$/[salvigénine]$_{tot}$ = 2,0.

La stœchiométrie des complexes ferriques a été évaluée par la méthode des variations continues et nous a permis de confirmer que la ladanéine forme des complexes de stœchiométrie 1:1 avec le Fe(III).

Nous avons ensuite considéré les complexes ferriques formés avec les autres analogues de la ladanéine. Les constantes de stabilité sont réunies dans le Tableau 3. L'ensemble des flavones forme des complexes de stabilité comparable. Même en milieu acide, il est important de noter que la formation des complexes ferriques induit une oxydation rapide de la ladanéine.

Tableau 3. Constantes de stabilité des complexes de Fe(III) avec la ladanéine et ses analogues.

Complexe	log K^*FFe	MCT (nm) (M^{-1} cm^{-1})
FOMe.Fe	6.0(3)	633(1560)
FH.Fe	5.4(6)	635(1200)
FFCF$_3$.Fe	5.8(4)	651(1050)
FCF$_3$.Fe	5.3(6)	650(1230)
FF.Fe	4.7(3)	655(910)
FOCF$_3$.Fe	5.8(3)	649(1040)
		σ σ

Pour raisons de solubilité du fer(III), nous avions, jusqu'à présent, réalisé des études de spéciation de nos flavones par le Fe(III) en milieu acide. Ces conditions sont, cependant, très éloignées des conditions physiologiques (pH du foie ~ 7). En effet, à pH 7,4, le Fe(III) forme des espèces hydroxylées insolubles. Afin de pouvoir étudier les complexes ferriques dans des conditions quasi-physiologiques, l'ajout d'un ligand exogène s'est avéré nécessaire pour assurer la solubilité de ce cation trivalent. L'acide nitrilotriacétique (NTA) a été choisi. La Figure 21 illustre le titrage spectrophotométrique (absorption) de la ladanéine par le FeNTA à pH 7,4. On peut ainsi observer que la bande II subit un déplacement bathochrome et hyperchrome tandis que la bande I diminue d'intensité sans déplacement significatif de sa position. D'autre part, l'ensemble des complexes ferriques examinés dans ce travail sont caractérisés par des bandes de transfert de charge phénolate-Fer(III) dans le visible.
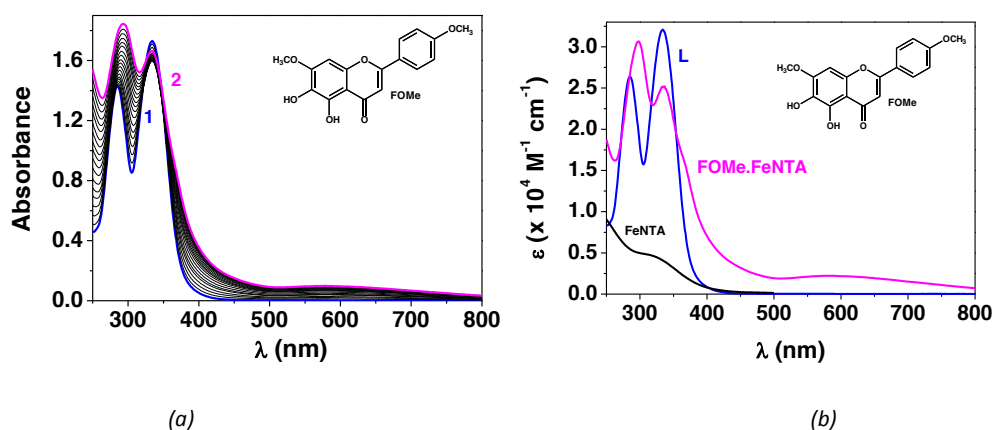

(a)   *(b)*

Figure 21. Titrage spectrophotométrique (absorption) de la ladanéine avec le FeNTA à pH 7,4. (a) Spectres d'absorption en fonction de $[FeNTA]_{tot}$ et (b) spectres électroniques d'absorption de la ladanéine et de ses complexes ternaires avec le fer(III) et le NTA. Solvant : CH_3OH/H_2O (80/20 par poids) ; pH = 7,4 (tampon Hepes) ; I = 0,1 M (Hepes) ; T = 25,0(2) °C ; I = 1 cm ; (a) (1) $[FOMe]_{tot}$ = 5,41 × 10^{-5} M ; (2) $[FeNTA]_{tot}/[FOMe]_{tot}$ = 2,0 ; (b) (1) $[FeNTA]_{tot}$ = 2,30 × 10^{-4} M ; (2) $[FOMe]_{tot}/[FeNTA]_{tot}$ = 1.51.

De manière intéressante, l'addition du NTA à pH 7,4 permet d'empêcher l'oxydation observée lorsque de la formation du complexe binaire Fe(III)-ladanéine en milieu acide. Ceci peut être expliqué par une modulation des propriétés rédox des complexes métalliques peu enclins à subir un échange électronique en présence de NTA.

Pour confirmer la stœchiométrie des complexes ternaires, nous avons ensuite mené une analyse par ESI-MS (Figure 22).
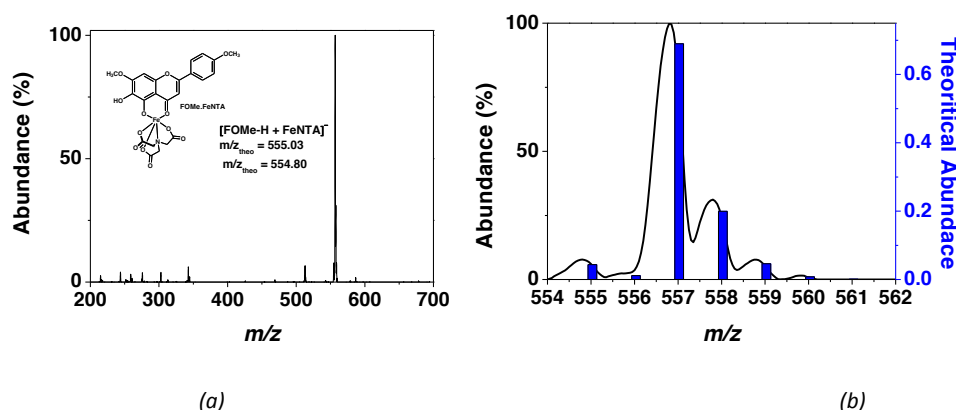

(a) *(b)*

Figure 22. Spectre ESI-MS du complexe ferrique de la ladanéine en présence de NTA. Solvant : CH_3OH/H_2O, voltage du capillaire = 4000 V. $[FOMe.FeNTA]_{tot}$ = 10^{-4} M ; mode négatif ; Fragmenteur = 150 V.

Complexes du Mg(II) et pharmacophores hybrides

Afin d'améliorer le faible temps de demi-vie de la ladanéine mesuré chez la souris (7.3 min dans le sérum), il a été décidé d'étudier les complexes de Mg(II) avec ces mêmes flavones, afin d'évaluer si la complexation par un cation inerte électrochimique était susceptible de protéger la flavones de la dégradation *in vivo*. La formation d'un premier complexe a été suivie par spectrophotométrie d'absorption par mélange de la ladanéine avec $MgCl_2$ dans un mélange binaire eau/acétonitrile (Figure 23). Cependant, le complexe formé est caractérisé par une stabilité insuffisante. L'utilisation du stéarate de Mg(II) a permis de conduire à la formation d'un complexe beaucoup plus stable, mais sa très faible solubilité nous a empêché de continuer l'étude.
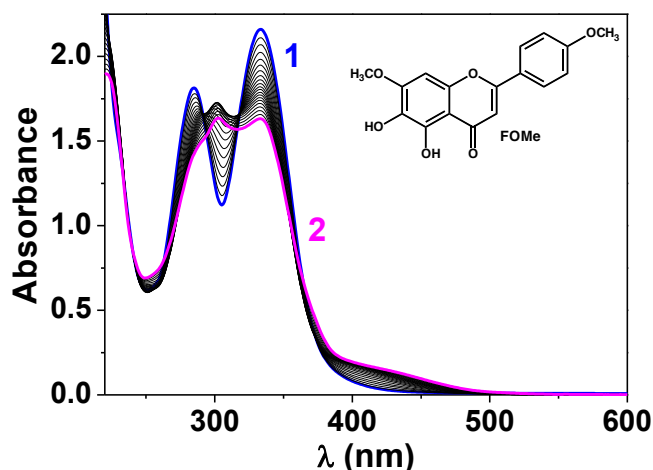
Figure 23. Titrage par spectrophotométrie d'absorption de la ladanéine par MgCl$_2$. Solvant : CH$_3$CN/H$_2$O (1:1 en volume) ; T = 25,0 °C ; l = 1 cm ; [**FOMe**]$_{tot}$ = 7,63 × 10^{-5} M ; (1) [MgCl$_2$]$_{tot}$/[**FOMe**]$_{tot}$ = 0 ; (2) [MgCl$_2$]$_{tot}$/[**FOMe**]$_{tot}$ = 185,8.

Les complexes ont été également étudiés dans le méthanol avec MgCl$_2$, le pidolate de Mg(II) et un précurseur de magnésium synthétisé au laboratoire et nommé Mg181. Les constantes de stabilité des complexes sont réunies dans le Tableau 4. On peut observer que les complexes les plus stables pour la ladanéine **FOMe** et la negletéine **FH** sont formés avec le pidolate de Mg(II) et Mg181. Par contre, pour les composés qui contiennent des atomes de fluor, les meilleurs résultats sont obtenus avec le MgPid et MgCl$_2$. Il est suggéré que la présence de plusieurs atomes de F au sein de Mg181 diminue la stabilité des complexes correspondants.

Tableau 4. Constantes de stabilité des différents complexes flavone-Mg(II). Solvant = CH$_3$OH ; T = 25 °C ; les erreurs sont donnés à 3σ avec σ = déviation standard.

	log $K^*_{F.MgX}$ (±3σ)		
	MgCl$_2$	**MgPid**	**Mg181**
FOMe	4.50(4)	4.92(7)	4.8(4)
FH	1.97(4)	4.38(5)	4.77(8)
FF	5.36(2)	5.09(3)	3.1(2)
FCF$_3$	4.4(2)	4.6(2)	<3
FFCF$_3$	4.93(2)	5.04(2)	<3
FOCF$_3$	5.47(4)	5.26(3)	4.1(2)

Les complexes ont aussi été étudiés par ESI-MS, et l'ensemble des complexes de magnésium ont pu être identifiés à l'exception de **FCF$_3$**.Mg181 and **FOCF$_3$**.Mg181, en accord avec la faible stabilité de ces espèces. Enfin, afin de confirmer la complexation du magnésium par la ladanéine et ses analogues (outre des caractérisations par RMN 1H et spectroscopie infrarouge), un déplacement des signaux caractéristiques a été observé lors de l'ajout de MgCl$_2$ lors de l'étude électrochimique.

L'activité antivirale du complexe **FOMe**.MgPid a été mesurée et est similaire à celle calculée pour la flavone libre, ce qui confirme que l'activité n'est pas perdue lorsque la flavone complexe un métal inerte. Si le nouveau complexe ne montre pas un temps de demi-vie amélioré (8 minutes), il est cependant beaucoup plus soluble et dispose d'une biodisponibilité orale.

Des tests biologiques avait démontré que la ladanéine possédait une activité antivirale[29] additive avec la chloroquine, composé utilisé pour traiter le paludisme. Il a donc été décidé de construire un double pharmacophore lié par le Mg(II). Cependant, par faute de temps, le projet n'a pu être achevé. Les étapes développées sont décrites au Schéma 5 ainsi que la structure chimique de la molécule finale cible.
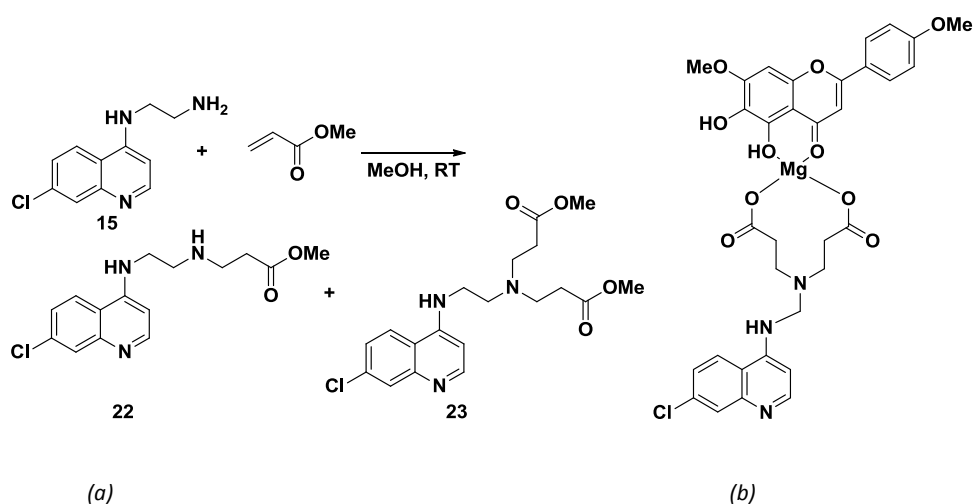

(a)   *(b)*

Schéma 5. (a) Réaction du produit **15** avec le méthyle acrylate pour donner les produits **22** et **23**. (b) Molécule hybride cible portant les deux pharmacophores.

Conclusion

Durant ces trois années de thèse de Doctorat, une nouvelle synthèse améliorée de la ladanéine a été développée. Cette nouvelle approche permet d'obtenir le produit désiré de façon beaucoup plus rapide, avec un meilleur rendement et sans avoir besoin d'avoir recours à des purifications fastidieuses par utilisation de colonne de silice ou de Sephadex LH-20.

Afin de mieux comprendre l'activité antivirale de ces composés, une étude physico-chimique a été entreprise. Les propriétés acido-basiques ont été étudiées. Les valeurs de pK_a ont été déterminées par spectrophotométrie d'absorption couplée à la pHmétrie et les valeurs mesurées ont été attribuées au groupement 6-OH des flavones. La cinétique d'oxydation en milieu basique a également été étudiée en détail en utilisant la spectrophotométrie d'absorption et la spectrométrie de masse en mode électrospray ESI-MS.

L'étude des propriétés électrochimiques des flavones a été également menée. Un processus irréversible à deux électrons a lieu entre -0,8 et +1,2 V et est assurément lié aux groupements présents sur le noyau A. Entre -2,35 et -1,2 V, un processus quasi-réversible à un électron correspondant à l'oxydoréduction de l'énone sur le cycle C a été mis en évidence.

Etant donné que le Fe(III) est probablement essentiel à l'activité antivirale des flavones (processus de bioactivation), une étude des complexes ferriques a été réalisée au moyen de la spectrophotométrie d'absorption. Toutes les flavones excepté le précurseur final **FP** complexent le Fe(III) au moyen de leurs sites 5-OH-4-carbonyle et forment des complexes 1:1 de stabilité comparable. Afin d'étudier ces mêmes complexes dans des conditions physiologiques, un ligand exogène (NTA) a été introduit et les complexes flavone.FeNTA ont été quantifiés par spectrophotométrie d'absorption et caractérisés par ESI-MS.

Le dernier aspect considéré dans mon travail de thèse a porté sur la mise au point d'une formulation qui puisse permettre d'améliorer le profil pharmacocinétique des flavones synthétisées. La complexation du magnésium a été ici privilégiée et l'étude des complexes de Mg(II) formés avec nos flavones a été effectuée. Le complexe FOMe.MgPid possède activité antivirale comparable à celle de la ladanéine seule mais avec une meilleure solubilité. Les premières étapes de la synthèse d'un composé hybride comportant deux pharmacophores aux modes d'action différents et liés au moyen d'un lien métallique ont été réalisées. Cependant, par faute de temps, le projet n'a pas pu être mené à sa fin et sera poursuivi ultérieurement.

Références bibliographiques

(1)   *Hepatology* **2002**, *36*, S3–S20.

(2)   Tanaka, Y.; Kurbanov, F.; Mano, S.; Orito, E.; Vargas, V.; Esteban, J. I.; Yuen, M.-F.; Lai, C.-L.; Kramvis, A.; Kew, M. C.; Smuts, H. E.; Netesov, S. V; Alter, H. J.; Mizokami, M. *Gastroenterology* **2006**, *130*, 703–714.

(3)   Moradpour, D.; Penin, F.; Rice, C. M. *Nat. Rev. Microbiol.* **2007**, *5*, 453–463.

(4)   Poynard, T.; Marcellin, P.; Lee, S. S.; Niederau, C.; Minuk, G. S.; Ideo, G.; Bain, V.; Heathcote, J.; Zeuzem, S.; Trepo, C.; Albrecht, J. *Lancet* **1998**, *352*, 1426–1432.

(5)   Zeuzem, S.; Feinman, S.; Rasenack, J.; Heathcote, J.; Lai, M.-Y.; Gane, E.; O'Grady, J.; Reichen, J.; Diago, M.; Lin, A.; Hoffman, J.; Brunda, M. M. J. *N. Engl. J. Med.* **2000**, *343*, 1666–1672.

(6)   Lawitz, E.; Mangia, A.; Wyles, D.; Rodriguez-Torres, M.; Hassanein, T.; Gordon, S. C.; Schultz, M.; Davis, M. N.; Kayali, Z.; Reddy, K. R.; Jacobson, I. M.; Kowdley, K. V; Nyberg, L.; Subramanian, G. M.; Hyland, R. H.; Arterburn, S.; Jiang, D.; McNally, J.; Brainard, D.; Symonds, W. T.; McHutchison, J. G.; Sheikh, A. M.; Younossi, Z.; Gane, E. J. *N. Engl. J. Med.* **2013**, *368*, 1878–1887.

(7)   Shirley, B. *Trends Plant Sci.* **1996**, 377–382.

(8)   Yoshioka, T.; Inokuchi, T.; Fujioka, S.; Kimura, Y. *Z. Naturforsch. C.* **2004**, *59*, 509–514.

(9)   Mo, Y.; Nagel, C.; Taylor, L. P. *Proc. Natl. Acad. Sci. U. S. A.* **1992**, *89*, 7213–7217.

(10)   Pietta, P. G. *J. Nat. Prod.* **2000**, *63*, 1035–1042.

(11)   Yoshida, M.; Sakai, T.; Hosokawa, N.; Marui, N.; Matsumoto, K.; Fujioka, A.; Nishino, H.; Aoike, A. *FEBS Lett.* **1990**, *260*, 10–13.

(12)   Duthie, G. G.; Duthie, S. J.; Kyle, J. A. *Nutr. Res. Rev.* **2000**, *13*, 79–106.

(13)   Wu, Y.; Wang, F.; Zheng, Q.; Lu, L.; Yao, H.; Zhou, C.; Wu, X.; Zhao, Y. *J. Biomed. Sci.* **2006**, *13*, 569–578.

(14)   Cushnie, T. P. T.; Lamb, A. J. *Int. J. Antimicrob. Agents* **2005**, *26*, 343–356.

(15)   Li, B. Q.; Fu, T.; Dongyan, Y.; Mikovits, J. A.; Ruscetti, F. W.; Wang, J. M. *Biochem. Biophys. Res. Commun.* **2000**, *276*, 534–538.

(16)   Geuenich, S.; Goffinet, C.; Venzke, S.; Nolkemper, S.; Baumann, I.; Plinkert, P.; Reichling, J.; Keppler, O. T. *Retrovirology* **2008**, *5*, 27.

(17)   Kostanecki, S. V.; Rozycki, A. *Berichte der Dtsch. Chem. Geselschaft* **1901**, *34*, 1901.

(18)   Auwers, K.; Müller, K. *Berichte der Dtsch. Chem. Geselschaft* **1908**, *41*, 4233–4241.

(19)   Allan, J.; Robinson, R. *J. Chem. Soc., Trans.* **1924**, 2192–2195.

(20)   Mahal, H. S.; Venkataraman, K. *J. Chem. Soc.* **1934**, 1932–1934.

(21)   Algar, J.; Flynn, J. *Proc. R. Irish Acad. Sect. B Biol. Geol. Chem. Sci.* **1934**, *42*, 1–8.

(22)   Khoobi, M.; Alipour, M.; Zarei, S.; Jafarpour, F.; Shafiee, A. *Chem. Commun.* **2012**, *48*, 2985–2987.

(23)   Selepe, M. a; Van Heerden, F. R. *Molecules* **2013**, *18*, 4739–4765.

(24) Yoshida, M.; Fujino, Y.; Doi, T. *Org. Lett.* **2011**, *13*, 4526–4529.

(25) Gampp, H.; Maeder, M.; Meyer, C. J.; Zuberbühler, A. D. *Talanta* **1986**, *33*, 943–951.

(26) Gampp, H.; Maeder, M.; Meyer, C. J.; Zuberbühler, A. D. *Talanta* **1985**, *32*, 257–264.

(27) Maeder, M.; Zuberbuhler, A. D. *Anal. Chem.* **1990**, 2220–2224.

(28) Gampp, H.; Maeder, M.; Meyer, J.; Zuberbühler, A. D. *Talanta* **1985**, *32*, 95–101.

(29) Pietschmann, T.; Haid, S.; Gentzsch, J.; Grethe, C.; Davioud-Charvet, E.; Lanfranchi, D.-A.; Elhabiri, M.; Benlloch-Martin, X. Flavone derivatives and their use. WO 2013/139487 A1, 2013.

Table of contents

Chapter I: General Introduction

1.1. Viruses

Viruses are biological entities that infect organisms all throughout nature, infecting plants, animals and bacteria alike. Viruses may cause diseases by using the metabolic machinery of its host to replicate. Many of the most serious illnesses known to man are caused by viruses, such as the Acquired Immunodeficiency Syndrome (AIDS) with around 35 million people infected worldwide and 1.5 million deaths in 2013, Ebola Hemorrhagic Fever (EHF) or, although already eradicated, smallpox, a virus known for centuries that caused many epidemics throughout the years.

Historically, in the late 19th century, Martinus Beijenrick and Dimitri Ivanovksi independently discovered an infectious agent from plant extracts.[1] They passed the extracts through filters and obtained an agent that was able to infect new plants, however, no bacteria could be cultured from the filtrates. Beijenrick named the agent a "virus", name that has been adopted and used ever since.

The perception of viruses radically changed in 1935 when Nobel Prize winner Wendel Stanley successfully crystallized the Tobacco Mosaic Virus (TMV, Figure 24) that had been previously studied by Beijenrick and Ivanovski.[2] Viruses were seen as an entity somewhere in between chemistry and biology, starting a great debate about whether or not viruses are living organisms. Nowadays, viruses are not considered as living organisms, but as biological entities, since they possess some of the properties of living systems (genome, adaptability). Nevertheless, they lack some of the basic attributes of life, such as being able to self-replicate or the ability to capture and store energy. Viruses need host factors and proteins to replicate themselves. It is hence accepted amongst biologists that the simplest system considered to be alive is a cell. Viruses are considered to be nonliving infectious agents. It is noteworthy that viruses have the highest proportion of proteins involved in information processes when compared to other organisms. This is because they rely on the biological machinery of the cell for their replication and energy needs.

When viruses are outside the host cells, they are called virions. A virion is basically a gene delivery system, and its main goal is to protect the genetic material and to facilitate its entry in a host cell. For that reason, the basic structure of a virus is composed of the genome packaged in a protein structure known as capsid.
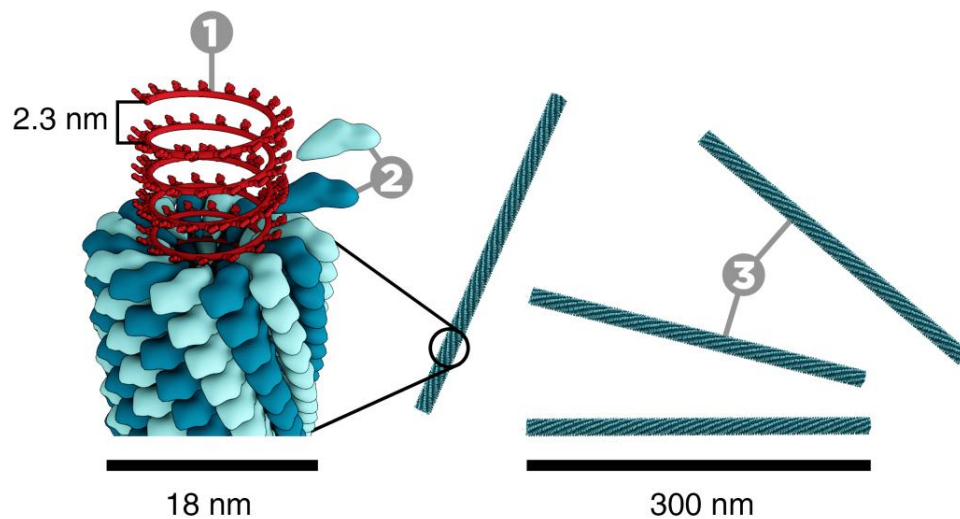
Figure 24. Structure of the tobacco mosaic virus, with the capsid in blue and the genetic material in red.

The genome can be either DNA- or RNA-based, single stranded (ss) or double stranded (ds) and arranged in a circular or linear structure. For example, parvoviruses are viruses with a single linear DNA strand. The major function of the capsid is to protect the genome, although it can exert other functions such as attachment to a host cell. Capsids can be arranged in different structures, forming helixes, icosahedra, rods, cones or other depending on the virus. The helix and icosahedron are the most common capsid structures. Viruses containing only a capsid are called non-enveloped viruses. Many viruses have a lipidic coat surrounding the capsid. These viruses are called enveloped viruses and will be further discussed in section 1.1.2.

1.1.1. Taxonomy

Even though a classification by species is apparently basic, it took virologists many years to start assigning viruses to different species. Finally, in 1991, the International Committee on Taxonomy of Viruses (ICTV) established the definition of viral species as the following: "*a virus species is a polythetic class of viruses that constitute a replicating lineage and occupy a particular ecological niche*". The principles of virus evolution are the same as for the rest of organisms, however, high-error rates, quasispecies and genetic exchange between large gene pools must be taken into account as well.

A virus classification is a tool that allows easy extrapolation of useful information from one virus to another. When a newly discovered virus is assigned to a certain category, a number of *a priori* properties can be assigned to it, awaiting confirmation. The first classification appeared in the 1920s, when viruses were described according to their effect on health (viruses causing liver problems were

put together in the "hepatitis viruses" group). However, it was not until the 1950s, with the help of the electron microscope, that a real classification was established. The main criterion chosen was the size and shape of the viral particle. Finally, it is only during the last years that a hierarchical classification was accepted. Nowadays, viruses are classified by their order, family, subfamily, genus and type species. This takes into account the type of nucleic acid (DNA or RNA), if it is single stranded (ss) or double stranded (ds), the use of a reverse transcription process and the sense of gene coding (positive or negative).

- Order (*-virales*)
- Family (*-viridae*)
- Subfamily (*-virinae*)
- Genus (*-virus*)
- Species

The ICTV considers there are seven major orders (*caudovirales*, *herpesvirales*, *ligamenvirales*, *mononegavirales*, *nidovirales*, *picornavirales* and *tymovirales*) and other virus families not assigned to an order, accounting for more than 2,500 viruses.

1.1.2. Enveloped Viruses

One structural feature that allows the classification of viruses is the presence or absence of a viral envelope. For nonenveloped viruses, the protein capsid protects the genome from the environment, whereas this role is partially fulfilled by the lipidic layer in enveloped viruses. Both capsids and viral envelopes are crucial to the survival of the virus, since they must allow the transport and delivery of the genetic material from one host cell to another. Viral capsids and envelopes are often formed by very few proteins, sometimes only one. However, they must perform various functional tasks. First, packing all the nucleic acids and proteins needed for an infective viral particle. Second, being stable enough to survive in the extracellular environment, bind and enter a new cell. Finally, the viral capsid or envelope must be readily disassembled once the virus enters the cell. Viruses can be classified according to the symmetry of the protein within the capsid, giving rise to five different categories:

- Helical nonenveloped virions
- Helical enveloped virions
- Icosahedral nonenveloped virions
- Icosahedral enveloped virions
- More complex virion structures

Helical virions have the genetic material organized around a central axis. An example of a nonenveloped helical virion is the tobacco mosaic virus, while an example of an enveloped helical virion is the rabies virus.[3] Regarding the icosahedral viruses, they form spherical particles with 2-, 3- and 5-fold axis of symmetry. We can cite *adenovirus*[4] as an example of nonenveloped virus and Herpes Simplex Virus (HSV)[5] as an enveloped one. Finally, the smallpox virus has a more complex structure as does not fit within the other categories.

Viruses containing a lipidic envelope include *Baculo-*,[6] *Bunya-*,[7] *Corona-*,[8] *Filo-*,[9] *Herpes-*,[10] *Lenti*,[11] *Orthomyxo-*,[12] *Paramyxo-*,[13] *Pox-*,[14] *Retro-*, *Rhabdo-*[15] and *Togaviridae*.[16] In any of these viruses, the function of the viral envelope is to form a membrane surrounding the nucleocapsid that contains the genetic material (Figure 25). Viral envelopes are formed by at least one lipidic bilayer, although on rare occasions more are present. Also, other viruses such as *Iridovirus* present a lipid membrane within the capsid and not surrounding it.[17] Embedded in the bilayer are proteins that play a critical role in virus entry. Generally, these proteins exert two functions, attachment to the cell surface and membrane fusion.
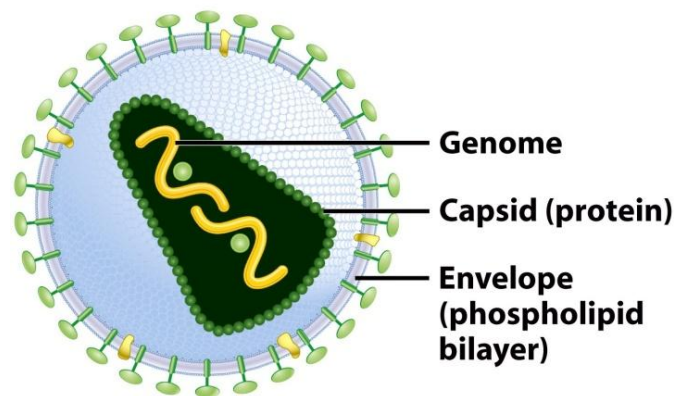
Figure 25. Basic structure of an enveloped virus.

Generally, the budding of the virion occurs when the nucleocapsid exits the cytoplasm and passes to the extracellular milieu. This means that in most cases, the lipidic bilayer forming the viral envelope comes from a pre-existing cytoplasmic membrane in the host cell. Nonetheless, the bilayer may be formed from the nuclear envelope, the Golgi apparatus and the endoplasmic reticulum.[18–20] Each virus utilizes a particular cell membrane to perform its budding. These lipidic envelopes are sensitive to chemical and physico-chemical conditions that disrupt them such as some solvents, extreme pHs, high temperatures or detergents.

Even though the bilayer is taken from the host cell, viruses embed their own proteins in them. These proteins can be classified in two different types, the integral and the peripheral. Integral proteins usually have three different domains, the extracellular domain, often glycosylated, which performs various tasks such as binding, fusion, etc. The transmembrane domain holds the protein in the viral envelope. Finally, the third domain, internal to the viral membrane may be used to select the protein to be included in the viral envelope. Peripheral viral proteins are attached to the membrane by a combination of hydrophobic and electrostatic interactions. Some of the peripheral proteins are thought to bring together the capsid and the envelope during viral assembly in the host cell.

Although the viral envelope is more fragile than a viral capsid, the presence of a viral envelope offers various advantages over a capsid. For example, *Influenza A virus* has a receptor-destroying enzyme which is believed to help during egress by preventing the virus from sticking to cells as well as preventing clumping of the virions.[21] In addition, the viral envelope protects the virion from antibody recognition and neutralization. Since the external proteins are often glycosylated, they trick the immune system and prevent the binding of antibodies. The presence of the lipidic bilayer also hides the virus internal proteins from the immune system, making it more difficult for the body to recognize the virus. It has been shown as well that certain viruses tolerate variations in the compositions of their lipidic envelope. A modification of the viral envelope to accommodate another viral protein can be feasible, while modification of a tight viral capsid is very difficult. Finally, viral entry and infection is easier because membrane fusion is greatly improved.

Naked virus entry is performed after an irreversible attachment to the cell surface followed by endocytosis. Enveloped viruses, on the other hand, first attach in a reversible manner that may lead to irreversible attachment. Then virus entry is either performed by fusion of the viral envelope with the cell membrane or endocytosis followed by fusion. Both processes involve the fusion of the viral bilayer with the cellular membrane, which does not occur spontaneously. Each virus possesses a glycoprotein that catalyzes this process. Some viruses fuse with the cell membrane in a pH-independent manner, such as HIV, whereas other viruses fuse *via* an acid-triggered fusion that exposes the fusion sequence of the protein, as can be found in influenza viruses.

1.2. Hepatitis C Virus

Amongst all enveloped viruses, Hepatitis C Virus (HCV) is one of the most widespread. Affecting more than 150 million people worldwide, it is estimated to cause around 500,000 deaths per year (2,600 deaths per year in France). In this section, the history of the discovery of the virus, its biological properties and the therapies used to fight its infection will be thoroughly discussed.

1.2.1. History of Hepatitis C Virus Infection

Viruses probably appeared with the dawn of life, and have evolved ever since. It is possible that HCV appeared hundreds of thousands of years ago and has been evolving since then. However, the oldest blood samples infected with the virus are 50 years old. During and after World War II, the increasing number of blood transfusions led to a raise in the cases of post-transfusion hepatitis. First, it was thought that two agents caused this disease, Hepatitis A Virus (HAV) and Hepatitis B Virus (HBV). However, it was discovered that HAV cannot be transmitted through blood contact.[22] During the 1960s and 1970s, scientists developed blood tests to identify Hepatitis B (1963) and A (1973). Surprisingly, it was found that many of the tested samples gave a negative result for both of the viruses.[23,24] Scientists called this new hepatitis form "non-A, non-B hepatitis" (NANBH). Because there was no way to test if a blood donor was infected with NANBH, patients that needed blood transfusion and medical staff were the most affected. Many efforts were put towards the identification of the agent causing NANBH. Further studies showed that the agent was most likely a small enveloped virus, because it was sensitive to organic solvents. Finally, in 1989 the virus was discovered by Bradley and Houghton.[25] Shortly after, in 1991, the first treatment with interferon (IFN) was approved by the FDA.[26] One year later, a blood test was made available to identify HCV in the blood transfusion supply.[27] It is estimated that 300,000 people were infected with HCV through blood transfusion only in the United States of America before the blood test was widely used. Since this moment, research in HCV started growing every year. Through a search of the term "HCV" using Scifinder, it can be seen that the number of publications has grown every year, from 15 in 1989 to more than 1,500 in the year 2013 (1,422 for 2014 – Scifinder consulted on November 12th).

1.2.2. Hepatitis C Virus Structure

Hepatitis C Virus is a *Hepacivirus*, belonging to the *Flaviviridae* family (Figure 26). It is an enveloped virus with a fairly small size of 55-65 nm and a 30 nm capsid. The capsid encloses a single-stranded positive-sense RNA molecule.

Until recently it was considered to be the only virus in its genus. However, other viruses belonging to the same genus were discovered.[29] The HCV particle is composed of a spherical viral envelope surrounding the icosahedral capsid and the genetic material (Figure 27). The 9.6 kb genome encodes one large polyprotein (3,000 aminoacids, Figure 28) that is further processed by viral and cellular proteases to produce the structural (Core,[30] E1 and E2) and non-structural (p7,[31] NS2, NS3, NS4A, NS4B, NS5A and NS5B) proteins.
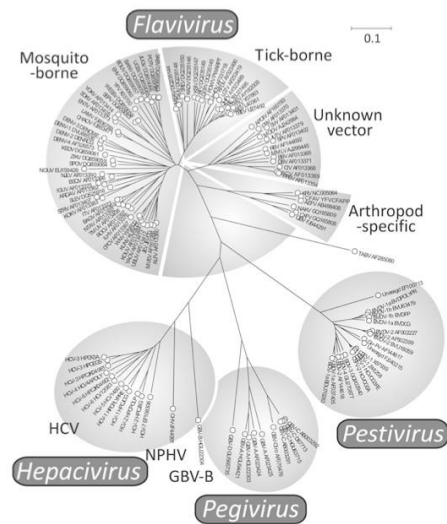
Figure 26. *Flaviviridae* phylogenetic tree.[28]
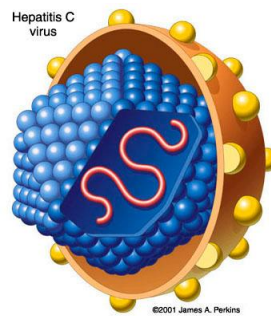
Figure 27. Structure of hepatitis C virus.
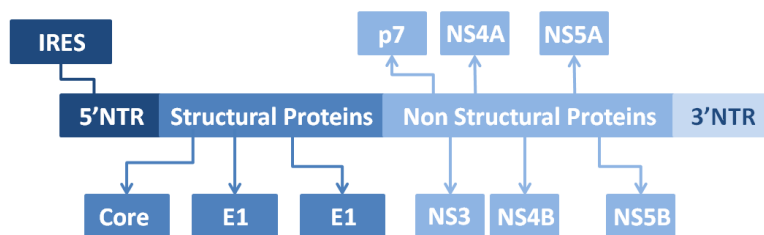
Figure 28. HCV genome and proteins.

Anchored in the lipidic layer are the two glycoproteins E1 and E2. These two proteins are highly glycosylated and do not need to be activated through a cleavage. They both have a large N-terminal ectodomain and a C-terminal transmembrane domain. Interestingly, the E2 glycoprotein has a hypervariable region that mutates frequently, allowing the development of a high number of immune escape variants. p7 is a small integral membrane protein, which probably functions as an ion channel and is essential for the production of infective virions.[31] As for the nonstructural proteins,

NS2 cleaves the polyprotein between NS2 and NS3 and appears to have a role in apoptosis and lipid metabolism among others. NS3, a helicase, forms a complex located in the endoplasmic reticulum (ER) with NS4A that cleaves the polyprotein after NS3 and is essential for the formation of the complex allowing viral replication. Also, the NS3/4A complex is thought to play a role in disrupting the response of the host immune system. NS4B is believed to be essential for viral replication, assembly and release of the virion and lipid metabolism. NS5A is associated to the ER and may have many functions. It is essential for viral replication, can be hyperphosphorylated and hence inhibit viral replication and is able to decrease the immune response of the host cell by inhibiting the protein kinase PKR. Finally, NS5B is a polymerase that uses an RNA template to build RNA. It is a key protein for viral replication. These will be further discussed in a following section.

1.2.3. Hepatitis C Virus Epidemiology

Although Hepatitis C is endemic worldwide, the prevalence of HCV infection varies depending on the region of the world. Prevalence is much higher in certain African and Asian countries while in Western Europe or North America it is much lower. For example, the prevalence rate in Bolivia is of 11 %, while in Cameroon is of 13 % or 18 % in Egypt. These figures are extremely high, especially when compared with European countries such as Germany (0.1 %), Ireland (0.1 %) or Austria (0.2 %). This data shows that HCV infection is much more important in developing countries. The very high prevalence in Egypt is most likely due to an antischistosomal treatment campaign during which syringes were reused from one patient to another.[32]
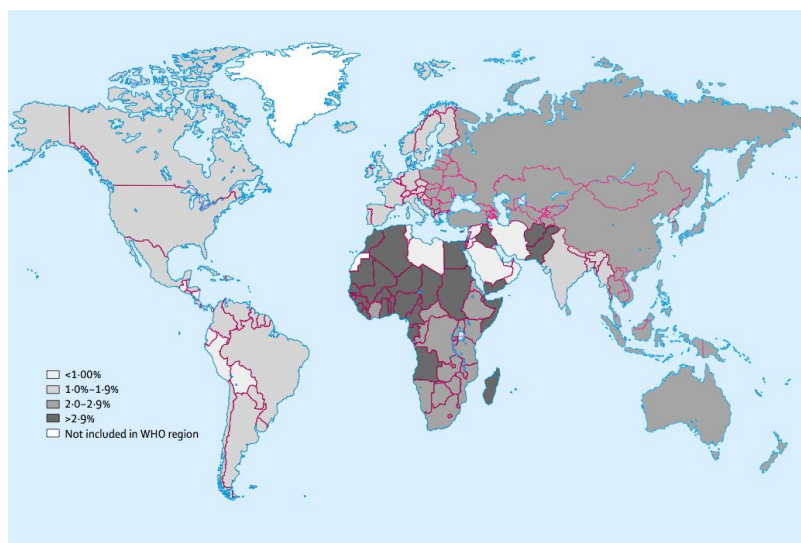
Figure 29. HCV infection epidemiology by country.[356]

Furthermore, since the virus has a long asymptomatic period,[33] these figures may not be very accurate, since many people may be living with HCV but remain undiagnosed.

Shortly after the discovery of HCV, it became apparent that there was a big difference between isolates from different individuals or countries. The variants were studied and gave rise to seven different HCV genotypes,[34] which vary in 35 % of their sequence.[34,35] These seven genotypes are further divided in 67 subtypes, which have a 15 % difference in their coding region. Certain genotypes are predominant in particular regions of the world. As it can be seen in Figure 30 genotype 1 is predominant in Western Europe and North America,[36] whereas genotype 4 is predominant in the Middle East.[28] A high number of subtypes are present in Africa and Southeast Asia, which may indicate the origin of the virus. Patients infected with genotype 1 are more prone to develop chronic infection and hepatocellular carcinoma.[37] Steatosis however, is most frequently observed in individuals infected by genotype 3.[38] Different genotypes also react differently to treatment. For example genotype 1 is more resistant to treatment than genotypes 2 and 3, with a clearance rate of only 40 to 50 % whereas the clearance rate for genotypes 2 and 3 is of 70 to 80 %.[39]

Not only there is a large number of genotypes and subtypes, but HCV rapidly generates virus variants known as quasispecies.[40] Even within a single infected individual, there does not exist one sole viral entity but a large amount of microvariants of a predominant sequence. These appear because of the high error rate (around 10^{-3} per site) when replicating and the lack of a proof-reading function in NS5B. Also the rate of replication is high with a half-life of three to five hours and a clearance rate of 10^{12} virions per day.[41,42] Assuming that 10 % of the hepatocytes are infected and that there are 2×10^{11} hepatocytes, each hepatocyte would produce around 50 virions per day.[42,43] Such a high replication rate coupled with the elevated error frequency causes the large amount of variants in the body.

Figure 30. HCV genotype distribution worldwide.

1.2.4. Hepatitis C Virus Natural History

The natural history of a disease is defined as the ordinary course of an illness from the moment of exposure to its resolution, as well as the factors that affect its incidence and 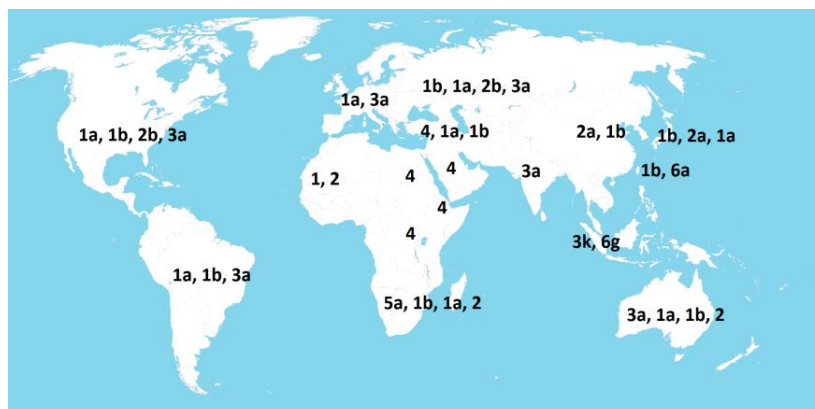distribution. In order to study and analyze the real natural history of a disease, there must be no intervention from the beginning until the resolution. Determining the natural history of HCV is extremely difficult due to different factors. HCV infection is often asymptomatic for long periods of time and its development is very slow, taking several decades since the exposure until removal or death. Also, treatment should be avoided in order to study the natural history of HCV infection, but obviously, that is not possible for ethical reasons.

HCV is mainly transmitted through exposure to infected blood.[44–46] During the first years of the disease, the main risk groups were post-transfusion patients,[45] medical staff through percutaneous exposure to blood,[47] intravenous drug users,[48] hemodialysis patients[49] or recipients of organs from an infected donor.[50] The virus can be contracted through other routes such as sexual contact or birth to an infected mother,[51] but the rates of infection are lower than through blood exposure. Nonetheless, with new screening methods in developed countries, HCV infection has greatly decreased, especially for patients and medical staff.

There are two different manifestations of hepatitis C, acute hepatitis C and chronic hepatitis C.

1.2.4a. Acute Hepatitis C

It is estimated that 30,000 cases of acute Hepatitis C happen each year. Acute hepatitis C is very difficult to study because it is infrequently diagnosed since most of the infected individuals show no symptoms whatsoever. Symptoms of acute Hepatitis C may include malaise, weakness, nausea, loss of appetite and jaundice.[33,52,53] Fulminant hepatitis only occurs in extremely rare cases.[54] Symptoms usually appear three to twelve weeks after exposure and HCV RNA is detectable in serum one to three weeks after exposure.[55] The antibody to HCV becomes positive one to two months after exposure. However, 30 % of patients test negative for anti-HCV when their symptoms start.[56] This makes anti-HCV testing unreliable to detect acute HCV infection. The criteria often used to define an acute HCV infection are the following: increase of alanine aminotransferase (ALT) to more than ten times its upper normal limit, test positive for HCV RNA and exposure to HCV until two months before the testing. However, no reliable assay has yet been developed to correctly differentiate between acute and chronic infection. After virus entry in the cell, interferons (IFN-α and IFN-ß) are produced within hepatocytes (interferons are proteins released by host cell in response to pathogen presence

in order to generate an immune response). This triggers a process that directs lymphocytes to the liver. These lymphocytes will then cause apoptosis on infected hepatocytes. Once the immune response is triggered, there may be clearance of the virus, which is estimated to happen in 20-25 % of cases.[55] Spontaneous viral clearance is favored by different factors such as young age, female sex[57] and symptomatic disease (jaundice).[33] It is also thought that clearance is linked to a smaller HCV quasispecies diversity.[58]

1.2.4b. Chronic Hepatitis C

It is considered that a person is infected with chronic hepatitis C when HCV RNA is persistent in the blood six months after onset of acute infection.[59] This happens to approximately 75-80 % of the patients. Spontaneous clearance is extremely rare once chronic hepatitis is established. Risk factors for developing chronic HCV infection are being more than 25 years old at the time of infection, male gender, having no symptoms during the acute phase, African American race, coinfection with HIV and use of immunosuppressants.[44] It is very likely that a large presence of quasispecies variants helps develop chronic hepatitis C.[58] Also, the genotype plays a role in the advancement of the disease. It has been reported that disease progression is accelerated in patients infected with genotype 3 (Figure 30).[60,61] As happens for acute hepatitis infection, most patients are unaware of their HCV infection and are not diagnosed until years later.

Chronic infection may lead to numerous extrahepatic conditions in up to 70 % of infected individuals.[62] They involve the renal, dermatologic and hematologic organ systems among others. Mixed cryoglobulinemia is the most common extrahepatic manifestation, found in 19 to 55 % of chronic hepatitis patients. Other frequent conditions are membranoproliferative glomerulonephritis,[63] porphyria cutaneous tarda,[64] lichen planus[65] and vitiligo.[66]

Another important condition caused by chronic HCV infection is liver fibrosis. Liver fibrosis is the excessive aggregation of scar tissue due to constant inflammation and liver cell death. The rate of liver fibrosis, however, varies greatly depending on the patient.[67] It might be limited to portal and periportal areas in a mild case, whereas more advanced cases may present bridging fibrosis. Liver fibrosis advances during many years, and may eventually lead to cirrhosis.

Around 15 % of the chronically infected individuals will develop cirrhosis.[68] Cirrhosis happens when there is a loss in liver function due to too much fibrous tissue. Some of the factors that increase the risk of advanced liver disease are chronic alcohol consumption (>30 g/day), older age at the time of infection, coinfection with HIV or HBV and male gender.[33] The progression of cirrhosis is usually

asymptomatic and patients often do not know they suffer from HCV infection until they present complications related with end-stage liver disease or HepatoCellular Carcinoma (HCC). The main symptoms of cirrhosis are ascites, gastrointestinal bleeding, hepatorenal syndrome and hepatic encephalopathy. Studies have shown that there is 5 % of probability to suffer an episode of hepatic decompensation at one year, whereas for 10 years it increases to 30 %.[69–71] As for liver fibrosis, the rate of development is dependent on the infected individual. It is estimated that it takes around 20 years since infection to the development cirrhosis.

Once cirrhosis has appeared, it may take around 3 years to develop hepatocellular carcinoma (appearing in 1 to 5 % of the patients), which develops from 1 % to 4 % per year.[72] HCC may appear in patients who have not developed cirrhosis, but the incidence is much higher amongst cirrhotic individuals. Chronic hepatitis accounts for 25 % of HCCs worldwide.[73] However, this figure is expected to increase because the majority of infections in Europe and North America occurred during the 1970s and 1980s and the development of the infection is very slow.

HCV infection increases the risk of mortality. Death is caused by either HCC or decompensated cirrhosis. Overall, 2-4 % of the individuals suffering HCV-related liver cirrhosis die annually.

In the future, it will be interesting to discover more accurate indicators to identify patients with a self-limited infection. Also, identifying new markers associated with the development of cirrhosis and HCC, so that patients can be diagnosed at an earlier stage of the infection.[33,44]
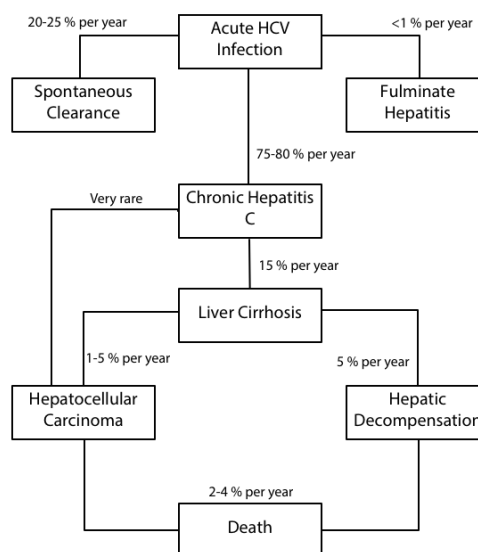

Figure 31. Scheme depicting HCV natural history.

1.2.5. HCV Reservoirs

The main reservoir of hepatitis C virus in the body is hepatocytes. Hepatocytes are the main cell type found in liver tissue. Nonetheless, HCV has been found in other cells such as peripheral blood mononuclear cells (PBMCs),[74,75] dendritic cells,[76] and B-[74] and T-lymphocytes.[77] It is likely that the expression of microRNA-122 facilitates HCV replication in non hepatic cells. HCV is well known for efficient reinfection after liver transplantation and alternative reservoirs to hepatocytes may play an important role in this. Interestingly, the quasispecies distribution is different between plasma and PMBCs, showing that HCV perpetuates in a different manner depending on the cell type.[78] It has also been proven that HCV replication can occur in cell types other than hepatocytes.[79] Indeed, replication was possible in a cell line derived from B-cell lymphoma,[80] that produced viral particles that were able to infect peripheral blood B cells. The role and significance of these reservoirs is yet not completely understood, but it is assumed that HCV induces defects when infecting these extrahepatic cells, causing dysfunctions of the cellular immune response. It is speculated that leukocyte compartments are used by HCV to manipulate the immune system and avoid eradication. Dendritic cells play a key role in the induction of immune responses, both innate and adaptive. HCV-infected dendritic cells may also have functional defects resulting in a poor antiviral response. In addition, it is assumed that infection of non hepatic cells leads to some extrahepatic conditions, which have been discussed in a previous section.

1.2.6. HCV Infection Systems

During the first two decades of the HCV pandemic, one of the major obstacles was the lack of an efficient replication system with which the replication of HCV could be studied. At first, some research efforts were put towards developing systems based on the cultivation of cells isolated from tissues of chronically infected patients, but results were unsatisfactory due to low levels of HCV replication.[81,82] Also, reproducibility was difficult to attain. Furthermore, since the replication levels were low, it was necessary to use highly sensitive methods to detect it. To detect a negative-sense RNA, believed to be indicative of virus replication, *in vitro* studies use strand-specific reverse transcriptase polymerase chain reaction (RT-PCR). This allowed for identification of low levels of HCV RNA, however, the method had several drawbacks such as potential for contamining and priming.[83,84] Overcoming these difficulties, Lanford and Iacovacci were successful in propagating serum-derived HCV in human and chimpanzee hepatocytes.[83,85] Although this first system allowed to gain insight in the basic principles of HCV infection, there were still some problems, especially low viral replication. It was also still difficult to analyze the viral cycle in detail.

Lohmann *et al.* then created a HCV minigenome obtained from liver-derived viral RNA.[86] Since the full-length genome did not replicate well, a shorter version was created. Blight also created HCV replicons from an HCV-H genotype 1a infectious clone.[87] These shorter replicons replicated to a high level, probably due to adaptative mutations of NS3, NS5A and NS5B to cell culture.[87–89] Subsequently, several groups produced full-length replicons with substitutions in the genes encoding the non-structural proteins that had enhanced RNA levels and replication frequency.[90–93] Nonetheless, the number of cells capable of replicating HCV RNA remained low even for adapted replicons, suggesting that acellular background could play a major role in replication efficiency. To overcome these problems, cells that supported viral replication were cured by treatment with IFN-α. Subsequently, the cells were cloned and tested for their ability to support HCV replication while infected with short and full-length replicons. A specific cell line arose as the most permissive towards HCV infection, Huh-7.5, with a 33-fold increase in the frequency of cells supporting HCV replication.[94] Indeed, a mutation present in this cell line inhibits the cellular antiviral response hence enhancing HCV RNA replication.[95]

Even if the replicon system provides great insight on HCV replication, it gives no information whatsoever on virus attachment and entry. There was need for a system providing information on the first steps of viral infection. After some attempts to generate HCV-like particles using *Baculovirus*[96] and Vesicular Stomatitis Virus (VSV)[97] that were mildly successful, several groups finally developed the HCV pseudoparticles (HCVpp) system, that allows the construction of replication-deficient HCV particles.[98–100] The HCVpp system permits to study virus binding, attachment and internalization.

Following this discovery, two different groups were able to produce infectious particles that replicated without adaptative mutations and also secreted viral particles in cell culture.[101–103] This is known as the HCV cell culture (HCVcc) system and allows the study of the HCV life cycle from entry to release. Both the HCVpp and HCVcc systems were great milestones in anti-HCV research, allowing for greater understanding on viral replication and possible therapeutic targets and agents. However an animal model allowing for greater insight was still needed.

For more than ten years, the chimpanzee was the only animal model available, which was used to characterize the agent causing NANBH[104] and to clone the HCV genome for the first time.[25] One of the advantages of the chimpanzee model is that the progression of the disease can be tracked from beginning to end, allowing the study of the acute infection, usually asymptomatic in humans and hence very difficult to study. An ideal animal model to study HCV would need to be affordable, easily available, reproducible and have an accurate representation of human HCV infection and disease.

Transgenic mouse models have been developed during the last decade, although with conflicting results. Recently, several groups reported the production of chimeric mice possessing human hepatocytes.[105,106] These mice have been successfully infected with HCV derived from human serum and supported viral replication, allowing the study of viral replication in a small animal model for the first time.

Nevertheless, there is still room for improvement. Chimpanzees are the closest model to humans but they are not used due to expense, ethical concerns and ban of biomedical research using chimpanzees. Also, mice models are unsuitable for the testing of an HCV vaccine because of their immunodeficiency. There is hence great need for new models that permit to link the *in vitro* models that are available today with the actual situation in an infected patient. Developing a preclinical animal method to test new compounds would possibly speed up the development of new antiviral drugs, avoiding the costly clinical trials for the first tests. Also, new animal models could be useful to analyze toxicities and potential drug-drug interactions. Anti-HCV vaccine research would also greatly benefit of a new animal model.

1.2.7. HCV Life Cycle

In this section the different steps of HCV entry, replication and assembly will be discussed. The HCV life cycle is a complex process involving many different factors (Figure 32).
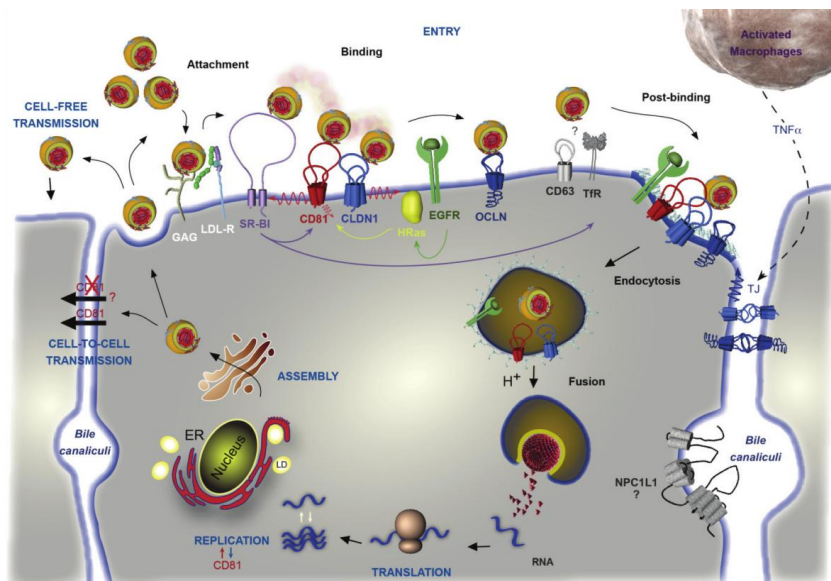
Figure 32. Hepatitis C virus life cycle.[107]

1.2.7a. HCV Entry

The first step in the life cycle of HCV is the attachment of the virus to the host cell. HCV circulates in the blood and may come in contact with hepatocytes. When the virus is close enough, it can bind certain receptors on the surface of the cell and enter the cell.
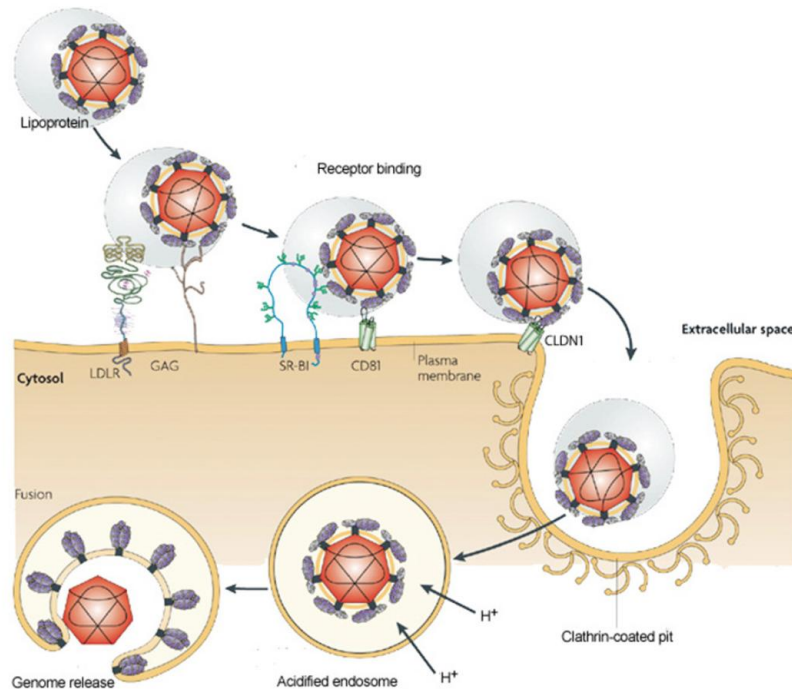
Figure 33. HCV entry in the cell.[108]

Initial attachment occurs through a low-affinity interaction with low-density-lipoprotein receptor (LDLR)[109] and glycosaminoglycans (GAGs).[110] Both are present on heparan sulfate proteoglycans (HSPGs)[111] and can interact with apoliprotein E (apoE),[112] which is present in the viral envelope. Using an apoE specific antibody blocks the attachment of HCV to the cell. Also, when using an HSPG binding molecule (for instance, heparin) attachment is inhibited, which suggests that both HSPGs and apoE are important for HCV virion binding. It is speculated that this is an electrostatic interaction and hence not specific, so that it only initiates the attachment. Since HCV virions are associated with low-density-lipoproteins (LDL) and very-low-density lipoproteins (VLDL),[113] LDLR plays an important role in establishing the first interactions between the virion and the host cell. It is suggested that a fraction of HCV particles are not internalized through the usual pathway but through an LDLR-dependent mechanism. However, the internalized particles are non productive.[114] LDLR may also be important for HCV replication because of its physiological function of contributing the hepatocytes

with cholesterol and other lipids, which are closely linked to RNA replication.[115] However, further studies are necessary to completely understand the role of LDLR in HCV entry.

Following primary attachment, viral envelope glycoprotein E2 binds Scavenger Receptor class B type I (SR-BI or SR-B1, Figure 33). SR-BI is an 82 kDa protein and is highly expressed in hepatocytes. It functions as a lipoprotein receptor mediating intake of high density lipoprotein (HDL), and VLDL among others.[116] It is thought that SR-BI acts concomitantly with another receptor present in the cell surface, CD81 (Cluster of Differentiation 81).[117] However it was shown that HCVcc bind SR-BI expressing cells and not CD81 expressing cells,[118] which may suggest that a first interaction with SR-BI is necessary prior to binding CD81. It is speculated that SR-BI has different roles in HCV entry. First, it may contribute to virus attachment through interaction with lipoproteins associated with the virion.[119] Second, since SR-BI has a physiological lipid transfer activity,[120] it mediates a post-binding event that is important for productive viral entry.[115] Finally, interacting with the hypervariable region 1 (HVR1) of E2[121,122] causes a conformational change in the viral envelope that exposes a key region allowing E2 to bind CD81.[123]

CD81, the first factor for HCV entry to be discovered,[124] is a 26 kDa, 236 amino acid protein[125] that belongs to the broad tetraspanin family and is widely expressed on the cell surface. It directly binds E2 after the conformational change at the large extracellular loop of CD81 with a species-specific interaction.[124] It is suggested that a minimal threshold of CD81 expression is necessary for the cells to be efficiently infected.[126] In addition, it has been shown that treatment of virus particles with soluble CD81 renders them sensitive to acidic pHs, showing that CD81 might help to prime HCV envelope proteins for low-pH activation during virus-entry.[107,127] It is proposed that when CD81 interacts with the viral particles, it triggers signaling responses that relocalize it from the basolateral surface towards tight junctions.[118] Finally, because E1 and E2 form a heterodimer, it has been hypothesized that E1 may play a critical role in the binding of E2 with CD81 and SR-BI by modulating the accessibility of the existing E2 binding domains.[128]

Claudin-1 (CLDN-1) is a 21 kDa plasma membrane expressed in most tissues and present at tight junctions and, at a lower level, the basolateral surface of hepatocytes.[129] CLDN-1 is a crucial HCV entry factor, since cells only expressing CD81 and SR-BI became sensitive to HCV infection only once they expressed CLDN-1.[118] It is speculated that CLDN-1 does not directly interact with the HCV glycoproteins but rather with CD81, allowing for an easier virus internalization.[118,130] However, a recent report suggested that E1 glycoprotein is crucial for the CLDN-1 step and that claudin-1 may actually bind E1 or a conformational domain formed by both glycoproteins. It has been suggested that interactions prior to the role of CLDN-1 may trigger a conformational change in the tight junction

protein required for HCV binding. Signaling pathways (PKA, RHO, EGFR and EPHA2)[122,131–134] between CD81 and CLDN1 are believed to also be necessary for a CD81-bound HCV particle to interact with CLDN-1. Indeed, inhibitors of these pathways block HCV entry. The interaction of the HCV-CD81 complex with CLDN1 induces clathrin-mediated endocytosis of the ternary complex.[135,136]
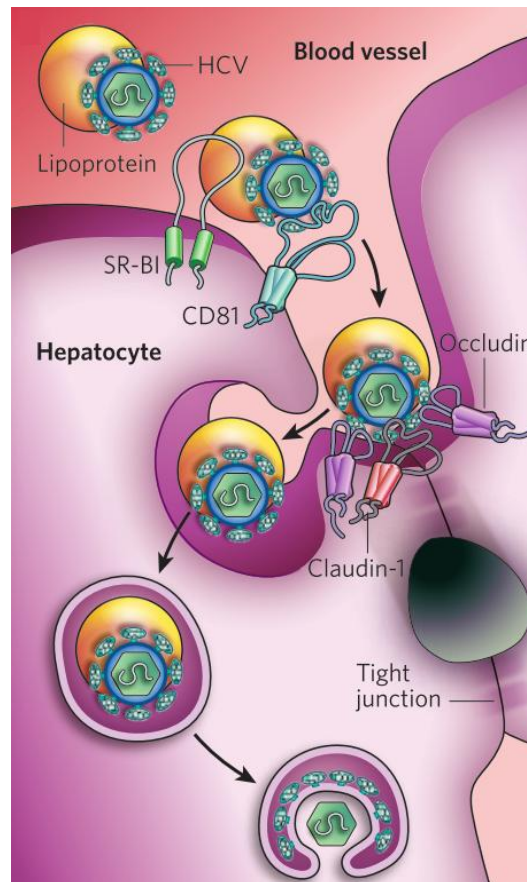
Figure 34. HCV entry through tight junctions.[137]

However, yet another factor is needed to achieve HCV entry in the cell. Occludin[138] (OCLN) is a 60 kDa tight junction protein that plays a role in a post-attachment step in HCV entry. Unlike CLDN-1, OCLN does interact with HCV glycoproteins.[139] It is not yet clear what role OCLN plays in HCV entry, but it has been suggested that it may be implied in the fusion process.[140]

Following the endocytosis, the HCV complex is moved to endosomal compartments, where SR-BI and NPC1L1 (which expression is needed for HCVcc infection to take place)[141] may further modify the virus and its lipoproteins. As explained before, the interaction between E2 and CD81 might prime HCV glycoproteins to respond the low pH in the compartment and induce fusion between the viral envelope and the endosomal membrane.[127] It is thought that low pH may trigger the exposure of the fusion peptide.[142] Also, it is suggested that E1 glycoprotein may play an important role in viral fusion

either by harboring itself a fusion peptide[143] or inducing a conformational change that exposes a hypothetical E2 fusion peptide.[128] Following fusion, the HCV genome is presumably released into the cytosol, where it is translated to initiate viral replication.

Recently, another factor that plays a role in HCV entry was discovered, transferrin receptor 1 (TfR1).[144] TfR1 is the main receptor for cellular iron uptake and is ubiquitously expressed in all tissues. Its specific role in HCV entry is not yet understood, but it probably acts in a post-binding step after CD81 during endocytosis.

Another important factor for HCV entry is the buoyant density of the viral particle. Fractions with the lower density showed the highest infectivity and fusogenicity.[145]

Finally, a crystal structure of the E2 glycoprotein has recently been obtained.[146] This outstanding finding will help gain insight into the specific interactions and conformational changes that happen throughout the HCV entry process.

1.2.7b. HCV Replication

Once the viral genome has been released into the cytoplasm after fusion, it is readily translated. It is suggested that HCV replication is mediated by an Internal Ribosome Entry Site (IRES)[147,148] rather than a cap-dependent mechanism, due to the fact that the HCV genome is not capped. The IRES binds 40S ribosomal subunits[149] and then, by recruiting other factors, induces a slow transition to the active 80S complex.[150]

The polyprotein is translated into three structural proteins (C, E1 and E2), one ion channel protein (p7) and six nonstructural proteins (NS2, NS3A, NS4A, NS4B, NS5A and NS5B) at the endoplasmic reticulum directed by the IRES (Figure 28). Then, host cell enzymes cleave the polyprotein co- and post-translationally. The C-NS2 region is processed by peptidases cleaving at the C/E1, E1/E2, E2/p7 and p7/NS2 regions.[151,152] However, not all cleavages are co-translational, since the formation of processing intermediates has been shown. The core protein (C) is further processed and transported from the endoplasmic reticulum to the surface of lipid droplets,[153] where HCV virion assembly happens. Following these cleavages, the polyprotein is further processed by the NS2/3 protease which cleaves the NS2/NS3 junction *via* a rapid intramolecular reaction.[154] Next, the final NS3-NS5B region is processed by the NS3 protease cleaving the polyprotein in the following order: NS3/4A, NS5A/B, NS4A/B and NS4A/5B.[155–158] Even after the cleavage of NS3, the substrate and the NS3 enzyme remain at close proximity, probably due to the formation of a high-order complex. NS3 also

plays an important role as a helicase. NS4A is thought to have an important role by catalyzing the enzymatic activity of NS3 *via* conformational changes in the NS3 proteinase.[159] The NS3-4A protease also diminishes the antiviral response of the host cell by impairing the immune response because it can cleave the Toll-like receptor 3 TRIF responsible of inducing IFN-β.[160]

NS4B is an integral membrane protein[161] that is thought to induce the formation of a membrane compartment ("membranous web"), which is presumed to be the site of viral replication.[162] NS5A is present in a basally phosphorylated form and a hyperphosphorylated form.[163] The state of phosphorylation is thought to be very important for viral replication, as it is present in other *Flaviviridae*.[164]

Finally NS5B is the RNA dependent RNA polymerase (NS5B RdRp).[165] It is responsible for synthesizing the complementary negative strand of the genome as a replication intermediate and then genomic RNA using the negative strand as template. NS5B is thought to act in conjunction with NS5A, using the latter as a cofactor.

Like all positive strand RNA viruses, HCV replication occurs on intracellular membranes. HCV forms a replication complex with all nonstructural proteins anchored to vesicular membranes formed by the endoplasmic reticulum. It is thought that cellular cofactors are also included in the replication complex. Although not yet completely understood, it is speculated that cellular cofactors PTB,[166] glyceraldehyde-3-phosphate dehydrogenase,[167] miRNAs,[168] p87[169] and p130[169] may be concerned in RNA replication.

1.2.7c. HCV Assembly

Before the viral particle is mature and ready to abandon the host cell, the nucleocapsid, genome and lipid bilayer must be assembled. However, a lot is still unknown about HCV assembly and egress.

The first step is to put together the three structural proteins E1, E2 and C and the viral RNA. The assembly of the HCV viral particle occurs by budding into the endoplasmic reticulum. The interaction between the matured core protein, which is relocated to lipid droplets[170] (consisting of a phospholipid monolayer surrounding a core formed by cholesterol and other lipids), and NS5A probably shifts RNA from translation or replication into virus packaging.[171] The relocation of C, controlled by DiacylGlycerolAcylTransferase-1 (DGAT1) probably drags the capsid proteins along the surface of the endoplasmic reticulum onto nascent lipid droplets.[172] An interaction of the core protein with specific regions of the 3' and 5' NTR of HCV RNA causes the core protein to oligomerize

and initiates the virus assembly reaction.[173] It is also speculated that the p7-NS2 complex brings together the E1-E2 and NS3-4A complexes,[174,175] whose interaction will then recruit the core protein from lipid droplets into sites of virus assembly.[176] Indeed, as happens for other flaviviruses, non-structural proteins are involved in a concerted process involving RNA encapsidation, capsid envelopment, budding and association with lipoproteins. Once all components are in close vicinity at the assembly site, genome encapsidation followed by capsid envelopment occur at the endoplasmic reticulum membrane. The specificity of the encapsidation is very likely due to the spatial proximity between the capsid and the newly replicated genome.

Virus particles are released from the cell through the secretory pathway, during which the virions acquire their low density when interacting with the VLDL machinery of the host cell, where apoliproteinE (apoE) is also present.[177] Interestingly, secreted particles have a lower density than those found within the cell, which suggests a lipoprotein-related maturation during release. In addition, during their course through the secretory pathway, and probably through the Golgi apparatus,[178] E1 and E2 are post-translationally modified. Finally, p7 protects the virus particles from exposure to low pH (pH < 5) when exiting the cell.[179] p7 increases proton conductance in vesicles and is able to rapidly equilibrate H$^+$ gradients. It is suggested that the viral particles induce the membrane curvature needed for release *via* a "pull" model in which the glycoproteins pull the membrane.[180]

Once the viral particles are ready, they are either secreted in the extracellular environment to infect other cells or do it directly *via* cell-to-cell transmission. Cell-to-cell transmission is widely used by viruses[181] and allows them to bypass the host cell immune system during chronic infection and spread faster.[182] Several entry factors are necessary for an effective HCV cell-to-cell transmission, SR-BI, CLDN, OCLN and the recently discovered NPC1L1.[183] There is controversy on whether or not CD81 is necessary for cell-to-cell transmission.

1.2.8. Anti-HCV Therapies

During the first decades of the HCV pandemic, therapies were neither very effective nor did they evolve rapidly, not adapted to unmet medical needs. The development of the HCV replicon system allowed for much greater insight into the viral life cycle, and the last ten years have been extremely successful for anti-HCV drug research. Many companies and groups have studied HCV and have found many therapeutic targets throughout the viral life cycle. New Directly Acting Antivirals (DAAs), which may probably set a new standard for anti-HCV therapy, have been approved for treatment in the last years or are still under development.

1.2.8a. IFN-Based Therapy

During the beginning of the discovery of NANBH, no specific treatment existed. Instead, it was recommended to have rest, a good diet and some medication, not specifically anti-HCV drugs.[184] The discovery of Hepatitis B Virus (HBV) spurred the interest in antihepatitis drugs. Many different compounds were tested and amongst them, interferon was the most effective one.[185]

Even before the pathogen causing Hepatitis C was discovered, IFN-α was tested in patients suffering from NANBH.[186,187] Treatment lasted for 24 weeks and the results obtained were quite low, yet encouraging. Sustained Virologic Response (SVR) was achieved in 6 % of the patients.[186,187] A sustained virologic response is defined as the absence of viremia 6 months after stopping antiviral treatment. During the 1990s the research with IFN continued and it was proven that longer treatment (48 weeks) afforded higher SVR (up to 16 %).

In parallel, another drug was under investigation, ribavirin (RBV). By itself, it did not lower HCV RNA levels.[188] Nonetheless, when used in double therapy with IFN-α, the SVR rates improved greatly, increasing to 34 % after 24 weeks and 42 % after 48 weeks.[189,190] In 2001, the standard treatment consisted in IFN-α injections three times per week and oral administration of ribavirin twice a day. In addition, it was found that patients infected with genotype 1 needed longer treatment and had a lower SVR than those infected with genotypes 2 or 3.

One of the main drawbacks of using IFN-α was that its half-life in the body is extremely short (4-5 hours). Hence, it was found that using a pegylated interferon (PEG-IFN), with improved half-life (40-80 hours), increased the SVR up to 55 % when used in conjunction with RBV for 48 weeks.[191,192] It also improved the treatment of patients infected with genotype 1, with cirrhosis or with high baseline levels of HCV RNA, which reacted poorly to treatment.[193] It is assumed that the use of PEG-IFN allows for constant high serum levels, which cause the uninterrupted antiviral response in the cell.

Another important drawback is the various side effects that interferon-based therapy causes.[194] Most common side effects include influenza-like symptoms, digestive dysfunction, depression[195] or thyroid disfunction.[196]

Mechanistically, interferons do not target a specific step in the viral life cycle but create a state of immune response within the cell.[197] Interferons are host proteins produces in response to an infection and have broad actions. There exist three types of interferons. Type I interferons (-α, -β, -ω) are produced by many cells as a response for viral infection.[198] They bind the IFN-α receptor, present

on every cell in the body, which in turn leads to a signaling cascade using the JAK-STAT pathway,[199] expressing interferon-stimulated genes (ISGs). This leads to a combined attack on the virus, so that resistant variants are extremely rare.[200] Indeed, when a patient is not responding to interferon is mainly because the cells are not responding rather than the virus being resistant to IFN.[201] IFN-α therapy is also meant to substitute the disrupted production of IFN in the cells by some of the HCV proteins, which deactivate signaling pathways and IFN production. Nevertheless, some of the expressed ISGs are very likely to cause some of the side effects seen with IFN-based therapies. Type II interferon (-γ) is produced by T cells but no effect against HCV has been observed.[202] Finally, type III interferons (-λ) have a similar antiviral effect to Type I IFNs, but achieve it by binding to a different receptor. In contrast to Type I IFNs, the receptor for Type III IFNs is only present in epithelial cells such as hepatocytes, not as widely distributed as the IFN-α receptor. This may be able to reduce IFN I associated side effects. Studies have been performed, but it remains to be seen if they are better than standard interferon.[203]

1.2.8b. Ribavirin

Ribavirin (RBV, Figure 35) is a guanosine nucleoside analogue. It was first approved for the therapy of Respiratory Syncytial Virus (RSV),[204] but it is active against many other viruses.[205] Among the viruses affected by RBV are some that resemble HCV, so in the 1990s a Ribavirin monotherapy study was performed. However, RBV showed very little antiviral effect.[206] Subsequently, a bitherapy of IFN with Ribavirin was evaluated, showing that the addition of RBV resulted in great improvement of SVR rates.[207] It became the standard of care of chronic HCV infection for a decade.
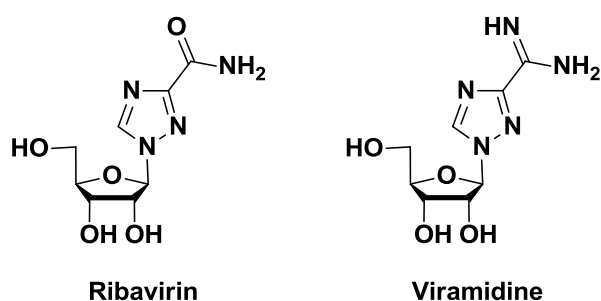
Figure 35. Chemical structure of Ribavirin and Viramidine.

Although RBV has been extensively used in anti-HCV therapy, the mechanism by which it exerts its antiviral activity has not yet been elucidated. Various mechanisms have been proposed.[208] The first proposed mechanism is that RBV causes viral mutagenesis causing nucleotide transitions.[209] Second, it is speculated that it may directly inhibit HCV RdRp hence inhibiting RNA replication. Third, it is

proposed that it might decrease the synthesis of GTP resulting in a lower viral replication. Fourth, it is suggested that it may increase the host cell immune response by Th2 response suppression and Th1 response induction. Finally, the fifth mechanism suggests that it modulates genes involved in interferon signaling, hence increasing the immune response of the cell. The fact that the mechanism of action has not yet been solved makes it difficult to further improve the antiviral effects of RBV.

A major drawback of using RBV that has caused many patients to abandon the therapy is its side effects. Side effects include anemia, fatigue, itch, sinusitis or abdominal pain.[210] In addition, increasing the RBV dose in order to improve SVR was associated with an increase of side effects.[211] A prodrug of RBV, Viramidine (Figure 35),[212] was developed. It causes less side effects but also displays a reduced antiviral action.[213]

It seems difficult to further improve the IFN-RBV dual therapy without more insight into the mode of action of RBV. Furthermore, many patients are either not eligible, have poor response to bitherapy or chose not to undergo dual therapy due to the many side effects. Anti-HCV drug research has dramatically increased in the last decade and new drugs are being released, but RBV will probably still continue to be used in conjunction with newly developed drugs.
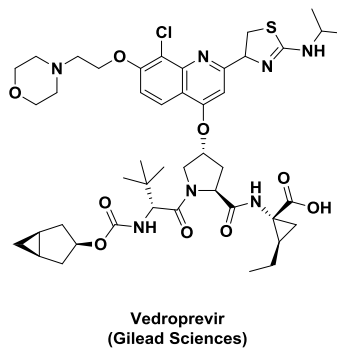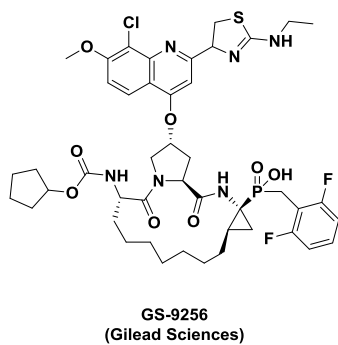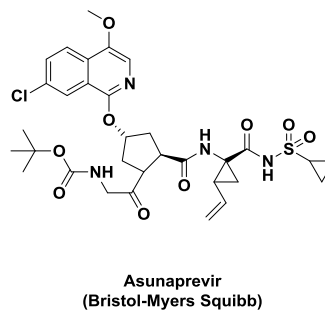
1.2.8c. Directly Acting Antivirals (DAAs)

In the recent years, several new drugs for the treatment of hepatitis C have been approved, starting a new era in anti-HCV therapy. By 2011, more than 50 companies were working on HCV and in 2013 clinical trials for more than 12 compounds were being conducted. These new compounds directly inhibit one or several steps in the viral life cycle. SVR rates have been improved for all genotypes and some studies show that interferon-based therapies may very soon be displaced by new therapies using DAAs as the major component. Indeed, soon there may exist an all-oral highly tolerable therapy to treat chronic HCV infections. It is interesting to highlight that, opposed to anti-HIV therapy, it has taken 22 years since the discovery of HCV to the arrival on the market of the first directly acting antiviral molecules. It is likely that it took so long because of the lack of effective ways to test the compounds *in vitro* and because the perceived market value was quite low.[214]

NS3/4A Protease Inhibitors

Three of the compounds that are going to be presented in this section (Telaprevir, Boceprevir and Simeprevir) are already on the market. Both Telaprevir and Boceprevir were approved in 2011 and were the first DAAs approved by the FDA. Simeprevir was approved in 2013 and is a second

generation NS3/4A inhibitor. Another eleven are still in clinical development. The structures of thirteen of the molecules are depicted in Figure 36.

Telaprevir
(Vertex)

Boceprevir
(Merck)

Faldaprevir
(Boehringer Ingelheim)

Asunaprevir
(Bristol-Myers Squibb)

GS-9256
(Gilead Sciences)

Vedroprevir
(Gilead Sciences)
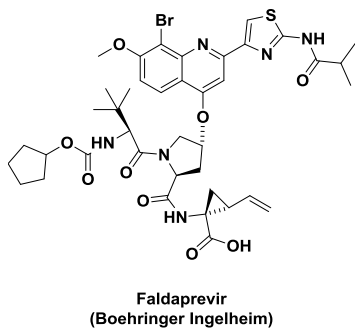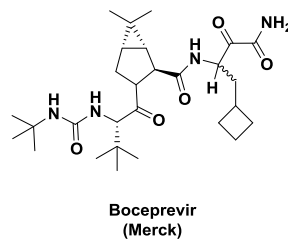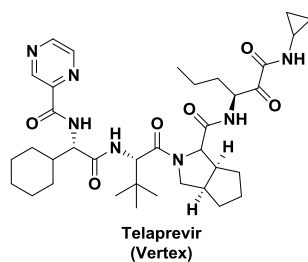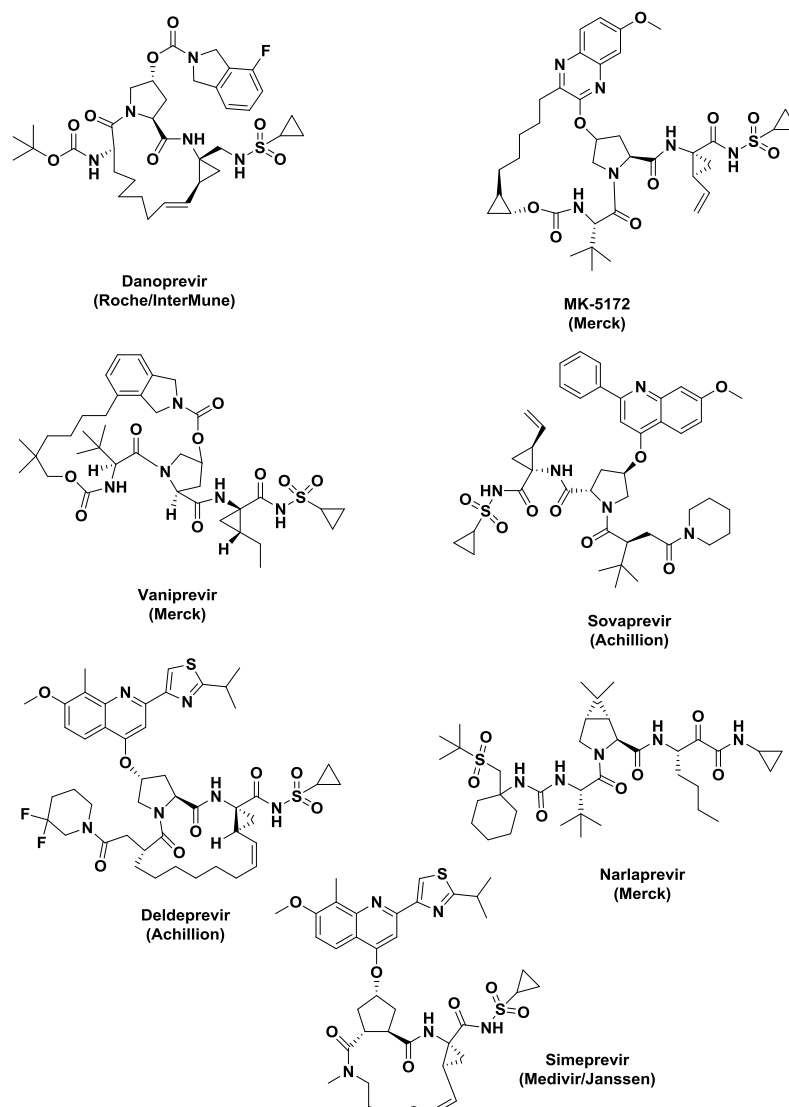
Figure 36. NS3/4A protein inhibitors approved or under development.

Telaprevir was developed by Vertex and was accepted by the FDA in 2011. It binds to the NS3/4A protease in a two step manner and dissociates the NS3/4A complex, effectively inhibiting the synthesis of proteins necessary for HCV replication.[215] Indeed, it prevents the cleavage of the polyprotein into its active forms (NS4A, NS4B, NS5A and NS5B). Telaprevir is specific and does not inhibit the activity of other proteases.[216] Triple therapy with IFN and RBV improves the SVR rates up to 75 % in genotype 1 patients with a shortening of the treatment time.[217] Telaprevir causes side effects such as rash, anemia or gastrointestinal effects.[217] Boceprevir was also approved in 2011 for triple therapy and its mechanism of action is probably the same as Telaprevir. SVR rates are also improved up to 75 % in genotype 1 patients.[218,219]

The major drawback of these first generation NS3/4A inhibitors is that they have a low genetic barrier to resistance and resistant mutations are already starting to appear.[220] That is why both Teleprevir and Boceprevir are approved in a triple therapy with IFN and RBV. Drug-drug interactions are also an important disadvantage of these first-wave inhibitors.

Simeprevir is a second generation NS3/4A inhibitor and has been approved by the FDA for triple therapy with IFN and RBV during 12 weeks. The main advantages of using this compound is that it is dosed once per day[221] and that additional anemia does not appear. SVR rates are increased up to 85 %.[222] Unfortunately, as for first-generation inhibitors, in patients with poor response the SVR diminishes due to the selection of Simeprevir-resistant variants.

A recent article by De Clercq[220] describes the main characteristics of the rest of NS3/4A inhibitors as well as other HCV inhibitors.

Although the SVR rates have been highly improved with the use NS3/4A inhibitors, response rates remain suboptimal. Furthermore, many patients do not tolerate the therapy and among those who can, side effects can be a big burden and lead to premature treatment discontinuation.

NS5A Protein Inhibitors

Because of its key role in viral replication and assembly, NS5A is a suitable target for antiviral therapy. Although their mode of action is yet unknown, it is suggested that NS5A inhibitors may act at the N-terminus of NS5A, maybe inhibiting hyperphosphorylation, which is key for the activity of the protein.[223] They have very low values of EC_{50} in the low nM and even pM range. However, they also show a very low barrier to resistance.[224] Even when the drug has not yet been administered, NS5A resistant variants are already present in the quasispecies pool. Once the DAA is administered, they may grow to high levels. So far, no NS5A inhibitor has been approved for therapeutic use.

Among the compounds that inhibit the NS5A protein, we can highlight Daclatasvir, with an EC_{50} of 50 pM against genotype 1a[225] or Ledispavir with SVR rates in conjunction with Sofosbuvir of 100%.[226] Structures of the molecules are depicted in Figure 37. It is speculated that the NS5A protein forms a dimer,[227] and that may be the reason why some of these symmetric compounds have such high potencies.

It is likely that NS5A will be approved for future anti-HCV therapies either in combination with IFN and RBV or in an all-oral therapy, mainly due to their specificity, potency and low EC_{50}. Furthermore,

second-wave inhibitors are already being developed, showing very similar efficacy and better resistance barrier.
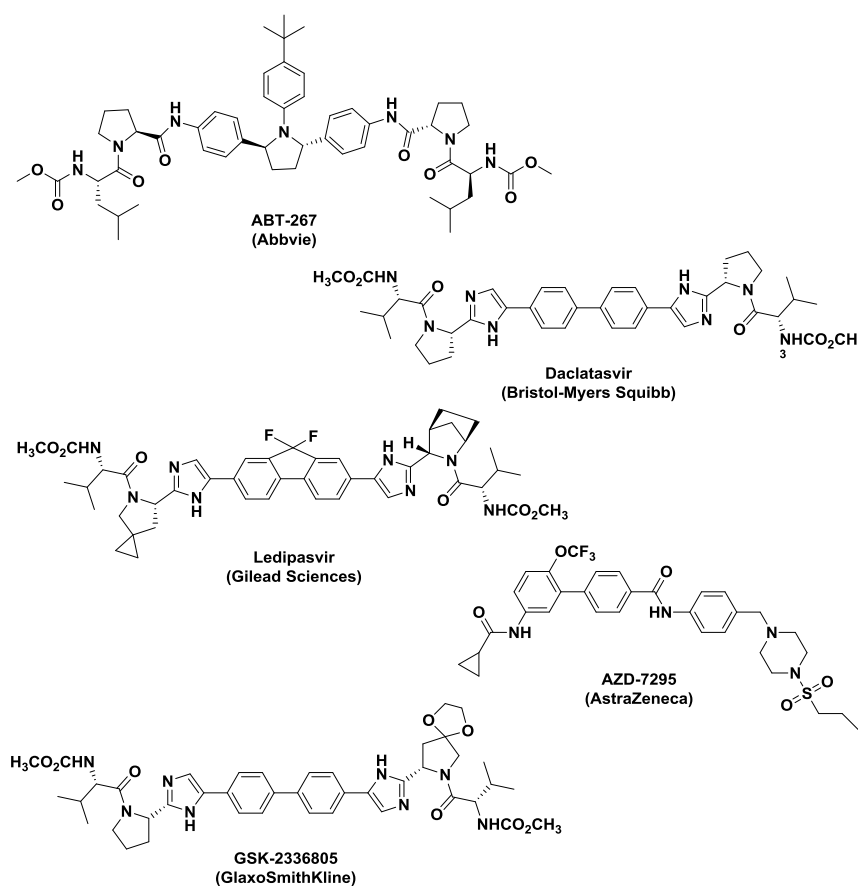
Figure 37. NS5A inhibitors under development.

NS5B Polymerase Inhibitors

NS5B polymerase inhibitors can be divided into two different classes of compounds, the nucleosidic type and the non-nucleosidic type. Nucleoside inhibitors are analogues of natural substrates of the NS5B RdRp that are incorporated into the synthesized RNA, promoting a chain termination reaction by binding the active site of NS5B.[228] They need to be phosphorylated to their triphosphate form in order to become active. NS5B is highly conserved across all different genomes and subtypes, so NS5B inhibitors are usually active against all genotypes and have high genetic resistance barriers.[229] Figure 38 depicts various nucleoside inhibitors.

Sofosbuvir
(Gilead Sciences)

GS-0938
(Gilead Sciences)

Mericitabine
(Roche)
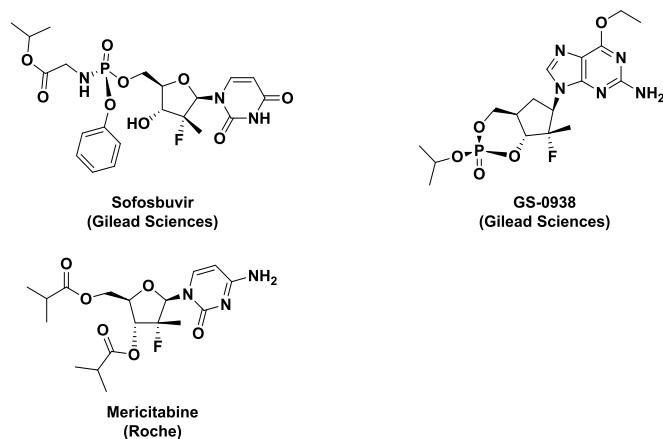
Figure 38. NS5B nucleosidic inhibitors approved or under development.

Non-nucleosidic inhibitors bind to one of the allosteric sites of the enzyme, inducing conformational changes in the protein that inhibit its polymerase activity.[230] In contrast to nucleosidic inhibitors, their activities are dependent on the genotype and have a much lower barrier to resistance. Nevertheless, since they bind to different allosteric sites, a therapy including several non-nucleoside inhibitors could be possible. Figure 39 depicts various non-nucleosidic inhibitors.

VX-222
(Vertex)

ABT-072
(AbbVie)

ABT-333
(AbbVie)

Deleobuvir
(Boehringer Ingelheim)

Tegobuvir
(Gilead Sciences)

Setrobuvir
(Anadys)

Filibuvir
(Pfizer)
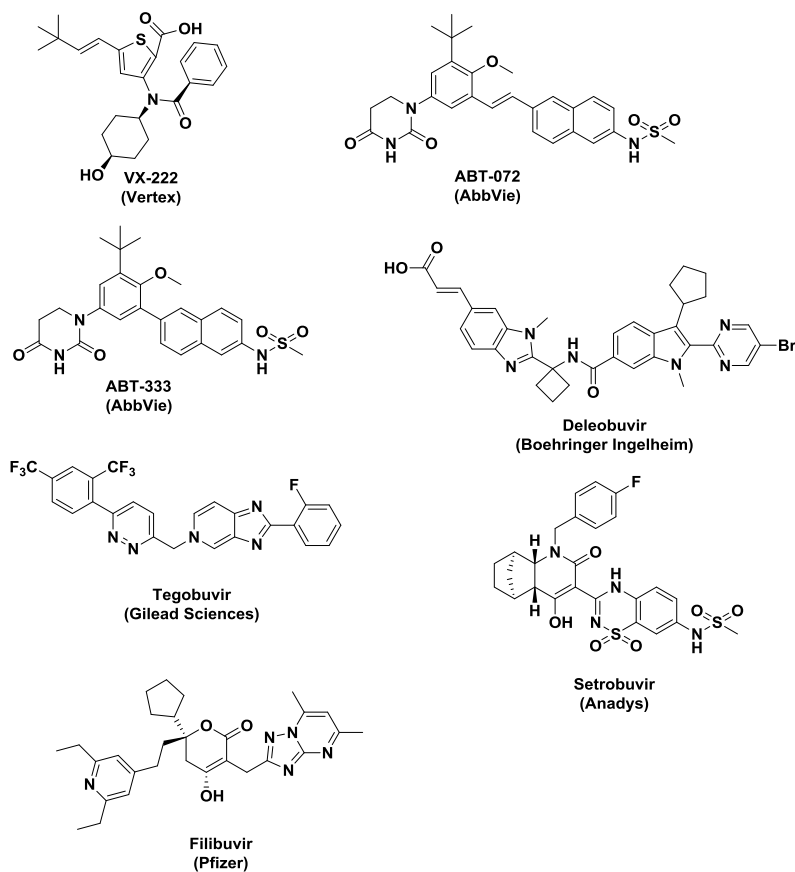
Figure 39. Non-nucleosidic NS5B inhibitors approved or under development.

Among all the NS5B nucleoside polymerase inhibitors, Sofosbuvir is probably the best known. It was approved by the FDA in 2013 for the treatment of chronic hepatitis C in combination with PEG-IFN and RBV for genotypes 1 and 4 and without IFN but in combination with RBV for the treatment of patients infected with genotypes 2 and 3. Furthermore, the discontinuation rate of the non-containing IFN therapy is very low and the side effects are less important than when using PEG-IFN.[231] The SVR rates obtained are excellent for most genotypes with the exception of genotype 3, for which a longer treatment is recommended. New combinations are being studied. For instance, patients chronically infected with HCV genotype 1 treated with a combination of Sofosbuvir and Ledipasvir (an NS5A inhibitor) showed SVR rates of up to 100 % after a 12 week treatment.
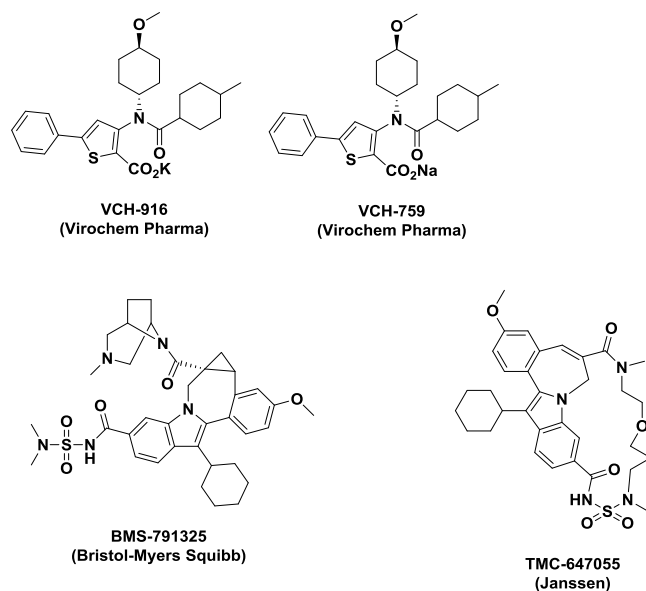
NS5B inhibitors are a promising new class of drugs showing great potency and SVR rates that could be very important in a future all-oral IFN-free therapy.

1.2.8d. Other Antiviral Agents

Many other drugs not targeting NS3/4A, NS5A or NS5B are also being developed. Some of these drugs are targeting host-cell proteins. For example, inhibitors of Cyclophilin A such as Alisporivir,[232] or inhibitors of miRNA 122 like Miravirsen.[233,234]

A new class of drugs under development is entry inhibitors, which attack the virus during the first steps of its life cycle. During viral entry, there are many different host-cell factors that can be therapeutic targets. Targeting the entry step is a promising approach because the infection may be

stopped before the genetic material enters inside the cell. Furthermore, entry inhibitors could be very useful for patients receiving liver grafts, since for now the therapies available have limited efficacy.[235] In addition, it is suggested that mutations in the elements needed for viral entry occur with a much lower frequency than for other viral proteins.[236,237] Furthermore, it is likely that entry inhibitors may be pangenotypic, because different genotypes have been shown to enter the cell through similar mechanisms.[238]

The development of entry inhibitors has been slow due to the lack of efficient small animal models and cell culture systems focusing on viral entry. It was in 2003 and 2005 that the HCVpp and the HCVcc models enabled the screening for entry inhibitors. Transgenic mouse models provide further insight for the study of entry inhibitors.

As of today, there are many different entry inhibitors being studied, ranging from antibodies targeting CD81 to small molecules such as Ezetimibe.[239] ITX5061 is a small molecule targeting SR-BI that is already being tested in phase 1b trials.[240] In the future, it is possible that entry inhibitors will be given in combination with DAAs, especially to avoid liver graft reinfection or in patients that have relapsed from previous therapies.
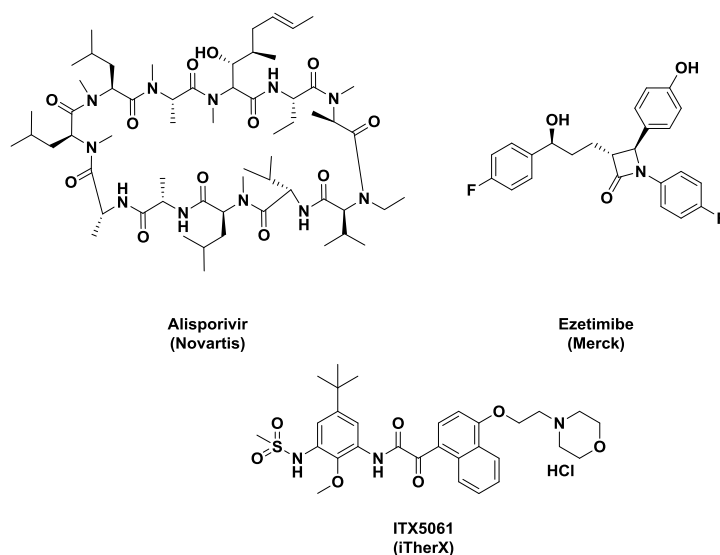

Figure 40. Other antiviral agents under study.

1.2.8.e. Future Therapies

It is very likely that anti-HCV research will continue to develop and evolve very rapidly. New anti-HCV treatments should further improve the problems observed with DAAs already on the market, namely better genetic barrier to resistance and less important side effects, while maintaining or improving

the potency and efficacy. The main goal for new therapies should be to provide a once-daily all-oral IFN-free therapy with great antiviral effects across all genotypes and genetic variants, which may be achieved by combining various drugs targeting different steps of the viral cycle. In addition, RBV should become less and less important in the years to come, eliminating the important side effects linked to it. The therapies could be composed of two DAAs combined with an agent targeting the host-cell such as an entry inhibitor.

As of today, a vaccine for HCV does not exist. The fact that no convenient small animal model was available for many years and that no crystal structure had been determined greatly hampered the research to find a vaccine. In addition, the great variability of HCV between different genotypes and subtypes makes developing an efficient vaccine a very difficult task. Neutralizing antibodies (nAbs) supposedly target the viral glycoprotein E2 and some of them have been shown to prevent HCV infection,[241,242] nevertheless, the virus escapes nAbs because of the high variability of its E2. Another approach is to target a conserved nonstructural protein and induce a broad T-cell response.[243] This discovery combined with the new animal methods and cell culture systems available are probably going to accelerate the development of an anti-HCV vaccine.

Even if DAAs have revolutionized anti-HCV treatment, most of the individuals chronically infected by HCV will not have access to the new drugs. Indeed, low-income countries are those with a higher hepatitis C burden and account for 80 % of the people infected with HCV worldwide. New treatments being developed are extremely costly. For instance, Sofosbuvir has a price of $1,000 per pill ($84,000 for the whole treatment, not counting the price of IFN and RBV). Interestingly, it is expected to be the best-selling drug of all time. In addition, the price of second generation NS3/4A inhibitor Simeprevir is also extraordinarily high at $66,000 for a 12-week treatment. The need for cheap drugs targeting different steps of the HCV life cycle is still very high.

1.3. Flavonoids

Flavonoids are naturally occurring polyphenolic compounds that are ubiquitously found throughout the plant kingdom. They occur in fruits, seeds, flowers and vegetables among others and are an important part of human diet. They have been widely studied and been reported to have a wide range of biological effects such as antiviral, anti-bacterial or antioxidant activities.

One of the first studies in flavonoids was made by Boyle in 1664, describing the effect of acids and bases on flavonoid pigments. The chemical composition of flavonoids was first reported in the 19th century. Since then, flavonoids have been extensively studied. Great progress has been made during

the last decades, especially because many biological activities of flavonoids have been reported, which has spurred the interest in this field.

1.3.1. Structure of Flavonoids

Flavonoids basic structure is characterized by the presence of a benzo-γ-pyrone motif, a C_6-C_3-C_6 carbon skeleton. The three different rings are referred to as A, B and C respectively and atom are numbered as depicted in Figure 41.
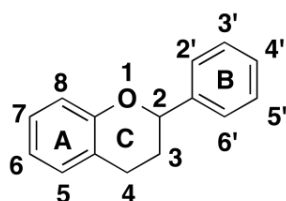
Figure 41. Basic structure of flavonoids.

Even though all flavonoids share a common structure, there exist a very wide range of different flavonoid structures. In fact, they form the largest group in the polyphenol family with over 6,000 compounds identified so far.[244] Flavans, flavanols (also called catechins), flavanones, flavanonols, flavones, flavonols, anthocyanidins and chalcones all belong to the flavonoid compound family (Figure 42). *Neo*flavonoids and *iso*flavonoids are also considered as flavonoids. Compared to flavonoids, the phenyl moiety is shifted to the 4 and 3 position respectively. Differently hydroxylated and saturated *neo*flavonoids and *iso*flavonoids exist as well. Finally, another type of flavonoid with a different structure when compared to the rest is aurones, whose C ring is a five-membered ring instead of a six-membered ring as for the rest of flavonoids. Flavonoids are usually found with various levels of hydroxylation, methoxylation, glycosylation or glucuronidation, which contributes to the great variety in structures and, therefore, to the great variety in biological properties.
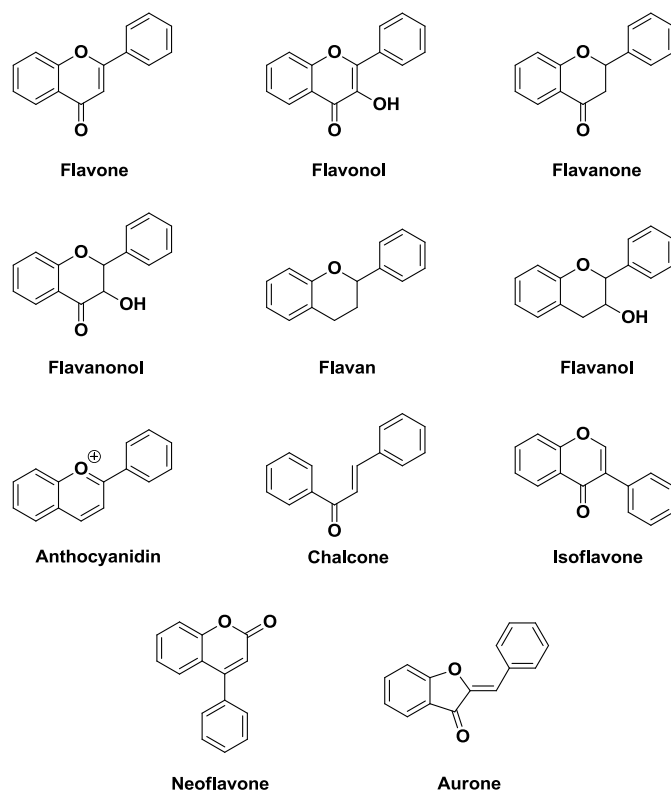
Figure 42. Structure of different flavonoids.

1.3.2. Occurrence and Role of Flavonoids

Flavonoids are present in most plants except *algae*,[245] and more particularly in photosynthesizing plants. Plant families have their specific patterns of flavonoids depending on the role the flavonoids accomplish. They are secondary metabolites synthesized through the flavonoid pathway in the cytosol, starting from phenylalanine and malonylCoA.[246] Once synthesized, they are transported to the appropriate compartment in which they will perform their role. They are mainly located in leaves,[247,248] the nucleus of mesophyll cells[244,249] as well as the chloroplast[250] and the vacuole.[244]

It is suggested that during the early days of life on Earth, flavonoids served to protect the plants from UV-B radiation when plants started to move from water to land.[251] UV-B can produce reactive oxygen species (ROS), affecting DNA, proteins and membranes. Mosses were probably the first plants to colonize land, and chalcones, flavonols and flavones can be found within them. Interestingly, no flavonoids are found in *algae*.

Even now, it is believed that one of the main functions of flavonoids is protecting the plant from UV radiation. It has been proposed that the phenolic compounds adjust the antioxidant system and

prevent the plant from mutagenesis. In addition, it has been shown that mutant plants that do not produce flavonoids are UV-hypersensitive.[252]

Another important role of flavonoids is as signaling compounds. Indeed, flavonoid compounds may act as allelochemicals.[253] Allelopathy is a chemical interaction between two plants. For instance, flavonoids may be transferred to the soil and inhibit the growth of another competitor plant. In addition, flavonoids may act as signaling compounds for microbes or bacteria.[254] Quercetin, a widely distributed flavone depicted in Figure 43, induces microbial inhibition.[255]
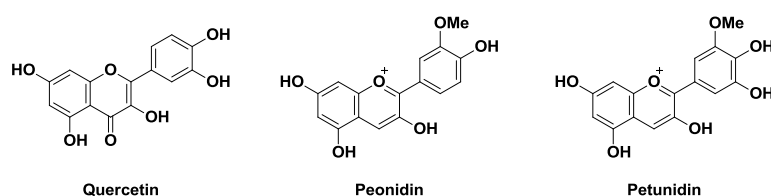

Figure 43. Structures of flavonoids quercetin, peonidin and petunidin.

A third basic function of flavonoids is pigmentation in fruits and flowers. Indeed, their role is to attract animals to flowers, so the pollen can be dispersed to other flowers. They also attract animals to fruits, so that the seed contained within may be scattered. Anthocyanins are the main component of pigments ranging from blue to red. For example, petunidin is present in flowers from *Vicia Villosa*[256] and peonidin is present in grapes.[257] Yellow colored flowers and fruits contain chalcones and aurones. The presence or lack of hydroxyl groups as well as their position play a critical role in the color diversity displayed by these compounds.

Flavonoids are also thought to have a role in plant growth, regulating it.[258] It has been suggested that they may be cofactors in the process of regulating the growth hormone auxin as well as its transport.[259] Furthermore, flavonoids are suggested to play a critical role in pollen fertility.[260,261]

Last but not least, flavonoids have an important function in plant defense. Many compounds have antifungal[262] and insecticide properties.[263] These defensive flavonoids can be induced either by the attack of a pathogen, and hence synthesized at the moment of the attack, or preformed, synthesized during the normal development of the plant.

1.3.3. Flavonoids and Human Diet

Flavonoids are part of the human and animal diet because they are present in most plants. They are present in both food and beverages. Red wine, tea, fruits, cereals, nuts and vegetables all contain

flavonoids. Depending on the food or beverage, levels and type of flavonoids vary. For example, green tea is the only drink containing GalloCatechin (GC), EpiGalloCatechin (EGC) and EpiGalloCatechin Gallate (EGCG).[264] In addition, up to 35 % of the dry matter of the tea is composed of flavonoids and other phenolic compounds.[245] Another flavonoid-containing food is black chocolate, which contains 610 mg/kg of catechins.[265] Flavonoids and polyphenols are also involved in the taste of food and beverages. [266]
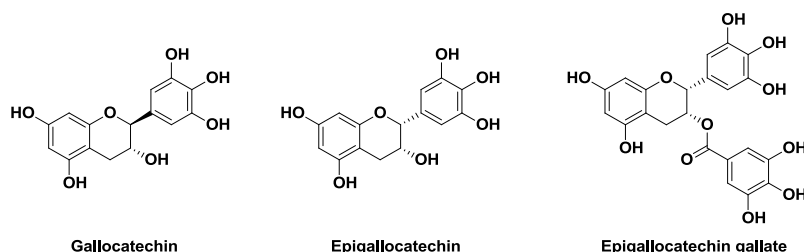
Figure 44. Structures of catechin derivatives present in green tea.

Accurate information on flavonoid dietary intake is not yet available. Several estimations have nonetheless been proposed. Kühnau estimated that about 1 g of flavonoids are ingested in the United States per day.[267–269] However, this is probably overestimated due to inaccuracy in the analytical methods available. Recently, it has been estimated that the intake of flavones, flavanones and flavonols per day is around 25 mg.[270] It is noteworthy that Phenol-Explorer (http://phenol-explorer.eu) constitutes the first comprehensive database on polyphenol content in foods (518 polyphenols are already available). Once ingested, flavonoids are probably digested and absorbed in the gut,[271] and then metabolized in the liver(Figure 45).[245] In turn, glycoside-containing flavonoids may be metabolized after bacterial glycosidases hydrolyze them, in the upper intestine.[272–275]
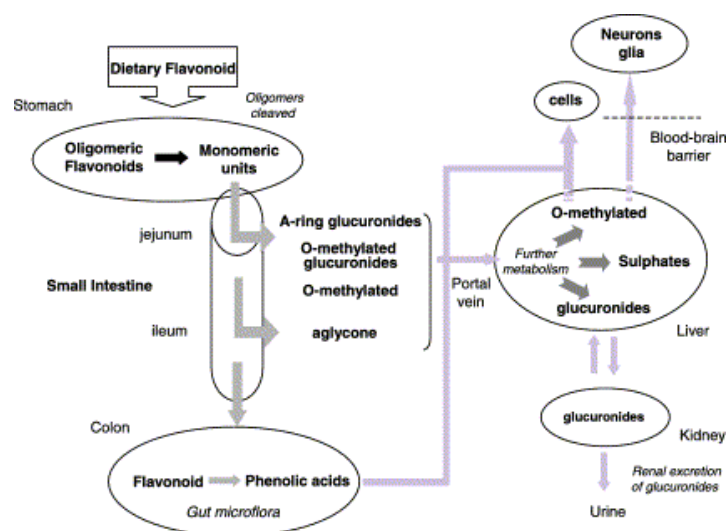
Figure 45. Summary of the formation of gastrointestinal tract and hepatic metabolites and conjugates of flavonoids in humans.[275]

1.3.4. Biological Activities of Flavonoids

Flavonoids have been known to exert numerous benefits (pleiotropic action) on humans. Herbal medicines have been used for centuries and now it is known that flavonoids are present in many of these traditional medicines. For instance, *Radix Scutellariae* is used by Chinese people to treat inflammatory diseases or diarrhea and it contains baicalein, baicalin and wogonin (Figure 46) among other polyphenols and flavonoids.[276] Flavonoids from various plants used in traditional Mexican medicine also show therapeutic effects against diarrhea.[277] Recently, interest in flavonoids has augmented because they have been found to produce diverse therapeutic effects.

Baicalein   **Baicalin**   **Wogonin**
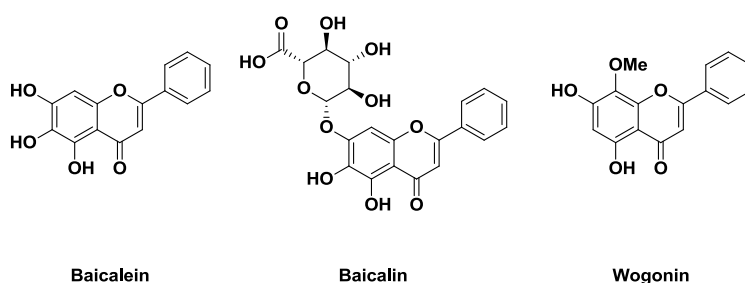
Figure 46. Structures of Baicalein, Baicalin and Wogonin

The main biological activity that has been studied for flavonoids is their antioxidant activity, even though they do not display the best antioxidant activity among polyphenols. During normal metabolism, ROS (Reactive Oxygen Species) are formed. They are believed to cause cellular aging,[278] mutagenesis or carcinogenesis.[279] It is indeed thought that ROS produce these effects by DNA damage or oxidation of LDL.[280] Flavonoids have been shown to be great radical scavengers[278] because

of their ability to react with free radicals and other active species. Indeed, the conjugated rings and hydroxyl groups allow them to act as radical scavengers, reducing the effect of ROS in the body. In addition, their ability to strongly chelate metals (prooxidant metal ions such as Cu(I) or Fe(II)) involved in radical generation may explain as well their global antioxidative effects.[281,282]

Flavonoids have also been shown to have anticarcinogenic activities.[283] Compounds such as quercetin,[284] genistein,[285] daidzein[286] (Figure 47) and EGCG[287] (Figure 44) have been reported to have anticarcinogenic effects. The mechanism of action is not yet clear, but it is suggested that flavonoids may affect tumoral initiation, promotion and progression.[283] It has been shown that citrus flavonoids (naringenin, eriodictyol, hesperetin, Figure 47) exhibit an antiproliferative activity on cancer cells.[288]
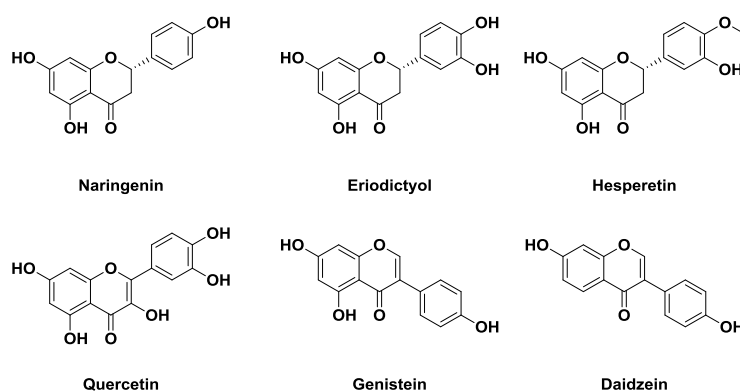
Figure 47. Structures of Naringenin, Eriodictyol, Hesperetin, Quercetin, Genistein and Daidzein.

By preventing the oxidation of LDLs and the aggregation of platelets, flavonoids have protective effects against heart disease. It has been suggested that flavonoid intake may reduce the risk of suffering from heart disease,[289] which is supported by the fact that countries with an elevated consumption of foods and beverages with a high content in flavonoids have lower rates of heart disease.[290,291]

Flavonoids show hepatoprotective activities as well. For example, flavonoids from *Laggera alata* have hepatoprotective activities against carbon tetrachloride (CCl_4) induced injury in hepatocytes.[292]

Furthermore, antibacterial activity has been reported for several flavonoids. Flavonoids such as apigenin or galangin (Figure 48) possess a strong antibacterial activity.[293] It is not surprising that flavonoids show this biological activity because they play an important role in plant defense, including bacterial infection.

Interestingly, flavonoids have also been reported to exert anti-inflammatory activities.[294] It is thought that they may impair the function of enzymes involved in the inflammatory process.

Another important biological effect of flavonoids is their antiviral effect. Indeed, many flavonoids such as baicalin[295,296] or robinetin[297] (Figure 48) inhibit HIV and Dengue Virus (DENV) infections. Luteolin has a synergistic effect in conjunction with kaempferol against Herpes Simplex Virus.[298]

Figure 48. Structures of Apigenin, Galangin and Robinetin.

Finally, flavonoids have also been reported to have antidiabetic,[299] antitrypanosomal,[300] antipsoriasis[301] and antineurodegenerative[302] activities.
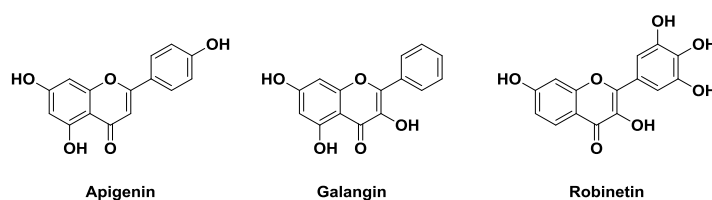
1.4. Background of the Project

Historically, the research project started when Prof. Dr. Oliver Keppler (HIV virologist) at the University of Heidelberg discovered that aqueous extracts from dried leaves from plants of the *Lamiaceae* family (lemon balm, peppermint and sage) displayed a potent anti-HIV activity in the low micromolar range,[303] both *in vitro* and *ex vivo*, with a novel mode of action. It was shown that the *Lamiaceae* extracts had an impact on the early steps of the viral life cycle, targeting the entry step of the virion. Interestingly, antiviral activity against surface-bound virions was greatly diminished, suggesting that the plant extracts exert their activity in a step prior to virion attachment. No cytotoxicity at antiviral concentrations was observed. In addition, the density of the virions was increased when exposed to *Lamiaceae* extracts, effectively decreasing their infectivity. This change in density is thought to be determinant for the antiviral activity displayed by the *Lamiaceae* extracts. It is noteworthy that the viral particles with the lower density showed the highest infectivity and fusogenicity.[145] For instance, the density of HCV circulating in blood is very heterogeneous, from very low to low (sharing common properties with LDL and VLDL), intermediate and high density fractions. The corresponding lipid-rich pattern of the low to very low density fractions affords appropriate infectivity to these virions. Last but not least, the extracts showed antiviral effects on other enveloped viruses but were not active against non-enveloped viruses, clearly suggesting that the viral lipidic envelope was upset on the presence of the active compound.
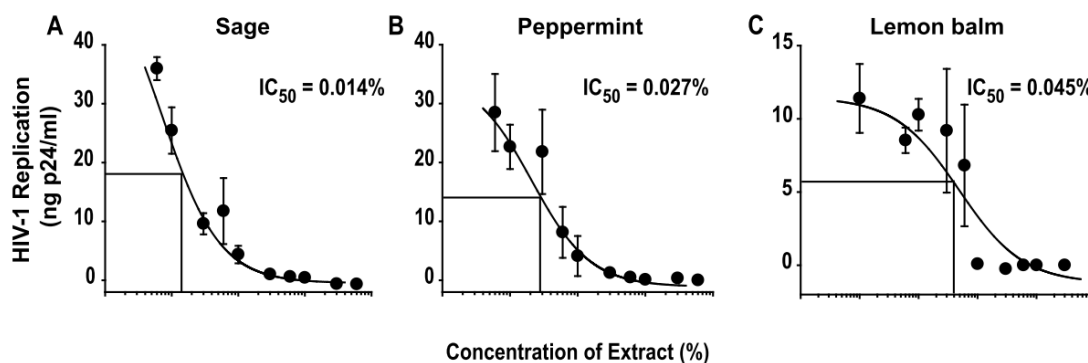
Figure 49. Anti-HIV activity displayed by the aqueous extracts of sage, peppermint and lemon balm.[303]

Following this discovery, a preparative bio-guided fractionation approach of *Marrubium peregrinum L* in close collaboration with the laboratory of Dr. Elisabeth Davioud-Charvet at the University of Heidelberg and the laboratory of Prof. François Bailleul at the University of Lille allowed the discovery of a novel antiviral lead structure, ladanein (designated as MP03, depicted in Figure 50).
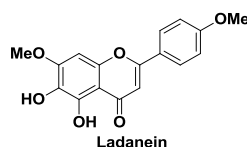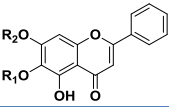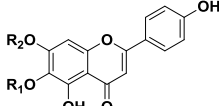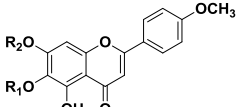
Figure 50. Structure of the antiviral flavone ladanein.

Ladanein shares an uncommon polysubstitution patterns on cycle A (5,6-dihydroxy-7-methoxy) with other flavonoids such as baicalein, for which numerous antiviral properties have been demonstrated (Table 1). Retaining a 5-OH substitution and an 8-free position, a survey of the literature shows that more than 160 flavones with H, OH, OMe, O-glucoside or O-glucuronide substitutions have been characterized until now. Table 1 gathers an exhaustive list of the flavones (26 compounds) with such an A-ring pattern for which antiviral activities have been reported in the literature. Among them, baicalein and baicalin have been undoubtedly the most studied flavones in regard of their antiviral activities. Other interesting feature is that most of infectious targets of these flavones are enveloped viruses and that no matter what the substitution on the B-cycle is, the antiviral activity is maintained for a wide range of viral pathogens. Even though not all viruses were studied, Table 1 shows that this class of compounds targets mainly HCV, HIV, Influenza, H1N1 and AMV viruses.

Table 1. Structure and antiviral activity of selected flavones displaying a 5,6,7-trihydroxylation pattern.

	R_1	R_2	Antiviral Activity Reported
Baicalein	H	H	JEV,[304] DENV,[305] RSV,[306] HIV,[307] PRRSV,[308] IBD,[309] HCMV,[310] H1N1,[311] Influenza,[312] Simian Virus,[313] Sendai Virus,[314] Epstein-Barr Virus,[315] AMV[316]
Baicalin	H	Glucuronide	Influenza,[318] H1N1,[319] RSV,[306] PRRSV,[308] IBD,[309] HSV,[320] HIV,[295,321] HMCV,[322] SARS,[323] HTLV-I[324]
Oroxylin A	CH_3	H	RSV[306]
Oroxylin A-7-glucuronide	CH_3	Glucuronide	HIV,[325] Influenza[326]

	R_1	R_2	Antiviral Activity Reported
Scutellarein	H	H	AMV,[327] Influenza,[326] HIV,[325] SARS[328]
Plantaginin	H	Glucoside	HIV[329]
Scutellarein B	H	Glucuronide	PRRSV,[308] SARS,[328] H1N1,[330] HIV,[331] Influenza[332]
Dinatin	CH_3	H	AMV,[327] H1N1,[330] Influenza,[326] HSV,[333] HIV[325]
Homoplataginin	CH_3	Glucoside	HIV[329]
Hispidulin-7-glucuronide	CH_3	Glucuronide	HSV[333]
Cirsimaritin	CH_3	CH_3	AMV,[327] HIV,[334] Influenza[326]

	R_1	R_2	Antiviral Activity Reported
Ladanein	H	CH_3	HIV, HCV, Herpes[335]
Salvigenin	CH_3	CH_3	Influenza[326]

	R_1	R_2	Antiviral Activity Reported
Nornepetin	H	H	AMV,[327] HIV[329]
Stereolensin	Glucoside	H	Epstein-Barr virus[336]
6-Hydroxyluteolin-7-glucoside	H	Glucoside	HIV[329]

JEV = Japanese Encephalitis Virus, DENV = Dengue Virus, RSV = Respiratory Syncytal Virus, HIV = Human Immunodeficiency Virus, PRRSV = Porcine Reproductive and Respiratory Syndrome Virus, IBD = Infectious Bursal Disease, HCMV = Human Cytomegalovirus, AMV = Avian myeloblastoma Virus, HSV = Herpes Simplex Virus, HTLV-I = Human T-Lymphotropic Virus, SARS = Severe Acute Respiratory Syndrome.

Concomitantly to the anti-HIV tests, the extracts were also tested against HCV by Prof. Thomas Pietschmann at the University of Hannover.[337] Following the characterization of the active compound, a rapid and straightforward synthesis of ladanein was developed at the laboratory of Dr. Davioud-Charvet and the resulting synthetic flavone (designated as BJ486K) was tested as well,

obtaining similar results. Both the plant extracts and the synthetic ladanein effectively inhibited HCV infection. They displayed a pangenotypic activity, affecting HCV entry in the cell. Furthermore, the entry step targeted is a post-attachment step. Cells were inoculated with a virus for 1 hour at 4 °C, so that virions were bound to the cell but did not enter it. In these conditions, ladanein showed a potent inhibition as well. Infection with virus mutants showing resistance against the entry inhibitor ITX5061[240] (SR-BI inhibitor, Figure 40) was also inhibited by the presence of ladanein.
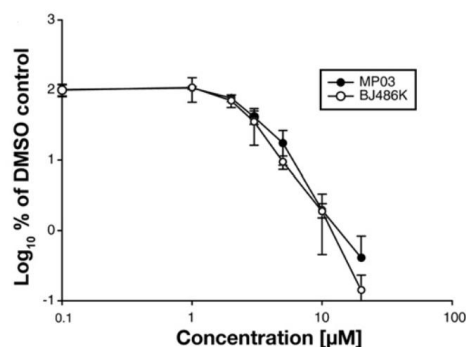
Figure 51. Anti-HCV activity of natural ladanein (MP03) and synthetic ladanein (BJ486K) in Huh7-Lunet/Cd81 cells inoculated with Luc-Jc1 virus particles for 48 hours.

It was also shown that a combination of ladanein and Cyclosporine A had a synergistic effect on the inhibition of HCV infection, while Chloroquine (an antimalarial drug, unpublished results) displayed an additive anti-HCV effect in conjunction with ladanein.[337]

Even though the synthetic route developed yielded the desired product with satisfactory purity, it had several drawbacks that had to be improved. The drawbacks and the new synthetic pathway will be thoroughly discussed in Chapter II.

Through an ICP-MS investigation, it was observed that the fractions from the extracts that had the higher activities were Fe- and Cu-enriched, so that it was suggested that metal chelation may play a critical role in the antiviral activity of the molecule. Indeed, in the presence of a strong iron chelator such as ferrioxamine (DFO), the antiviral activity of the flavone is abolished. Furthermore, it was proved that ladanein forms a 1:1 complex with Fe(III) through the β-hydroxyketone site and that iron catalyzes the degradation of the flavone (Chapter V). However, the complex can be stabilized if a ternary complex is formed with the addition of an exogenous ligand such as nitrilotriacetic acid (NTA). It has been suggested that the degradation products might be due to uncontrolled polymerization and C,C- and C,O-coupling reactions. These aspects will be discussed in the following chapter.

Recently, interest in flavonoids and polyphenols has increased because they have been found to possess many different biological properties, including antiviral properties. Indeed, various polyphenols have been reported to have anti-HCV properties (see Table 1 for ladanein analogues and Table 2 for other virucidal compounds).[338]

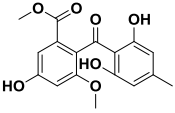There are many examples of compounds targeting HCV virion entry. For example, sulochrin inhibits HCV entry and has an additive activity in conjunction with IFN-α or Telaprevir. In addition, some funicone derivatives such as deoxyfunicone or 3-*O*-methylfunicone display an improved anti-HCV activity.[339] Silibinin also displayed an important anti-HCV activity by allegedly blocking clathrin-mediated endocytosis.[145] Furthermore, its derivatives have an antiviral activity as well.[340] EGCG, mainly found in green tea, inhibits hepatitis C virus infection by effectively blocking its entry.[341] It is suggested that it interacts with virion surface proteins and competes with heparan sulfate.[342] Curcumin is also a well-known polyphenol that inhibits HCV entry, affecting membrane fluidity and cell-to-cell transmission.[343] Finally, honokiol has been reported to block HCV entry in the cell.[344]

Several polyphenols have also been reported to block other stages in the HCV life cycle. Various polyphenols isolated from *Galla chinese* and *Exoecaria agallocha L.* act as NS3 inhibitors.[345,346] Psammaplin A[347] and proanthocyanidin[348] inhibit the viral NS3 protein as well. Various compounds have also been reported to inhibit HCV replication by targeting the NS5 viral protein. For instance, quercetin, naringenin and catechin exert their antiviral activity by blocking NS5A.[349] The flavonoid luteolin has been shown to block the NS5B protein.[350] Other compounds target the same protein such as apigenin[350] and wedelolactone.[351]

Finally apigenin decreases the level of mature miR122,[352] hence decreasing viral infection. Other compounds have been studied but the precise step on which they exert their activity has not yet been elucidated. For example, dihydroquercetin,[353] xanthohumol[354] or caffeic acid phenethyl ester (CAPE) and its derivatives[355] display antiviral activities as well.

Table 2. Structure of selected polyphenols affecting HCV entry steps.

Compounds	Agents blocking HCV entry	
	Source	HCV targets, properties and ref
Sulochrin	*Fungal* metabolite isolated from *Penicillium sp.* and *Asperigillus*	**Ref. 339** Blocks entry step and shows an additive activity with IFN-α or Telaprevir Active on genotypes 1a, 1b, and 2a.
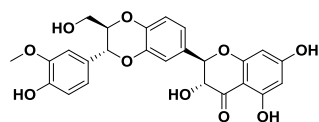
Silibinin	Flavanolignans Extract from milk thistle seeds 0.08%	**Ref. 145** Blocks clathrin-mediated endocytosis Bioavailability 0.4-1.3 µg/L
Deoxyfunicone	Isolated from *Penicillium citreonigrum* and *T. Flavus*	**Ref. 339** Displays an antiviral activity 5 times more potent than sulochrin
3-O-methylfunicone	Isolated from a soil strain of *P. Pinophilum*.	**Ref. 339** Similar potency to Deoxyfunicone
EGCG	Most abundant catechin in green tea (50 % of total catechins, *Camellia sinensis*) (27.16 mg/100 ml)	**Ref 341** Inhibits HCV attachment as well as cell-to-cell spread
Curcumin	Principal curcuminoid of the South Asian spice turmeric 3.14% by weight of the pure turmeric powder	**Ref. 343** Affects membrane fluidity and cell-to-cell transmission
Honokiol	Bark, seed cones, and leaves of trees belonging to *Magnolia obovata*.	**Ref. 344** Inhibition of HCV entry as well as replication
Agents blocking other step of the HCV life cycle		
Psammaplin A	Present in several marine sponges including *Pseudoceratina purpurea*	**Ref. 347** Inhibits NS3 activity by inhibiting the NS3 ATPase activity
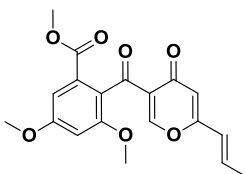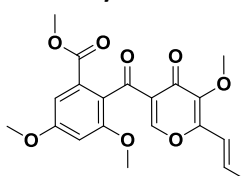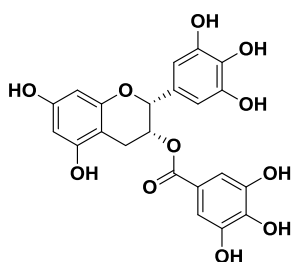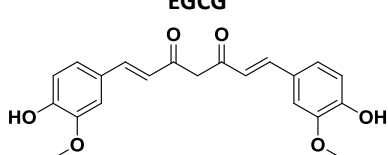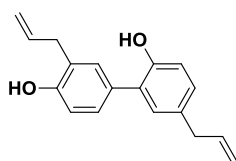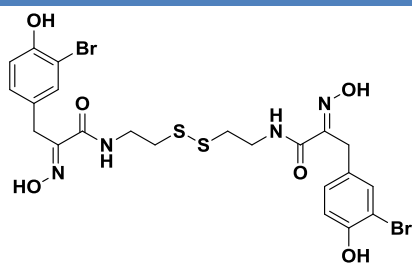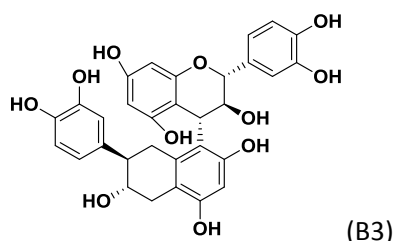
Proanthocyanidins (B3)	Extracted from blueberry leaves (*Vaccinium virgatum*).	**Ref. 348** Inhibition of NS3, greater activity with a polymerization degree of 8 to 9.
Quercetin	Present in many foods and beverages such as berries (42 mg/100 g) or chocolate (25 mg/100g)	**Ref. 349** NS5A inhibitor. Inhibits intracellular virion assembly as well.
Naringenin	Found in grapefruits, oranges and tomatoes.	**Ref. 349** Lower potency than Quercetin. NS5A inhibitor. Blocks virion assembly
Catechin	Found in cocoa (108 mg/100g), plum juice (25 mg/100g),	**Ref. 349** Lower potency than Quercetin. NS5A inhibitor. Blocks virion assembly
Luteolin	Present in sage (33 mg/100 g), thyme (40 mg/100 g) and artichoke (42 mg/100 g)	**Ref. 350** NS5B inhibitor
Apigenin	Present inchamomile tea (*Matricaria chamomilla*)	**Ref. 350** NS5B inhibitor Decreases the level of mature miR122
Wedelolactone	Isolated from *Eclipta alba* (false daisy) and *Wedelia calendulacea*	**Ref. 351** NS5B RdRp inhibitor
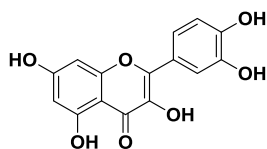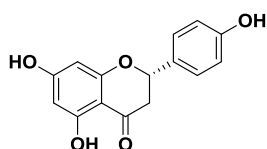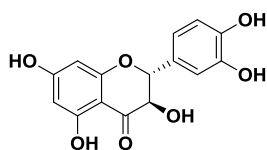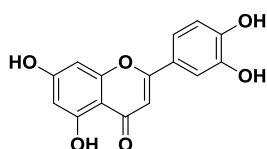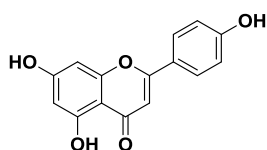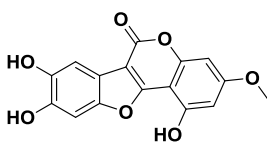
New compounds that are easily accessible everywhere in the world and can be obtained at a low price will probably be of great importance for the future treatment of HCV infection. As discussed in a previous section, the majority of people infected with HCV live in low-income countries, where new treatments incorporating DAAs will not be available and affordable to everyone. Compounds that can be either extracted from plants used in traditional medicine or that are inexpensive will probably lead to less expensive treatments which will be available and accessible for people living in low-income countries.

Entry inhibitors are becoming increasingly important in anti-HCV research because they exert their biological activity before the virion has infected the cell and started producing genetic material that will remain within the cell. Even if DAAs provide better results than bitherapy with IFN-α and RBV, resistant variants are already starting to appear. Combination therapies will therefore be needed in order to treat hepatitis C, and entry inhibitors could play an important role. Furthermore, some patients still need an alternative therapy since they do not tolerate well the current therapies. Entry inhibitors may also play an important role in patients undergoing liver transplant, since reinfection after liver graft occurs in a majority of the patients. Moreover, entry inhibitors have been shown to be less genotype-dependent and have a higher genetic barrier to resistance, due to the fact that the entry process is conserved between different variants and even different enveloped viruses. A possible combination of DAAs and entry inhibitors is a promising new therapy for anti-HCV infection. Because the compounds have different modes of action, it is possible to observe synergistic or additive effects.

Towards these objectives, the aims of my PhD project were:

- To develop a new synthetic pathway allowing for better yields and a quicker access to analogues of ladanein,
- To study the physico-chemical properties of both the lead flavone and different analogues,
- To improve the bioavailability and $t_{1/2}$ of the lead compound *via* the formation of metallic compounds,
- To study the synthesis of a bi-drug complex between ladanein and a chloroquine analogue.

References

(1)   Zaitlin, M. *Discov. Plant Biol.* **1998**, 105–110.

(2)   Stanley, W. M. *Science* **1935**, *81*, 644–645.

(3)   Albertini, A.; Wernimont, A. K.; Muziol, T.; Ravelli, R. B. G.; Clapier, C. R.; Schoehn, G.; Weissenhorn, W.; Ruigrok, R. W. H. *Science* **2006**, *313*, 360–363.

(4)   Reddy, V. S.; Natchiar, S. K.; Stewart, P. L.; Nemerow, G. R. *Science* **2010**, *329*, 1071–1075.

(5)   Pilling, A.; Rosenberg, M. F.; Willis, S. H.; Jäger, J.; Cohen, G. H.; Eisenberg, R. J.; Meredith, M.; Holzenburg, A.; Ja, J. **1999**.

(6)   Ikeda, M.; Hamajima, R.; Kobayashi, M. *Entomol. Sci.* **2014**, n/a – n/a.

(7)   Soldan, S. S.; González-Scarano, F. *J. Neurovirol.* **2005**, *11*, 412–423.

(8)   Siddell, S. G.; Anderson, R.; Cavanagh, D.; Fujiwara, K.; Klenk, H. D.; Macnaughton, M. R.; Pensaert, M.; Stohlman, S. A.; Sturman, L.; Van der Zeijst, B. A. M. *Intervirology* **1983**, 181–189.

(9)   Ascenzi, P.; Bocedi, A.; Heptonstall, J.; Capobianchi, M. R.; Di Caro, A.; Mastrangelo, E.; Bolognesi, M.; Ippolito, G. *Mol. Aspects Med.* **2008**, *29*, 151–185.

(10)   Foulon, T. *Comp. Immunol. Microbiol. Infect. Dis.* **1992**, *15*, 13–29.

(11)   Clements, J.; Zink, M. *Clin. Microbiol. Rev.* **1996**, *9*, 100–117.

(12)   Neumann, G.; Brownlee, G.; Fodor, E.; Kawaoka, Y. *Biol. Negat. Strand Viruses Power Reverse Genet.* **2004**, 121–143.

(13)   Kingsbury, D. W.; Bratt, M. A.; Choppin, P. W.; Hanson, R. P.; Hosaka, Y.; Ter Meulen, V.; Norrby, E.; Plowright, W.; Rott, R.; Wunner, W. H. *Intervirology* **1978**, *10*, 137–152.

(14)   McFadden, G. *Nat. Rev. Microbiol.* **2005**, *3*, 201–213.

(15)   Brown, F.; Bishop, D. H. L.; Crick, J.; Francki, R. I. B.; Holland, J. J.; Hull, R.; Johnson, K.; Martelli, G.; Murphy, F. A.; Obijeski, J. F.; Peters, D.; Pringle, C. R.; Reichmann, M. E.; Schneider, L. G.; Shope, R. E.; Simpson, D. I. H.; Summers, D. F.; Wagner, R. . *Intervirology* **1979**, *12*, 1–7.

(16)   Westaway, E.; Brinton, M.; Gaidamovich, S. Y.; Horzinek, M. C.; Igarashi, A.; Kääriäinen, L.; Lvov, D. K.; Porterfield, J. S.; Russell, P. K.; Trent, D. W. *Intervirology* **1985**, *24*, 125–139.

(17)   Yan, X.; Chipman, P. R.; Battisti, A. J.; Bergoin, M.; Rossmann, M. G.; Baker, T. S. *Microsc. Microanal.* **2005**, *11*, 134–135.

(18)   Sodeik, B.; Doms, R. W.; Ericsson, M.; Hiller, G.; Machamer, C. E.; van't Hof, W.; van Meer, G.; Moss, B.; Griffiths, G. *J. Cell Biol.* **1993**, *121*, 521–541.

(19)   Suhy, D. A.; Giddings, T. H.; Kirkegaard, K. *J. Virol.* **2000**, *74*, 8953–8965.

(20)   Cobbold, C.; Whittle, J.; Wileman, T. *J. Virol.* **1996**, *70*, 8382–8390.

(21)   Air, G. M.; Laver, W. G. *Proteins* **1989**, *6*, 341–356.

(22)   Lima, L. R.; Almeida, A. J. De; Tourinho, R. D. S.; Hasselmann, B.; Lewis Ximenez, L. L.; De Paula, V. S. *PLoS One* **2014**, *9*, e102925.

(23)   Prince, A.; Grady, G.; Hazzi, C.; Brotman, B. *Lancet* **1974**, 241–246.

(24)   Feinstone, S.; Kapikian, A. *N. Engl. J. Med.* **1975**, *292*, 767–770.

(25)   Choo, Q. L.; Kuo, G.; Weiner, A. J.; Overby, L. R.; Bradley, D. W.; Houghton, M. *Science* **1989**, *244*, 359–362.

(26)   Davis, G. L.; Balart, L. A.; Schiff, E. R.; Lindsay, K.; Bodenheimer, H. C.; Perrillo, R. P.; Carey, W.; Jacobson, I. M.; Payne, J.; Dienstag, J. L.; Van Thiel, D. H.; Tamburro, C.; Lefkowitch, J.; Albrecht, J.; Meschievitz, C.; Ortego, T. J.; Gibas. *J. Hepatol.* **1990**, *11*, S31–S35.

(27)   Kiyosawa, K.; Sodeyama, T.; Tanaka, E.; Gibo, Y.; Yoshizawa, K.; Nakano, Y.; Furuta, S.; Akahane, Y.; Nishioka, K.; Purcell, R. H. *Hepatology* **1990**, *12*, 671–675.

(28)   Chamberlain, R. W.; Adams, N.; Saeed, A. A.; Simmonds, P.; Elliott, R. M. *J. Gen. Virol.* **1997**, *78 (Pt 6)*, 1341–1347.

(29)   Lauck, M.; Sibley, S. D.; Lara, J.; Purdy, M. A.; Khudyakov, Y.; Hyeroba, D.; Tumukunde, A.; Weny, G.; Switzer, W. M.; Chapman, C. A.; Hughes, A. L.; Friedrich, T. C.; O'Connor, D. H.; Goldberg, T. L. *J. Virol.* **2013**, *87*, 8971–8981.

(30)   Gawlik, K.; Gallay, P. A. *Immunol. Res.* **2014**.

(31)   Griffin, S. D. C.; Beales, L. P.; Clarke, D. S.; Worsfold, O.; Evans, S. D.; Jaeger, J.; Harris, M. P. G.; Rowlands, D. J. *FEBS Lett.* **2003**, *535*, 34–38.

(32)   Frank, C.; Mohamed, M. K.; Strickland, G. T.; Lavanchy, D.; Arthur, R. R.; Magder, L. S.; El Khoby, T.; Abdel-Wahab, Y.; Aly Ohn, E. S.; Anwar, W.; Sallam, I. *Lancet* **2000**, *355*, 887–891.

(33)   Maasoumy, B.; Wedemeyer, H. *Best Pract. Res. Clin. Gastroenterol.* **2012**, *26*, 401–412.

(34)   Smith, D. B.; Bukh, J.; Kuiken, C.; Muerhoff, A. S.; Rice, C. M.; Stapleton, J. T.; Simmonds, P. *Hepatology* **2014**, *59*, 318–327.

(35)   Simmonds, P. *J. Gen. Virol.* **2004**, *85*, 3173–3188.

(36)   McOmish, F.; Yap, P. L.; Dow, B. C.; Follett, E. A.; Seed, C.; Keller, A. J.; Cobain, T. J.; Krusius, T.; Kolho, E.; Naukkarinen, R. *J. Clin. Microbiol.* **1994**, *32*, 884–892.

(37)   Kobayashi, M.; Tanaka, E.; Sodeyama, T.; Urushihara, A.; Matsumoto, A.; Kiyosawa, K. *Hepatology* **1996**, *23*, 695–699.

(38)   Rubbia-Brandt, L.; Quadri, R.; Abid, K. *J. Hepatol.* **2000**, *33*, 106–115.

(39)   Manns, M. P.; Wedemeyer, H.; Cornberg, M. *Gut* **2006**, *55*, 1350–1359.

(40)   Martell, M.; Esteban, J.; Quer, J.; Genescà, J.; Weiner, A.; Esteban, R.; Guardia, J.; Gómez, J. *J. Virol.* **1992**, *66*, 3225–3229.

(41)   Ramratnam, B.; Bonhoeffer, S.; Binley, J.; Hurley, A.; Zhang, L.; Mittler, J. E.; Moore, J. P.; Perelson, A. S.; Ho, D. . *Lancet* **1999**, *354*, 1782–1785.

(42)   Neumann, A. U.; Lam, N. .; Dahari, H.; Gretch, D. R.; Wiley, T. E.; Layden, T. J.; Perelson, A. S. *Science (80-.).* **1998**, *282*, 103–107.

(43)   Bartenschlager, R.; Lohmann, V. *J. Gen. Virol.* **2000**, *81*, 1631–1648.

(44)   Chen, S. L.; Morgan, T. R. *Int. J. Med. Sci.* **2006**, *3*, 47–52.

(45)   Ascione, A.; Tartaglione, M. T.; Di Constanzo, G. G. *Dig. Liver Dis.* **2007**, *1*, 37–40.

(46)   Lauer, G.; Walker, B. *N. Engl. J. Med.* **2001**, *345*, 41–52.

(47)   Beltrami, E.; Williams, I.; Shapiro, C. N.; Chamberland, M. *Clin. Microbiol. Rev.* **2000**, *13*, 385–407.

(48)   Vidal-Trécan, G.; Coste, J.; Varescon-Pousson, I.; Christoforov, B.; Boissonnas, A. *Eur. J. Epidemiol.* **2000**, *16*, 439–445.

(49)   Vallet-Pichard, A.; Pol, S. *Clin. Res. Hepatol. Gastroenterol.* **2013**, *37*, 340–346.

(50)   Pereira, B.; Milford, E.; R.L., K.; Quan, S.; Sayre, K. R.; Johnson, P. J.; Wilber, J. C.; Levey, A. S. *N. Engl. J. Med.* **1992**, *327*, 910–915.

(51)   Roberts, E. A.; Yeung, L. *Hepatology* **2002**, *36*, S106–S113.

(52)   Orland, J. R.; Wright, T. L.; Cooper, S. *Hepatology* **2001**, *33*, 321–327.

(53)   Chung, R. *Clin. Infect. Dis.* **2005**, *2696*.

(54)   Farci, P.; Alter, H.; Shimoda, A.; Govindarajan, S.; Cheung, L. C.; Melpolder, J. C.; Sacher, R. A.; Shih, J. W.; Purcell, R. H. *N. Engl. J. Med.* **1996**, *335*, 631–634.

(55)   Thimme, R.; Oldach, D.; Chang, K. M.; Steiger, C.; Ray, S. C.; Chisari, F. V. *J. Exp. Med.* **2001**, *194*, 1395–1406.

(56)   Farci, P.; Alter, H.; Wong, D.; Miller, R. H.; Shih, J. W.; Jett, B.; Purcell, R. H. *N. Engl. J. Med.* **1991**, *325*, 98–104.

(57)   Bakr, I.; Rekacewicz, C.; El Hosseiny, M.; Ismail, S.; El Daly, M.; El-Kafrawy, S.; Esmat, G.; Hamid, M. A.; Mohamed, M. K.; Fontanet, A. *Gut* **2006**, *55*, 1183–1187.

(58)   Farci, P.; Shimoda, A.; Coiana, A.; Diaz, G.; Peddis, G.; Melpolder, J. C.; Strazzera, A.; Chien, D. Y.; Munoz, S. J.; Balestrieri, A.; Purcell, R. H.; Alter, H. *Science (80-.).* **2000**, *288*, 339–344.

(59)   Seeff, L. B.; Hoofnagle, J. H. *Hepatology* **2002**, *36*, S1–S2.

(60)   Bochud, P.-Y.; Cai, T.; Overbeck, K.; Bochud, M.; Dufour, J.-F.; Müllhaupt, B.; Borovicka, J.; Heim, M.; Moradpour, D.; Cerny, A.; Malinverni, R.; Francioli, P.; Negro, F. *J. Hepatol.* **2009**, *51*, 655–666.

(61)   Westin, J.; Nordlinder, H.; Lagging, M.; Norkrans, G.; Wejstål, R. *J. Hepatol.* **2002**, *37*, 837–842.

(62)   Sène, D.; Limal, N.; Cacoub, P. *Metab. Brain Dis.* **2004**, *19*, 357–381.

(63)   Johnson, R. J.; Gretch, D. R.; Yamabe, H.; Hart, J.; Bacchi, C. E.; Hartwell, P.; Couser, W. G.; Corey, L.; Wener, M. H.; Alpers, C. E.; Willson, R. *N. Engl. J. Med.* **1993**, *328*, 465–470.

(64)   Ryan Caballes, F.; Sendi, H.; Bonkovsky, H. L. *Liver Int.* **2012**, *32*, 880–893.

(65)   Lodi, G.; Pellicano, R.; Carrozzo, M. *Oral Dis.* **2010**, *16*, 601–612.

(66)   Jackson, J. M. *Dermatol. Clin.* **2002**, *20*, 449–458.

(67)   Poynard, T.; Bedossa, P.; Opolon, P. *Lancet* **1997**, *349*, 825–832.

(68)   *Hepatology* **2002**, *36*, S3–S20.

(69)   Fattovich, G.; Giustina, G.; Degos, F.; Tremolada, F.; Diodati, G.; Almasio, P.; Nevens, F.; Solinas, Ø. A.; Mura, D.; Brouwer, J. T.; Thomas, H.; Njapoum, C.; Casarin, C.; Bonetti, P.; Fuschi, P.; Basho, J.; Tocco, Ø. A.; Bhalla, A.; Galassini, R.; Noventa, F.; Schalm, S. W.; Realdi, G. *Gastroenterology* **1997**, *112*, 463–472.

(70)   Serfaty, L.; Aumaître, H.; Chazouillères, O.; Bonnand, A. M.; Rosmorduc, O.; Poupon, R. E.; Poupon, R. *Hepatology* **1998**, *27*, 1435–1440.

(71)   Hu, K. Q.; Tong, M. J. *Hepatology* **1999**, *29*, 1311–1316.

(72)   Lok, A. S.; Seeff, L. B.; Morgan, T. R.; Di Bisceglie, A. M.; Sterling, R. K.; Curto, T. M.; Everson, G. T.; Lindsay, K. L.; Lee, W. M.; Bonkovsky, H. L.; Dienstag, J. L.; Ghany, M. G.; Morishima, C.; Goodman, Z. D. *Gastroenterology* **2009**, *136*, 138–148.

(73)   Tanaka, Y.; Kurbanov, F.; Mano, S.; Orito, E.; Vargas, V.; Esteban, J. I.; Yuen, M.-F.; Lai, C.-L.; Kramvis, A.; Kew, M. C.; Smuts, H. E.; Netesov, S. V; Alter, H. J.; Mizokami, M. *Gastroenterology* **2006**, *130*, 703–714.

(74)   Baré, P.; Massud, I.; Parodi, C.; Belmonte, L.; García, G.; Nebel, M. C.; Corti, M.; Pinto, M. T.; Bianco, R. P.; Bracco, M. M.; Campos, R.; Ares, B. R. *J. Gen. Virol.* **2005**, *86*, 1717–1727.

(75)   Zignego, A. L.; Macchiad, D.; Monti, M.; Thiers, V.; Mazzettid, M.; Maggid, E.; Romagnanl, S.; Gentilini, P.; Brtchot, C. *J. Hepatol.* **1992**, *15*, 382–386.

(76)   Goutagny, N.; Fatmi, A.; De Ledinghen, V.; Penin, F.; Couzigou, P.; Inchauspé, G.; Bain, C. *J. Infect. Dis.* **2003**, *187*, 1951–1958.

(77)   Sarhan, M. A.; Pham, T. N. Q.; Chen, A. Y.; Michalak, T. I. *J. Virol.* **2012**, *86*, 3723–3735.

(78)   Okuda, M.; Hino, K.; Korenaga, M.; Yamaguchi, Y.; Katoh, Y.; Okita, K. *Hepatology* **1999**, *29*, 217–222.

(79)   Blackard, J. T.; Kemmer, N.; Sherman, K. E. *Hepatology* **2006**, *44*, 15–22.

(80)   Sung, V. M.; Shimodaira, S.; Doughty, A. L.; Picchio, G. R.; Can, H.; Yen, T. S. B.; Karen, L.; Levine, A. M.; Lai, M. M. C.; Lindsay, K. L. *J. Virol.* **2003**, *77*, 2134–2146.

(81)   Seipp, S.; Mueller, H. M.; Pfaff, E.; Stremmel, W.; Theilmann, L.; Goeser, T. *J. Gen. Virol.* **1997**, *78*, 2467–2476.

(82)   Tagawa, M.; Kato, N.; Yokosuka, O.; Ishikawa, T.; Ohto, M.; Omata, M. *J. Gastroenterol. Hepatol.* **1995**, *10*, 523–527.

(83)   Lanford, R.; Sureau, C.; Jacob, J.; White, R.; Fuerst, T. *Virology* **1994**, *202*, 606–614.

(84)   Gunji, T.; Kato, N.; Hijikata, M.; Hayashi, K.; Saitoh, S.; Shimotohno, K. *Arch. Virol.* **1994**, *134*, 293–302.

(85)   Iacovacci, S.; Manzin, A.; Barca, S.; Sargiacomo, M.; Serafino, A.; Valli, M. B.; Macioce, G.; Hassan, H. J.; Ponzetto, A.; Clementi, M.; Peschle, C.; Carloni, G. *Hepatology* **1997**, *26*, 1328–1337.

(86)   Lohmann, V.; Körner, F.; Koch, J.-O.; Herian, U.; Theilmann, L.; Bartenschlager, R. *Science* **1999**, *285*, 110–113.

(87)   Blight, K. J.; Kolykhalov, A. A.; Rice, C. M. *Science* **2000**, *290*, 1972–1974.

(88)   Krieger, N.; Lohmann, V.; Bartenschlager, R. *J. Virol.* **2001**, *75*, 4614–4624.

(89)   Lohmann, V.; Körner, F. *J. Virol.* **2001**, *75*, 1437–1449.

(90)   Pietschmann, T.; Lohmann, V.; Kaul, A. *J. Virol.* **2002**, *76*, 4008–4021.

(91)   Ikeda, M.; Yi, M.; Li, K.; Lemon, S. *J. Virol.* **2002**, *76*, 2997–3006.

(92)   Blight, K. J.; McKeating, J. A.; Marcotrigiano, J.; Rice, C. M. *J. Virol.* **2003**, *77*, 3181–3190.

(93)   Kato, N.; Sugiyama, K.; Namba, K.; Dansako, H.; Nakamura, T.; Takami, M.; Naka, K.; Nozaki, A.; Shimotohno, K. *Biochem. Biophys. Res. Commun.* **2003**, *306*, 756–766.

(94)   Blight, K. J.; Mckeating, J. A.; Rice, C. M. *J. Virol.* **2002**, *76*, 13001–13014.

(95)   Sumpter, R.; Loo, Y.; Foy, E.; Li, K.; Yoneyama, M.; Fujita, T.; Lemon, S. M.; Gale, M. *J. Virol.* **2005**, *79*, 2689–2699.

(96)   Baumert, T.; Ito, S.; Wong, D.; Liang, T. *J. Virol.* **1998**, *72*, 3827–3836.

(97)   Buonocore, L.; Blight, K.; Rice, C.; Rose, J. *J. Virol.* **2002**, *76*, 6865–6872.

(98)   Drummer, H. E.; Maerz, A.; Poumbourios, P. *FEBS Lett.* **2003**, *546*, 385–390.

(99)   Bartosch, B.; Vitelli, A.; Granier, C.; Goujon, C.; Dubuisson, J.; Pascale, S.; Scarselli, E.; Cortese, R.; Nicosia, A.; Cosset, F.-L. *J. Biol. Chem.* **2003**, *278*, 41624–41630.

(100)   Hsu, M.; Zhang, J.; Flint, M.; Logvinoff, C.; Cheng-Mayer, C.; Rice, C. M.; McKeating, J. A. *Proc. Natl. Acad. Sci. U. S. A.* **2003**, *100*, 7271–7276.

(101)   Lindenbach, B. D.; Evans, M. J.; Syder, A. J.; Wölk, B.; Tellinghuisen, T. L.; Liu, C. C.; Maruyama, T.; Hynes, R. O.; Burton, D. R.; McKeating, J. A.; Rice, C. M. *Science* **2005**, *309*, 623–626.

(102)   Yi, M.; Villanueva, R. A.; Thomas, D. L.; Wakita, T.; Lemon, S. M. *Proc. Natl. Acad. Sci. U. S. A.* **2006**, *103*, 2310–2315.

(103)   Wakita, T.; Pietschmann, T.; Kato, T.; Date, T.; Miyamoto, M.; Zhao, Z.; Murthy, K.; Habermann, A.; Kräusslich, H.-G.; Mizokami, M.; Bartenschlager, R.; Liang, T. J. *Nat. Med.* **2005**, *11*, 791–796.

(104)   Alter, H.; Holland, P.; Purcell, R.; Popper, H. *Lancet* **1978**, 459–463.

(105)   Meuleman, P.; Libbrecht, L.; De Vos, R.; de Hemptinne, B.; Gevaert, K.; Vandekerckhove, J.; Roskams, T.; Leroux-Roels, G. *Hepatology* **2005**, *41*, 847–856.

(106)   Mercer, D.; Schiller, D.; Elliott, J.; Douglas, D.; Hao, C.; Rinfret, A.; Addison, W. R.; Fischer, K. P.; Churchill, T. A.; Lakey, J. R. T.; Tyrrell, D. L. J.; Kneteman, N. M. *Nat. Med.* **2001**, *7*, 927–933.

(107)   Fénéant, L.; Levy, S.; Cocquerel, L. *Viruses* **2014**, *6*, 535–572.

(108)   Moradpour, D.; Penin, F.; Rice, C. M. *Nat. Rev. Microbiol.* **2007**, *5*, 453–463.

(109)   Agnello, V.; Abel, G.; Elfahal, M.; Knight, G. B.; Zhang, Q. X. *Proc. Natl. Acad. Sci. U. S. A.* **1999**, *96*, 12766–12771.

(110)   Germi, R.; Crance, J.-M.; Garin, D.; Guimet, J.; Lortat-Jacob, H.; Ruigrok, R. W. H.; Zarski, J.-P.; Drouet, E. *J. Med. Virol.* **2002**, *68*, 206–215.

(111)   Barth, H.; Schafer, C.; Adah, M. I.; Zhang, F.; Linhardt, R. J.; Toyoda, H.; Kinoshita-Toyoda, A.; Toida, T.; Van Kuppevelt, T. H.; Depla, E.; Von Weizsacker, F.; Blum, H. E.; Baumert, T. F. *J. Biol. Chem.* **2003**, *278*, 41003–41012.

(112)   Jiang, J.; Wu, X.; Tang, H.; Luo, G. *PLoS One* **2013**, *8*, e67982.

(113)   Bartenschlager, R.; Penin, F.; Lohmann, V.; André, P. *Trends Microbiol.* **2011**, *19*, 95–103.

(114)   Albecka, A.; Belouzard, S.; Op de Beeck, A.; Descamps, V.; Goueslain, L.; Bertrand-Michel, J.; Tercé, F.; Duverlie, G.; Rouillé, Y.; Dubuisson, J. *Hepatology* **2012**, *55*, 998–1007.

(115)   Bartosch, B.; Dubuisson, J. *Viruses* **2010**, *2*, 692–709.

(116)   Connelly, M. A.; Klein, S. M.; Azhar, S.; Abumrad, N. A.; Williams, D. L. *J. Biol. Chem.* **1999**, *274*, 41–47.

(117)   Zeisel, M. B.; Koutsoudakis, G.; Schnober, E. K.; Haberstroh, A.; Blum, H. E.; Cosset, F.-L.; Wakita, T.; Jaeck, D.; Doffoel, M.; Royer, C.; Soulier, E.; Schvoerer, E.; Schuster, C.; Stoll-Keller, F.; Bartenschlager, R.; Pietschmann, T.; Barth, H.; Baumert, T. F. *Hepatology* **2007**, *46*, 1722–1731.

(118)   Evans, M. J.; von Hahn, T.; Tscherne, D. M.; Syder, A. J.; Panis, M.; Wölk, B.; Hatziioannou, T.; McKeating, J. A.; Bieniasz, P. D.; Rice, C. M. *Nature* **2007**, *446*, 801–805.

(119)   Maillard, P.; Huby, T.; Andréo, U.; Moreau, M.; Chapman, J.; Budkowska, A. *FASEB J.* **2006**, *20*, 735–737.

(120)   Dreux, M.; Dao Thi, V. L.; Fresquet, J.; Guérin, M.; Julia, Z.; Verney, G.; Durantel, D.; Zoulim, F.; Lavillette, D.; Cosset, F.-L.; Bartosch, B. *PLoS Pathog.* **2009**, *5*, e1000310.

(121)   Scarselli, E.; Ansuini, H.; Cerino, R.; Roccasecca, R. M.; Acali, S.; Filocamo, G.; Traboni, C.; Nicosia, A.; Cortese, R.; Vitelli, A. *EMBO J.* **2002**, *21*, 5017–5025.

(122)   Dao Thi, V. L.; Granier, C.; Zeisel, M. B.; Guérin, M.; Mancip, J.; Granio, O.; Penin, F.; Lavillette, D.; Bartenschlager, R.; Baumert, T. F.; Cosset, F.-L.; Dreux, M. *J. Biol. Chem.* **2012**, *287*, 31242–31257.

(123)   Bankwitz, D.; Steinmann, E.; Bitzegeio, J.; Ciesek, S.; Friesland, M.; Herrmann, E.; Zeisel, M. B.; Baumert, T. F.; Keck, Z.; Foung, S. K. H.; Pécheur, E.-I.; Pietschmann, T. *J. Virol.* **2010**, *84*, 5751–5763.

(124)   Pileri, P.; Uematsu, Y.; Campagnoli, S.; Galli, G.; Falugi, F.; Petracca, R.; Weiner, A. J.; Houghton, M.; Rosa, D.; Grandi, G.; Abrignani, S. *Science* **1998**, *282*, 938–941.

(125)   Levy, S.; Nguyen, V. Q.; Andria, M. L.; Takahashi, S. *J. Biol. Chem.* **1991**, *266*, 14597–14602.

(126)   Koutsoudakis, G.; Herrmann, E.; Kallis, S.; Bartenschlager, R.; Pietschmann, T. *J. Virol.* **2007**, *81*, 588–598.

(127)   Sharma, N. R.; Mateu, G.; Dreux, M.; Grakoui, A.; Cosset, F.-L.; Melikyan, G. B. *J. Biol. Chem.* **2011**, *286*, 30361–30376.

(128)   Douam, F.; Dao Thi, V. L.; Maurin, G.; Fresquet, J.; Mompelat, D.; Zeisel, M. B.; Baumert, T. F.; Cosset, F.-L.; Lavillette, D. *Hepatology* **2014**, *59*, 776–788.

(129)   Morita, K.; Furuse, M.; Fujimoto, K.; Tsukita, S. *Proc. Natl. Acad. Sci. U. S. A.* **1999**, *96*, 511–516.

(130)   Harris, H. J.; Davis, C.; Mullins, J. G. L.; Hu, K.; Goodall, M.; Farquhar, M. J.; Mee, C. J.; McCaffrey, K.; Young, S.; Drummer, H.; Balfe, P.; McKeating, J. A. *J. Biol. Chem.* **2010**, *285*, 21092–21102.

(131)   Brazzoli, M.; Bianchi, A.; Filippini, S.; Weiner, A.; Zhu, Q.; Pizza, M.; Crotta, S. *J. Virol.* **2008**, *82*, 8316–8329.

(132)   Farquhar, M. J.; Harris, H. J.; Diskar, M.; Jones, S.; Mee, C. J.; Nielsen, S. U.; Brimacombe, C. L.; Molina, S.; Toms, G. L.; Maurel, P.; Howl, J.; Herberg, F. W.; van Ijzendoorn, S. C. D.; Balfe, P.; McKeating, J. A. *J. Virol.* **2008**, *82*, 8797–8811.

(133)   Zona, L.; Lupberger, J.; Sidahmed-Adrar, N.; Thumann, C.; Harris, H. J.; Barnes, A.; Florentin, J.; Tawar, R. G.; Xiao, F.; Turek, M.; Durand, S. C.; Duong, F. H. T.; Heim, M. H.; Cosset, F.-L.; Hirsch, I.; Samuel, D.; Brino, L.; Zeisel, M. B.; Le Naour, F.; McKeating, J. A.; Baumert, T. F. *Cell Host Microbe* **2013**, *13*, 302–313.

(134)   Lupberger, J.; Zeisel, M. B.; Xiao, F.; Thumann, C.; Fofana, I.; Zona, L.; Davis, C.; Mee, C. J.; Turek, M.; Gorke, S.; Royer, C.; Fischer, B.; Zahid, M. N.; Lavillette, D.; Fresquet, J.; Cosset, F.-L.; Rothenberg, S. M.; Pietschmann, T.; Patel, A. H.; Pessaux, P.; Doffoël, M.; Raffelsberger, W.; Poch, O.; McKeating, J. A.; Brino, L.; Baumert, T. F. *Nat. Med.* **2011**, *17*, 589–595.

(135)   Blanchard, E.; Belouzard, S.; Goueslain, L.; Wakita, T.; Dubuisson, J.; Wychowski, C.; Rouillé, Y. *J. Virol.* **2006**, *80*, 6964–6972.

(136)   Meertens, L.; Bertaux, C.; Dragic, T. *J. Virol.* **2006**, *80*, 11571–11578.

(137)   Pietschmann, T. *Nature* **2009**, *457*.

(138)   Ploss, A.; Evans, M. J.; Gaysinskaya, V. A.; Panis, M.; You, H.; de Jong, Y. P.; Rice, C. M. *Nature* **2009**, *457*, 882–886.

(139)   Benedicto, I.; Molina-Jiménez, F.; Barreiro, O.; Maldonado-Rodríguez, A.; Prieto, J.; Moreno-Otero, R.; Aldabe, R.; López-Cabrera, M.; Majano, P. L. *Hepatology* **2008**, *48*, 1044–1053.

(140)   Benedicto, I.; Molina-Jiménez, F.; Bartosch, B.; Cosset, F.-L.; Lavillette, D.; Prieto, J.; Moreno-Otero, R.; Valenzuela-Fernández, A.; Aldabe, R.; López-Cabrera, M.; Majano, P. L. *J. Virol.* **2009**, *83*, 8012–8020.

(141)   Sainz, B.; Barretto, N.; Martin, D. N.; Hiraga, N.; Imamura, M.; Hussain, S.; Marsh, K. A.; Yu, X.; Chayama, K.; Alrefai, W. A.; Uprichard, S. L. *Nat. Med.* **2012**, *18*, 281–285.

(142)   Kielian, M. *Virology* **2006**, *344*, 38–47.

(143)   Drummer, H. E.; Boo, I.; Poumbourios, P. *J. Gen. Virol.* **2007**, *88*, 1144–1148.

(144)   Martin, D. N.; Uprichard, S. L. *Proc. Natl. Acad. Sci. U. S. A.* **2013**, *110*, 10777–10782.

(145)   Blaising, J.; Pécheur, E.-I. *Biochimie* **2013**, *95*, 96–102.

(146)   Khan, A. G.; Whidby, J.; Miller, M. T.; Scarborough, H.; Zatorski, A. V; Cygan, A.; Price, A. A.; Yost, S. A.; Bohannon, C. D.; Jacob, J.; Grakoui, A.; Marcotrigiano, J. *Nature* **2014**, *509*, 381–384.

(147)   Tsukiyama-Kohara, K.; Iizuka, N.; Kohara, M.; Nomoto, A. *J. Virol.* **1992**, *66*, 1476–1483.

(148)   Wang, C.; Sarnow, P.; Siddiqui, A. *J. Virol.* **1993**, *67*, 3338–3344.

(149)   Lindenbach, B. D.; Rice, C. M. *Nature* **2005**, *436*, 933–938.

(150)   Otto, G. A.; Puglisi, J. D. *Cell* **2004**, *119*, 369–380.

(151)   Grakoui, A.; McCourt, D.; Wychowski, C.; Feinstone, S. M.; Rice, C. M. *J. Virol.* **1993**, *67*, 2832–2843.

(152)   Lin, C.; Lindenbach, B.; Pragai, B.; McCourt, D. W.; Rice, C. M. *J. Virol.* **1994**, *68*, 5063–5073.

(153)   Barba, G.; Harper, F.; Harada, T.; Kohara, M.; Goulinet, S.; Matsuura, Y.; Eder, G.; Schaff, Z.; Chapman, M. J.; Miyamura, T.; Bréchot, C. *Proc. Natl. Acad. Sci. U. S. A.* **1997**, *94*, 1200–1205.

(154)   Grakoui, A.; McCourt, D. W.; Wychowski, C.; Feinstone, S. M.; Rice, C. M. *Proc. Natl. Acad. Sci. U. S. A.* **1993**, *90*, 10583–10587.

(155)   Tanji, Y.; Hijikata, M.; Hirowatari, Y.; Shimotohno, K. *J. Virol.* **1994**, *68*, 8418.

(156)   Failla, C.; Tomei, L.; Francesco, R. De. *J. Virol.* **1995**, *69*, 1769–1777.

(157)   Bartenschlager, R.; Ahlborn-Laake, L.; Mous, J.; Jacobsen, H. *J. Virol.* **1994**, *68*, 5045–5055.

(158)   Lin, C.; Prágai, B. M.; Grakoui, A.; Xu, J.; Rice, C. M. *J. Virol.* **1994**, *68*, 8147–8157.

(159)   Kim, J. L.; Morgenstern, K. A.; Lin, C.; Fox, T.; Dwyer, M. D.; Landro, J. A.; Chambers, S. P.; Markland, W.; Lepre, C. A.; O'Malley, E. T.; Harbeson, S. L.; Rice, C. M.; Murcko, M. A.; Caron, P. R.; Thomson, J. A. *Cell* **1996**, *87*, 343–355.

(160)   Li, K.; Foy, E.; Ferreon, J. C.; Nakamura, M.; Ferreon, A. C. M.; Ikeda, M.; Ray, S. C.; Gale, M.; Lemon, S. M. *Proc. Natl. Acad. Sci. U. S. A.* **2005**, *102*, 2992–2997.

(161)   Hügle, T.; Fehrmann, F.; Bieck, E.; Kohara, M.; Kräusslich, H. G.; Rice, C. M.; Blum, H. E.; Moradpour, D. *Virology* **2001**, *284*, 70–81.

(162)   Egger, D.; Wölk, B.; Gosert, R.; Blum, H. E.; Moradpour, D.; Bienz, K. *J. Virol.* **2002**, *76*, 5974–5984.

(163)   Quintavalle, M.; Sambucini, S.; Di Pietro, C.; De Francesco, R.; Neddermann, P. *J. Virol.* **2006**, *80*, 11305–11312.

(164)   Reed, K. E.; Gorbalenya, A. E.; Rice, C. M. *J. Virol.* **1998**, *72*, 6199–6206.

(165)   Behrens, S. E.; Tomei, L.; De Francesco, R. *EMBO J.* **1996**, *15*, 12–22.

(166)   Chung, R. T.; Kaplan, L. M. *Biochem. Biophys. Res. Commun.* **1999**, *254*, 351–362.

(167)   Petrik, J.; Parker, H.; Alexander, G. J. *J. Gen. Virol.* **1999**, *80*, 3109–3113.

(168)   Jopling, C. L. *Biochem. Soc. Trans.* **2008**, *36*, 1220–1223.

(169)   Inoue, Y.; Miyazaki, M.; Ohashi, R.; Tsuji, T.; Fukaya, K.; Kouchi, H.; Uemura, T.; Mihara, K.; Namba, M. *Biochem. Biophys. Res. Commun.* **1998**, *245*, 198–203.

(170)   McLauchlan, J.; Lemberg, M.; Hope, G.; Martoglio, B. *EMBO J.* **2002**, *21*, 3980–3988.

(171)   Shimoike, T.; Mimori, S.; Tani, H.; Matsuura, Y.; Miyamura, T. *J. Virol.* **1999**, *73*, 9718–9725.

(172)   Herker, E.; Harris, C.; Hernandez, C.; Carpentier, A.; Kaehlcke, K.; Rosenberg, A. R.; Farese, R. V.; Ott, M. *Nat. Med.* **2010**, *16*, 1295–1298.

(173)   Nakai, K.; Okamoto, T.; Kimura-Someya, T.; Ishii, K.; Lim, C. K.; Tani, H.; Matsuo, E.; Abe, T.; Mori, Y.; Suzuki, T.; Miyamura, T.; Nunberg, J. H.; Moriishi, K.; Matsuura, Y. *J. Virol.* **2006**, *80*, 11265–11273.

(174)   Jirasko, V.; Montserret, R.; Lee, J. Y.; Gouttenoire, J.; Moradpour, D.; Penin, F.; Bartenschlager, R. *PLoS Pathog.* **2010**, *6*, e1001233.

(175)   Popescu, C.-I.; Callens, N.; Trinel, D.; Roingeard, P.; Moradpour, D.; Descamps, V.; Duverlie, G.; Penin, F.; Héliot, L.; Rouillé, Y.; Dubuisson, J. *PLoS Pathog.* **2011**, *7*, e1001278.

(176)   Lindenbach, B. D.; Rice, C. M. *Nat. Rev. Microbiol.* **2013**, *11*, 688–700.

(177)   Gastaminza, P.; Cheng, G.; Wieland, S.; Zhong, J.; Liao, W.; Chisari, F. V. *J. Virol.* **2008**, *82*, 2120–2129.

(178)   Vieyres, G.; Thomas, X.; Descamps, V.; Duverlie, G.; Patel, A. H.; Dubuisson, J. *J. Virol.* **2010**, *84*, 10159–10168.

(179)   Wozniak, A. L.; Griffin, S.; Rowlands, D.; Harris, M.; Yi, M.; Lemon, S. M.; Weinman, S. A. *PLoS Pathog.* **2010**, *6*, e1001087.

(180)   Vieyres, G.; Dubuisson, J.; Pietschmann, T. *Viruses* **2014**, *6*, 1149–1187.

(181)   Johnson, D.; Huber, M. *J. Virol.* **2002**, *76*, 1–8.

(182)   Sattentau, Q. *Nat. Rev. Microbiol.* **2008**, *6*, 815–826.

(183)   Brimacombe, C. L.; Grove, J.; Meredith, L. W.; Hu, K.; Syder, A. J.; Flores, M. V.; Timpe, J. M.; Krieger, S. E.; Baumert, T. F.; Tellinghuisen, T. L.; Wong-Staal, F.; Balfe, P.; McKeating, J. A. *J. Virol.* **2011**, *85*, 596–605.

(184)   Strader, D. B.; Seeff, L. B. *Clin. Liver Dis.* **2012**, *1*, 6–11.

(185)   Greenberg, H.; Pollard, R.; Lutwick, L. I.; Gregory, P. B.; Robinson, W. S.; Merigan, T. C. *N. Engl. J. Med.* **1976**, *295*, 517–522.

(186)   Bisceglie, A. Di; Martin, P.; Kassianides, C.; Lisker-Melman, M.; Murray, L.; Waggoner, J.; Goodman, Z.; Banks, S. M.; Hoofnagle, J. H. *N. Engl. J. Med.* **1989**, *321*, 1506–1510.

(187)   Davis, G. L.; Balart, L. A.; Schiff, E. R.; Lindsay, K.; Bodenheimer, H. C.; Perrillo, R. P.; Carey, W.; Jacobson, I. M.; Payne, J.; Dienstag, J. L.; VanThiel, D. H.; Tamburro, C.; Lefkowitch, J.; Albrecht, J.; Meschievitz, C.; Ortego, T. J.; Gibas, A. *N. Engl. J. Med.* **1989**, *321*, 1501–1506.

(188)   Dusheiko, G.; Main, J.; Thomas, H.; Reichard, O.; Lee, C.; Dhillon, A.; Rassam, S.; Fryden, A.; Reesink, H.; Bassendine, M.; Norkrans, G.; Cuypers, T.; Lelie, N.; Telfer, P.; Watson, J.; Weegink, C.; Sillikens, P.; Weiland, O. *J. Hepatol.* **1996**, *25*, 591–598.

(189)   Poynard, T.; Marcellin, P.; Lee, S. S.; Niederau, C.; Minuk, G. S.; Ideo, G.; Bain, V.; Heathcote, J.; Zeuzem, S.; Trepo, C.; Albrecht, J. *Lancet* **1998**, *352*, 1426–1432.

(190)   McHutchison, J.; Gordon, S.; Schiff, E. R.; Shiffman, M. L.; Lee, W. M.; Rustgi, V. K.; Goodman, Z. D.; Ling, M.-H.; Cort, S.; Albrecht, J. *N. Engl. J. Med.* **1998**, *339*, 1485–1492.

(191)   Zeuzem, S.; Feinman, S.; Rasenack, J.; Heathcote, J.; Lai, M.-Y.; Gane, E.; O'Grady, J.; Reichen, J.; Diago, M.; Lin, A.; Hoffman, J.; Brunda, M. M. J. *N. Engl. J. Med.* **2000**, *343*, 1666–1672.

(192)   Lindsay, K. L.; Trepo, C.; Heintges, T.; Shiffman, M. L.; Gordon, S. C.; Hoefs, J. C.; Schiff, E. R.; Goodman, Z. D.; Laughlin, M.; Yao, R.; Albrecht, J. K. *Hepatology* **2001**, *34*, 395–403.

(193)   Manns, M. P.; McHutchison, J. G.; Gordon, S. C.; Rustgi, V. K.; Shiffman, M.; Reindollar, R.; Goodman, Z. D.; Koury, K.; Ling, M.; Albrecht, J. K. *Lancet* **2001**, *358*, 958–965.

(194)   Okanoue, T.; Sakamoto, S.; Itoh, Y.; Minami, M.; Yasui, K.; Sakamoto, M.; Nishioji, K.; Katagishi, T.; Nakagawa, Y.; Tada, H.; Sawa, Y.; Mizuno, M.; Kagawa, K.; Kashima, K. *J. Hepatol.* **1996**, *25*, 283–291.

(195)   Hauser, P.; Khosla, J.; Aurora, H.; Laurin, J.; Kling, M. A.; Hill, J.; Gulati, M.; Thornton, A. J.; Schultz, R. L.; Valentine, A. D.; Meyers, C. A.; Howell, C. D. *Mol. Psychiatry* **2002**, *7*, 942–947.

(196)   Roti, E.; Minelli, R.; Giuberti, T.; Marchelli, S.; Schianchi, C.; Gardini, E.; Salvi, M.; Fiaccadori, F.; Ugolotti, G.; Neri, T. M.; Braverman, L. E. *Am. J. Med.* **1996**, *101*, 482–487.

(197)   Feld, J. J.; Hoofnagle, J. H. *Nature* **2005**, *436*, 967–972.

(198)   Bekisz, J.; Schmeisser, H.; Hernandez, J.; Goldman, N. D.; Zoon, K. C. *Growth Factors* **2004**, *22*, 243–251.

(199)   Murray, P. J. *J. Immunol.* **2007**, *178*, 2623–2629.

(200)   Schoggins, J. W.; Wilson, S. J.; Panis, M.; Murphy, M. Y.; Jones, C. T.; Bieniasz, P.; Rice, C. M. *Nature* **2011**, *472*, 481–485.

(201)   Hoofnagle, J. H.; Seeff, L. B. *N. Engl. J. Med.* **2006**, *355*, 2444–2451.

(202)   Soza, A.; Heller, T.; Ghany, M.; Lutchman, G.; Jake Liang, T.; Germain, J.; Hsu, H. H.; Park, Y.; Hoofnagle, J. H. *J. Hepatol.* **2005**, *43*, 67–71.

(203)   Ramos, E. L. *J. Interferon Cytokine Res.* **2010**, *30*, 591–595.

(204)   Taber, L.; Knight, V.; Gilbert, B.; McClung, H. W.; Wilson, S. Z.; Norton, H. J.; Thurson, J. M.; Gordon, W. H.; Atmar, R. L.; Schlaudt, W. R. *Pediatrics* **1983**, *72*, 613–618.

(205)   Sidwell, R. B.; Huffman, J. H.; Khare, G. P.; Allen, L. B.; Witkowsi, J. T.; Robins, R. K. *Science* **1972**, *84*, 1971–1972.

(206)   Bisceglie, A. M. Di; Conjeevaram, H. S.; Fried, M. W.; Sallie, R.; Park, Y.; Yurdaydin, C.; Swain, M.; Kleiner, D. E.; Mahaney, K.; Hoofnagle, J. H. *Ann. Intern. Med.* **1995**, *123*, 897–903.

(207)   Brillanti, S.; Garson, J.; Foli, M.; Whitby, K.; Masci, C.; Miglioli, M.; Barbara, L. *Gastroenterology* **1994**, *107*, 812–817.

(208)   Koh, C.; Liang, T. J. *Antiviral Res.* **2014**, *104*, 34–39.

(209)   Hofmann, W. P.; Polta, A.; Herrmann, E.; Mihm, U.; Kronenberger, B.; Sonntag, T.; Lohmann, V.; Schönberger, B.; Zeuzem, S.; Sarrazin, C. *Gastroenterology* **2007**, *132*, 921–930.

(210)   Fried, M. W. *Hepatology* **2002**, *36*, S237–S244.

(211)   Jacobson, I. M.; Brown, R. S.; McCone, J.; Black, M.; Albert, C.; Dragutsky, M. S.; Siddiqui, F. A.; Hargrave, T.; Kwo, P. Y.; Lambiase, L.; Galler, G. W.; Araya, V.; Freilich, B.; Harvey, J.; Griffel, L. H.; Brass, C. A. *Hepatology* **2007**, *46*, 982–990.

(212)   Wu, J. Z.; Lin, C.; Hong, Z. *J. Antimicrob. Chemother.* **2003**, *52*, 543–546.

(213)   Benhamou, Y.; Afdhal, N. H.; Nelson, D. R.; Shiffman, M. L.; Halliman, D. G.; Heise, J.; Chun, E.; Pockros, P. J. *Hepatology* **2009**, *50*, 717–726.

(214)   Kwong, A. *ACS Med. Chem. Lett.* **2014**, *5*, 214–220.

(215)   Matthews, S. J.; Lancaster, J. W. *Clin. Ther.* **2012**, *34*, 1857–1882.

(216)   Perni, R. B.; Almquist, S. J.; Byrn, R. A.; Chandorkar, G.; Chaturvedi, P. R.; Lawrence, F.; Decker, C. J.; Dinehart, K.; Cynthia, A.; Harbeson, S. L.; Heiser, A.; Kalkeri, G.; Kolaczkowski, E.; Lin, K.; Luong, Y.; Govinda, B.; Taylor, W. P.; Thomson, J. A.; Tung, R. D.; Wei, Y.; Kwong, A. D.; Lin, C. *Antimicrob. Agents Chemother.* **2006**, *50*, 899–909.

(217)   Jacobson, I. M.; McHutchison, J. G.; Dusheiko, G.; Di Bisceglie, A. M.; Reddy, K. R.; Bzowej, N. H.; Marcellin, P.; Muir, A. J.; Ferenci, P.; Flisiak, R.; George, J.; Rizzetto, M.; Shouval, D.; Sola, R.; Terg, R. A.; Yoshida, E. M.; Adda, N.; Bengtsson, L.; Sankoh, A. J.; Kieffer, T. L.; George, S.; Kauffman, R. S.; Zeuzem, S. *N. Engl. J. Med.* **2011**, *364*, 2405–2416.

(218)   Berman, K.; Kwo, P. Y. *Clin. Liver Dis.* **2009**, *13*, 429–439.

(219)   Poordad, F.; McCone, J.; Bacon, B. R.; Bruno, S.; Manns, M. P.; Sulkowski, M. S.; Jacobson, I. M.; Reddy, R.; Goodman, Z. D.; Boparai, N.; DiNubile, M. J.; Sniukene, V.; Brass, C. A.; Albrecht, J.; Bronowicki, J.-P. *N. Engl. J. Med.* **2011**, *364*, 1195–1206.

(220)   De Clercq, E. De. *Biochem. Pharmacol.* **2014**, *89*, 441–452.

(221)   Hayashi, N.; Seto, C.; Kato, M.; Komada, Y.; Goto, S. *J. Gastroenterol.* **2014**, *49*, 138–147.

(222)   Zeuzem, S.; Berg, T.; Gane, E.; Ferenci, P.; Foster, G. R.; Fried, M. W.; Hezode, C.; Hirschfield, G. M.; Jacobson, I.; Nikitin, I.; Pockros, P. J.; Poordad, F.; Scott, J.; Lenz, O.; Peeters, M.; Sekar, V.; De Smedt, G.; Sinha, R.; Beumont-Mauviel, M. *Gastroenterology* **2014**, *146*, 430–441.e6.

(223)   Qiu, D.; Lemm, J. A.; O'Boyle, D. R.; Sun, J.-H.; Nower, P. T.; Nguyen, V.; Hamann, L. G.; Snyder, L. B.; Deon, D. H.; Ruediger, E.; Meanwell, N. A.; Belema, M.; Gao, M.; Fridell, R. A. *J. Gen. Virol.* **2011**, *92*, 2502–2511.

(224)   Gao, M. *Curr. Opin. Virol.* **2013**, *3*, 514–520.

(225)   Belema, M.; Meanwell, N. A. *J. Med. Chem.* **2014**, *57*, 5057–5071.

(226)   Link, J. O.; Taylor, J. G.; Xu, L.; Mitchell, M.; Guo, H.; Liu, H.; Kato, D.; Kirschberg, T.; Sun, J.; Squires, N.; Parrish, J.; Keller, T.; Yang, Z.-Y.; Yang, C.; Matles, M.; Wang, Y.; Wang, K.; Cheng, G.; Tian, Y.; Mogalian, E.; Mondou, E.; Cornpropst, M.; Perry, J.; Desai, M. C. *J. Med. Chem.* **2014**, *57*, 2033–2046.

(227) O'Boyle, D. R.; Sun, J.-H.; Nower, P. T.; Lemm, J. A.; Fridell, R. A.; Wang, C.; Romine, J. L.; Belema, M.; Nguyen, V. N.; Laurent, D. R. S.; Serrano-Wu, M.; Snyder, L. B.; Meanwell, N. A.; Langley, D. R.; Gao, M. *Virology* **2013**, *444*, 343–354.

(228) Patil, V. M.; Gupta, S. P.; Samanta, S.; Masand, N. *Curr. Med. Chem.* **2011**, *18*, 5564–5597.

(229) McCown, M. F.; Rajyaguru, S.; Le Pogam, S.; Ali, S.; Jiang, W.-R.; Kang, H.; Symons, J.; Cammack, N.; Najera, I. *Antimicrob. Agents Chemother.* **2008**, *52*, 1604–1612.

(230) Wang, M.; Ng, K. K.-S.; Cherney, M. M.; Chan, L.; Yannopoulos, C. G.; Bedard, J.; Morin, N.; Nguyen-Ba, N.; Alaoui-Ismaili, M. H.; Bethell, R. C.; James, M. N. G. *J. Biol. Chem.* **2003**, *278*, 9489–9495.

(231) Cada, D. J.; Cong, J.; Baker, D. E. *Hosp. Pharm.* **2014**, *49*, 466–478.

(232) Gallay, P. A.; Lin, K. *Drug Des. Devel. Ther.* **2013**, *7*, 105–115.

(233) Janssen, H. L. A.; Reesink, H. W.; Lawitz, E. J.; Zeuzem, S.; Rodriguez-Torres, M.; Patel, K.; van der Meer, A. J.; Patick, A. K.; Chen, A.; Zhou, Y.; Persson, R.; King, B. D.; Kauppinen, S.; Levin, A. A.; Hodges, M. R. *N. Engl. J. Med.* **2013**, *368*, 1685–1694.

(234) Gebert, L. F. R.; Rebhan, M. A. E.; Crivelli, S. E. M.; Denzler, R.; Stoffel, M.; Hall, J. *Nucleic Acids Res.* **2014**, *42*, 609–621.

(235) Crespo, G.; Mariño, Z.; Navasa, M.; Forns, X. *Gastroenterology* **2012**, *142*, 1373–1383.e1.

(236) Zeisel, M. B.; Fofana, I.; Fafi-Kremer, S.; Baumert, T. F. *J. Hepatol.* **2011**, *54*, 566–576.

(237) Keck, Z.; Li, S. H.; Xia, J.; von Hahn, T.; Balfe, P.; McKeating, J. A.; Witteveldt, J.; Patel, A. H.; Alter, H.; Rice, C. M.; Foung, S. K. H. *J. Virol.* **2009**, *83*, 6149–6160.

(238) Fofana, I.; Jilg, N.; Chung, R. T.; Baumert, T. F. *Antiviral Res.* **2014**, *104*, 136–142.

(239) Garcia-Clavo, M.; Lisnock, J.-M.; Bull, H. G.; Hawes, B. E.; Burnett, D. A.; Braun, M. P.; Crona, J. H.; Davis, H. R.; Dean, D. C.; Detmers, P. A.; Graziano, M. P.; Hughes, M.; MacIntyre, D. E.; Ogawa, A.; O'Neill, K. A.; Iyer, S. P. N.; Shevell, D. E.; Smith, M. M.; Tang, Y. S.; Makarewicz, A. M.; Ujjainwalla, F.; Altmann, S. W.; Chapman, K. T.; Thornberry, N. A. *Proc. Natl. Acad. Sci. U. S. A.* **2005**, *102*, 8132–8137.

(240) Syder, A. J.; Lee, H.; Zeisel, M. B.; Grove, J.; Soulier, E.; Macdonald, J.; Chow, S.; Chang, J.; Baumert, T. F.; McKeating, J. A.; McKelvy, J.; Wong-Staal, F. *J. Hepatol.* **2011**, *54*, 48–55.

(241) Pestka, J. M.; Zeisel, M. B.; Bläser, E.; Schürmann, P.; Bartosch, B.; Cosset, F.-L.; Patel, A. H.; Meisel, H.; Baumert, J.; Viazov, S.; Rispeter, K.; Blum, H. E.; Roggendorf, M.; Baumert, T. F. *Proc. Natl. Acad. Sci. U. S. A.* **2007**, *104*, 6025–6030.

(242) Raghuraman, S.; Park, H.; Osburn, W. O.; Winkelstein, E.; Edlin, B. R.; Rehermann, B. *J. Infect. Dis.* **2012**, *205*, 763–771.

(243) Man John Law, L.; Landi, A.; Magee, W. C.; Lorne Tyrrell, D.; Houghton, M. *Emerg. Microbes Infect.* **2013**, *2*, e79.

(244) Agati, G.; Azzarello, E.; Pollastri, S.; Tattini, M. *Plant Sci.* **2012**, *196*, 67–76.

(245) Bravo, L. *Nutr. Rev.* **1998**, *56*, 317–333.

(246) Shirley, B. *Trends Plant Sci.* **1996**, 377–382.

(247) Tattini, M.; Gravano, E.; Pinelli, P.; Mulinacci, N.; Romani, A. *New Phytol.* **2000**, *148*, 69–77.

(248)   Liu, L.; Gitz, D.; McClure, J. *Physiol. Plant.* **1995**, *93*, 725–733.

(249)   Agati, G.; Stefano, G.; Biricolti, S.; Tattini, M. *Ann. Bot.* **2009**, *104*, 853–861.

(250)   Agati, G.; Matteini, P.; Goti, A.; Tattini, M. *New Phytol.* **2007**, *174*, 77–89.

(251)   Agati, G.; Brunetti, C.; Di Ferdinando, M.; Ferrini, F.; Pollastri, S.; Tattini, M. *Plant Physiol. Biochem.* **2013**, *72*, 35–45.

(252)   Ryan, K. G.; Swinny, E. E.; Winefield, C.; Markham, K. R. *Z. Naturforsch. C.* **2001**, *56*, 745–754.

(253)   Correa, J.; Souza, I.; Ladeira, A. M.; Young, M. C. M.; Aragushi, M. *Allelopath. J.* **2000**, *7*, 225–233.

(254)   Hassan, S.; Mathesius, U. *J. Exp. Bot.* **2012**, *63*, 3429–3444.

(255)   Averett, J.; Banks, W.; Boehme, D. *Biochem. Syst. Ecol.* **1978**, *6*, 6–8.

(256)   Catalano, G.; Fossen, T.; Andersen, Ø. M. *J. Agric. Food Chem.* **1998**, *46*, 4568–4570.

(257)   Do, C.; Cormier, F. *Plant Cell. Tissue Organ Cult.* **1991**, *24*, 49–54.

(258)   Yoshioka, T.; Inokuchi, T.; Fujioka, S.; Kimura, Y. *Z. Naturforsch. C.* **2004**, *59*, 509–514.

(259)   Peer, W. A.; Murphy, A. S. *Trends Plant Sci.* **2007**, *12*, 556–563.

(260)   Van der Meer, I. M.; Stam, M. E.; van Tunen, A. J.; Mol, J. N.; Stuitje, A. R. *Plant Cell* **1992**, *4*, 253–262.

(261)   Mo, Y.; Nagel, C.; Taylor, L. P. *Proc. Natl. Acad. Sci. U. S. A.* **1992**, *89*, 7213–7217.

(262)   Tomas-Barberán, F.; Msonthi, J.; Hostettmann, K. *Phytochemistry* **1988**, *27*, 753–755.

(263)   Salunke, B. K.; Kotkar, H. M.; Mendki, P. S.; Upasani, S. M.; Maheshwari, V. L. *Crop Prot.* **2005**, *24*, 888–893.

(264)   Arts, I. C.; van De Putte, B.; Hollman, P. C. *J. Agric. Food Chem.* **2000**, *48*, 1752–1757.

(265)   Arts, I. C.; van de Putte, B.; Hollman, P. C. *J. Agric. Food Chem.* **2000**, *48*, 1746–1751.

(266)   Drewnowski, A.; Henderson, S. A.; Shore, A. B. *Am. J. Clin. Nutr.* **1997**, *66*, 391–397.

(267)   Kühnau, J. *World Rev. Nutr. Diet.* **1976**, *24*, 117–191.

(268)   Pierpoint, W. S. *Prog. Clin. Biol. Res.* **1986**, *213*, 125.

(269)   Brat, P.; Georgé, S.; Bellamy, A.; Du Chaffaut, L.; Scalbert, A.; Mennen, L.; Arnault, N.; Amior, M. J. *J. Nutr.* **2006**, *136*, 2368.

(270)   Justesen, B. U.; Knuthsen, P.; Andersen, N. L.; Leth, T.; Wine, R. *Scand. J. Nutr.* **2000**, *44*, 158–160.

(271)   Cook, N.; Samman, S. *J. Nutr. Biochem.* **1996**, *2863*, 66–76.

(272)   Hollman, P.; De Vries, J. H. M.; Van Leeuwen, S. D.; Mengelers, M. J. B.; Katan, M. B. *Am. J. Clin. Nutr.* **1995**, *62*, 1276–1282.

(273)   King, R.; Broadbent, J.; Head, R. *J. Nutr.* **1996**, 176–182.

(274)   Manach, C.; Scalbert, A.; Morand, C.; Rémésy, C.; Jiménez, L. *Am. J. Clin. Nutr.* **2004**, *79*, 727–747.

(275)   Spencer, J. P. .; Abd El Mohsen, M. .; Rice-Evans, C. *Arch. Biochem. Biophys.* **2004**, *423*, 148–161.

(276)   Han, J.; Ye, M.; Xu, M.; Sun, J.; Wang, B.; Guo, D. *J. Chromatogr. B. Analyt. Technol. Biomed. Life Sci.* **2007**, *848*, 355–362.

(277)   Barbosa, E.; Calzada, F.; Campos, R. *J. Ethnopharmacol.* **2007**, *109*, 552–554.

(278)   Pietta, P. G. *J. Nat. Prod.* **2000**, *63*, 1035–1042.

(279)   Birt, D. F.; Hendrich, S.; Wang, W. *Pharmacol. Ther.* **2001**, *90*, 157–177.

(280)   Chen, K. *Free Radic. Biol. Med.* **2003**, *35*, 117–132.

(281)   Afanas'ev, I. B.; Dorozhko, A. I.; Brodskii, A. V.; Kostyuk, V. A.; Potapovitch, A. I. *Biochem. Pharmacol.* **1989**, *3*, 1763–1769.

(282)   Morel, I.; Lescoat, G.; Cogrel, P.; Sergent, O.; Pasdeloup, N.; Brissot, P.; Cillard, P.; Cillard, J. *Biochem. Pharmacol.* **1993**, *45*, 13–19.

(283)   Kandaswami, C.; Kanadaswami, C.; Lee, L.-T.; Lee, P.-P. H.; Hwang, J.-J.; Ke, F.-C.; Huang, Y.-T.; Lee, M.-T. *In Vivo* **2005**, *19*, 895–909.

(284)   Yoshida, M.; Sakai, T.; Hosokawa, N.; Marui, N.; Matsumoto, K.; Fujioka, A.; Nishino, H.; Aoike, A. *FEBS Lett.* **1990**, *260*, 10–13.

(285)   Peterson, G.; Barnes, S. *Biochem. Biophys. Res. Commun.* **1991**, *179*, 661–667.

(286)   Coward, L.; Barnes, N. C.; Setchel, K. D. R.; J, S. B. *J. Agric. Food Chem.* **1993**, *41*, 1961–1967.

(287)   Chen, Z. P.; Schell, J. B.; Ho, C. T.; Chen, K. Y. *Cancer Lett.* **1998**, *129*, 173–179.

(288)   Kandaswami, C.; Perkins, E.; Soloniuk, D. S.; Drzewiecki, G.; Middleton, E. *Cancer Lett.* **1991**, *56*, 147–152.

(289)   Duthie, G. G.; Duthie, S. J.; Kyle, J. A. *Nutr. Res. Rev.* **2000**, *13*, 79–106.

(290)   Renaud, S.; de Lorgeril, M. *Lancet* **1992**, *339*, 1523–1526.

(291)   Mennen, L. I.; Malvy, D.; Galan, P.; Preziosi, P.; Bertrais, S.; Bruckert, E.; Maurel, M.; Franchisseur, C.; Hercberg, S. *Nutr. Res.* **2003**, *23*, 879–890.

(292)   Wu, Y.; Wang, F.; Zheng, Q.; Lu, L.; Yao, H.; Zhou, C.; Wu, X.; Zhao, Y. *J. Biomed. Sci.* **2006**, *13*, 569–578.

(293)   Cushnie, T. P. T.; Lamb, A. J. *Int. J. Antimicrob. Agents* **2005**, *26*, 343–356.

(294)   Ferrándiz, M. L.; Alcaraz, M. J. *Agents Actions* **1991**, *32*, 283–288.

(295)   Li, B. Q.; Fu, T.; Dongyan, Y.; Mikovits, J. A.; Ruscetti, F. W.; Wang, J. M. *Biochem. Biophys. Res. Commun.* **2000**, *276*, 534–538.

(296)   Moghaddam, E.; Teoh, B.-T.; Sam, S.-S.; Lani, R.; Hassandarvish, P.; Chik, Z.; Yueh, A.; Abubakar, S.; Zandi, K. *Sci. Rep.* **2014**, *4*, 5452.

(297)   Fesen, M.; Pommier, Y.; Leteurtre, F.; Hiroguchi, S.; Yung, J.; Kohn, K. W. *Biochem. Pharmacol.* **1994**, *48*, 595–608.

(298)   Amoros, M.; Simõs, C.; Girre, L. *J. Nat. Prod.* **1992**, *55*, 1732–1740.

(299)   Vessal, M.; Hemmati, M.; Vasei, M. *Comp. Biochem. Physiol. C. Toxicol. Pharmacol.* **2003**, *135C*, 357–364.

(300)   Tasdemir, D.; Kaiser, M.; Brun, R.; Schmidt, T. J.; Tosun, F.; Rüedi, P.; Yardley, V.; Ru, P. *Antimicrob. Agents Chemother.* **2006**, *50*, 1352–1364.

(301)   Dhanabal, S. P.; Muruganantham, N.; Basavaraj, K. H.; Wadhwani, A.; Shamasundar, N. M. *J. Pharm. Pharmacol.* **2012**, *64*, 1501–1509.

(302)   Onozuka, H.; Nakajima, A.; Matsuzaki, K.; Shin, R.; Ogino, K.; Saigusa, D.; Tetsu, N.; Yokosuka, A.; Sashida, Y.; Mimaki, Y.; Yamakuni, T.; Ohizumi, Y. *J. Pharmacolocy Exp. Ther.* **2008**, *326*, 739–744.

(303)   Geuenich, S.; Goffinet, C.; Venzke, S.; Nolkemper, S.; Baumann, I.; Plinkert, P.; Reichling, J.; Keppler, O. T. *Retrovirology* **2008**, *5*, 27.

(304)   Johari, J.; Kianmehr, A.; Mustafa, M. R.; Abubakar, S.; Zandi, K. *Int. J. Mol. Sci.* **2012**, *13*, 16785–16795.

(305)   Zandi, K.; Teoh, B.-T.; Sam, S.-S.; Wong, P.-F.; Mustafa, M. R.; Abubakar, S. *BMC Complement. Altern. Med.* **2012**, *12*, 214.

(306)   Ma, S.-C.; Du, J.; But, P. P.-H.; Deng, X.-L.; Zhang, Y.-W.; Ooi, V. E.-C.; Xu, H.-X.; Lee, S. H.-S.; Lee, S. F. *J. Ethnopharmacol.* **2002**, *79*, 205–211.

(307)   Li, B.-W.; Zhang, F.-H.; Serrao, E.; Chen, H.; Sanchez, T. W.; Yang, L.-M.; Neamati, N.; Zheng, Y.-T.; Wang, H.; Long, Y.-Q. *Bioorg. Med. Chem.* **2014**, *22*, 3146–3158.

(308)   Cheng, J.; Sun, N.; Zhao, X.; Niu, L.; Song, M.; Sun, Y.; Jiang, J.; Guo, J.; Bai, Y.; He, J.; Li, H. *J. Microbiol. Biotechnol.* **2013**, *23*, 1076–1083.

(309)   Sun, Y.; Song, M.; Niu, L.; Bai, X.; Sun, N.; Zhao, X.; Jiang, J.; He, J.; Li, H. *Pharm. Biol.* **2013**, *51*, 1137–1143.

(310)   Cotin, S.; Calliste, C.-A.; Mazeron, M.-C.; Hantz, S.; Duroux, J.-L.; Rawlinson, W. D.; Ploy, M.-C.; Alain, S. *Antiviral Res.* **2012**, *96*, 181–186.

(311)   Su, Z.-Z.; Dou, J.; Xu, Z.-P.; Guo, Q.-L.; Zhou, C.-L. *Chin. J. Nat. Med.* **2012**, *10*, 415–420.

(312)   Sithisarn, P.; Michaelis, M.; Schubert-Zsilavecz, M.; Cinatl, J. *Antiviral Res.* **2013**, *97*, 41–48.

(313)   Seguin, S. P.; Ireland, A. W.; Gupta, T.; Wright, C. M.; Miyata, Y.; Wipf, P.; Pipas, J. M.; Gestwicki, J. E.; Brodsky, J. L. *Antiviral Res.* **2012**, *96*, 70–81.

(314)   Dou, J.; Chen, L.; Xu, G.; Zhang, L.; Zhou, H.; Wang, H.; Su, Z.; Ke, M.; Guo, Q.; Zhou, C. *Arch. Virol.* **2011**, *156*, 793–801.

(315)   Koyama, J.; Morita, I.; Kobayashi, N.; Konoshima, T.; Takasaki, M.; Osakai, T.; Tokuda, H. *Cancer Lett.* **2008**, *263*, 61–66.

(316)   Inouye, Y.; Yamaguchi, K.; Take, Y.; Nakamura, S. *J. Antibiot. (Tokyo).* **1989**, *XLII*, 1523–1525.

(317)   Cheng, K.; Wu, Z.; Gao, B.; Xu, J. *Cell Biochem. Biophys.* **2014**, *70*, 1305–1309.

(318)   Qi, X.; Yu, H.; Sun, Y.; Cheng, H.; Zhang, C. *J. Pure Appl. Microbiol.* **2013**, *7*, 1317.

(319)   Nayak, M. K.; Agrawal, A. S.; Bose, S.; Naskar, S.; Bhowmick, R.; Chakrabarti, S.; Sarkar, S.; Chawla-Sarkar, M. *J. Antimicrob. Chemother.* **2014**, *69*, 1298–1310.

(320)   Lyu, S.; Rhim, J.; Park, W. *Arch. Pharm. Res.* **2005**, *28*, 1293.

(321)   Sudha, K.; Subhashini, R.; Shobana, K.; Thiagarajan, B. *Int. J. Med. Eng. Inform.* **2012**, *4*, 140.

(322)   Evers, D. L.; Chao, C.-F.; Wang, X.; Zhang, Z.; Huong, S.-M.; Huang, E.-S. *Antiviral Res.* **2005**, *68*, 124–134.

(323)   Yuen, K.; Chen, F.; Chan, K.; Kao, Y. Baicalin and its derivatives as a treatment for SARS coronavirus infection or other related infections. CN 1901921A, 2004.

(324)   Baylor, N.; Fu, T.; Yan, Y.; Ruscetti, F. *J. Infect. …* **1992**, *165*, 433.

(325)   Kusumoto, I.; Hattori, M.; Miyaichi, Y.; Tomimori, T.; Hanaoka, M.; Namba, T. *Shoyakugaku Zasshi* **1991**, *45*, 240.

(326)   Nagai, T.; Miyaichi, Y.; Tomimori, T.; Suzuki, Y.; Yamada, H. *Chem. Pharm. Bull. (Tokyo).* **1990**, *38*, 1329.

(327)   Phosrithong, N.; Samee, W.; Ungwitayatorn, J. *Med. Chem. Res.* **2011**, *21*, 559–567.

(328)   Keum, Y.-S.; Jeong, Y.-J. *Biochem. Pharmacol.* **2012**, *84*, 1351–1358.

(329)   Nishibe, S.; Murai, M. *Food Food Ingred J Jpn* **1995**, *166*, 43.

(330)   Mercader, A. G.; Pomilio, A. B. *Eur. J. Med. Chem.* **2010**, *45*, 1724–1730.

(331)   Zhang, G.-H.; Wang, Q.; Chen, J.-J.; Zhang, X.-M.; Tam, S.-C.; Zheng, Y.-T. *Biochem. Biophys. Res. Commun.* **2005**, *334*, 812–816.

(332)   Liu, A.-L.; Wang, H.-D.; Lee, S. M.; Wang, Y.-T.; Du, G.-H. *Bioorg. Med. Chem.* **2008**, *16*, 7141–7147.

(333)   Schnitzler, P.; Nolkemper, S.; Stintzing, F. C.; Reichling, J. *Phytomedicine* **2008**, *15*, 62–70.

(334)   Wu, T.-S.; Tsang, Z.-J.; Wu, P.-L.; Lin, F.-W.; Li, C.-Y.; Teng, C.-M.; Lee, K.-H. *Bioorg. Med. Chem.* **2001**, *9*, 77–83.

(335)   Pietschmann, T.; Haid, S.; Gentzsch, J.; Grethe, C.; Davioud-Charvet, E.; Lanfranchi, D.-A.; Elhabiri, M.; Benlloch-Martin, X. Flavone derivatives and their use, WO2013139487A1.

(336)   Akihisa, T.; Kawashima, K.; Orido, M.; Akazawa, H.; Matsumoto, M.; Yamamoto, A.; Ogihara, E.; Fukatsu, M.; Tokuda, H.; Fuji, J. *Chem. Biodivers.* **2013**, *10*, 313–327.

(337)   Haid, S.; Novodomská, A.; Gentzsch, J.; Grethe, C.; Geuenich, S.; Bankwitz, D.; Chhatwal, P.; Jannack, B.; Hennebelle, T.; Bailleul, F.; Keppler, O. T.; Poenisch, M.; Bartenschlager, R.; Hernandez, C.; Lemasson, M.; Rosenberg, A. R.; Wong-Staal, F.; Davioud-Charvet, E.; Pietschmann, T. *Gastroenterology* **2012**, *143*, 213–222.e5.

(338)   Calland, N.; Dubuisson, J.; Rouillé, Y.; Séron, K. *Viruses* **2012**, *4*, 2197–2217.

(339)   Nakajima, S.; Watashi, K.; Kamisuki, S.; Tsukuda, S.; Takemoto, K.; Matsuda, M.; Suzuki, R.; Aizaki, H.; Sugawara, F.; Wakita, T. *Biochem. Biophys. Res. Commun.* **2013**, *440*, 515–520.

(340)   Polyak, S. J.; Oberlies, N. H.; Pécheur, E.-I.; Dahari, H.; Ferenci, P.; Pawlotsky, J.-M. *Antivir. Ther.* **2013**, *18*, 141–147.

(341)   Ciesek, S.; von Hahn, T.; Colpitts, C. C.; Schang, L. M.; Friesland, M.; Steinmann, J.; Manns, M. P.; Ott, M.; Wedemeyer, H.; Meuleman, P.; Pietschmann, T.; Steinmann, E. *Hepatology* **2011**, *54*, 1947–1955.

(342)   Colpitts, C. C.; Schang, L. M. *J. Virol.* **2014**, *88*.

(343)   Anggakusuma; Colpitts, C. C.; Schang, L. M.; Rachmawati, H.; Frentzen, A.; Pfaender, S.; Behrendt, P.; Brown, R. J. P.; Bankwitz, D.; Steinmann, J.; Ott, M.; Meuleman, P.; Rice, C. M.; Ploss, A.; Pietschmann, T.; Steinmann, E. *Gut* **2013**, 1137–1149.

(344)   Lan, K.-H.; Wang, Y.-W.; Lee, W.-P.; Lan, K.-L.; Tseng, S.-H.; Hung, L.-R.; Yen, S.-H.; Lin, H.-C.; Lee, S.-D. *Liver Int.* **2012**, *32*, 989–997.

(345)   Duan, D.; Li, Z.; Luo, H.; Zhang, W.; Chen, L.; Xu, X. *Bioorg. Med. Chem. Lett.* **2004**, *14*, 6041–6044.

(346)   Li, Y.; Yu, S.; Liu, D.; Proksch, P.; Lin, W. *Bioorg. Med. Chem. Lett.* **2012**, *22*, 1099–1102.

(347)   Salam, K. A.; Furuta, A.; Noda, N.; Tsuneda, S.; Sekiguchi, Y.; Yamashita, A.; Moriishi, K.; Nakakoshi, M.; Tsubuki, M.; Tani, H.; Tanaka, J.; Akimitsu, N. *J. Nat. Med.* **2013**, *67*, 765–772.

(348)   Takeshita, M.; Ishida, Y.-I.; Akamatsu, E.; Ohmori, Y.; Sudoh, M.; Uto, H.; Tsubouchi, H.; Kataoka, H. *J. Biol. Chem.* **2009**, *284*, 21165–21176.

(349)   Khachatoorian, R.; Arumugaswami, V.; Raychaudhuri, S.; Yeh, G. K.; Maloney, E. M.; Wang, J.; Dasgupta, A.; French, S. W. *Virology* **2012**, *433*, 346–355.

(350)   Liu, M.-M.; Zhou, L.; He, P.-L.; Zhang, Y.-N.; Zhou, J.-Y.; Shen, Q.; Chen, X.-W.; Zuo, J.-P.; Li, W.; Ye, D.-Y. *Eur. J. Med. Chem.* **2012**, *52*, 33–43.

(351)   Kaushik-Basu, N.; Bopda-Waffo, A.; Talele, T. T.; Basu, A.; Costa, P. R. R.; da Silva, A. J. M.; Sarafianos, S. G.; Noël, F. *Nucleic Acids Res.* **2008**, *36*, 1482–1496.

(352)   Shibata, C.; Ohno, M.; Otsuka, M.; Kishikawa, T.; Goto, K.; Muroyama, R.; Kato, N.; Yoshikawa, T.; Takata, A.; Koike, K. *Virology* **2014**, *462-463*, 42–48.

(353)   Weidmann, A. E. *Eur. J. Pharmacol.* **2012**, *684*, 19–26.

(354)   Lou, S.; Zheng, Y.-M.; Liu, S.-L.; Qiu, J.; Han, Q.; Li, N.; Zhu, Q.; Zhang, P.; Yang, C.; Liu, Z. *Planta Med.* **2014**, *80*, 171–176.

(355)   Shen, H.; Yamashita, A.; Nakakoshi, M.; Yokoe, H.; Sudo, M.; Kasai, H.; Tanaka, T.; Fujimoto, Y.; Ikeda, M.; Kato, N.; Sakamoto, N.; Shindo, H.; Maekawa, S.; Enomoto, N.; Tsubuki, M.; Moriishi, K. *PLoS One* **2013**, *8*, e82299.

(356)   Shepard, C. W.; Finelli, L.; Alter, M. J. *Lancet. Infect. Dis.* **2005**, *5*, 558–567.

Chapter II. Synthesis of Flavones and Evaluation of their Antiviral Activity.

In this chapter, we will first describe the different synthetic routes to flavonoids, using either the classic reactions such as the Algar-Flynn-Oyamada reaction or the Baker-Venkataraman rearrangement or the newly developed synthesis using the Suzuki coupling reaction or *o*-alkynoylphenols. The former synthesis used in the laboratory to prepare ladanein will be then commented and special emphasis will be focused afterwards on the significant improvements that have been made during my PhD to finally establish the new improved synthesis. This methodological approach allowed for easy incorporation of functional diversity in the B-ring of the flavone core. Finally, the antiviral activities of ladanein and the newly synthesized analogues will be presented.

2.1. Syntheses of Flavonoids

As previously stated in this manuscript, flavonoids have been extensively studied because of their wide range of biological properties and application as well as their ubiquitously presence in our daily life (human diet such as vegetables, fruits, foods or beverages). It is then not surprising that chemists have been interested in finding routes to synthesize different flavonoids. For instance, Kostanecki described in 1901 how to synthesize coumarins and chromones.[1] Shortly after, in 1908, Auwers reported a reaction allowing the transformation of a flavonol into a coumarone.[2] Since then, the syntheses of flavones and other members of the flavonoid family have been widely studied. Some of the most important flavonoid-forming reactions will be discussed in the following section.

As stated just above, one of the first examples of synthesis of flavonoids was reported by Kostanecki in 1901.[1,3] The reaction involves an alkyl *o*-hydroxyaryl ketone, an aliphatic acid anhydride and the corresponding carboxylate sodium salt to yield coumarins and chromones, depending on the conditions. The proposed mechanism can be found in Scheme 1.

Another reaction discovered in the early 20th century is the Auwers reaction.[2] The Auwers synthesis yields flavonols when using coumarones as starting material (Scheme 2). The product from the aldol condensation between the coumarone and a benzaldehyde can be brominated to yield the flavonol after treatment with KOH.

An important synthetic achievement for the preparation of flavonoids during the 20th century is the Allan-Robinson reaction, reported first in 1924 (Scheme 3).[4] It can be considered a variant of the Kostanecki reaction using aromatic acid anhydrides instead of aliphatic ones.
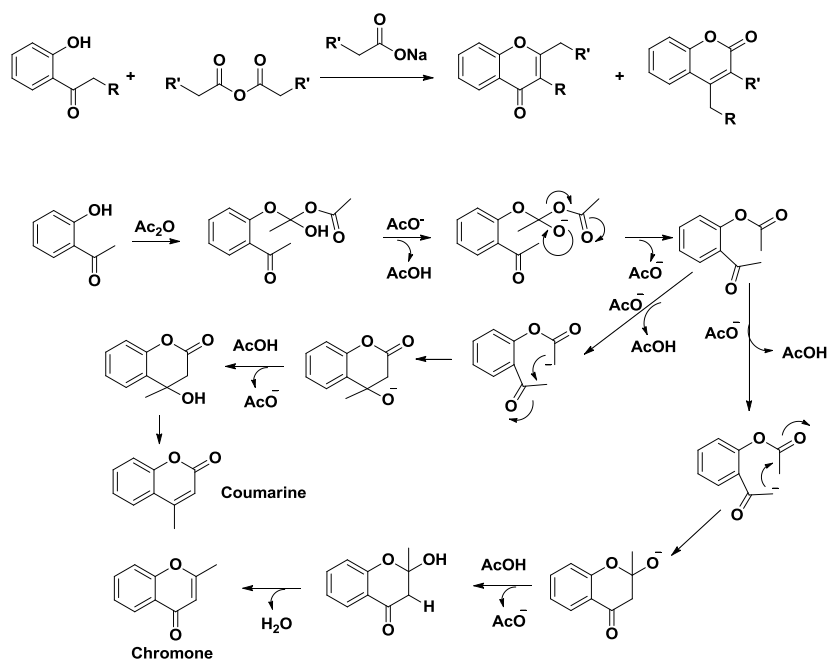
**Scheme 1.** Example and proposed mechanism of the Kostanecki reaction.
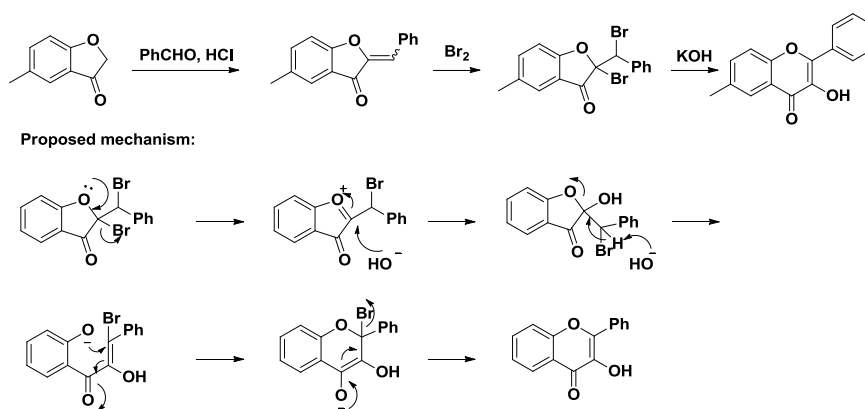
Scheme 2. Example of the Auwers synthesis of flavonols.
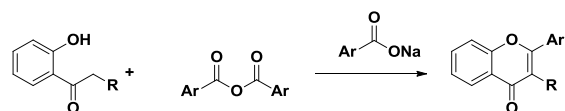

Scheme 3. The Allan-Robinson reaction.

The Baker-Venkataraman rearrangement has been widely used to synthesize flavones since it was first reported in 1933.[5,6] It corresponds to the rearrangement of *o*-acyloxyketones into β-diketones under basic conditions, and it has become a very used reaction in flavone chemistry (Scheme 4).
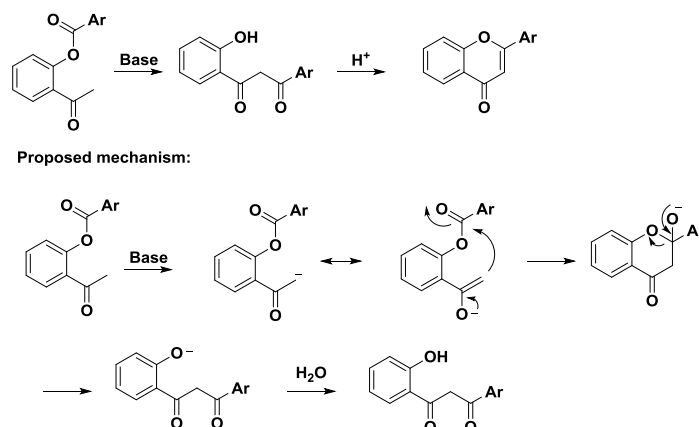
Scheme 4. Mechanism of the Baker-Venkataraman rearrangement.

Finally, the last so called "classic" reaction to synthesize flavonoids is the Algar-Flynn-Oyamada reaction, that proceeds through an oxidative cyclization of 2'-hydroxy-chalcones to yield flavonols or aurones (Scheme 5).[7,8] Depending on the substituents present in the chalcone or the conditions, the formation of flavonols or aurones is favored.
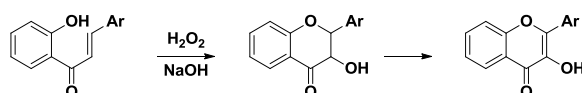
**Scheme 5.** The Algar-Flynn-Oyamada cyclization of chalcones.

The proposed mechanism is depicted in Scheme 6. First, the chalcone is converted to an epoxide, which may suffer a nucleophilic attack on the α-position, leading to an aurone, or in the β position, which leads to a dihydroflavonol that is further oxidized to flavonol.
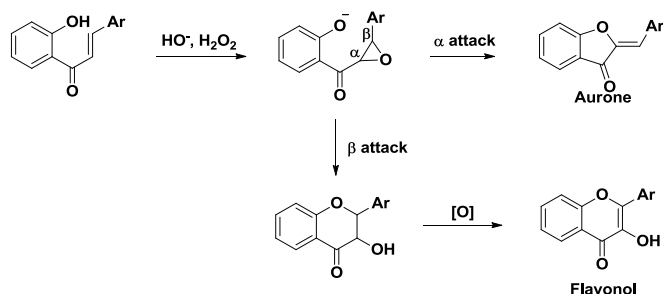
**Scheme 6.** Proposed mechanism for the Algar-Flynn-Oyamada reaction.

Research to find new routes to synthesize flavonoids is still ongoing. For example, Capretta *et al.* reported the use of Sonogashira-Carbonylation-Annulation reaction to form flavones under microwave (MW) irradiation, with moderate to good yields and short reaction times (Scheme 7).[9]

Liang *et al.* also reported the synthesis of flavones through a Sonogashira reaction but using water as solvent.[10] Alper *et al.* reported a similar synthesis of chromones and flavones using ionic liquids.[11]
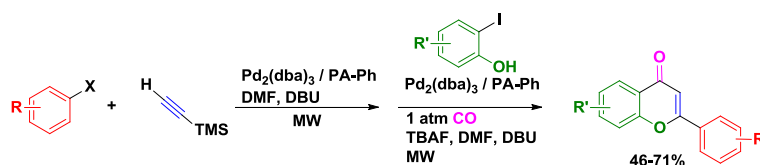

Scheme 7. Use of the Sonogashira cross-coupling to synthesize flavones.

The use of Heck reaction to synthesize *neo*flavones has also been reported.[12] Using a coumarin as starting material, it is reacted with a phenylboronic acid in presence of oxygen, Pd(II) and 1,10-phenantroline as a ligand, giving good yields and regioselectivity (Scheme 8). Interestingly, the reaction works as well when using chromones instead of coumarins to obtain flavones.
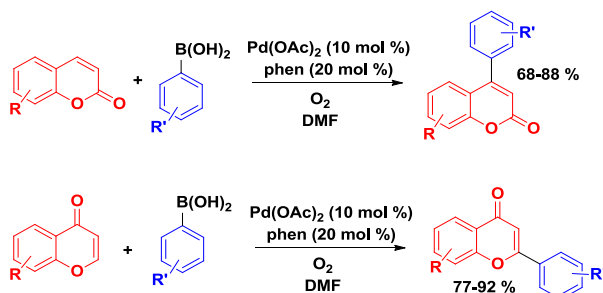
Scheme 8. Formation of *neo*flavones and flavones *via* a Heck reaction.

Chalcones have also been synthesized using the Heck reaction starting from an α,β-unsaturated ketone and an aryl iodide (Scheme 9). The chalcones can then be further cyclized to flavanones or flavones.[13]
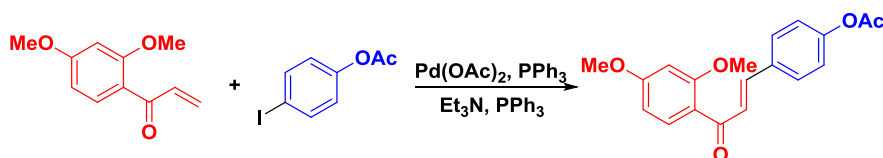
Scheme 9. Heck reaction to form chalcones.

Another cross-coupling reaction was studied by Min *et al.*[14] They reported the C-H functionalization of chromones at C2 position with non-activated arene compounds (Scheme 10). Regioselectivity for this reaction is high and achieved when a carboxylic acid is added to the mixture. If no carboxylic acid is present, the major product is functionalized at the C3 position. A wide range of chromones and arene compounds can be used with good to excellent yields.
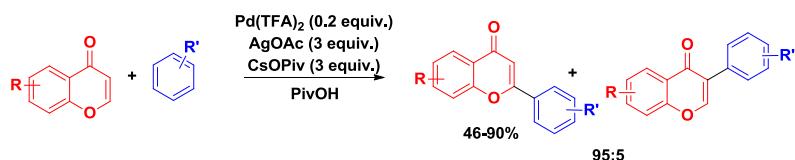
Scheme 10. Regioselective oxidative cross-coupling to yield flavones and isoflavones.

The use of the Suzuki-Miyaura coupling for the synthesis of flavonoids has also been reported. A recent review by van Heerden *et al.* provides a more in-depth discussion about the use of the Suzuki-Miyaura coupling towards the formation of flavonoids.[15] The Suzuki-Miyaura coupling has been successfully used to obtain chalcones[16] and bichalcones,[17] flavones[18] and biflavones,[19] isoflavones[20,21] and neoflavones.[22] Some examples are depicted in Scheme 11.
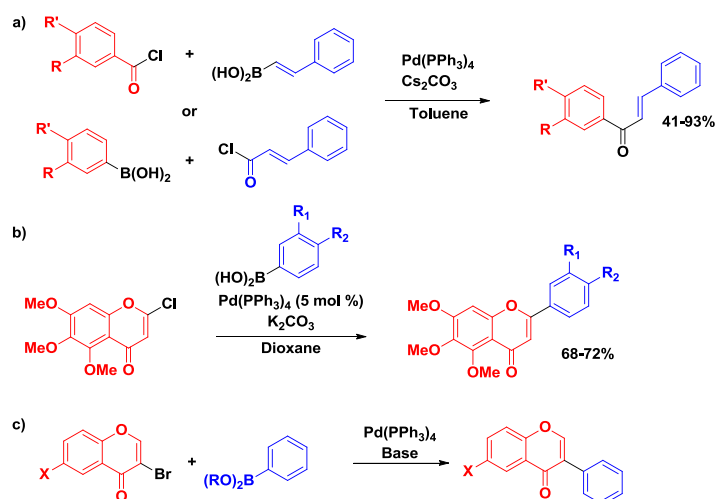

Scheme 11. (*a*) Synthesis of chalcones *via* a Suzuki-Miyaura coupling. (*b*) Synthesis of flavones using chromones and phenylboronic acids. (*c*) Synthesis of *iso*flavones by means of a Suzuki-Miyaura reaction.

The Diels-Alder reaction is a very well-known reaction in which a diene and a dienophile form a 6-membered ring. Among numerous other systems, this reaction has also been applied to the synthesis of flavonoids. Menichetti *et al.* reported the use of a hetero Diels-Alder reaction to synthesize various thiaflavans,[23,24] which can be further oxidized to thiaflavanols (Scheme 12).
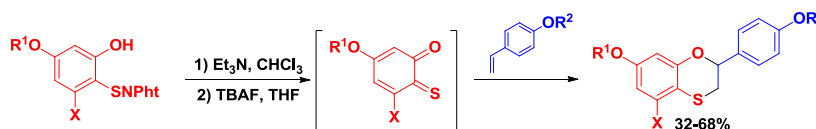
Scheme 12. Synthesis of thiaflavans by means of a Diels-Alder reaction.

Cavaleiro and coworkers reported the synthesis of flavones using a Diels-Alder reaction. However, unlike Menichetti *et al.*, they used the cycloaddition step to build the B-ring instead of the central C-cycle (Scheme 13).[25]
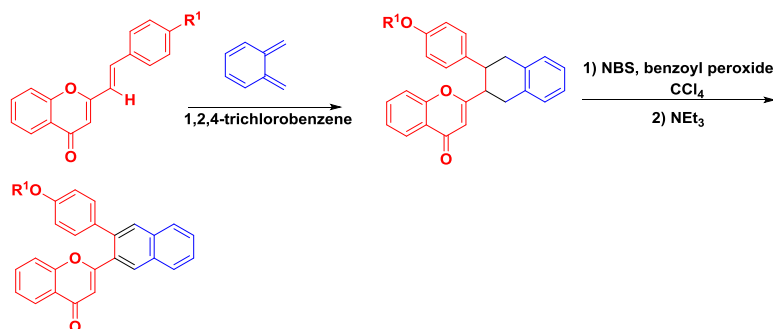
Scheme 13. Synthesis of the B-cycle of a flavone using a Diels-Alder reaction.

Flavans have been synthesized using a tandem one-pot synthesis with a Knoevenagel reaction followed by a Diels-Alder cycloaddition.[26] Using silica-HClO$_4$ as the catalyst, Vishwakarma and coworkers synthesized various flavans starting from phloroglucinol and formaldehyde (Scheme 14). If DDQ is added, the obtained flavans are oxidized to flavones (Scheme 14).
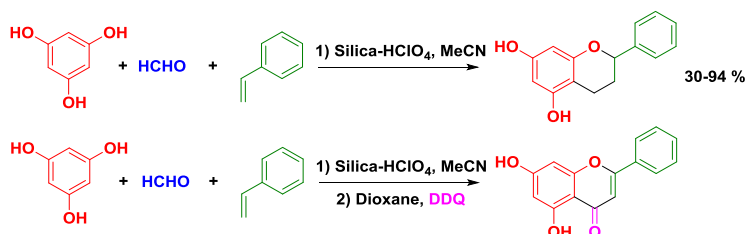
Scheme 14. Synthesis of flavans and flavones using silica-HClO$_4$.

As discussed before, the Algar-Flynn-Oyamada reaction affords flavonols or aurones from chalcones by using hydrogen peroxide. However, other methods can be used in order to form the C-cycle. For instance, FeCl$_3$.6H$_2$O was recently reported to promote ring closure in 2'-amino- and 2'-hydroxy-chalcones to yield quinolines and flavones respectively (Scheme 15).[27]
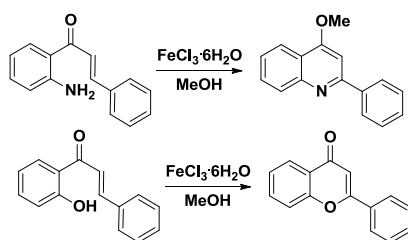
Scheme 15. Formation of flavones from chalcones by C-ring closure promoted by FeCl$_3$.6H$_2$O.

I_2/DMSO and $NaIO_4$/DMSO can also be used to cyclize chalcones into flavones,[28,29] as well as hypervalent iodine reagent such as iodosobenzene diacetate.[30] Chalcones may also be transformed into flavones using a Wacker-related oxidation.[31]

o-Alkynoylphenols have been used to form flavones or aurones. Yoshido and coworkers reported that flavones may be synthesized by means of a TfOH-promoted intramolecular cyclization of *o*-alkynoylphenols (Scheme 16).[32] The reaction was selective yielding only the flavone product and no aurone by-product was formed due to the presence of TfOH.
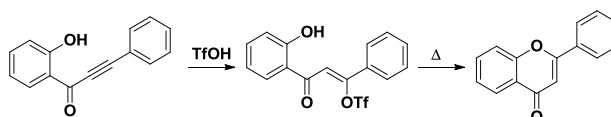
Scheme 16. TfOH-promoted synthesis of flavones from *o*-alkynoylphenol.

Later, the same group reported the use of DMAP as a catalyst for the cyclization reaction of *o*-alkynoylphenols.[33] When using DMAP, flavones were the major product obtained through a 6-*endo* cyclization. Aurones were obtained as the major product through a 5-*exo* cyclization when using K_2CO_3 in EtOH. *O*-alkynoylphenols cyclization is also promoted by Et_2NH,[34] I_2/CAN,[35] KF[36] and palladium.[37]

2.2. Former Synthesis

When this research project started, it was found that the active molecule from the extracts of *Marrubium Peregrinum* was the flavone ladanein. A synthesis was then developed in order to obtain the synthetic version of ladanein and further continue the biological tests. At that time, the main objective was to obtain an appropriate quantity of the product to validate the initial hypothesis that ladanein was the main biologically active compound. In that context, a robust and straightforward synthetic route was designed. This synthesis is depicted in Scheme 17.
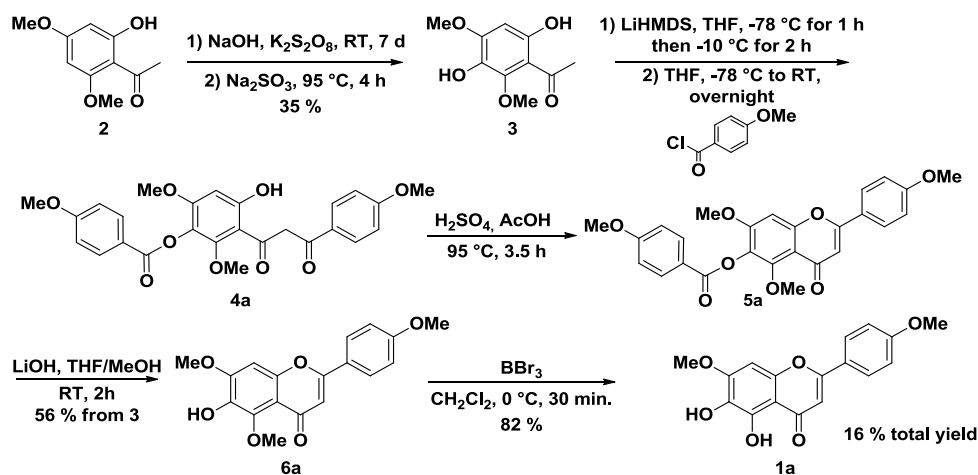
Scheme 17. Former synthesis of ladanein (**1a**) developed in the laboratory.

The synthesis starts from the commercially available 4,6-dimethoxy-2-hydroxy acetophenone **2**, which undergoes an Elbs oxidation[38] in order to form the dihydroxylated acetophenone **3** with 35 % yield after a silica gel column chromatography. Then, treatment with lithium hexamethyldisilazane (LiHMDS) in THF at -78 °C for 1 hour, then -10 °C for 2 hours yields the lithium anion, which is subsequently reacted with commercial 4-methoxybenzoyl chloride, leading to diketone **4a**, which is used without further purification. Compound **4a** was cyclized under acidic conditions in the presence of H_2SO_4 and acetic acid at 95 °C to yield flavone **5a**, which is readily saponified in the presence of LiOH in THF/MeOH. The saponification affords product **6a** in 56 % yield from acetophenone **3**, and it is purified by silica gel column chromatography. Finally, ladanein **1a** is obtained *via* a demethylation step using BBr_3 in dichloromethane. The final product is obtained in 82 % yield after purification through a Sephadex LH-20 column. Ladanein is therefore obtained after a 5-step long sequence with an overall yield of 16 %.

However, the synthetic route has four major drawbacks that needed to be improved. First, the synthesis starts with an Elbs oxidation to form product **3**. This oxidation of compound **2** (a commercially available but rather expensive product, 200 € for 5 g) is a low-yielding reaction (35 % on average) that takes seven days. Furthermore, half of the unreacted starting material **2** has to be recovered by means of an extremely laborious work-up and purification process.

Second, even though LiHMDS, which is used to form the diketone **4**, is commercially available, its quality is inconsistent between different batches, a fact that seriously diminishes the reproducibility and the possibility to scale-up the reaction.

Third, ladanein is obtained after a demethylation step using BBr$_3$. Nevertheless, it undergoes degradation when purification through silica gel column chromatography is attempted. Because of this, a purification using Sephadex LH-20 was necessary in order to obtain pure ladanein **1a**. Sephadex LH-20 is widely used in natural product chemistry. Separation depends on the size of the molecule, adsorption and other mechanisms. To purify ladanein, several consecutive columns were often needed. Sephadex columns need a long preparation and usually take a much longer time than silica gel purifications. Furthermore, even though Sephadex LH-20 can be reutilized, it is a very expensive material (330 € for 50 g).

Finally, products **3** and **6** needed to be purified through time-consuming silica gel column chromatography, a purification method that is much more expensive than recrystallization and is less adapted to industrial processes and large amounts.

Due to these downsides, the first goal of my PhD was to develop a new general synthesis to gain access to different analogues of ladanein in a more efficient manner, in order to continue the biological tests and to tailor new possible formulations.

2.3. Improved Synthesis

It was decided that the same reaction to form the flavone core should be kept, because of its robustness. The first objective was to improve the synthesis of the dihydroxylated acetophenone **3**, the initial precursor of ladanein.

For that, a new pathway was designed starting from the commercially available and cheap syringaldehyde **7** (105 € for 100 g). The proposed synthesis of **3** is depicted in Scheme 18. Through a Baeyer-Villiger reaction, compound **8** could be formed and then yield dihydroquinone **9** after reaction with HCl. After acetylation to yield product **10**, a Fries reaction could yield the desired acetophenone **3**.
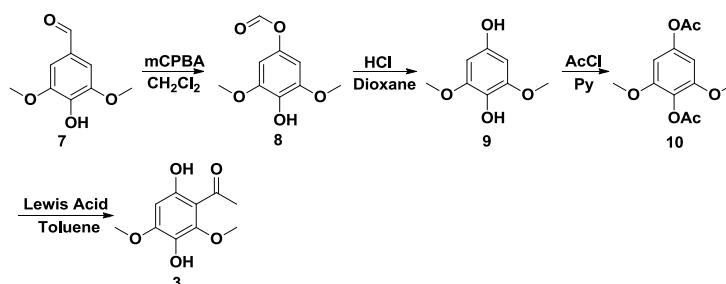
Scheme 18. Designed improved synthesis of acetophenone **3**.

Even though it involved more steps than the previous Elbs oxidation, it was supposed to be a much faster route with better yields. Furthermore, the starting material was far cheaper than the starting material used in the former synthesis.

Nonetheless, reaction of product **8** to yield hydroquinone **9** did not take place. Instead, the corresponding oxidized quinone **11** (Scheme 19) was obtained in 29 % yield after a two day-long reaction and a laborious purification through silica gel column chromatography. This setback was used as a new starting point.

2,6-dimethoxyquinone (**11**) is a commercially available product that is cheaper than 4,6-dimethoxy-2-hydroxy acetophenone (190 € for 25 g). It was used as the starting product for the new synthesis of the initial precursor **3** (Scheme 19). In order to obtain the diacetylated compound **10**, 2,6-dimethoxyquinone undergoes a reductive acetylation in the presence of Zn powder, HCl and acetic anhydride at 0°C for five minutes to yield **10** with quantitative yield.[39]

So as to find the best conditions for the Fries rearrangement, a thorough screening of different Lewis acids and experimental conditions were carried out and are summarized in Table 1. The best conditions were found to be boron trifluoride etherate in toluene under reflux (entry 9). Even though the use of microwave (MW) irradiation (entry 10) afforded acetophenone **3** with slightly increased yield, it was discarded because the scale-up was not possible with the equipment available in the laboratory.

Table 1. Reaction conditions of the screening for the Fries rearrangement.

Entry	Lewis acid	Temp (°C)	Reaction time (h)	Equiv.	Solvent	Yield (3) %
1	$BF_3 \cdot Et_2O$	120	3	20	Toluene	50
2	BCl_3	110	24	3	Toluene	0
3	BBr_3	110	4	3	Toluene	0
4	$B(OH)_3$	70	4	6	THF	0
5	$AlCl_3$	110	2	3	Toluene	0
6	$TiCl_4$	110	72	3	Toluene	30
7	$ZrCl_4$	110	1.5	3	Toluene	0
8	$SnCl_4$	110	2	3	Toluene	0
9	$BF_3 \cdot Et_2O$	110	18	3	Toluene	70
10	$BF_3 \cdot Et_2O$	130 (MW)	1	3	Toluene	85

Finally, using three equivalents of boron trifluoride etherate in toluene at 110 °C overnight, acetophenone **3** was obtained in 70 % yield. A byproduct was obtained in 30 % yield, the acetylated acetophenone **12** (Scheme 19). After a filtration through a silica gel pad, a mixture of **3** and **12** is obtained. Both products can be separated by silica gel column chromatography or recrystallization. However, it is not necessary because the mixture can be used in the next reaction as **12** can be used as starting material to synthesize ladanein as well. It is noteworthy that the quality of $BF_3 \cdot Et_2O$ is very important for the outcome of the reaction. Better yields are obtained with fresh Lewis acid.
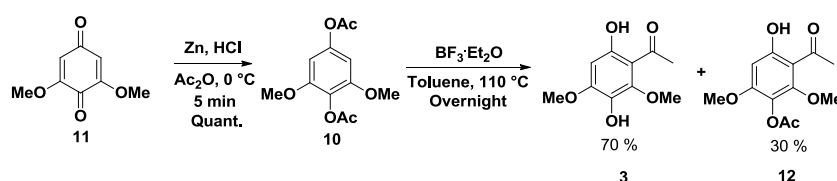
Scheme 19. Improved pathway to initial precursors **3** and **12**.

Both reactions were performed on a 30 g scale and allow the access to initial precursor **3** in one day whereas the old reaction took seven days. The yield is also improved compared to the Elbs oxidation.

The synthesis continues with the formation of the diketone **4**. The reaction is carried out in the presence of LiHMDS. To avoid the reproducibility concerns of the commercial LiHMDS, the base was synthesized reacting freshly distilled HMDS with *n*-BuLi at 0°C,[40] with superior quality and a lower price than the commercially available LiHMDS. The base was added to a solution of acetophenone **3** at -78°C. Once the acetophenone was deprotonated, *p*-methoxybenzoyl chloride was added to the mixture and allowed to react overnight to yield compound **4**. Without further purification, the diketone was cyclized under acidic conditions in the presence of H_2SO_4 and acetic acid, yielding flavone **5**. Saponification to obtain the final precursor **6** was performed with LiOH in a mixture of THF and CH_3OH. After three successive reactions without purification, a silica gel column chromatography was necessary to obtain the desired product with the former synthesis. Nonetheless, the purification had to be done very carefully in order to obtain the product with satisfactory purity.

Hence, a direct recrystallization of the crude mixture was tested. However, too many impurities were present and it was not possible to correctly purify the product by recrystallizing it. It was then decided to design a new work-up protocol (depicted in Figure 1) taking advantage of the acido-basic properties of the flavone.
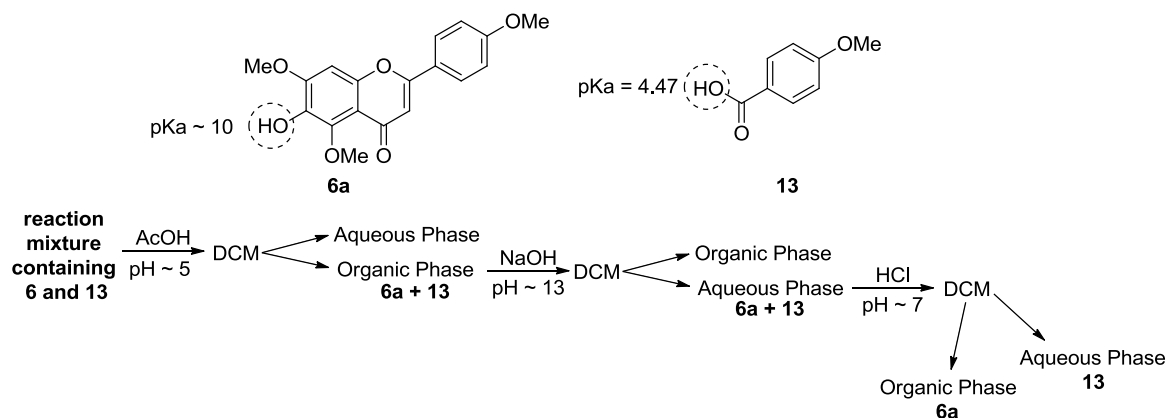
Figure 1. Protonation constants (pK_a) of the flavone (**6a**) and the carboxylic acid (**13**) and work-up strategy to purify **6a**. The pK_a of **6a** was estimated on the basis of the values determined for ladanein (see next chapter) and that of *p*-anisic acid (**13**) is taken from the literature.

After the saponification of **5a**, flavone **6a** is present in the crude product alongside other impurities and carboxylic acid **13**. Once the saponification reaction is complete, acetic acid is added until the pH is around 5. Then, the solution is extracted with DCM. At this point, both the flavone and the carboxylic acid are protonated and present in the organic phase, whereas some impurities are disposed of in the aqueous phase. Subsequently, the organic phase is thoroughly washed with NaOH, so that both the flavone and *p*-anisic acid are deprotonated and present in the aqueous phase. Careful acidification to pH 7 and subsequent extraction with DCM allows separating the carboxylic acid from the flavone, because the latter is protonated and is transferred to the organic phase while the acid remains deprotonated and remains soluble in the aqueous phase. Finally, final precursor **6a** can be recrystallized from water/EtOAc with 72 % yield.

The final drawback of the former synthesis was the use of a Sephadex LH-20 column after the demethylation step with BBr_3 in order to purify ladanein, since it is sensitive to silica gel and decomposes in its presence. Therefore, a direct recrystallization after the demethylation reaction was attempted, but with unsatisfactory results. A reaction with a different demethylating agent ($AlCl_3$ in the presence of NaI) was tested as well, but it leads to polymerization of the product. Finally, $MgBr_2 \cdot Et_2O$ in acetonitrile at 80°C yielded 75 % of the desired product **1a** after recrystallization from DCM. This inexpensive Lewis acid was easily synthesized from magnesium turnings and 1,2-dibromoethane.[41]

Reactions from the mixture of **3** and **12** to the demethylation step with $MgBr_2.Et_2O$ were performed in a 5 g scale. The improved synthetic pathway is depicted in Scheme 20. It is a 6-step long sequence with 54 % overall yield that can be performed in a week and with no chromatographic purification needed.
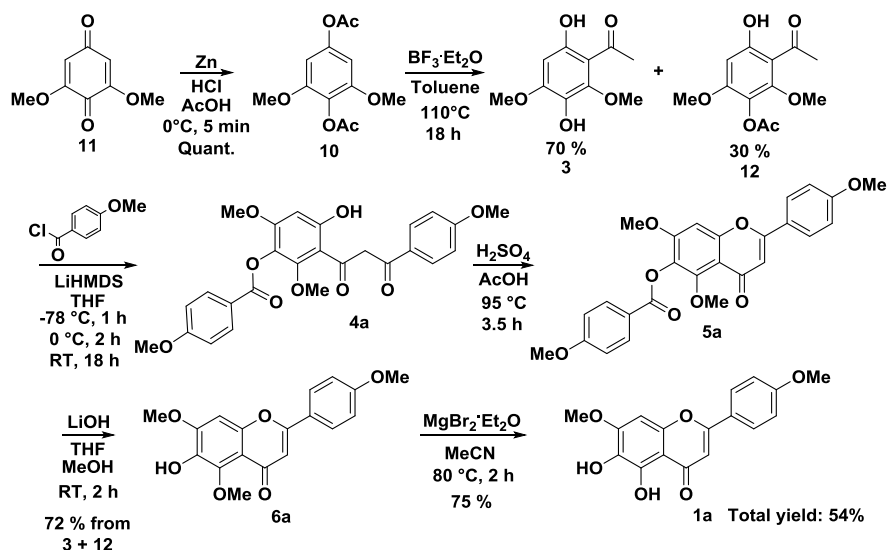
Scheme 20. Improved synthetic route to ladanein.

Analogues bearing different groups in the 4'-position were easily synthesized using the same pathway as ladanein **1a**, using a different acyl chloride after the obtention of the mixture of **3** and **12**. Our synthetic approach revealed to be a robust and straightforward synthetic route and allowed the introduction of diverse functionality on the B-ring while maintaining intact the A- and C-rings which are expected to be of crucial importance for the antiviral properties. As can be seen from **Figure 2**, the other analogues were obtained in a lower overall yield. It is important to note that these yields are not optimized. However, the lower yields could be due to the formation of a 3' product after opening of the flavones during the cyclization. Also, it is possible that the diketone **4**, which is in equilibrium with the corresponding enol form, is not as reactive for the rest of coumpounds.
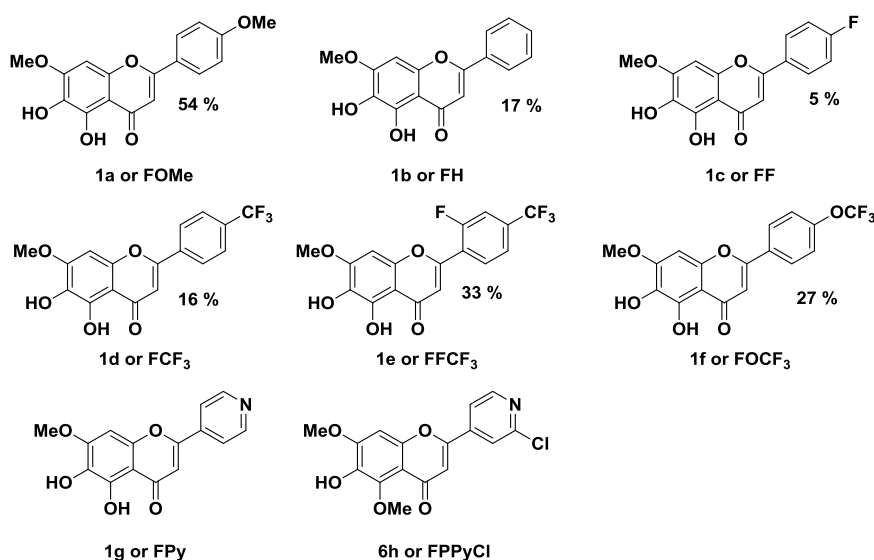

Figure 2. Different analogues prepared using the improved route.

One of the shortcomings of this synthetic approach to flavones can be seen with the synthesis of analogues **1g** and **6h**. Indeed, since both molecules possess another atom that can be protonated, the acido-basic work-up is therefore not well adapted for the synthesis of these compounds. A new work-up procedure or purification through silica gel column chromatography is thus needed to isolate the pure products.

2.4. Pricing of the Synthetic Ladanein

As discussed in a previous section, there are many new DAAs and other therapeutic agents already on the market or in the final stages of development. Nonetheless, the price of these new drugs is so high ($84,000 for Sofosbuvir and $66,000 for Simeprevir) that people on low-income countries, which account for 80 % of the global HCV infected people, have no access to these highly potent compounds. Furthermore, there is a big debate within insurance companies in the United States on whether or not they are going to pay for such expensive treatments. Hence, even in developed countries only people with a good insurance will be eligible for treatment with the newly developed drugs. It is therefore of crucial interest to develop new compounds that have a lower price and that can be accessible to most of the infected individuals.

Previously, it was discussed that ladanein can be extracted from plants. Also two syntheses were developed in our team. It was deemed interesting to calculate how much would cost to obtain one gram of ladanein with the different methods to obtain it.

The process to extract ladanein from plants was described by Thierry Hennebelle in his PhD thesis (University of Lille, 2006) and is depicted in Figure 3. In order to obtain 1 g of ladanein from dried plants, it would be necessary to start from 3.125 kg of dried *Marrubium Peregrinum* L. The dried matter should be turned into powder and then put in contact with 12.5 L of DCM during 24 h for the first extraction. This process should be repeated twice, so that the first step is 3 days long and needs 37.5 L of DCM. Once evaporated, 100 g of extract would be obtained. To further purify this extract, a Sephadex LH-20 column would be needed. Then, with the 1.55 g of flavone mixture obtained after the Sephadex column, a silica gel column chromatography should be performed to finally yield 1 g of ladanein. This method is clearly not well adapted to obtain bulk quantities of flavone because it is very time-consuming, expensive and would require a huge amount of solvents and purification materials. Only the 37.5 L of dichloromethane used for the first extraction already costs more (80 €) than obtaining 1 g of ladanein with the improved synthesis, without adding the costs of the Sephadex LH-20, silica gel and the solvents needed to perform the columns.
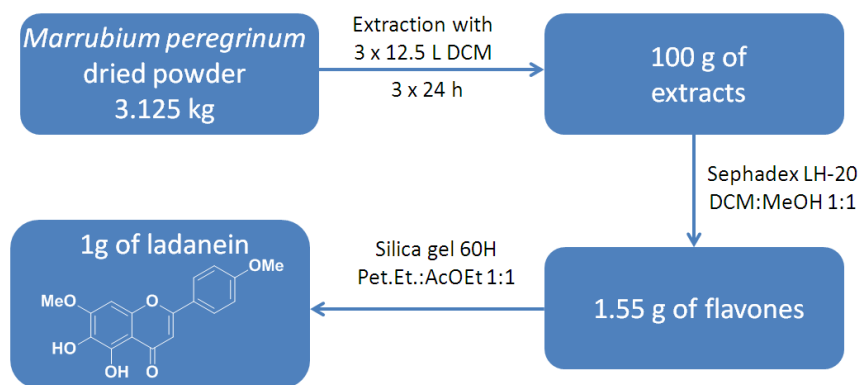
Figure 3. Process necessary to obtain 1 g of ladanein from dried plant matter.

For the former and the new synthesis, prices have been calculated for each step taking into account reagents, solvents and other necessary chemicals such as silica gel and magnesium sulfate. Table 2 summarizes the cost of each step for both syntheses as well as the total cost to obtain 1 g of pure ladanein.

Table 2. Step by step and total costs of both the former and improved syntheses. (*) The price of Sephadex LH-20 is not taken into account for this step since it can be reused.

For 1 g of pure ladanein	Former synthesis	New synthesis
Elbs oxidation	€120	-
Reductive acetylation	-	€13
Fries rearrangement	-	€12
Baker-Venkataraman	€15	€7
Cyclisation	€0.5	€0.5
Saponification	€21	€1
Demethylation	€21*	€1.50
Total	€177.5	€35

As it can be seen, the new synthesis affords pure ladanein with a much lower price than the former synthesis. The initial precursor was obtained *via* an Elbs oxidation from an expensive starting material, whereas now it can be obtained in two steps with high yield and from a cheap starting material, which significantly brings down the cost. Also, since no chromatographic column is needed, the use of expensive silica gel can be avoided. Synthesizing the LiHMDS needed for the formation of diketone **4** instead of using the commercial one divides the cost of this step by two, ensuring reproducibility at the same time. Cyclization remains unchanged between both syntheses. The formation of the final precursor **6** is much cheaper because of the new work-up procedure developed

and the avoidance of a silica gel chromatographic column. Finally, using $MgBr_2.Et_2O$ instead of BBr_3 also brings down the price of the demethylation step. It is noteworthy that because Sephadex LH-20 can be reutilized several times, its price has not been taken into account for this comparison. Also, the salary of the staff needed to perform the synthesis has not been taken into account. Overall, the old synthesis is more than five times as expensive as the newly developed one. Human costs (*i.e.* time spent on the synthesis of ladanein) were not taken into account for this comparison and would undoubtedly widen the gap between the two synthetic routes.

2.5. Antiviral Activities

The antiviral activities of the newly synthesized compounds were measured in close collaboration with the group of Prof. Thomas Pietschmann (HCV virologist, Department of Experimental Virology, TWINCORE - Centre for Experimental and Clinical Infection Research, Hannover, Germany). The results are depicted in Figure 4.
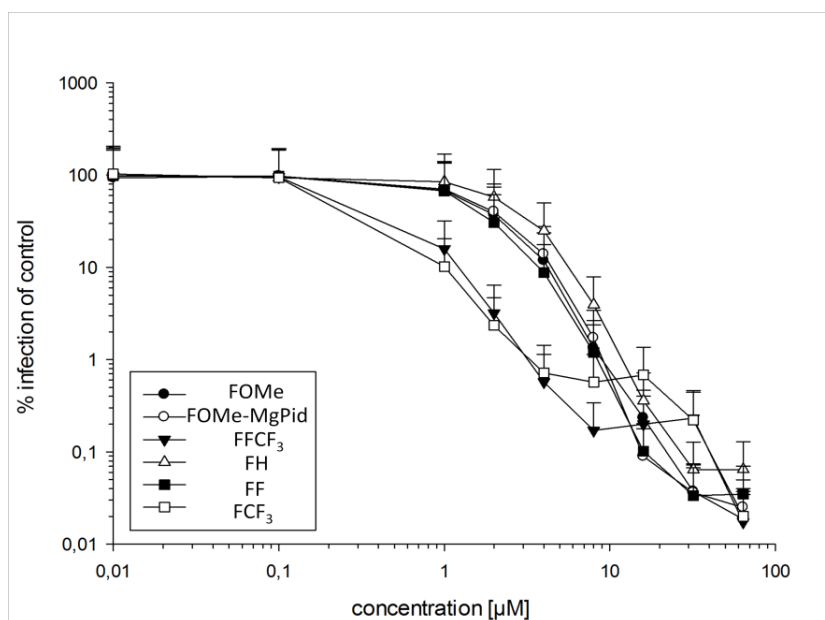
Figure 4. Anti-HCV activities of ladanein **FOMe**, its analogues and its magnesium pidolate complex. Summary of four independent experiments. Jc-R2a reporter virus was preincubated with indicated concentration of inhibitors for 30 min at 37 °C prior to infection of Huh-7.5 cells. Cells were subsequently lysed for 72 h and luciferase activity was then measured.[42]

As it can be observed, most of the compounds tested (**FOMe/1a**, **FH/1b**, **FF/1c**, **FCF₃/1d**, **FFCF₃/1e** and **FOCF₃/1f**, Figure 2 and Table 3) display comparable anti-HCV activities. Nonetheless, three compounds stand out of the rest with an improved antiviral activity, namely **FCF₃/1d** (black triangles, Figure 2), **FFCF₃/1e** (white squares, Figure 2) and **FOCF₃/1f** (Table 3). It is noteworthy that for a same compound (*e.g.* ladanein **FOMe**), two different but rather close EC_{50} values were obtained and can be

explained by the fact that they were measured from two different batches originating from the former (BJ486K) and the new syntheses. Interestingly, the presence of the highly electron-withdrawing groups CF_3 and OCF_3 is much likely one of the determining factors that improve the antiviral activity of these compounds, demonstrating that further subtle modification of the B-ring could still lead to an improvement of the antiviral properties. The EC_{50} values obtained for the flavones are summarized in Table 3. This enhanced activity may be due to an improved solubility of the fluorine-containing analogues as well as halogen bonding.

Table 3. EC_{50} values obtained for the different analogues.

Compounds	EC_{50} (µM)
FOMe/1a	1.6[a] / 2[b]
FH/1b	2.4[a]
FF/1c	1.4[a]
FCF$_3$/1d	0.3[c] / 0.2[c]
FFCF$_3$/1e	0.36[a]
FOCF$_3$/1f	0.3[d]
[a] New synthesis. [b] Former synthesis (labeled BJ486K). [c] Former synthesis (labeled BJ751-1). [d] Former synthesis (labeled BJ755-3)	

2.6. Conclusion

In conclusion, a new straightforward, cheap, less-time consuming and purification-free synthesis of flavones has been developed. The former synthesis used in the laboratory involved an expensive starting material, low-yielding reactions and time-consuming purification steps either by silica gel column chromatography or Sephadex LH-20. The improved synthesis is based on two high yielding reactions leading to initial precursors **3** and **12** *via* a reductive acetylation and a Fries rearrangement, respectively. This approach to the initial precursor is much faster and with better yield. The formation of the flavone is done by a Baker-Venkataraman reaction followed by an acidic cyclization. The use of freshly prepared LiHMDS allows for better reproducibility. The work-up procedure taking advantage of the acido-basic properties of the flavone allows us to obtain the final precursor **6** without purification through silica gel column chromatography, which was necessary with the previous synthetic route. Finally, the desired flavone is obtained by means of a demethylation step using $MgBr_2$ etherate and not BBr_3, yielding the pure product after recrystallization instead of the expensive and time-consuming Sephadex LH-20 column. Furthermore, the newly developed route

provides a much cheaper access to the desired compound. Overall, the new synthesis allows us to obtain ladanein with 54 % overall yield in the course of a week whereas the former synthesis yielded the desired compound with 16 % yield in three weeks time.

This synthetic route has been successfully applied to different ladanein analogues which differ by the substitution pattern on the B-ring. Introduction of electron-withdrawing substituents on the B-cycle (*i.e.* fluoride containing moieties) still led to efficient anti-HCV compounds with improved antiviral activities (*i.e.* from 5 to 10-fold decrease of the EC_{50} with respect to flavone lacking substituent on the B-ring).

EXPERIMENTAL SECTION

Generality

Commercially available starting materials were purchased from Sigma-Aldrich, ABCR GmbH & Co. KG, Alfa Aesar, and Apollo Scientific and were used without further purification. Solvents were obtained from Sigma-Aldrich and Carlos Erba. Unless noticed reagent grade was used for reactions and column of chromatography and analytical grade was used for recrystallization. Dichloromethane (DCM) was distilled over CaH_2 under argon. Tetrahydrofuran (THF) was dried by passage through an activated alumina column under argon. Hexamethyldisilazane (HMDS) was freshly distilled before use.

All reactions were performed in standard glassware. Microwave reactions were carried out on a Biotage Initiator™ apparatus; supplier standard microwave vials were used. Thin Layer Chromatography (TLC) were used to monitor reactions (*vide infra*).

Crude mixtures were purified either by recrystallization or by flash column chromatography. The latter were performed using silica gel 60 (230-400 mesh, 0.040-0.063 mm) purchased from E. Merck. Automatic flash chromatographies were carried out in a Biotage Puriflash apparatus with UV-Vis detection at 254 nm (unless otherwise specified).

Monitoring and primary characterization of products were achieved by Thin Layer Chromatography on aluminum sheets coated with silica gel 60 F254 purchased from E. Merck. Eluted TLC's were revealed under UV (325 nm and 254 nm).

Nuclear Magnetic Resonance (NMR) spectra were recorded on a Bruker AC 300 or Bruker AC 400 with solvent peaks as reference. Carbon multiplicities were assigned by Distortionless Enhancement by Polarization Transfer (DEPT) experiments. In the following NMR assignments, coupling constants (*J*) will be expressed in Hertz (Hz), multiplicity are described with (s) as singlet, (d) as doublet, (t) as triplet and (q) as quadruplet.

Infrared (IR) spectra (cm^{-1}) were recorded neat on a Perkin-Elmer Spectrum One Spectrophotometer. HRMS were obtained from "Service commun d'analyses" from the University of Strasbourg. Melting points were measured on a Stuart Melting Point 10 apparatus and are given uncorrected; when measured after recrystallization, the solvent is mentioned between brackets. (dec = decomposition).

In the following sections, solvents will be abbreviated as follows: DCM: dichloromethane; EtOAc: Ethyl acetate; Tol.: toluene; Et_2O: diethyl ether; THF: tetrahydrofurane; MeOH: methanol.

Synthesis of the Flavones

4-(Acetyloxy)-3,5-dimethoxyphenyl Acetate (10)
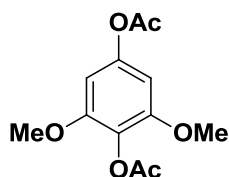
White solid
Chemical formula: $C_{12}H_{14}O_6$
Molecular weight: 254.24 g/mol
Yield: quantitative

A cold (0 °C) solution of concentrated HCl (40 mL, excess) and Ac2O (225 mL, excess) was added to a mixture of 2,6- dimethoxy-1,4-benzoquinone (11) (9.90 g, 59 mmol, 1 equiv) and activated Zn powder (29.03 g, 444 mmol, 7.5 equiv). The mixture was stirred at 0 °C for 5 min. Et_2O (300 mL) was added, and the solid was filtrated. The organic phase was washed with water and brine, dried over magnesium sulfate, and concentrated under reduced pressure, adding toluene to coevaporate the acetic acid, to yield a white solid (14.62 g, 58 mmol, quantitative yield).
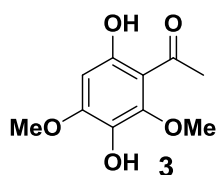
^{1}H NMR (CDCl$_3$; 300 MHz): δ (ppm) 6.40 (s, 2 H), 3.81 (s, 6 H), 2.34 (s, 3 H), 2.31 (s, 3 H)
^{13}C NMR (CDCl$_3$; 75 MHz): δ (ppm) 169.4, 168.8, 152.6, 149.1, 126.6, 99.1, 56.4, 21.3, 20.6
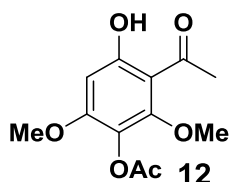**mp**: 126 °C
IR (neat, cm^{-1}): 1754, 1615, 1504, 1423, 1179, 1129, 1018, 983, 909, 831, 567

1-(3,6-Dihydroxy-2,4-dimethoxyphenyl)ethan-1-one (3) and 3-Acetyl-4-hydroxy-2,6-dimethoxyphenyl Acetate (12)

Yellow solid
Chemical formula: $C_{10}H_{12}O_5$
Molecular weight: 212.20 g/mol

White solid
Chemical formula: $C_{12}H_{14}O_6$
Molecular weight: 254.24 g/mol

$BF_3 \cdot Et_2O$ (15 mL, 118.4 mmol, 3 equiv) was added dropwise to a solution of 4-(acetyloxy)-3,5-dimethoxyphenyl acetate 10 (10.04 g, 39.5 mmol, 1 equiv) in tol. (200 mL), and the mixture was heated to 110 °C for 18 h. Then, water (100 mL) and a saturated solution of NH4Cl (100 mL) were added, and the aqueous phase was extracted three times with EtOAc. The separated organic layer was washed with water and brine, dried over magnesium sulfate, and concentrated under reduced pressure to yield a brown solid. The solid was diluted in DCM, filtered through silica gel, and solvent evaporated under reduced pressure to yield a mixture of 3 and 12 (yellow solid, 8.84 g of a 67:33 mixture of 3 (70% corrected yield) and 12 (30% corrected yield)). The solid was used without further purification.

For product **3**:

^{1}H NMR (CDCl$_3$; 300 MHz): δ (ppm) 13.20 (s, 1 H), 6.28 (s, 1 H), 5.10 (s, 1 H), 3.98 (s, 3 H), 3.94 (s, 3 H), 2.69 (s, 3 H)
^{13}C NMR (CDCl$_3$; 75 MHz): δ (ppm) 203.6, 159.1, 154.3, 147.6, 131.5, 108.7, 95.7, 60.9, 56.5, 31.8
mp: 162 °C
IR (neat, cm^{-1}): 3261, 1630, 1594, 1499, 1433, 1230, 1078, 959, 892, 820, 593

For product **12**:

^{1}H NMR (CDCl$_3$; 300 MHz): 13.52 (s, 1 H), 6.31 (s, 1 H), 3.91 (s, 3 H), 3.86 (s, 3 H), 2.67 (s, 3 H), 2.36 (s, 3 H)
^{13}C NMR (CDCl$_3$; 75 MHz): 203.3, 168.9, 163.9, 158.5, 154.6, 125.8, 108.6, 96.7, 61.6, 56.5, 31.8, 20.6
**mp**: 103 °C
IR (neat, cm^{-1}): 1762, 1594, 1444, 1360, 1261, 1202, 1156, 1103, 1080, 926, 817, 503

General Procedure for the Synthesis of the Final Precursors

A solution of LiHMDS was prepared by adding *n*-BuLi (1.6 M in hexane, 7.5 equiv.) to a solution of freshly distilled HMDS (7.9 equiv.) in dry THF at 0 °C. The mixture was stirred at that temperature for 30 min and then was added dropwise to a mixture of product **3** and **12** in dry THF under Ar atmosphere and at -78 °C. The mixture was stirred for 1 h at -78 °C, 2 h at -10 °C and cooled down again to -78 °C. A solution of the respective benzoyl chloride (2 equiv.) in dry THF was added and the reaction was stirred for 1 h at -78 °C and at RT overnight. The solution was then poured into a mixture of crushed ice and concentrated HCl, extracted three times with DCM, dried over MgSO$_4$ and the solvent was removed under reduced pressure to yield a brown solid which was used without further purification.

Then, the crude was dissolved in acetic acid and H$_2$SO$_4$ was added. The mixture was stirred at 95 °C for 3.5 h to 6 h. The solvent was then evaporated under reduced pressure, water was added and the aqueous phase was extracted three times with DCM. The organic phase was dried over Mg SO$_4$ and the solvent was evaporated under reduced pressure to yield a dark brown solid which was used without further purification.

Finally, the crude product was dissolved in THF and a solution of LiOH (excess) in MeOH was added. The reaction was stirred at RT for 2 h. Then, the solution was poured into water, and AcOH was added until the pH was around 5. The aqueous phase was extracted three times with DCM, and the organic phase was thoroughly washed with a 0.5 M solution of NaOH. The aqueous phase was then acidified to neutral pH with a 1 M solution of HCl, and the aqueous phase was extracted three times with DCM. After concentration under reduced pressure and a recrystallization from water/EtOAc, the pure desired final precursor was obtained.

6-Hydroxy-5,7-dimethoxy-2-(4-methoxyphenyl)-4H-chromen-4-one (6a)
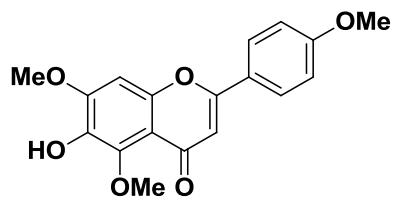
Light-brown solid
Chemical formula: $C_{18}H_{16}O_6$
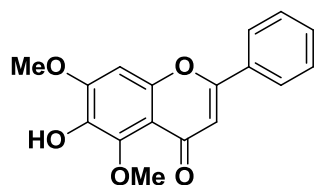**Molecular weight: 328.32 g/mol**
Yield: 72 %

Synthesized from a mixture of product **3** and **12** (4.94 g) using the procedure described above to obtain 5.15 g (15.7 mmol, 72 % yield).

^{1}H NMR (CDCl$_3$; 300 MHz): δ (ppm) 7.84 (d, *J* = 8.9 Hz, 2 H), 7.02 (d, *J* = 8.9 Hz, 2 H), 6.84 (s, 1 H), 6.61 (s, 1 H), 5.93 (s, 1 H), 4.04 (s, 3 H), 4.03 (s, 3 H), 3.90 (s, 3 H)
^{13}C NMR (CDCl$_3$; 75 MHz): δ (ppm) 177.0, 162.1, 161.4, 152.1, 151.9, 144.0, 136.6, 127.6, 124.0, 114.4, 112.3, 106.9, 96.2, 62.6, 56.4, 55.5
mp: 222-223 °C
IR (neat, cm^{-1}): 3281, 1602, 1498, 1358, 1249, 1182, 1111, 838, 827, 555

6-hydroxy-5,7-dimethoxy-2-phenyl-4H-chromen-4-one (6b)

Light-brown solid
Chemical formula: $C_{17}H_{14}O_5$
Molecular weight: 298.29 g/mol
Yield: 21 %

Synthesized from product **12** (0.582 g, 2.29 mmol) using the procedure described above to obtain 142 mg (0.48 mmol, 21 % yield).

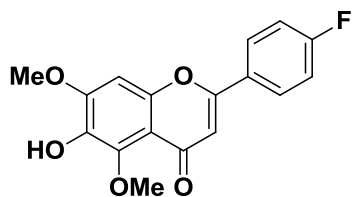**^{1}H NMR (CDCl$_3$; 300 MHz)**: δ (ppm) 7.90 (m, 2 H), 7.53 (m, 3 H), 6.88 (s, 1 H), 6.71 (s, 1 H), 5.96 (s, 1 H), 4.05 (s, 6 H).
^{13}C NMR (CDCl$_3$; 75 MHz): δ (ppm) 177.3, 161.6, 152.5, 152.3, 144.2, 137.0, 131.9, 131.5, 129.2, 126.2, 114.2, 112.6, 108.4, 96.5, 62.8, 56.7.
mp: 211-212 °C
IR (neat, cm^{-1}): 3261, 1633, 1596, 1463, 1359, 1201, 1109, 949, 768, 686

6-Hydroxy-5,7-dimethoxy-2-(4-fluorophenyl)-4H-chromen-4-one (6c)

Brown solid
Chemical formula: $C_{17}H_{13}FO_5$
Molecular weight: 316.28 g/mol
Yield: 10 %

Synthesized from product **3** (1 g, 4.71 mmol) using the procedure described above to obtain 149 mg (0.47 mmol, 10 % yield).

^{1}H NMR (CDCl$_3$; 300 MHz): δ (ppm) 7.90 (dd, *J* = 8.9 Hz, 5.4 Hz, 2H), 7.22 (t, *J* = 8.9 Hz, 2H), 6.86 (s, 1H), 6.65 (s, 1H), 5.91 (s, 1H), 4.04 (s, 6H)
^{13}C NMR (DMSO-*d$_6$*; 75 MHz): δ (ppm) 175.8, 162.7, 159.1, 153.5, 150.8, 144.2, 137.7, 128.6 (d, *J* = 9.3 Hz), 127.7 (d, *J* = 3.2 Hz), 116.1 (d, *J* = 21.9 Hz) 112.0, 107.2, 96.8, 61.2, 56.3
mp: 244-245 °C
IR (neat, cm^{-1}): 3324, 1635, 1600, 1200, 1095, 1038, 849, 812, 550, 505, 470

6-Hydroxy-5,7-dimethoxy-2-(4-(trifluoromethyl)phenyl)-4H-chromen-4-one (6d)
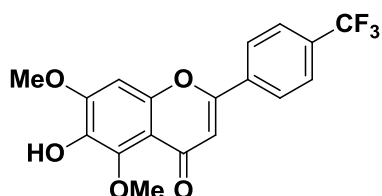
Light-brown solid
Chemical formula: $C_{18}H_{13}F_3O_5$
Molecular weight: 366.29 g/mol
Yield: 27 %

Synthesized from product **3** (1 g, 4.71 mmol) using the procedure described above to obtain 465 mg (1.27 mmol, 27 % yield).

^{1}H NMR (MeOD; 300 MHz): δ (ppm) 8.24 (d, *J* = 8.5 Hz, 2H), 7.90 (d, *J* = 8.5 Hz, 2H), 7.18 (s, 1H), 6.87 (s, 1H), 4.07 (s, 3H), 3.91 (s, 3H)
^{13}C NMR (DMSO-*d$_6$*; 75 MHz): δ (ppm) 175.7, 158.3, 153.7, 150.8, 144.2, 137.8, 135.1, 131.2 (q, *J* = 33 Hz), 126.8, 125.9 (q, *J* = 4.7 Hz), 125.7, 112.2, 108.8, 96.8, 61.2, 56.3
mp: 247-248 °C
IR (neat, cm^{-1}): 3315, 1316, 1297, 1109, 1093, 1065, 1013, 855, 832, 817, 503

2-(2-fluoro-4-(trifluoromethyl)phenyl)-6-hydroxy-5,7-dimethoxy-4H-chromen-4-one (6e)
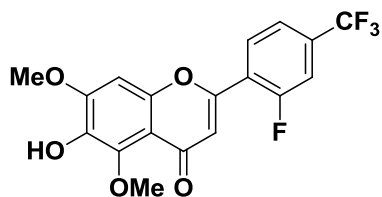
Light-brown solid
Chemical formula: $C_{18}H_{12}F_4O_5$
Molecular weight: 384.28 g/mol
Yield: 42 %

Synthesized from product **12** (0.995 g, 3.93 mmol) using the procedure described above to obtain 629 mg (1.64 mmol, 42 % yield).

^{1}H NMR (DMSO-d_6; 300 MHz): δ (ppm) 9.21 (s, 1H), 8.27 (t, *J* = 8.5 Hz, 1H), 8.00 (d, *J* = 11.1 Hz, 1H), 7.85 (d, *J* =8.5 Hz, 1H), 7.16 (s, 1H), 6.68 (s, 1H), 3.97 (s, 3H), 3.79 (s, 3H)
^{13}C NMR (CDCl$_3$; 75 MHz): δ (ppm) 175.3, 161.0, 157.6, 154.4, 153.8, 150.9, 144.1, 137.9, 130.7, 121.9, 114.7, 112.9, 112.0, 96.7, 61.2, 56.3
mp: 248-249 °C
IR (neat, cm^{-1}): 3302, 1637, 1626, 1495, 1424, 1330, 1123, 1111, 869, 820

6-Hydroxy-5,7-dimethoxy-2-(4-(trifluoromethoxy)phenyl)-4H-chromen-4-one (6f)

Light-brown solid
Chemical formula: $C_{18}H_{13}F_3O_6$
Molecular weight: 382.29 g/mol
Yield: 36 %

Synthesized from product **3** (500 mg, 2.36 mmol) using the procedure described above to obtain 325 mg (0.85 mmol, 36 % yield).

**^{1}H NMR (CDCl$_3$; 400 MHz)**: δ (ppm) 7.93 (d, *J* =9.1 Hz, 2H), 7.36 (d, *J* =9.1 Hz, 2H), 6.85 (s, 1H), 6.66 (s, 1H), 5.94 (s, 1H), 4.04 (s, 3H), 4.03 (s, 3H)
^{13}C NMR (CDCl$_3$; 100 MHz): δ (ppm) 177.0, 160.2, 152.7, 152.2, 151.5, 151.4, 144.2, 137.1, 130.4, 127.9, 121.3, 112.63, 108.7, 96.5, 62.8, 56.7
mp: 218-219 °C
IR (neat): 3294, 1242, 1199, 1109, 1150, 1178, 1091, 1088, 856, 824, 499

General Procedure for the Synthesis of the Deprotected Flavones

To a solution of the respective final precursor (1 equiv.) in acetonitrile was added $MgBr_2$ (3 equiv.) and the reaction mixture was stirred for 3 h at 80 °C. The reaction was monitored by TLC using DCM:EtOAc 1:1 as eluent. Once all starting material had been consumed, a 0.5 M solution of HCl was added to the mixture and the aqueous phase was extracted three times with EtOAc. The organic phase was then washed three times with a 0.5 M solution of HCl and once with water and brine. The organic layer was then dried over $MgSO_4$, concentrated under reduced pressure and recrystallized from DCM to yield the desired product.

5,6-Dihydroxy-7-methoxy-2-(4-methoxyphenyl)-chromen-4-one (1a, FOMe)
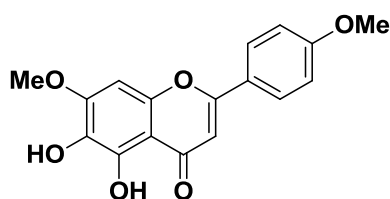
Yellow solid
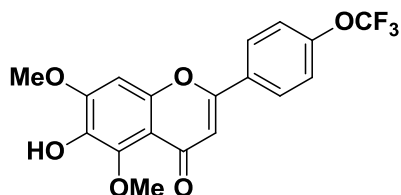Chemical formula: $C_{17}H_{14}O_6$
Molecular weight: 314.29 g/mol
Yield: 75 %

Synthesized from product **6a** (3.91 g, 11.92 mmol) using the procedure described above to obtain 2.86 g (9.1 mmol, 75 % yield).

^{1}H NMR (DMSO-d_6; 300 MHz): δ (ppm) 12.62 (s, 1 H), 8.73 (s, 1 H), 8.07 (d, *J* = 8.8 Hz, 2 H), 7.13 (d, *J* = 8.8 Hz, 2 H), 6.96 (s, 1 H), 6.91 (s, 1 H), 3.94 (s, 3 H), 3.88 (s, 3 H)
^{13}C NMR (DMSO-d_6; 75 MHz): δ (ppm) 182.2, 163.3, 162.2, 154.4, 149.6, 146.2, 129.9, 128.2, 123.0, 114.5, 105.1, 103.1, 91.2, 56.3, 55.5
mp: 215 °C, dec
IR (neat, cm^{-1}): 3518, 1482, 1464, 1359, 1248, 1179, 1108, 1035, 830, 803, 558
HRMS (ESI$^+$): 315.09 [M+H]$^+$ (calc. 315.08).

5,6-dihydroxy-7-methoxy-2-phenyl-4H-chromen-4-one (1b, FH)
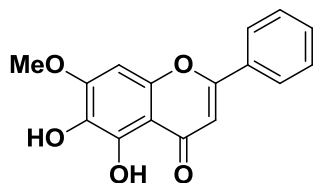
Yellow solid
Chemical formula: $C_{16}H_{12}O_5$
Molecular weight: 284.26 g/mol
Yield: 79 %

Synthesized from product **6b** (142 mg, 0.43 mmol) using the procedure described above to obtain 106 mg (0.34 mmol, 79 % yield).

¹H NMR (Acetone-d_6; 300 MHz): δ (ppm) 12.58 (s, 1 H), 8.08 (m, 2 H), 7.60 (m, 3 H), 6.91 (s, 1 H), 6.80 (s, 1 H), 4.01 (s, 3 H)
¹³C NMR (DMSO-d_6; 75 MHz): δ (ppm) 182.3, 163.2, 154.6, 149.8, 146.1, 132.0, 130.9, 130.1, 129.1, 126.3, 105.3, 104.7, 91.3, 56.4
mp: 216-217 °C, dec
IR (neat, cm⁻¹): 3442, 1667, 1585, 1498, 1450, 1364, 1205, 1083, 806, 726
HRMS (ESI⁺): 285.07 [M+H]⁺ (calc. 285.07)

5,6-Dihydroxy-7-methoxy-2-(4-fluorophenyl)-4H-chromen-4-one (1c, FF)
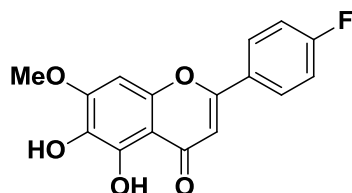
Yellow solid
Chemical formula: $C_{16}H_{11}FO_5$
Molecular weight: 302.25 g/mol
Yield: 40 %

Synthesized from product **6c** (150 mg, 0.47 mmol) using the procedure described above to obtain 56 mg (0.19 mmol, 40 % yield).

¹H NMR (DMF-d_7; 300 MHz): δ (ppm) 12.58 (s, 1 H), 9.00 (s, 1 H), 8.23 (dd, *J* = 9.0 Hz, *J* = 5.3 Hz, 2 H), 7.46 (t, *J* = 8.8 Hz, 2 H), 7.03 (s, 1 H), 6.95 (s, 1 H), 4.01 (s, 3 H).
No ¹³C NMR was could be obtained due to the low quantity of product available.
mp: 226-228 °C
IR (neat, cm⁻¹): 3324, 1354, 1223, 1181, 1159, 1113, 825, 549, 513, 495, 470
HRMS (ESI⁺): 303.07 [M+H]⁺ (calc. 303.06)

5,6-Dihydroxy-7-methoxy-2-(4-(trifluoromethyl)phenyl)-4H-chromen-4-one (1d, FCF$_3$)
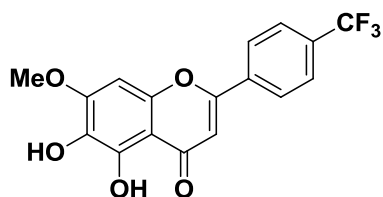
Yellow solid
Chemical formula: C$_{17}$H$_{11}$F$_3$O$_5$
Molecular weight: 352.26 g/mol
Yield: 58 %

Synthesized from product **6d** (250 mg, 0.68 mmol) using the procedure described above to obtain 139 mg (0.39 mmol, 58 % yield).

^{1}H NMR (DMSO-d_6; 300 MHz): δ (ppm) 12.39 (s, 1H), 8.91 (s, 1H), 8.33 (d, *J* = 8.3 Hz, 2H), 7.97 (d, *J* = 8.3 Hz, 2H), 7.15 (s, 1H), 7.01 (s, 1H), 3.97 (s, 3H)
^{13}C NMR (DMSO-d_6; 75 MHz): δ (ppm) 182.2, 161.3, 154.8, 149.8, 146.0, 134.7, 131.6, 130.2, 127.1, 125.9 (q, *J* = 4.1 Hz), 125.6, 106.2, 105.4, 91.3, 56.3
mp: 247-248 °C
IR (neat, cm^{-1}): 3358, 1317, 1123, 1108, 1066, 1014, 836, 819, 786, 568, 498
HRMS (ESI$^+$): 353.06 [M+H]$^+$ (calc. 353.06)

2-(2-fluoro-4-(trifluoromethyl)phenyl)-5,6-dihydroxy-7-methoxy-4H-chromen-4-one (1e, FFCF$_3$)
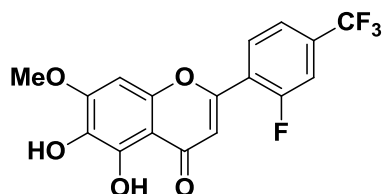
Yellow solid
Chemical formula: C$_{17}$H$_{10}$F$_4$O$_5$
Molecular weight: 370.25 g/mol
Yield: 79 %

Synthesized from product **6e** (200 mg, 0.52 mmol) using the procedure described above to obtain 151 mg (0.41 mmol, 79 % yield).

^{1}H NMR (DMSO-d_6; 300 MHz): δ (ppm) 12.29 (s, 1H), 8.92 (s, 1H), 8.28 (t, *J* = 8.6 Hz, 1H), 8.03 (d, *J* = 10.8 Hz, 1H), 7.87 (d, *J* = 8.6 Hz, 1H), 6.97 (s, 1H), 6.86 (s, 1H), 3.97 (s, 3H)
^{13}C NMR (DMSO-d_6; 75 MHz): δ (ppm) 181.8, 161.1, 157.65, 155.0, 150.0, 145.9, 131.0, 130.9, 130.4, 123.3, 122.0, 121.1, 114.8, 110.3, 105.4, 91.4, 56.4.
mp: 217-218 dec
IR (neat, cm^{-1}): 3302, 1609, 1495, 1428, 1331, 1250, 1129, 1110, 877, 580
HRMS (ESI$^+$): 371.05 [M+H]$^+$ (calc. 371.05)

5,6-Dihydroxy-7-methoxy-2-(4-(trifluoromethoxy)phenyl)-4H-chromen-4-one (1f, FOCF₃)
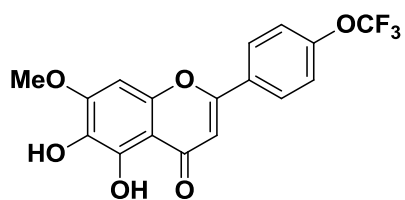
Yellow solid
Chemical formula: $C_{17}H_{11}F_3O_6$
Molecular weight: 368.26 g/mol
Yield: 75 %

Synthesized from product **6f** (154 mg, 0.40 mmol) using the procedure described above to obtain 111 mg (0.30 mmol, 75 % yield).

¹H NMR (MeOD; 300 MHz): δ (ppm) 8.18 (d, *J* = 8.9 Hz, 2H), 7.51 (d, *J* = 8.9 Hz, 2H), 6.92 (s, 1H), 6.85 (s, 1H), 4.04 (s, 3H)

¹³C NMR (CDCl₃; 75 MHz): δ (ppm) 182.3, 162.7, 153.1, 151.6, 150.7, 145.5, 129.8, 128.0, 121.2, 119.4, 105.9, 105.7, 90.5, 56.5

mp: 247-248 °C

IR (neat, cm⁻¹): 1245, 1199, 1155, 1107, 836, 802, 602, 572, 538, 503

HRMS (ESI⁺): 369.06 [M+H]⁺ (calc. 369.05)

References

(1)   Kostanecki, S. V.; Rozycki, A. *Berichte der Dtsch. Chem. Geselschaft* **1901**, *34*, 1901.

(2)   Auwers, K.; Müller, K. *Berichte der Dtsch. Chem. Geselschaft* **1908**, *41*, 4233–4241.

(3)   Wang, Z. In *Comprehensive Organic Name Reactions and reagents*; Wiley, 2010; pp. 1679–1682.

(4)   Allan, J.; Robinson, R. *J. Chem. Soc., Trans.* **1924**, 2192–2195.

(5)   Baker, W. *J. Chem. Soc.* **1933**, 1381–1389.

(6)   Mahal, H. S.; Venkataraman, K. *J. Chem. Soc.* **1934**, 1932–1934.

(7)   Oyamada, T. *Bull. Chem. Soc. Jpn.* **1935**, *10*, 182–186.

(8)   Algar, J.; Flynn, J. *Proc. R. Irish Acad. Sect. B Biol. Geol. Chem. Sci.* **1934**, *42*, 1–8.

(9)   Awuah, E.; Capretta, A. *Org. Lett.* **2009**, *11*, 3210–3213.

(10)   Liang, B.; Huang, M.; You, Z.; Xiong, Z. *J. Org. Chem.* **2005**, *70*, 6097–6100.

(11)   Yang, Q.; Alper, H. *J. Org. Chem.* **2010**, *75*, 948–950.

(12)   Khoobi, M.; Alipour, M.; Zarei, S.; Jafarpour, F.; Shafiee, A. *Chem. Commun.* **2012**, *48*, 2985–2987.

(13)   Bianco, A.; Cavarischia, C.; Farina, A.; Guiso, M.; Marra, C. *Tetrahedron Lett.* **2003**, *44*, 9107–9109.

(14)   Min, M.; Choe, H.; Hong, S. *Asian J. Org. Chem.* **2012**, *1*, 47–50.

(15)   Selepe, M. a; Van Heerden, F. R. *Molecules* **2013**, *18*, 4739–4765.

(16)   Eddarir, S.; Cotelle, N.; Bakkour, Y.; Rolando, C. *Tetrahedron Lett.* **2003**, *44*, 5359–5363.

(17)   Mihigo, S. O.; Mammo, W.; Bezabih, M.; Andrae-Marobela, K.; Abegaz, B. M. *Bioorg. Med. Chem.* **2010**, *18*, 2464–2473.

(18)   Kraus, G. a; Gupta, V. *Org. Lett.* **2010**, *12*, 5278–5280.

(19)   Muller, D.; Fleury, J.-P. *Tetrahedron Lett.* **1991**, 2229–2232.

(20)   Hoshino, Y.; Miyaura, N.; Suzuki, A. *Bull. Chem. Soc. Jpn.* **1988**, *61*, 3008–3010.

(21)   Wei, G.; Yu, B. *European J. Org. Chem.* **2008**, *18*, 3156–3163.

(22)   Donnelly, D. M. X.; Finet, J.-P.; Guiry, P. J.; Rea, M. D. *Synth. Commun.* **1999**, *29*, 2719–2730.

(23) Menichetti, S.; Nativi, C. *J. Sulfur Chem.* **2004**, *25*, 317–327.

(24) Menichetti, S.; Aversa, M. C.; Cimino, F.; Contini, A.; Viglianisi, C.; Tomaino, A. *Org. Biomol. Chem.* **2005**, *3*, 3066–3072.

(25) Silva, A. M. S.; Silva, A. M. G.; Tomé, A. C.; Cavaleiro, J. A. S. *European J. Org. Chem.* **1999**, 135–139.

(26) Bharate, S. B.; Mudududdla, R.; Bharate, J. B.; Battini, N.; Battula, S.; Yadav, R. R.; Singh, B.; Vishwakarma, R. a. *Org. Biomol. Chem.* **2012**, *10*, 5143–5150.

(27) Kumar, K. H.; Perumal, P. T. *Tetrahedron* **2007**, *63*, 9531–9535.

(28) Li, Z.-Y.; Cao, X.; Wang, X.; Guo, Q.-L.; You, Q.-D. *Org. Prep. Proced. Int.* **2009**, *41*, 327–330.

(29) Hans, N.; Grover, S. K. *Synth. Commun.* **1993**, *23*, 1021–1023.

(30) Litkei, G.; Gulacsi, K.; Antus, S.; Blaskbb, G. *Liebigs Ann.* **1995**, 1711–1715.

(31) Lorenz, M.; Kabir, M. S.; Cook, J. M. *Tetrahedron Lett.* **2010**, *51*, 1095.

(32) Yoshida, M.; Fujino, Y.; Doi, T. *Org. Lett.* **2011**, *13*, 4526–4529.

(33) Yoshida, M.; Fujino, Y.; Saito, K.; Doi, T. *Tetrahedron* **2011**, *67*, 9993–9997.

(34) Torii, S.; Okumoto, H.; Xu, L. H.; Sadakane, M.; Shostakovsky, M. V.; Ponomaryov, A. B.; Kalinin, V. N. *Tetrahedron* **1993**, *49*, 6773–6784.

(35) Likhar, P. R.; Subhas, M. S.; Roy, M.; Roy, S.; Kantam, M. L. *Helv. Chim. Acta* **2008**, *91*, 259–264.

(36) Nakatani, K.; Okamoto, A.; Saito, I. *Tetrahedron* **1996**, *52*, 9427–9446.

(37) Ciattini, P. G.; Morera, E.; Ortar, G.; Rossi, S. S. *Tetrahedron* **1991**, *47*, 6449–6456.

(38) Sethna, S. *Chem. Rev.* **1951**, 91–101.

(39) Smith, L. R.; Mahoney, N.; Molyneux, R. J. *J. Nat. Prod.* **2003**, *66*, 169–176.

(40) Danheiser, R. L.; Miller, R. F.; Brisbois, R. G. *Org. Synth.* **1996**, *73*, 134.

(41) Black, T.; McDermott, T.; Brown, G. *Tetrahedron Lett.* **1991**, *32*, 6501–6502.

(42) Haid, S.; Novodomská, A.; Gentzsch, J.; Grethe, C.; Geuenich, S.; Bankwitz, D.; Chhatwal, P.; Jannack, B.; Hennebelle, T.; Bailleul, F.; Keppler, O. T.; Poenisch, M.; Bartenschlager, R.; Hernandez, C.; Lemasson, M.; Rosenberg, A. R.; Wong-Staal, F.; Davioud-Charvet, E.; Pietschmann, T. *Gastroenterology* **2012**, *143*, 213–222.e5.

Chapter III. Evaluation of the Acido-Basic Properties of the Flavones

In order to evaluate the competition between protons and iron(III) (see next chapter) and their possible role in the antiviral activity of the compounds, it was first decided to determine the acido-basic properties of the free flavones synthesized during the course of my PhD. As discussed in Chapter 2, the flavones have been labeled with respect to the substituent or substituents present in ring B (Figure 1) except for the 2-phenyl-chromone model (flavone **F**) and the final precursor to ladanein (**FP**). Apigenin (5,7,4'-trihydroxyflavone) and salvigenin (the O6-methylated derivative of ladanein) have been considered as well. On the other hand, the reported acido-basic properties of epigallocatechin gallate (EGCG), curcumin and some of their derivatives, compounds that also display anti HCV properties, will be herein discussed together with the lead compound ladanein **FOMe** and its derivatives (Figure 2).

In this chapter, we will first describe the structural characteristics at the solid state of ladanein (from both natural and synthetic sources) and compare these data to closely related analogues such as baicalein, salvigenin, pectolarigenin or cirsimaritin. Only flavones bearing the 5,6,7-trihydroxylation pattern on cycle A have been considered for this study. However, the B-cycle can either present no substituent at all or be mono- or polyhydroxylated. In addition to the flavones presented here, a broad range of methoxylated, glycosylated, glucuronidated derivatives (presumably resulting from metabolic reactions) on cycles A and B can also be found in nature. A well known example is the 7-glucuronide analogue of baicalein (baicalin) which is present in the roots of *Scutellaria baicalensis* (a Chinese medicinal plant) and is also found as a metabolite of baicalein in animals and humans after intake. Both baicalein and baicalin show interesting and potent antiviral activities (*e.g.* Dengue virus DENV).[1] After this structural consideration, we will then present the acido-basic properties of ladanein and the synthetic analogues (Figure 1) and discuss these data with respect to EGCG and curcumin. In the last section of this chapter, we will focus on the base-oxidation/degradation kinetics of ladanein, which are anticipated to play a key role in the bioactivation of ladanein.
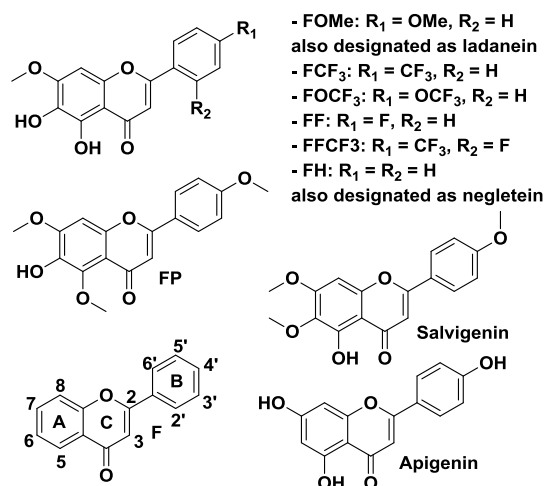
Figure 1. Chemical structures of the flavones considered in this work together with some model flavonoid compounds (salvigenin and apigenin).
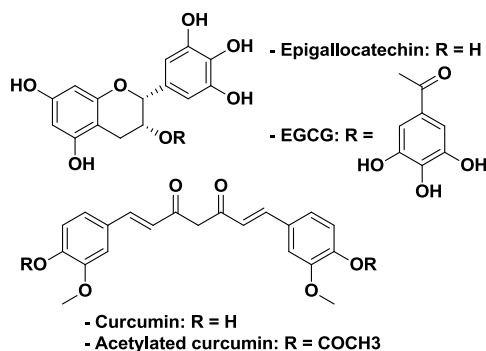
Figure 2. Chemical structures of curcumin (and its acetylated derivative) and of epigallocatechin gallate EGCG (and of the deacylated analogue epigallocatechin).

3.1. X-ray Structural Properties of Extracted and Synthetic Ladanein (FOMe), of its Final Precursor (FP) and of Closely Related Flavones

In the following section, we will first present and discuss the X-ray structural data obtained for ladanein **FOMe** and the final precursor **FP** and discuss these data with respect to closely related systems reported in the literature such as baicalein (5,6,7-trihydroxyflavone), salvigenin (5-hydroxy-6,7,4'-trimethoxyflavone), pectolarigenin (5,7-dihydroxy-6,4'-dimethoxyflavone), cirsimaritin (5,4'-dihydroxy-6,7-dimethoxyflavone) or eupatorin (5,3'-dihydroxy-6,7,4'-trimethoxyflavone). The X-ray structures of the closely related flavones ladanein,[2] salvigenin[3], baicalein[4], pectolarigenin[5], cirsimaritin[6] and eupatorin[7] are first presented in Figure 3. Table 1 gathers some important structural data (bond lengths, torsion angles...). To our best knowledge, these corresponding X-ray data together with those measured for 5,7,3'-trihydroxy-6,4',5'-trimethoxy-flavone[8] and 5,6,7,5'-

tetramethoxy-3',4'-methylenedioxyflavone monohydrate[9] are the only structural data available for this class of compounds.
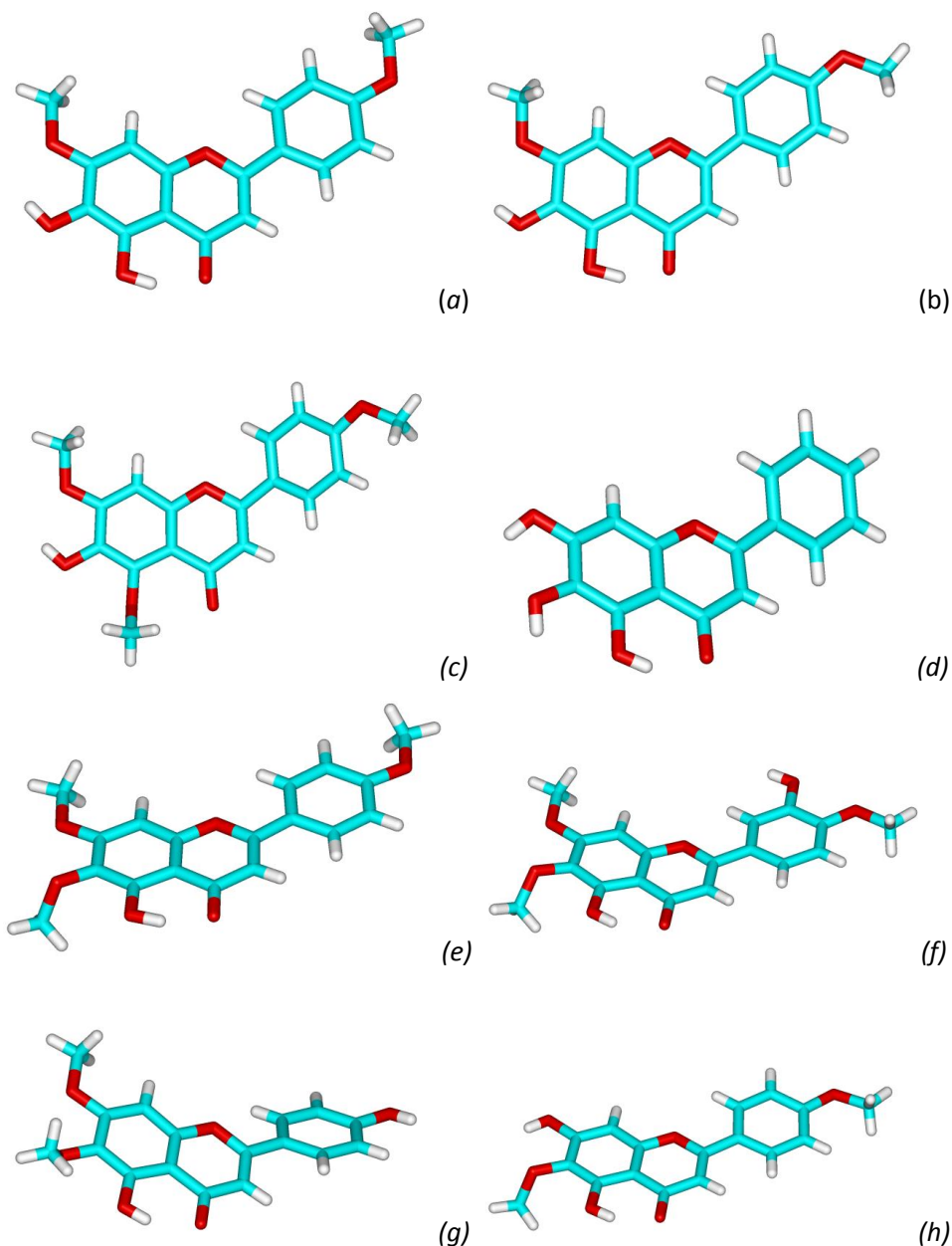
Figure 3. X-ray structures of ladanein (**FOMe**) from natural (*a*) and synthetic (*b*) sources, (*c*) the final precursor **FP** of ladanein, (*d*) baicalein, (*e*) salvigenin, (*f*) eupatorin, (g) cirsimaritin and (h) pectolarigenin.

First, the X-ray data (Table 1) obtained for ladanein **FOMe** from extraction and synthesis was considered, and close similarities between the two solid-state structures were found. The small differences observed might be due to the presence of a methanol molecule in the crystal lattice, which co-crystallizes with synthetic ladanein and interacts with the 6-OH group through hydrogen bonds (two ladanein molecules are brought together through two bridging methanol molecules with

bond lengths of $CH_3OH\cdots O_6H$ = 2.215 Å and $O_6H\cdots OHCH_3$ = 1.900 Å). For natural **FOMe**, the two ladanein molecules are organized in another symmetrical arrangement, each 6-OH group from the A ring interacting through hydrogen bonding with the methoxy group present on the 4' carbon atom of the B ring of the adjacent molecule ($O_6H\cdots OCH_3$) (Figure 4).

(*a*)

(*b*)
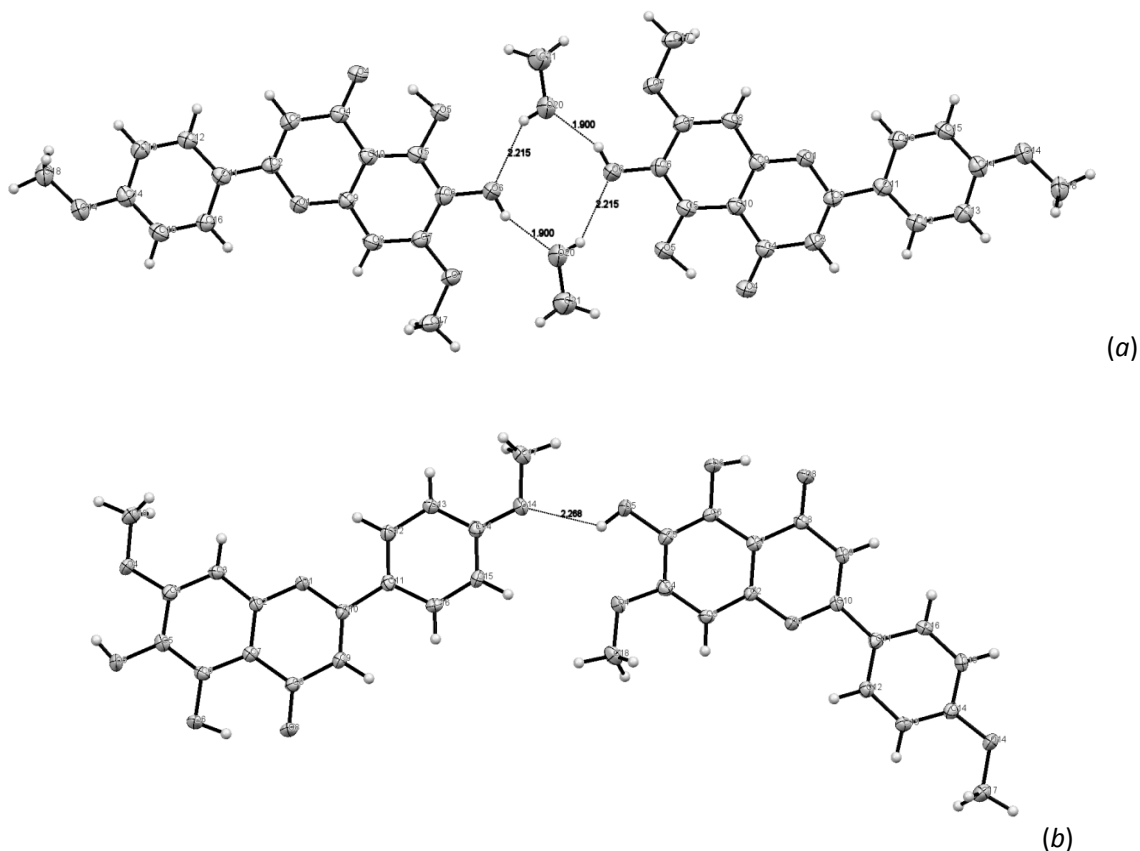
Figure 4. Ladanein stacking along the *a* dimension for the synthetic (a) and natural (b) flavones.

Similarly to most compounds containing benzopyran moiety, this unit was found to be almost coplanar; the dihedral angle between the planes of rings A and C ranging from 0.27° for synthetic ladanein to 2.75° for eupatorin. The planarity of the benzopyran moiety thus confirms the aromatic character of this subunit. The C_2-$C_{1'}$ bond that connects rings B and C is usually described as a single bond having free rotation. Therefore, it is expected that the two rings are not to be coplanar. However, the C_2-$C_{1'}$ bond distance ranges from 1.464 Å for synthetic ladanein to 1.482 Å for 5,7,3'-trihydroxy-6,4',5'-trimethoxyflavone. This means that the bond has a clear partial double-bond character, since a bond length value of 1.54 Å is expected for a pure single bond. Hence, the contribution of a resonance structure in which a C_2-$C_{1'}$ double bond is present and the molecule adopts a planar conformation is quite important. For flavones containing a 4'-methoxy substituent (ladanein, salvigenin, eupatorin and pectolarigenin), mesomeric effects (Scheme 1) from the methoxy

donor group to the 4-carbonyl acceptor unit may account for the small torsion angle measured between the phenyl B ring and the benzopyran A-C moiety (O_1-C_2-$C_{1'}$-$C_{2'}$ angle from 0.07° to 7.42°). As a consequence, these five related flavones display an almost planar conformation. For the final precursor **FP**, it is possible that a steric interaction between the 5-methoxy and 4-carbonyl groups has a more important effect than these electronic effects, hence, the O_1-C_2-$C_{1'}$-$C_{2'}$ angle is increased up to 18.96°. Interestingly, cirsimaritin displays an O_1-C_2-$C_{1'}$-$C_{2'}$ torsion angle of 22.59°. This might be due to π-π interactions and to hydrogen bonding between the 4'-OH group of a flavone and the 6-OCH_3 ($O_{4'}H^{...}O_6CH3$ = 1.947 Å) and 7-OCH_3 ($O_{4'}H^{...}O_7CH_3$ = 2.739 Å) of an adjacent molecule (Figure 5).
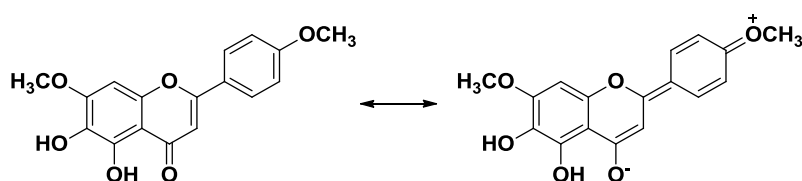
Scheme 1. Mesomeric effects for ladanein.
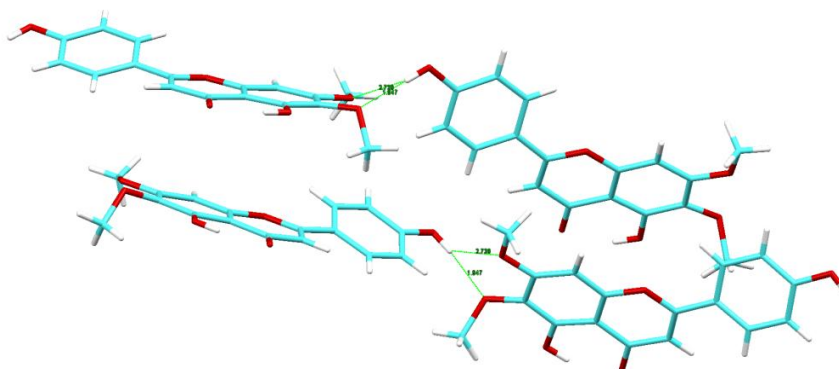
Figure 5. Arrangement and interactions between Cirsimaritin molecules in the crystal lattice.

Conformational energy analysis of the flavonoid skeleton revealed that the lowest potential energy corresponding to a non-planar conformation involves a torsion angle O_1–C_2–$C_{1'}$–$C_{2'}$ of about 22.8°.[10] This torsion angle represents a balance between the attractive interaction from a planar structure that provides the framework for a more extensive mesomeric effect and the repulsive steric interactions that would result from the close vicinity of the two *ortho* hydrogen atoms of the B ring with the C ring. However, the difference in energy between the lowest energy non planar conformation and the planar one is very weak (only *ca.* 0.7 kcal mol^{-1}). In the absence of mesomeric driving force, as happens for baicalein, the torsion angle O_1–C_2–$C_{1'}$–$C_{2'}$ was found to range from 8.52° to 20.01°. Whatever the flavonoid considered, the C_2–C_3 bond length was found to be slightly lower than a pure double bond (a bond length value of 1.339 Å is expected for a pure double bond) which

can be explained by mesomeric effect of the C-ring (Scheme 2). Hence, the bond does not have a complete double bond character, as can be observed for baicalein (1.355-1.360 Å), salvigenin (1.347 Å), ladanein (1.355-1.356 Å), pectolarigenin (1.350 Å), cirsimaritin (1.354 Å) or eupatorin (1.352 Å). The C_4–O_4 bond length is also increased (1.256-1.263 Å for baicalein, 1.257 Å for salvigenin and 1.258-1.265 Å for ladanein, 1.264 Å for eupatorin) compared to flavones having a larger dihedral angle (a bond length value of 1.213 Å is expected for a pure C=O double bond).[11] In addition to the mesomeric effect, the increased length of the C_4–O_4 double bond may also be explained by a strong intramolecular hydrogen bond between O_4 and O_5H. Indeed, in the case of the final precursor **FP** for which the O_4-O_5H hydrogen bond has been suppressed by O-alkylation, the C_4–O_4 (1.240 Å) and C_2–C_3 (1.338 Å) bond lengths approach the ideal values for C=O and C=C double bonds, respectively.
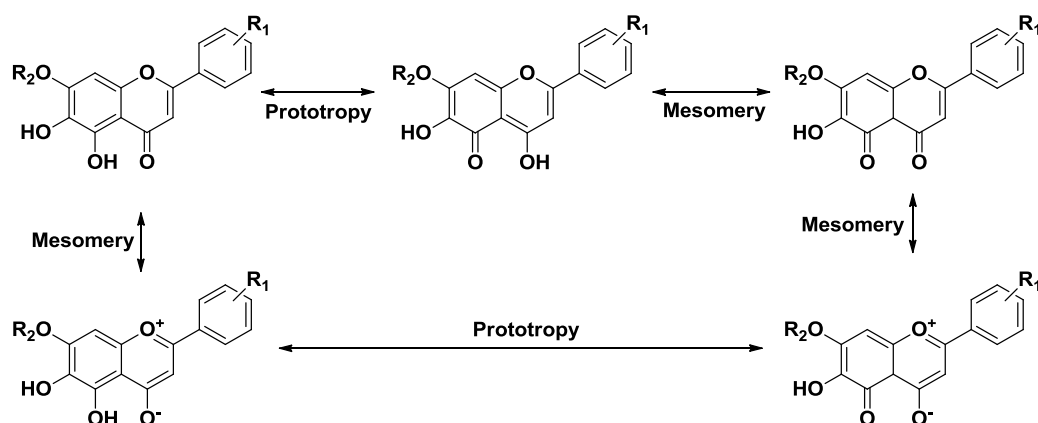
Scheme 2. Examples of mesomeric and prototropic effects which might explain the structural features observed for salvigenin and ladanein.

From this brief structural analysis, it appears that the exocyclic oxygen O_4 along with the B-ring substitution pattern, are of great importance to maintain the planarity of the flavone structure. Inducing a partial negative charge on O_4 *via* hydrogen bond also increases the contribution of this mesomeric effect and hence contributes to the planarity of the molecule. Baicalein has a strong hydrogen bond (1.736-1.854 Å for O_5H–O_4) and two weaker hydrogen bonds (2.421-2.541 Å for O_6H–O_5, 2.200-2.267 Å for O_7H–O_6), while salvigenin (1.685 Å for O_5H–O_4) only possesses one strong hydrogen bond. Interestingly, cirsimaritin (1.847 Å for O_5H–O_4) and eupatorin (1.864 Å for O_5H–O_4) both display the same substitution pattern as salvigenin on cycle A, but possess a much weaker hydrogen bond. For baicalein, the hydrogen bonds arrangement adopts an anti-clockwise orientation.[12] For ladanein, the situation is in an interesting contrast with a strong hydrogen bond between O_4 and O_5H (1.619-1.712 Å, anti-clockwise orientation), while O_6H establishes a weaker interaction with O_7CH_3 (2.206-2.327 Å) with a clockwise orientation.

Table 1. Solid state structural characteristics of the flavones considered in this work together with those reported for salvigenin and baicalein.

Structural parameters	Ladanein FOMe (natural)	Ladanein FOMe (synthetic)	Final precursor FP	Baicalein	Salvigenin
C_2-$C_{1'}$ (Å)	1.473	1.464	1.467	1.471/1.469/1.476	1.467
C_2-C_3 (Å)	1.355	1.356	1.338	1.360/1.360/1.355	1.347
C_3-C_4 (Å)	1.436	1.424	1.440	1.427/1.432/1.431	1.426
C_4-O_4 (Å)	1.265	1.258	1.240	1.263/1.261/1.256	1.257
O_5H-O_4 (Å)	1.712	1.619	-	1.815/1.736/1.854	1.685
O_6H-O_5 (Å)	-	-	-	2.426/2.421/2.541	-
O_6H-O_7CH_3 (Å)	2.206	2.327	2.287	-	-
O_7H-O_6 (Å)	-	-	-	2.267/2.200/2.227	-
A-C (°)	1.77	0.27	1.29	0.79/2.46/2.34	0.80
O_1-C_2-$C_{1'}$-$C_{2'}$ (°)	2.14	0.93	18.96	20.01/9.13/8.52	4.38

Structural parameters	Pectolarigenin	Cirsimaritin	Eupatorin	5,7,3'-trihydroxy-6,4',5'-trimethoxy-flavone	5,6,7,5'-tetramethoxy-3',4'-methylenedioxy-flavone
C_2-$C_{1'}$ (Å)	1.470	1.468	1.467	1.482	1.470
C_2-C_3 (Å)	1.350	1.354	1.352	1.340	1.347
C_3-C_4 (Å)	1.430	1.426	1.425	1.438	1.436
C_4-O_4 (Å)	1.255	1.256	1.265	1.260	1.240
O_5H-O_4 (Å)	1.847	1.847	1.864	1.850	-
O_7H-O_6 (Å)	2.284	-		2.38	-
A-C (°)	1.51	2.20	2.75	1.37	1.95
O_1-C_2-$C_{1'}$-$C_{2'}$ (°)	7.42	22.59	0.04	4.29	0.15

A semi-empirical method (AM1 method)[13] was used in order to model the structure of ladanein and other synthetic analogues with the aim of evidencing any influence of the B-ring substitution (H, OCH₃, F, OCF₃, CF₃, F/CF₃) on important structural parameters. Table 2 gathers the corresponding structural characteristics and shows a relatively good agreement between the calculated and experimental parameters for ladanein **FOMe** and its final precursor **FP**. It is noteworthy that the hydrogen bond pattern of the A-ring was constrained in order to fit to the solid-state properties. Obviously, this approach should be used only as a rough evaluation and cannot account for solution properties. The difference in energy between the lowest energy for the anticlockwise/clockwise and the anticlockwise conformations is only *ca.* 1 kcal mol^{-1} (Figure 6). For **FFCF₃**, which has a fluorine atom on the *ortho* position of the B ring, repulsive steric interactions lead to a torsion angle of about

33°. Unexpectedly, a torsion angle of about 27° is also reached for the 4'-trifluoromethoxy substitution. In all remaining cases, the A/C and B rings approach ideal planarity.
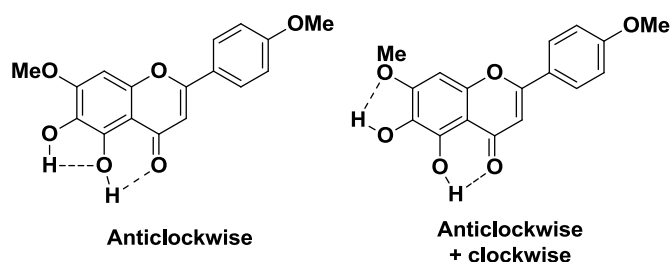

Figure 6. Anticlockwise and anticlockwise/clockwise conformations of hydrogen bonds present in ladanein.

Table 2. Structural characteristics gained from optimization with a semi-empirical method (AM1, Hyperchem) of the flavones considered in this work.

Structural parameters	FOMe	FOMe AM1	FP	FP AM1	FCF$_3$ AM1	FOCF$_3$ AM1	FF AM1	FFCF$_3$ AM1	FH AM1
C$_2$-C$_{1'}$ (Å)	1.473/1.464	1.462	1.467	1.462	1.466	1.463	1.464	1.465	1.465
C$_2$-C$_3$ (Å)	1.355/1.356	1.354	1.338	1.351	1.352	1.352	1.353	1.350	1.353
C$_3$-C$_4$ (Å)	1.436/1.424	1.458	1.440	1.464	1.462	1.460	1.460	1.463	1.460
C$_4$-O$_4$ (Å)	1.265/1.258	1.245	1.240	1.237	1.244	1.244	1.244	1.243	1.245
O$_5$H-O$_4$ (Å)	1.712/1.619	1.987	-	-	1.992	1.989	1.990	1.991	1.988
O$_6$H-O$_7$CH$_3$ (Å)	2.206/2.327	2.226	2.287	2.231	2.228	2.228	2.227	2.235	2.227
A-C (°)	1.77/0.27	0.07	1.29	2.58	0.05	0.17	0.04	0.19	0.04
O$_1$-C$_2$-C$_{1'}$-C$_{2'}$ (°)	2.14/0.93	0.39	18.96	26.76	0.02	27.14	0.04	33.55	0.04
The O$_6$H-O$_7$CH$_3$ was fixed to be compared with the X-ray data. The minimum of energy indeed shows the same hydrogen bond pattern than that of baicalein (anticlockwise orientation).									

3.2. Absorption Spectrophotometric Titrations *versus* pH

All flavones (**FOCH$_3$, FOCF$_3$, FF, FFCF$_3$, FH and FCF$_3$,** Figure 1) possess two ionizable deprotonation sites (namely, the 5-OH and 6-OH units). Since these flavonoid compounds are chromophoric systems in the UV region, it was decided to perform absorption spectrophotometric titrations as a function of pH. As these compounds are sparingly soluble in pure water (*ca.* 10^{-5} - 10^{-4} M, Table 3), their protolytic properties have been investigated in a mixed solvent composed of 80 % of methanol and 20% of water (*w/w*).

Table 3. Chemical characteristics of the flavones considered in this work.

compound	Formula	MM (g mol^{-1})	logP$_{calculated}$
F	$C_{15}H_{10}O_2$	222.24	3.07
FH/Negletein	$C_{16}H_{12}O_5$	284.27	2.17
FOMe/Ladanein	$C_{17}H_{14}O_6$	314.29	2.04
FOCF$_3$	$C_{17}H_{11}F_3O_6$	302.06	3.69
FF	$C_{16}H_{11}FO_5$	284.26	2.33
FFCF$_3$	$C_{17}H_{10}F_4O_5$	370.26	3.25
FCF$_3$	$C_{17}H_{11}F_3O_5$	352.27	3.09
FP	$C_{18}H_{16}O_6$	328.32	2.30
Salvigenin	$C_{18}H_{16}O_6$	328.32	2.30
Apigenin	$C_{15}H_{10}O_5$	270.24	1.90
Curcumin	$C_{21}H_{20}O_6$	368.38	2.56
epigallocatechin	$C_{15}H_{14}O_7$	306.27	1.11
EGCG	$C_{22}H_{18}O_{11}$	458.38	2.07

Absorption spectra of flavones and flavonols are usually characterized by two intense absorption bands (labeled I and II) lying in the UV region. Band I is typically centered between 320 and 380 nm, while band II lies at higher energies (240 - 270 nm).[14] These absorption bands arise from π-π* transitions of the compounds.[15,16] Band I of related flavones is usually assumed to be associated to the cinnamoyl system (B-C rings), while band II originates from the benzoyl moiety (A ring) (Figure 7).
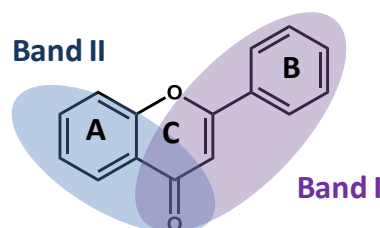
Figure 7. Main chromophores assumed to be responsible for the absorptions I and II.

Nonetheless, the situation is more complex since X-ray structural data and theoretical calculations done on various flavonoids (flavone,[17] quercetin,[15] isoquercitrin[18]) have shown that the electronic transitions responsible of absorption bands I and II may result from electronic redistribution on the whole molecule due to mesomeric or inductive effects. Figure 8 depicts the HOMO and LUMO levels of ladanein (calculated with the semi-empirical method AM1 using Hyperchem) which confirms that the HOMO-LUMO transition involves the system as a whole. Indeed, the electronic density of the HOMO of ladanein is mainly localized on the chromone part (A and C-ring) of ladanein whereas the electronic density of the LUMO is mainly centered on the B-ring (Figure 8). The π-π* transition,

observed at 335 nm (Table 4), can thus be regarded as a charge transfer (CT) from the benzoyl moiety to the cinnamoyl moiety. Solvatochromic properties support these facts and have been reported for the lower energy band (band I) of the absorption spectrum 7-hydroxyflavone derivatives in agreement with its resonance structure.[19] In addition, it has been also shown that the HOMO presents a great dependence with respect to substitution. Substitution on the A ring usually gives rise to an electronic localization on the A ring (stabilization of the HOMO) while the substitution on the B ring would lead to the localization of the electronic density on the B ring (destabilization of the HOMO and stabilization of the LUMO). This spectral feature can be clearly evidenced when comparing the 2-phenyl-chromone (flavone **F**, λ^{max} (band I) = 295 nm) to negletein **FH** (λ^{max} (band I) = 321 nm) and ladanein **FOMe** (λ^{max} (band I) = 335 nm). The computed electronic spectrum of the neutral and the deprotonated forms are also provided in Figure 8. Finally, Table 4 gathers the absorption spectrophotometric properties of the flavones.
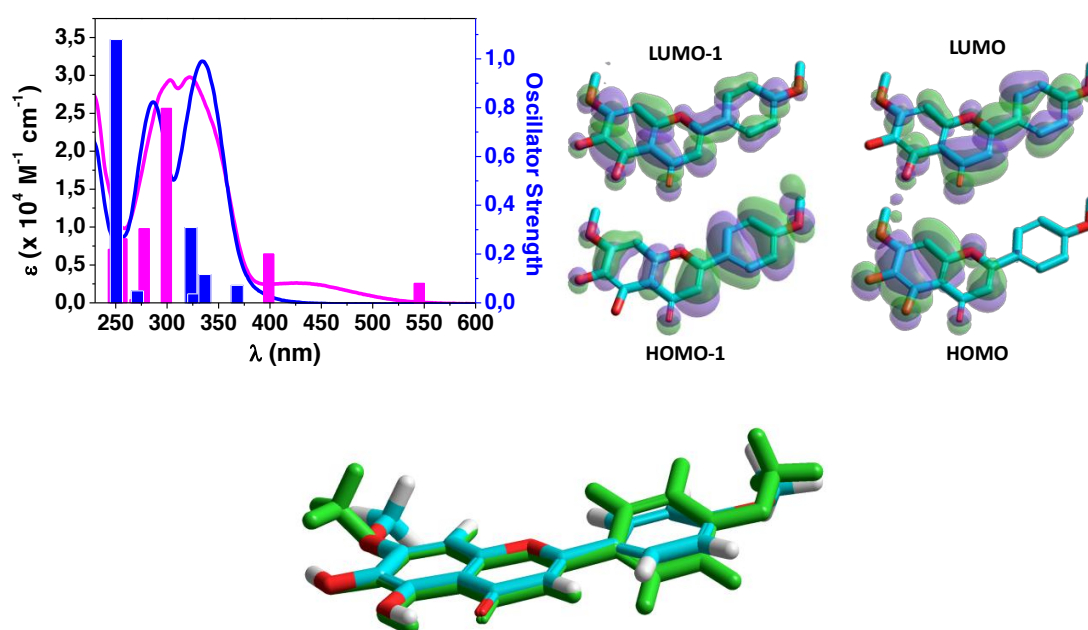
Figure 8. (top-left) Electronic absorption spectrum of the neutral (blue) and monodeprotonated (pink) states of ladanein (**FOMe**) compared to its simulated ones (using AM1/CI with Hyperchem 7.5 program). (top-right) HOMO and LUMO levels of ladanein (**FOMe**) under its neutral form. (bottom) Overlapped optimized structures of the neutral and monodeprotonated forms of ladanein showing significant torsion of the B ring with respect to the planar A-C plane upon deprotonation of the 6-OH group. This would suggest consequent loss of conjugation of the cinnamoyl-type moiety.

Table 4. Absorption characteristics of the flavones considered in this work.

compound[a]	Protonated		6-Monodeprotonated		
	Band I $\lambda^{max} (\varepsilon^{\lambda max})$ nm $(10^4 M^{-1} cm^{-1})$	Band II $\lambda^{max} (\varepsilon^{\lambda max})$ nm $(10^4 M^{-1} cm^{-1})$	Band I $\lambda^{max} (\varepsilon^{\lambda max})$ nm $(10^4 M^{-1} cm^{-1})$	Band II $\lambda^{max} (\varepsilon^{\lambda max})$ nm $(10^4 M^{-1} cm^{-1})$	Additional Band $\lambda^{max} (\varepsilon^{\lambda max})$ nm $(10^4 M^{-1} cm^{-1})$
Flavone F	295 (2.03)	252 (1.68)	na	na	na
FH/Negletein	321 (1.57)	277 (2.44)	317 (1.73)	275 (2.05)	423 (0.18)
FOMe/Ladanein	335 (3.19)	286 (2.65)	322 (2.98)	303 (2.94)	424 (0.26)
Salvigenin	332 (3.35)	276 (2.45)	na	na	na
FP	325 (3.02)	277 (2.01)	301 (3.04)		395 (0.61)
FOCF₃	321 (1.04)	277 (1.71)	314 (1.16)	278 (1.35)	424 (0.11)
FF	321 (1.29)	278 (2.00)	315 (1.40)	280 (1.70)	405 (0.15)
FFCF₃	320 (1.17)	273 (2.01)	326 (1.33)	262 (2.13)	450 (0.19)
FCF₃	322 (1.52)	277 (2.74)	326 (1.73)	272 (2.40)	446 (0.22)
Apigenin[b]	338 (2.11)	268 (1.85)	na	na	na

[a] Solvent: CH_3OH/H_2O (80/20 *w/w*); I = 0.1 M NEt_4ClO_4; T = 25(2)° C . The errors on the λ and ε are estimated to be $\pm$ 1 nm and 10%, respectively. [b] Solvent: CH_3OH/H_2O (80/20 *w/w*); I = 0.1 M $NaClO_4$ (see ref. 20). na = not applicable

To exemplify the absorption spectral variations induced by the medium acidity, Figure 9 and Figure 10 depict the absorption spectrophotometric titrations as a function of pH of two flavones (ladanein **FOMe** and the final precursor **FP**), both bearing a 4'-methoxy group on the B-ring. Deprotonation of the 6-OH group induces large absorption spectral changes. Band II is bathochromically shifted while band I experiences a hypsochromic shift. As a consequence, the two absorptions apparently blend into a single absorption centered at about 300 nm. This feature is in agreement with the fact that the two chromophoric units responsible of bands I and II do not behave independently. The significant alteration of the absorption properties of ladanein or **FP** upon 6-OH deprotonation can be related to the mesomeric effect of the methoxy group borne by the B-ring (Figure 8).

As a relevant example of the other flavones considered in this work (**FH**, **FF**, **FCF₃**, **FFCF₃** and **FOCF₃**), Figure 11 depicts the absorption variation triggered by pH for negletein **FH**. It is noteworthy that none of these compounds possesses a (+M) OCH_3 substituent group in the B ring (the B-substituents are mainly –I or –M directing groups). As a consequence, the increase of pH induces only weak hypo- or hyperchromic shifts of the bands II and I, respectively. In addition, similarly to **FOMe** and **FP**, absorption of much lower intensity emerges in visible region (~ 450 nm) upon deprotonation of the 6-OH group. Interestingly, this new absorption band is much more dependent on the nature of the B-cycle substituent (λ^{max} = 395 nm for **FP** to 446 nm for **FCF₃**).

(a)

(b)

Figure 9. (a) Absorption spectrophotometric titration of ladanein (designated as **FOMe**) as a function of pH and (b) electronic absorption spectra of the protonated species of ladanein. Solvent: CH_3OH/H_2O (80/20 *w/w*); I = 0.1 M (NEt_4ClO_4); T = 25.0(2) °C; l = 1 cm; $[\textbf{FOMe}]_{tot}$ = 3.12 x 10^{-5} M; (**1**) pH = 6.99; (**2**) pH = 12.15.

(a)

(b)

Figure 10. (a) Absorption spectrophotometric titration of the final precursor of ladanein (designated as **FP**) as a function of pH and (b) electronic absorption spectra of the protonated species of **FP**. Solvent: CH_3OH/H_2O (80/20 *w/w*); I = 0.1 M (NEt_4ClO_4); T = 25.0(2) °C; l = 1 cm; $[\textbf{FP}]_{tot}$ = 3.05 x 10^{-5} M; (**1**) pH = 5.52; (**2**) pH = 11.85.

(a)   *(b)*

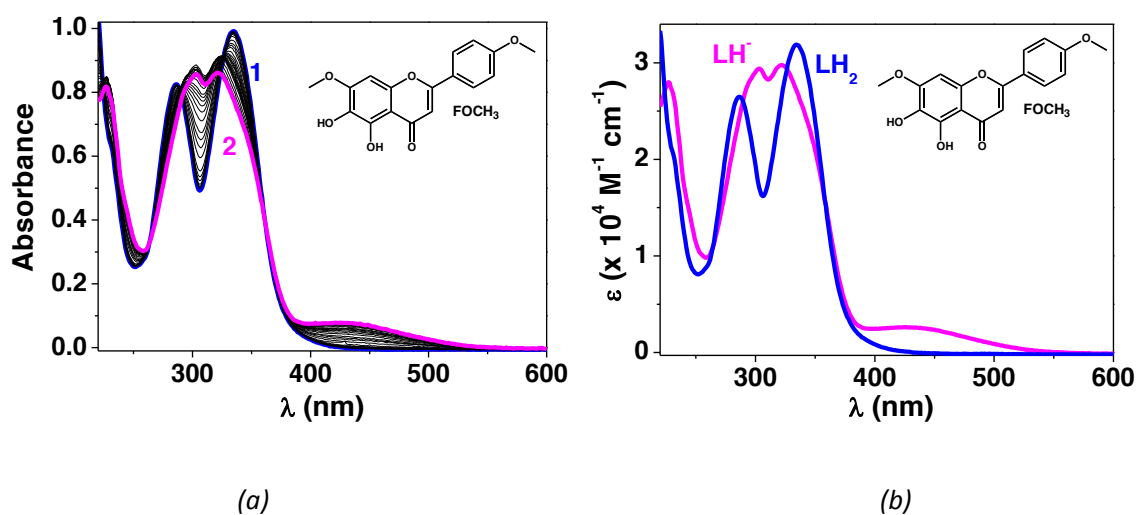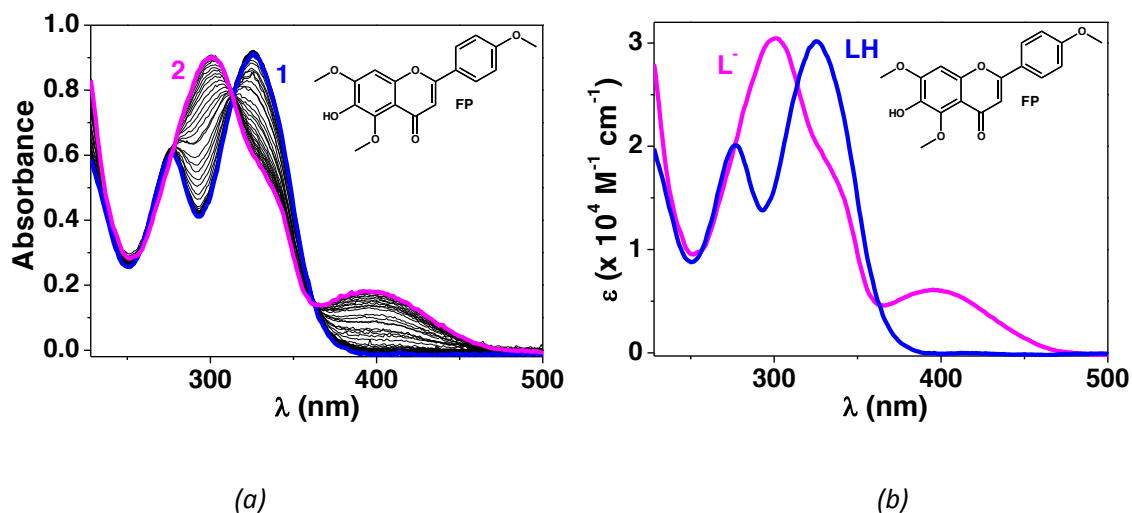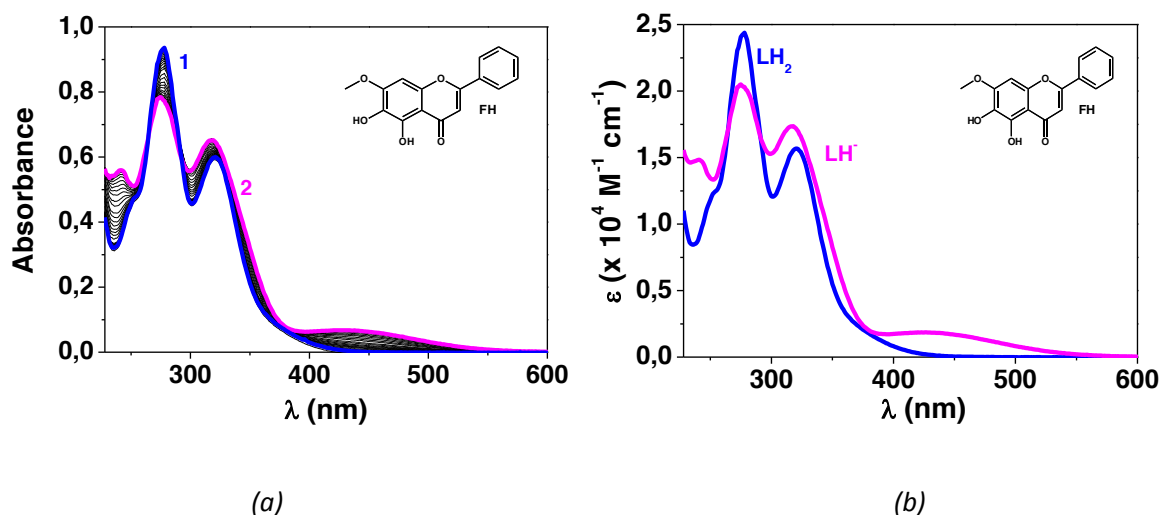**Figure 11.** (a) Absorption spectrophotometric titration of negletein **FH** as a function of pH and (b) electronic absorption spectra of the protonated species of **FH**. Solvent: CH_3OH/H_2O (80/20 *w/w*); I = 0.1 M (NEt_4ClO_4); T = 25.0(2) °C; l = 1 cm; $[\textbf{FP}]_{tot}$ = 3.08 x 10^{-5} M; (**1**) pH = 5.13; (**2**) pH = 11.05.

In summary, substituents on the B-ring (F, CF_3, OCF_3) with predominant –I or -M character[21-23] have little influence in the position of both bands I and II, while significant bathochromic shifts are measured for ladanein (**FOMe**) bearing a methoxy substituent on B-ring with predominant mesomeric nature (-I, +M). This indicates the occurrence of a resonance structure (Scheme 1) that might play an important role in the electronic properties of the molecule (donor-acceptor conjugated system) is in excellent agreement with the X-ray structural data and the AM1 optimization data. Furthermore, no matter which protonated neutral species is considered, Figure 12 and Table 4 clearly show that the substitution of B-ring does not significantly alter the absorption properties of the flavone, while A-substitution (i.e. methylation of the 5- or 7-OH group) markedly modifies the absorption of the flavone core. In contrast, **FFCF₃** displays a different behavior, probably due to the *ortho*-substitution by a fluoride atom leading to steric constrains. Last but not least, the position of weak absorption lying at lower energies for the deprotonated species significantly depends on the substitution pattern of the B-ring.
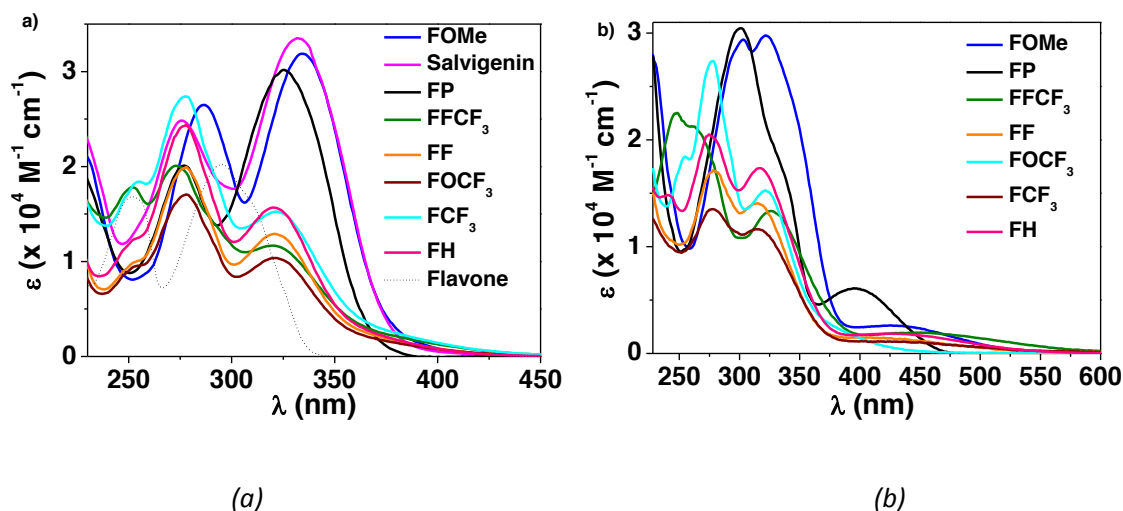
Figure 12. Electronic absorption spectrum of the neutral *(a)* and deprotonated *(b)* states of the flavone series considered in this work. Solvent: CH_3OH/H_2O (80/20 *w/w*); I = 0.1 M (NEt_4ClO_4); T = 25.0(2) °C

The absorption spectrophotometric and potentiometric data sets were processed using statistical tools[24] and allowed us to calculate the protonation constants of the 6-OH group as well as the electronic spectra of the corresponding protonated species (Figure 9, Figure 10, Figure 11 and Table 4). The pK_a values measured for our flavones series are gathered in Table 5. It is important to highlight that the protonation constant of the 5-OH group was not accessible under our experimental conditions (CH_3OH/H_2O 80/20 *w/w*). On the basis of the 5-hydroxy-flavone (pK_a = 11.44 in dioxane/water 1/1 *w/w*[25] and pK_a = 11.34 in CH_3OH/water 1/1 *w/w*[26]), the 5-OH pK_a value was estimated to be > 12 due to a strong intramolecular hydrogen bond with the β-carbonyl group.[27] The carbonyl-oxygen at the 4-position has been also demonstrated to display weak basic properties in the ground state (Scheme 3), its pK_a values being measured at < 0.[28] In the excited state, the pK_a* are dramatically increased (pK_a* ranging from 4 to 7) as a result an ESIPT process - Excited State Intramolecular Proton Transfer - (intramolecular and/or solvent assisted proton transfer). However, we will not discuss this feature in this report since the low pK_a values measured for related flavones are much likely not involved in the biological properties displayed by ladanein and its analogues.
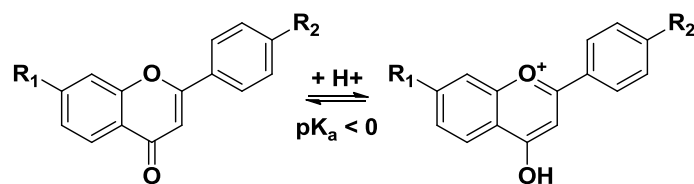
Scheme 3. Acido-basic properties of the C_4 carbonyl unit.[28] The protonated species adopts a flavylium-type structure with absorption lying at lower energies with respect to the neutral form.

The acido-basic properties were compared to the very scarce physico-chemical data available in the literature for closely related flavones (scutellarin B, 5,6,4'-trihydroxy-7-O-glucuronide-flavone). At a first glance, the pK_a values are not strongly influenced by the substitution pattern of the B-cycle in agreement with the observations obtained for the absorption spectrophotometric properties. For instance, ladanein **FOMe** has a slightly more basic 6-OH which may be due to the +M effect of the 4'-methoxy group (Scheme 1) that affects the 2-phenyl-chromone core. The basicity of the 6-OH group may also slightly increase in the case of the final precursor (**FP**, absence of O_4-HO_5 hydrogen bond) and **FFCF$_3$** (steric interaction). Nonetheless, the difference remains a small one and in a biological medium all flavones would be present in the same state.

Table 5. Acido-basic properties of the flavones considered in this work.[a]

Compounds	log K^H (6-OH) ($\pm\sigma$)
F	na
FH/Negletein	9.75(9)
FOMe/ Ladanein	10.33(5)
Salvigenin	nd
FP	10.10(3)
FOCF$_3$	9.47(6)
FF	9.87(5)
FFCF$_3$	10.15(2)
FCF$_3$	10.08(3)
Scutellarin B	10.19/7.77[b]

[a] Solvent: CH_3OH/H_2O (80/20 w/w); I = 0.1 M (NEt_4ClO_4); T = 25.0(2) °C. [b] phosphate buffers. na = not applicable

No matter the flavone considered, the neutral species remains the predominant one under the neutral pH conditions measured in the liver[29] (Figure 13) and probably indicates that the acido-basic properties are not the key physico-chemical parameters responsible for the antiviral activity. This feature can be also observed for other natural compounds displaying anti-HCV properties (inhibition of the virion entry as for ladanein) such as curcumin or epigallocatechin gallate EGCG (Figure 2 and Table 6). The basic pK_a values indeed demonstrate that the protolytic properties of EGCG or curcumin do not allow the explanation of the antiviral behavior of these compounds.

Table 6. Acido-basic properties of other natural polyphenolic compounds displaying anti-HCV properties with the same mode of action.

Compounds	$\log K_1^H$	$\log K_2^H$	$\log K_3^H$	Conditions
Curcumin[30]	10.69	9.3	8.54	CH_3OH/H_2O (50/50 v/v); I = 0.1 M ($NaNO_3$); T = 25.0(2) °C
Acetylated curcumin[30]	8.75	-	-	CH_3OH/H_2O (50/50 v/v); I = 0.1 M ($NaNO_3$); T = 25.0(2) °C
EGCG[31]	$\log K_5^H$ = 11.2; $\log K_6^H$ = 9.43; $\log K_7^H$ = 8.74; $\log K_8^H$ = 7.55			H_2O; I = 0.1 M (KCl); T = 25.0(2) °C

(a)   *(b)*
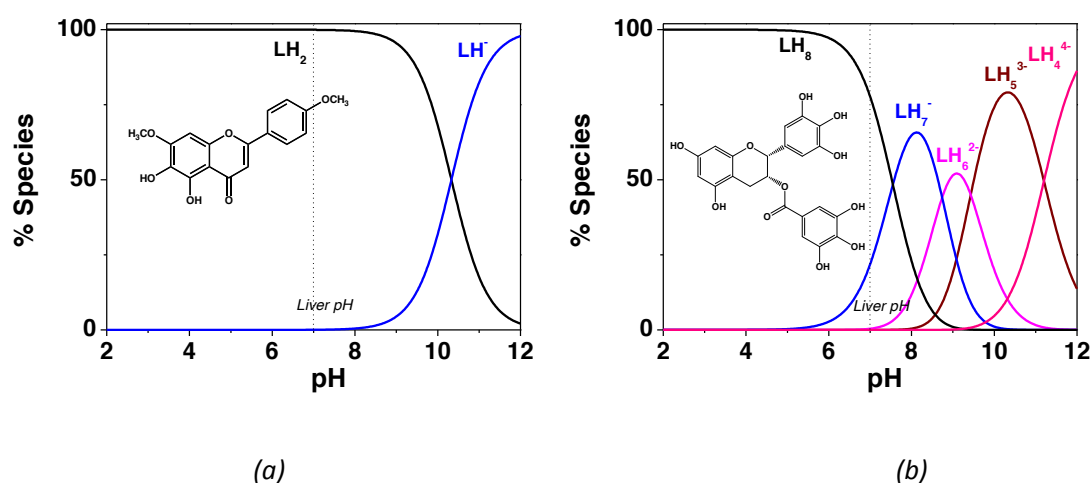
Figure 13. Distribution diagrams of the protonated species of *(a)* ladanein **FOMe** and *(b)* EGCG as a function of pH. [ligand] = 10^{-6} M (close to the EC_{50} values, see the chapter on synthesis); I = 0.1 M; T = 25°C.

3.3. Stability of the Flavones and Oxidation Kinetics

Oxidative coupling of free radical species derived from phenolic substrates is widely recognized to be a main pathway by which many natural products of complex nature are biosynthesized. Phenolic oxidative couplings involve either oxido-reductive enzymes (laccases, peroxidases and tyrosinases) or metal/O_2/pH reagents. Lignin, for instance, is formed by phenolic oxidative coupling of hydroxycinnamoyl alcohol monomers, brought about by peroxidase enzymes. Oxido-reductive enzymes are also able to transform phenols through oxidative coupling reactions with production of polymeric products by self-coupling or cross-coupling with other molecules. On the other hand, oxidative dimerization of phenols can be promoted stoichiometrically by Fe(III)[32] and catalytically by Cu(II) complexes[33] or transition metals.[34] Deprotonation of the phenol (under aerobic conditions) also influences the coupling mechanism. The mechanism of this reaction is well accepted[35] as involving

one electron oxidation of the phenolate anion to generate the phenoxy radical which then reacts with molecular oxygen to form the *para*-peroxy-cyclohexadienone. Finally, loss of water produces the *para*-benzoquinone. Competitive reaction of the phenoxy radical with molecular oxygen at the *ortho* position would lead to the *ortho*-benzoquinone. The usual side reactions also involve the phenoxy radical and *ortho-para* and *para-para C-C* or *C-O* coupling leading to bisquinone-methides, bisphenol or oligomeric derivatives (Figure 14).
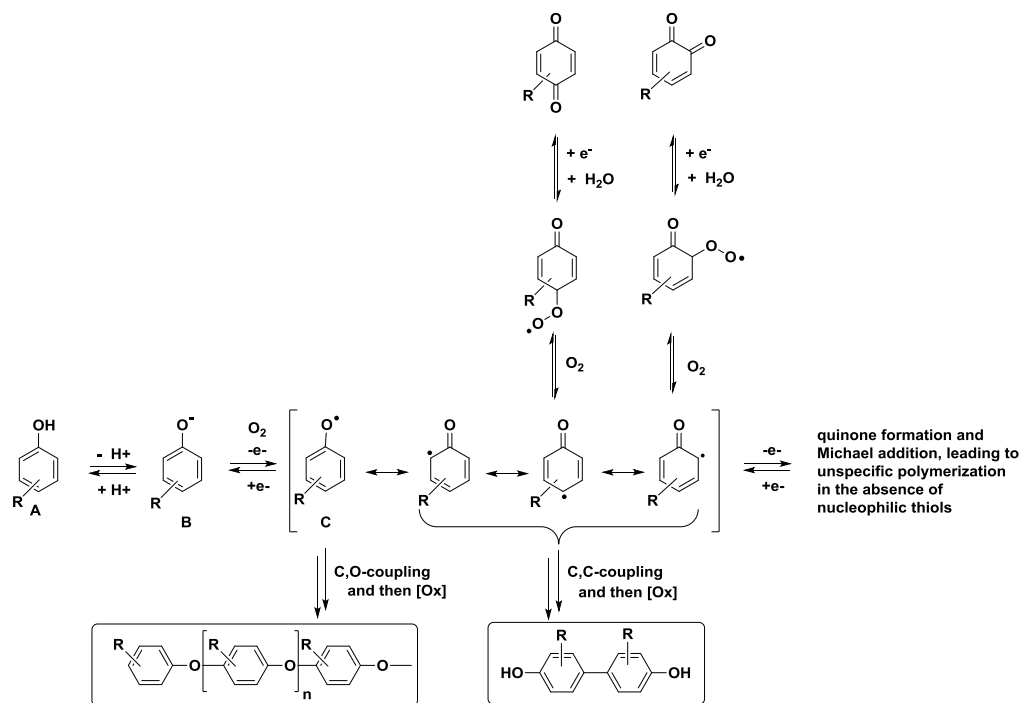

Figure 14. Potential pathways for the oxidative coupling of phenolic compounds.

The mechanism of oxidation of polyphenols and their stability in solution depends on pH and therefore on their acido-basic properties.[36] Oxidative degradation processes of flavonoids involve chemical reactions such as hydroxylation or dimerization.[37] For instance, oxidation of the flavonol quercetin, one of the most studied compounds, by means of hydroxyl free radicals (generated by $CuSO_4/H_2O_2$) leads to the formation of unstable Cu^{2+} chelates and subsequent production of low-molecular-weight compounds such as 3,4-dihydroxybenzoic acid and gallic acid.[38] Formation of 4,6-dihydroxy-2-(3,4-dihydroxybenzoyloxy)benzoic acid from quercetin and derivatives bearing a catechol group on the B-ring was also found in the presence of other unidentified oxidation products.[39] In other reports, 18 possible oxidation products of quercetin were identified by GC–MS and LC–MS analysis, including 3,4-dihydroxybenzoic acid and gallic acid.[40] Auto-oxidation of quercetin in alkaline solution has also been thoroughly investigated.[41,42] It has also been reported that

quercetin oxidation may lead to the formation of a Diels-Alder adduct when a diquinone is formed in cycle B.[43]
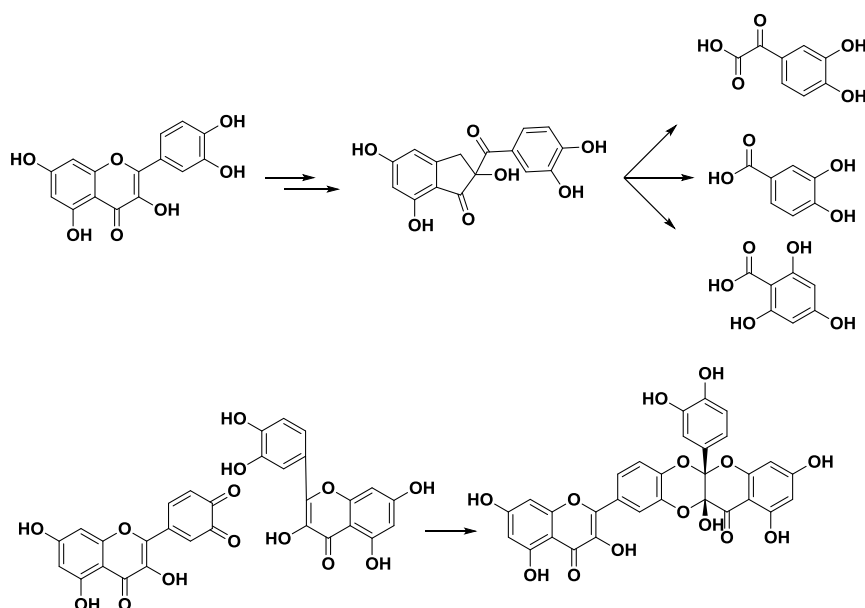
Scheme 4. Formation of the decomposition products of quercetin.

With respect to flavones bearing the 5,6,7-trihydroxylation pattern on cycle A, the reports on oxidation/degradation products are extremely scarce. We can, however, mention the study performed by D. Zhong *et al.*[44] who measured the stability of baicalin in buffered aqueous solutions at different pHs and in biological fluids, such as plasma, urine or tissue homogenates *in vitro*. The degradation of baicalin was pH- and temperature-dependent. An oxidation–reduction reaction intermediated by phenoxyl radicals is the major degradation process for baicalin in plasma and urine *in vitro*, whereas it mainly undergoes hydrolysis and phase II metabolic pathways when introduced in tissue homogenates.
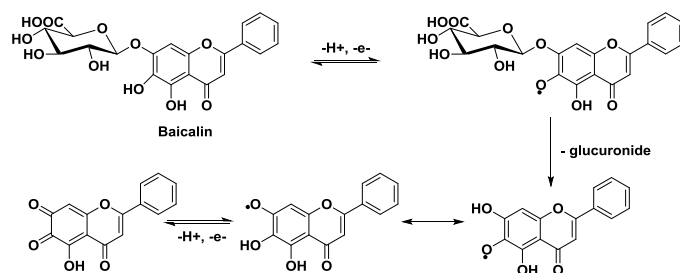
Scheme 5. Suggested degradation profile of baicalin in aqueous solution at pH 9.0.[44]

With the aim of better understanding the oxidation mechanism of ladanein and its analogues, we then examined the oxidation kinetics of ladanein and two of its analogues, **FH** and **FCF₃,** in methanol/water mixture (80/20 *w/w*) in the presence of base (NEt₄OH) and under aerobic conditions. Figure 15 first demonstrates that ladanein and closely related derivatives are stable in solution in the absence of base either under aerobic or anaerobic conditions.
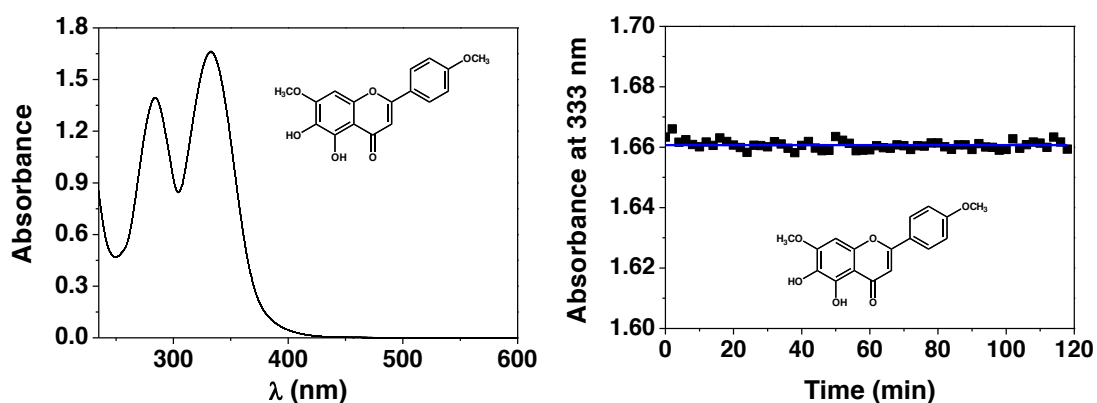
Figure 15. Absorption spectrophotometric spectra of solution of ladanein as a function of time (2 h). Solvent: CH₃OH/H₂O (80/20 *w/w*); *T* = 25.0(2) °C. [**FOMe**]$_{tot}$ = 5.2 x 10⁻⁵ M; *l* = 1 cm.

Upon addition of base, which is anticipated to trigger deprotonation of the 6-OH group of ladanein, a slow oxidation/degradation process inducing significant spectral changes can be observed as a function time (Figure 16). It is indeed noteworthy that the first spectrum recorded just after addition of the base closely matches with the electronic spectrum of the deprotonated species of ladanein **FOMe** (Figure 12b).
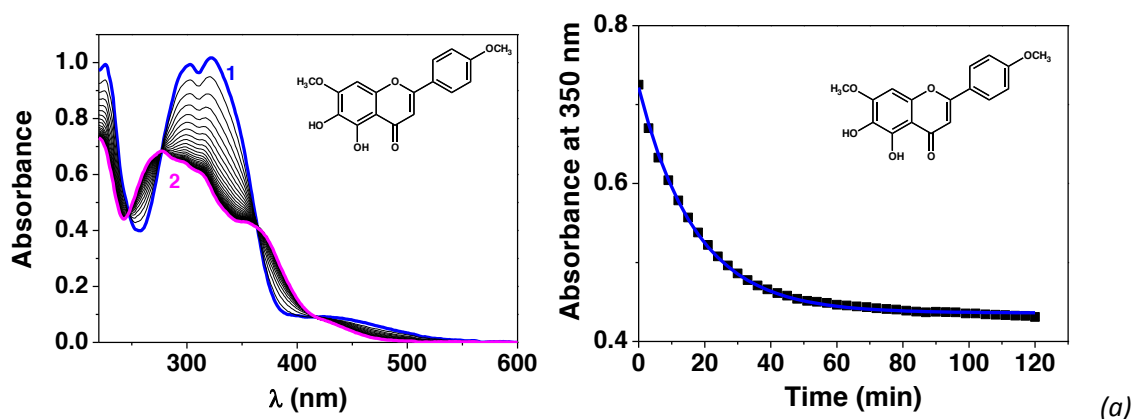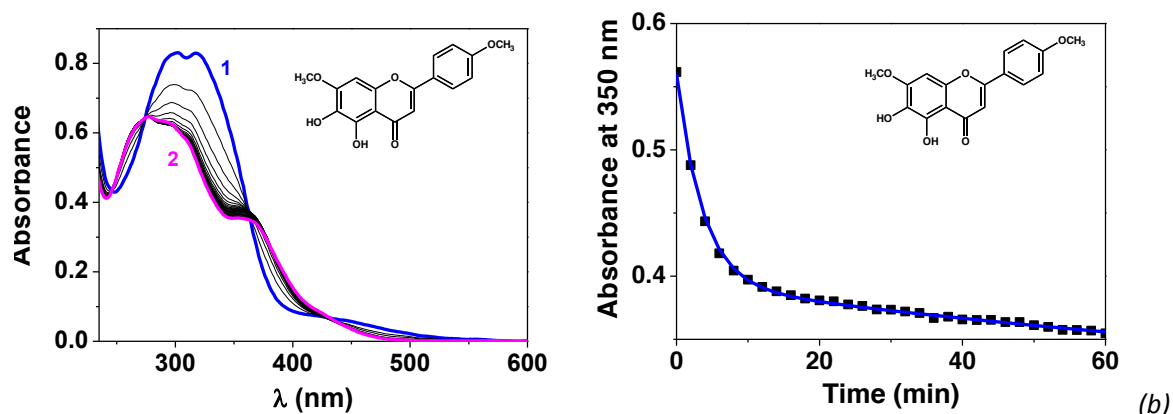

(a)

Figure 16. Absorption spectrophotometric spectra of solution of ladanein as a function of time (2 h) with the presence of base. Solvent: CH_3OH/H_2O (80/20 *w/w*); I = 0.1 M NEt_4ClO_4; T = 25.0(2) °C. (*a*) [**FOMe**]$_{tot}$ = 4.83 x 10^{-5} M; [NEt_4OH]$_{tot}$ = 9.63 x 10^{-4} M; (*b*) [**FOMe**]$_{tot}$ = 4.27 x 10^{-5} M; [NEt_4OH]$_{tot}$ = 8.75 x 10^{-3} M; l = 1 cm.

Figure 16 shows the time dependence of the absorption spectra of ladanein **FOMe** on exposure to air and addition of base. The absorption spectrum of the deprotonated form of ladanein is characterized by absorptions with maxima at 226 nm, 303 nm, and 322 nm (Table 4). During the first step of the oxidation/degradation, the two main absorption bands at 303 nm and 322 nm disappear while new absorptions appear at 277 nm and 354 nm. Isosbestic points at 248 nm, 277 nm and 416 nm clearly demonstrate the formation of only one predominant species during this first step. A second test was performed with an increased concentration of base, which led to the same observations (as well as a speed up of the oxidation kinetics, as discussed below). In addition, there is a further decrease of the absorption at 354 nm suggesting the formation of another minor product in a much slower kinetic step.

To gain further insight into the oxidation mechanism of free ladanein **FOMe**, we recorded electrospray mass spectra of the flavone in the presence of base (Figure 17) at different times after its addition (t = 0 and 15 minutes). In the absence of base (NH_4OH), the ESI-MS$^+$ spectrum of ladanein is characterized by peaks (*i.e.* mono-isotopic peak) at *m/z* = 315.15, 337.15, 353.05 and 651.3 corresponding to [**FOMe**+H]$^+$ (*m/z*$_{calc}$ = 315.09), [**FOMe**+Na]$^+$ (*m/z*$_{calc}$ = 337.07), [**FOMe**+K]$^+$ (*m/z*$_{calc}$ = 353.04) and [(**FOMe**)$_2$+Na]$^+$ (*m/z*$_{calc}$ = 651.15). Upon addition of base, new peaks whose intensity increase over time emerge (*e.g. m/z* = 264.15, 367.15, 399.15 and 969.4). Even though, the general profile of the ESI-MS$^+$ spectra is not significantly altered, some peaks provided valuable information. Indeed, the characteristic peaks of ladanein (*m/z* = 315.15, 337.15, 651.3) evidenced more intricate isotopic profiles which can be related to the oxidation ladanein into the corresponding quinone (resulting from -2e$^-$/-H$^+$ or -2e$^-$/-2H$^+$ oxidation). No loss of the 7-substituent (as seen for baicalin,

Scheme 5) is evidenced and importantly, no low-molecular-weight compounds are observed, as happens for quercetin (flavones/flavonols bearing a catechol unit on the B-ring, Scheme 4).
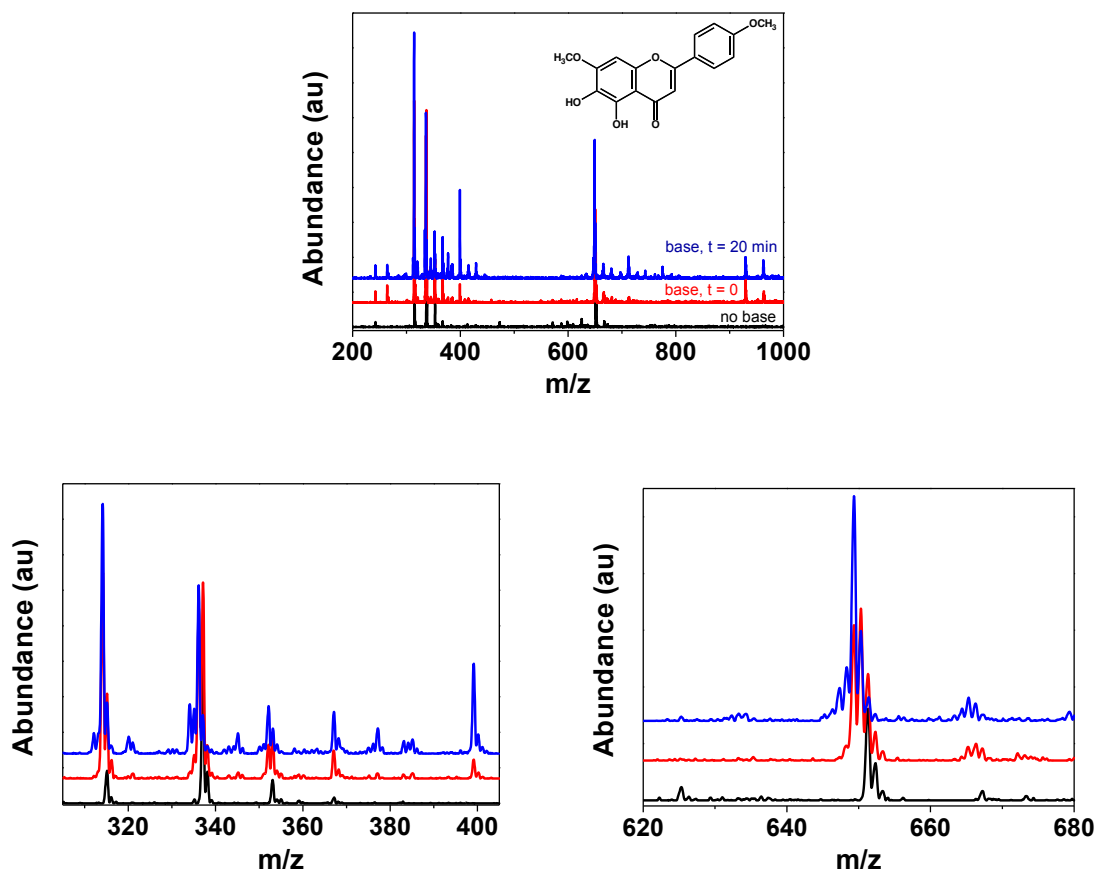
Figure 17. ESI-MS spectra of ladanein as a function of time (0 and 20 minutes) in the presence of base (NH_4OH). Solvent: CH_3OH/H_2O (80/20 *w/w*. (*a*) [**FOMe**]$_{tot}$ = 5 x 10^{-5} M; NH_4OH (0.01 *v/v*). Fragmentor = 100 V.

Upon close examination of the oxidation/degradation kinetics of the flavone, not only one but two rate limiting steps could be evidenced within the time range examined (2 hours) and in the presence of a high excess of base (NEt_4OH). For each of the two rate limiting steps and no matter the wavelength considered, the absorbances follow an exponential variation with time thus indicating a first-order reaction with respect to ladanein **FOMe**. The statistical processing of the absorption data versus time allowed the calculation of the pseudo-first order rate constants k^{obs}_1 and k^{obs}_2 (s^{-1}) related to the two stepwise oxidation processes (Figure 18b) as well as the electronic spectra of the oxidation products (Figure 18a). The pseudo-first order rate constants k_1^{obs} and k_2^{obs} linearly vary with [NEt_4OH] demonstrating that the oxidation/degradation processes are first-order reactions with respect to the base. These kinetic data clearly show that the deprotonation of the 6-OH is a key process triggering the oxidation of the flavones. The first step is characterized by a bimolecular rate

constant k_1 of 0.68(7) M^{-1} s^{-1}. The second slower step evidenced under our experimental conditions is associated to a bimolecular rate constant k_2 (1.42(3) x 10^{-3} M^{-1} s^{-1}), which is 50 times lower than k_1.

(a)   *(b)*
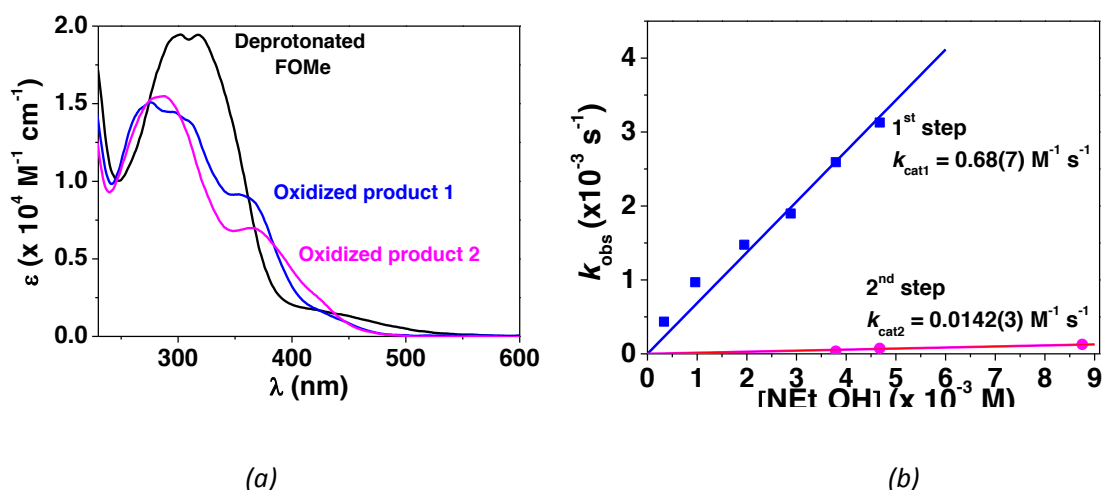
Figure 18. *(a)* Electronic absorption spectra of the oxidation/degradation products of ladanein **FOMe** and *(b)* variation of the pseudo-first order rate constants of the oxidation processes. Solvent: CH$_3$OH/H$_2$O (80/20 *w/w*); *I* = 0.1 M NEt$_4$ClO$_4$; *T* = 25.0(2) °C. (*a*) [**FOMe**]$_{tot}$ = 4-5 x 10^{-5} M.

To gain further insight on this process, the oxidation kinetics of two analogues of ladanein were studied, namely negletein **FH** and **FCF$_3$**. Figure 19 depicts the variation in absorption experienced during oxidation of the two flavones following deprotonation of the 6-OH unit. Interestingly, these spectral variations are comparable to those evidenced for ladanein with the first oxidation product characterized by absorption maxima at 362 nm and 259 nm for **FH** and 366 nm and 256 nm for **FCF$_3$**, respectively. Whatever the flavone considered, the band I centered on the benzoyl-type unit is then the most affected one, suggesting that the oxidation/degradation reactions involve the A-ring. The oxidation/degradation mechanism is seemingly shared by ladanein and its closely related analogues.

The flavones considered in this work were studied as well under apparent conditions ([NEt$_4$OH]$_{tot}$ = 9.50 x 10^{-4} M and [Flavone]$_{tot}$ = 4.7-4.8 x 10^{-5} M (Table 7). Even though weak differences can be observed for their oxidation kinetics (*i.e.* that can be attributed to their different acido-basic properties), the oxidation/degradation products apparently shared common features as shown by their comparable absorption spectrophotometric characteristics thus indicating the major role of the A-ring.

Table 7. Oxidation/degradation properties of the flavones considered in this work.[a]

Compounds	k_{obs} (x 10^{-4} s^{-1})	Oxidation product λ^{max} ($\epsilon^{\lambda max}$)
F	na	na
FH/Negletein	9.77	259(1.54)/362(0.77)
FOMe/ Ladanein	9.67	258(1.66)/351(0.84)
FP	no oxidation	na
FOCF$_3$	5.03	258(1.66)/362(0.76)
FF	10.27	259(1.56)/362(0.85)
FFCF$_3$	6.23	254(1.99)/363(0.98)
FCF$_3$	7.20	256(1.41)/366(0.73)
[a] Solvent: CH$_3$OH/H$_2$O (80/20 w/w); I = 0.1 M (NEt$_4$ClO$_4$); T = 25.0(2) °C. [NEt$_4$OH]$_{tot}$ = 9.50 x 10^{-4} M; na = not applicable		
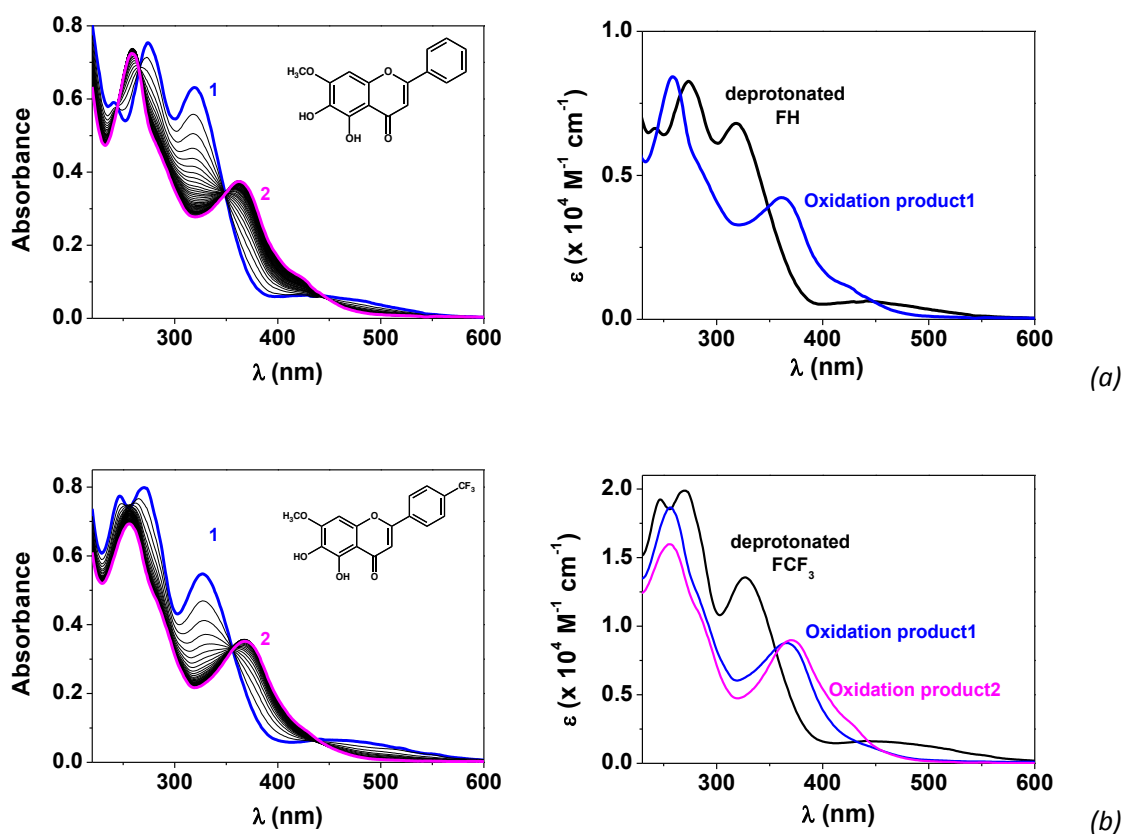
Figure 19. Variation of the absorption spectrophotometric spectra of solution of *(a)* **FH** and *(b)* **FCF$_3$** as a function of time (2 h) in the presence of base. Solvent: CH$_3$OH/H$_2$O (80/20 *w/w*); I = 0.1 M NEt$_4$ClO$_4$; T = 25.0(2) °C. (*a*) [**FH**]$_{tot}$ = 4.83 x 10^{-5} M; [NEt$_4$OH]$_{tot}$ = 9.63 x 10^{-4} M; (*b*) [**FCF$_3$**]$_{tot}$ = 4.27 x 10^{-5} M; [NEt$_4$OH]$_{tot}$ = 8.75 x 10^{-3} M; l = 1 cm.

The behavior of the final precursor **FP** was also studied using the same spectrophotometric method. Interestingly, no oxidation/degradation was observed for this compound within the time range examined, which suggests that the presence of a hydroxyl group in 5 may be necessary for this process to occur.
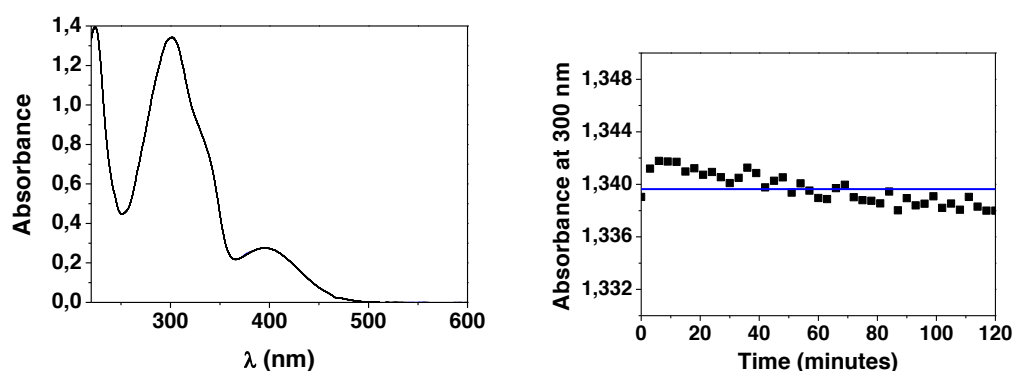
Figure 20. Absorption spectrophotometric spectra of solution of the final precursor **FP** as a function of time (2 h) with the presence of base. Solvent: CH_3OH/H_2O (80/20 *w/w*); I = 0.1 M NEt_4ClO_4; T = 25.0(2) °C. [**FP**]$_{tot}$ = 4.71 x 10^{-5} M; [NEt_4OH]$_{tot}$ = 9.42 x 10^{-4} M, l = 1 cm.

Taken together, the physico-chemical data suggest that deprotonation in aerobic conditions of the 6-OH group of ladanein and its analogues triggers the 1 e$^-$ oxidation of the corresponding phenolate. In contrast to baicalin, no demethylation of the 7-position occurs. From the results obtained for the tests performed on the final precursor **FP**, it can be suggested that the presence of 5-OH is necessary for this oxidative/degradation process to take place. Furthermore, it has been proven that **FP** displays no antiviral activity at all, so it may be possible that oxidation/degradation and antiviral activity are linked. In Scheme 6 we suggest a mechanism which ladanein and its derivatives may undergo when in presence of a base and leading to a quinone as the major product.
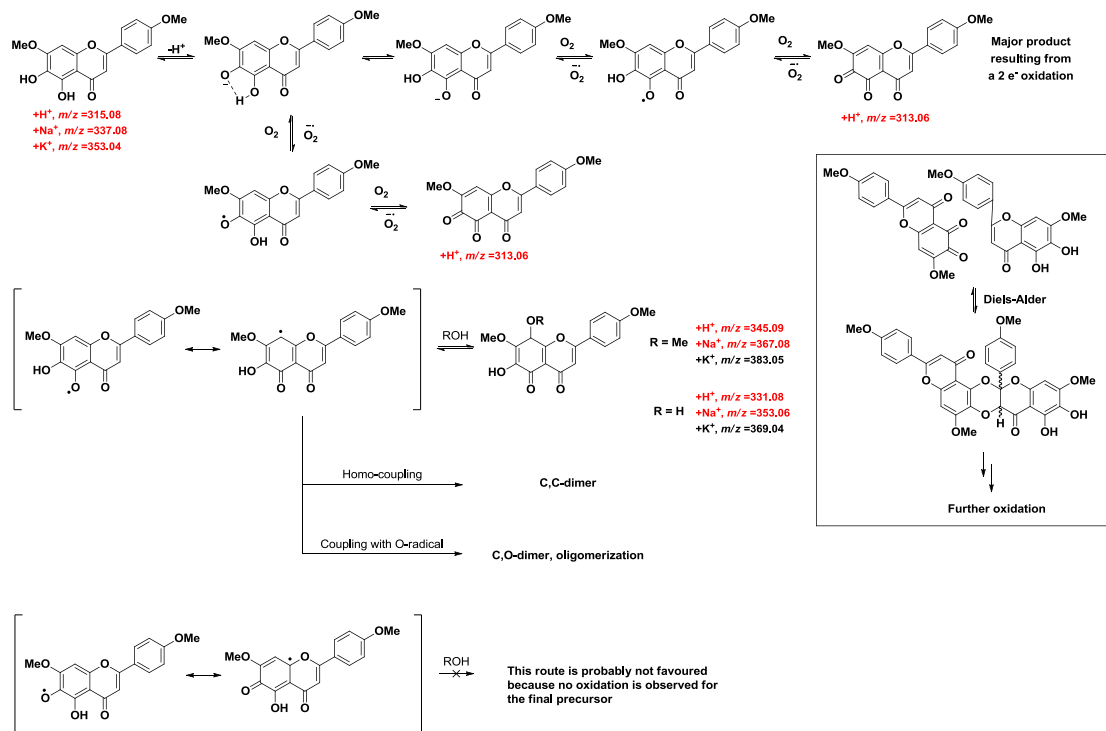
Scheme 6. Proposed mechanism that ladanein and its derivatives may undergo in presence of base. In red, the masses that have been observed by mass spectrometry.

Taken together, our data further confirmed observations made in my research group by previous colleagues. An HPLC analysis indeed showed that ladanein **FOMe** from extraction source was subjected to degradation in solution over the time by possible formation of the quinone following 2 electrons oxidation in absence of metal with significant loss of antiviral (HIV) activity (Figure 21).

Figure 21. Degradation of ladanein **FOMe** (fraction S3F4 found to be the most active) in solution in the presence of air revealed by HPLC and time-dependent decay of anti-HIV potency of fraction S3F4 in single round infection experiments.

3.4. Conclusion

In conclusion, in this chapter we have described the acido-basic properties of the synthesized flavones, bearing different substituents on cycle B. It is important to mention that very few physico-chemical studies of this type of compounds can be found in the litera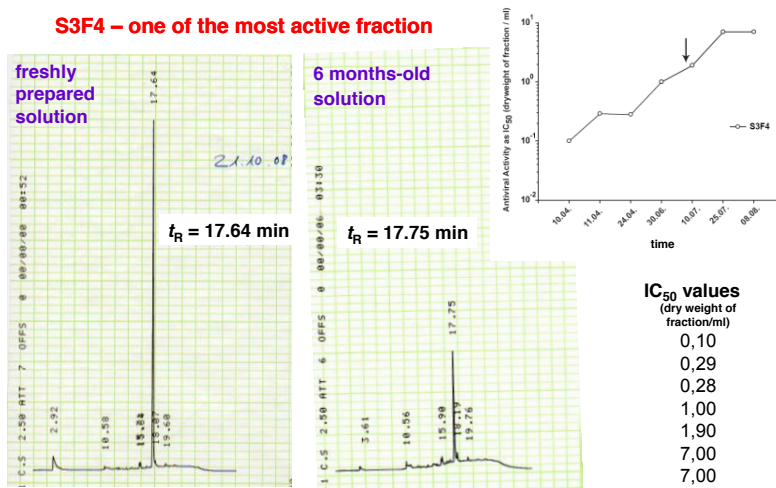ture. The acido-basic properties of this series of compounds were determined by spectrophotometric *vs.* pH titrations. Only one pKa value could be determined and it is suggested that it belongs to the 6-OH group and not the 5-OH since the latter forms a strong hydrogen bond with the adjacent carbonyl group. The substituent on the B-ring does not appear to have a very strong influence on the acido-basic properties of the groups on the A-ring, since the values do not change significantly between flavones bearing either electron donating or withdrawing groups. The results obtained are comparable to those of other antiviral polyphenols such as curcumin or EGCG, all of the compounds being in the protonated form in the liver. As stated previously, the pK_a values do not significantly change between different flavones except for **FOMe**, which may be explained because of the higher planarity of this compound compared to the rest.

The stability of the flavones at different pH values has been studied. The compounds are stable at acidic and neutral pH in MeOH/H$_2$O. However, the deprotonation in the 6-OH position triggers a slow degradation/oxidation process. A kinetic study of this process was performed by UV-Vis spectrometry and it was found that a 2-step oxidation takes place with similar rate constants values. The absorption spectra of all the flavones show similar features, so it can be suggested that it is a shared process. The oxidation was also studied by ESI-MS, and it was found that addition, oxidation and hydrolysis products may be formed during this process.

Overall, the substituent present in cycle B does not seem to be primordial for the acido-basic properties. Rather, it modulates the properties of the flavones, making it possible to have a great structural diversity in that cycle.

EXPERIMENTAL SECTION

Starting Materials and Solvents

Distilled water was further purified by passing it through a mixed bed of ion-exchanger (Bioblock Scientific R3-83002, M3-83006) and activated carbon (Bioblock Scientific ORC-83005) and was de-oxygenated by CO_2- and O_2-free argon (Sigma Oxiclear cartridge) before use. Spectrophotometric grade methanol (Merck, p.a.) and water were de-oxygenated by CO_2- and O_2-free argon (Sigma Oxiclear cartridge). All the stock solutions were prepared by weighing solid products using an AG 245 Mettler Toledo analytical balance (precision 0.01 mg). The ionic strength was maintained at 0.1 M with n-tetrabutylammonium perchlorate (NEt_4ClO_4, Fluka, puriss), and all measurements were carried out at 25.0(2) °C. All stock solutions were prepared using an AG 245 Mettler Toledo analytical balance (precision 0.01 mg). *CAUTION! Perchlorate salts combined with organic ligands are potentially explosive and should be handled in small quantities and with the adequate precautions.*[45]

Spectrophotometric Titrations versus pH

Spectrophotometric titrations as a function of pH of the free flavones were performed to evaluate their protolytic properties. For the sake of solubility, the flavones were dissolved in a mixed solvent made of 80% of methanol (Merck) and 20% of water by weight. Stock solutions of the flavones were first prepared by quantitative dissolution of the corresponding solid samples in methanol. The flavone solutions were then diluted in CH_3OH/H_2O solvent (80/20 by weight) containing the supporting electrolyte at 0.1 M (NEt_4ClO_4, Fluka, puriss). An aliquot of 40 mL of the solutions was then introduced into a jacketed cell (Metrohm) maintained at 25.0(2) °C by the flow of a Lauda E200 thermostat under Ar atmosphere. The free hydrogen ion concentration was measured with a combined glass electrode (Metrohm 6.0234.500, Long Life) and an automatic titrator system 794 Basic Titrino (Metrohm) connected to a microcomputer (Tiamo light 1.2 program for the acquisition of the potentiometric data). The Ag/AgCl reference glass electrode was filled with NaCl (0.1 M, Fluka, p.a.). The combined glass electrode was calibrated as a hydrogen concentration probe by titrating known amounts of perchloric acid ($\sim 7 \times 10^{-2}$ M from $HClO_4$, Prolabo, normapur, 70% min) with CO_2-free tetraethylammonium hydroxide solution ($\sim 7 \times 10^{-2}$ M from Aldrich, purum, ~ 40 % in water).[46] The $HClO_4$ and NEt_4OH solutions were freshly prepared just before use in CH_3OH/H_2O solvent and titrated with sodium tetraborate decahydrate ($B_4Na_2O_7.10H_2O$, Fluka, puriss, p.a.) and potassium hydrogen phthalate ($C_8H_5KO_3$, Fluka, puriss, p.a.), respectively, using methyl orange (RAL) and phenolphthalein (Prolabo, purum) as the indicators. The initial pH of the flavone solution was adjusted to ~ 2 with $HClO_4$ (Prolabo, normapur, 70% min), and the titrations of the free flavone (5 <

pH < 12) were then carried out by addition of known volumes of NEt_4OH solutions with an Eppendorf microburette. Special care was taken to ensure that complete equilibration was attained. Absorption spectra versus pH were then recorded using a Varian CARY 50 spectrophotometer fitted with Hellma optical fibers (Hellma, 041.002-UV) and an immersion probe made of quartz suprazil (Hellma, 661.500-QX). The temperature was maintained at 25.0(2) °C with the help of a Lauda E200 thermostat.

Analysis and Processing of the Spectroscopic Data

The spectrophotometric data were analysed with Specfit[47] programs which adjust the absorptivities and the stability constants of the species formed at equilibrium. Specfit uses factor analysis to reduce the absorbance matrix and to extract the eigenvalues prior to the multiwavelength fit of the reduced data set according to the Marquardt algorithm.[48,49]

Electrospray Mass Spectrometric Measurements

Electrospray mass spectra of the flavones and their oxidation products under basic conditions (addition of 0.1% NH_4OH *v/v*) were obtained with an Agilent Technologies 6120 quadrupole equipped with an electrospray (ESI) interface. Solutions (5×10^{-5} M) of the flavones have been prepared in water in the absence of any background salt. The sample solutions were continuously introduced into the spectrometer source with a syringe pump (Kd Scientific) with a flow rate of 600 $\mu L.h^{-1}$. For electrospray ionization, the drying gas was heated at 250 °C and its flow was set at 6 $L.min^{-1}$. The capillary exit voltage was fixed at 5 kV and the skimmer voltage was varied from 20 to 150 V in order to optimize the signal responses. Scanning was performed from m/z = 100 to 1500.

Oxidation Kinetics

The oxidation kinetics of the free flavones under basic conditions was sufficiently slow to be monitored by conventional absorption spectrophotometry. For **FOMe** ($4\text{-}5 \times 10^{-5}$ M), the oxidation kinetics of the flavone was studied for $[OH^-]$ ranging from 3.33×10^{-4} M to 8.75×10^{-3} M (at least ten times more concentrated solutions of OH^- with respect to MP03 impose pseudo-first order conditions) in CH_3OH/H_2O solvent (80:20 by weight) and absorption spectra (200 – 800 nm) were recorded as a function of time in a time span of 2 hours. For the other flavone derivatives, the oxidation kinetics was studied under apparent conditions (i.e. the flavone and base concentrations were kept constant whatever the flavone considered). The temperature was maintained at 25.0(2) °C

with the help of a Lauda E200 thermostat. The spectrophotometric data were analyzed with the Specfit program.[45-49]

X-ray of ladanein (FOMe) from natural and synthetic sources as well as of the final precursor (FP)

Natural ladanein: yellow crystal (plate), dimensions 0.40 x 0.31 x 0.02 mm^3, crystal system monoclinic, space group P2$_1$/c, Z=4, a=7.1846(19) Å, b=26.741(7) Å, c=7.2404(19) Å, alpha=90 deg, beta=92.287(6) deg, gamma=90 deg, V=1390.0(6) Å^3, rho=1.502 g/cm^3, T=200(2) K, Theta$_{max}$= 28.41 deg, radiation Mo Kalpha, lambda=0.71073 Å, 0.3 deg omega-scans with CCD area detector, covering a whole sphere in reciprocal space, 14338 reflections measured, 3469 unique (R(int)=0.0436), 2818 observed (I >2σ(I)), intensities were corrected for Lorentz and polarization effects, an empirical absorption correction was applied using SADABS[1] based on the Laue symmetry of the reciprocal space, mu=0.12mm^{-1}, T$_{min}$=0.96, T$_{max}$=1.00, structure solved by direct methods and refined against F^2 with a Full-matrix least-squares algorithm using the SHELXTL-PLUS (5.10) software package[2], 218 parameters refined, hydrogen atoms were treated using appropriate riding models, except of H5 and H6 at the hydroxyl groups, which were refined isotropically, goodness of fit 1.30 for observed reflections, final residual values R1(F)=0.092, wR(F^2)=0.169 for observed reflections, residual electron density -0.32 to 0.44 eÅ^{-3}.

Synthetic ladanein FOMe: yellow crystal (platte), dimensions 0.20 x 0.14 x 0.06 mm^3, crystal system triclinic, space group P $\overline{1}$, Z=2, a=6.8268(10) Å, b=7.6728(11) Å, c=15.650(2) Å, alpha=83.681(3) deg, beta=85.254(3) deg, gamma=86.152(3) deg, V=810.6(2) Å^3, rho=1.419 g/cm^3, T=274(2) K, Theta$_{max}$= 28.34 deg, radiation Mo Kalpha, lambda=0.71073 Å, 0.3 deg omega-scans with CCD area detector, covering a whole sphere in reciprocal space, 8504 reflections measured, 3986 unique (R(int)=0.0265), 2853 observed (I >2σ(I)), intensities were corrected for Lorentz and polarization effects, an empirical absorption correction was applied using SADABS[1] based on the Laue symmetry of the reciprocal space, mu=0.11mm^{-1}, T$_{min}$=0.98, T$_{max}$=0.99, structure solved by direct methods and refined against F^2 with a Full-matrix least-squares algorithm using the SHELXTL-PLUS (6.10) software package[2], 241 parameters refined, hydrogen atoms were treated using appropriate riding models, except of the hydrogen atoms of the hydroxy groups, which were refined isotropically, goodness of fit 1.14 for observed reflections, final residual values R1(F)=0.077, wR(F^2)=0.162 for observed reflections, residual electron density -0.30 to 0.35 eÅ^{-3}.

Final precursor: yellowish crystal (polyhedron), dimensions 0.39 x 0.08 x 0.06 mm^3, crystal system orthorhombic, space group Pbca, Z=8, a=14.659(2) Å, b=9.8378(11) Å, c=21.236(2) Å, alpha=90 deg, beta=90 deg, gamma=90 deg, V=3062.5(6) Å^3, rho=1.424 g/cm^3, T=200(2) K, Theta$_{max}$= 25.00 deg,

radiation Mo Kalpha, lambda=0.71073 Å, 0.3 deg omega-scans with CCD area detector, covering the asymmetric unit in reciprocal space with a mean redundancy of 2.6 and a completeness of 99% up to a resolution of 0.77 Å, 5200 reflections measured, 2657 unique (R(int)=0.0679), 1308 observed (I >2σ(I)), intensities were corrected for Lorentz and polarization effects, an empirical absorption correction was applied using SADABS based on the Laue symmetry of the reciprocal space, mu=0.11mm^{-1}, T$_{min}$=0.96, T$_{max}$=0.99, structure solved by direct methods and refined against F^2 with a Full-matrix least-squares algorithm using the SHELXTL-PLUS (5.10) software package, 224 parameters refined, hydrogen atoms were treated using appropriate riding models, except of H6 at the hydroxyl oxygen atom H6, which was refined isotropically, goodness of fit 0.94 for observed reflections, final residual values R1(F)=0.050, wR(F^2)=0.082 for observed reflections, residual electron density -0.26 to 0.24 eÅ^{-3}.

References

(1)   Moghaddam, E.; Teoh, B-T.; Sam, S-S.; Lani, R.; Hassandarvish, P.; Chik, Z.; Yueh, A.; Abubakar, S. and Zandi, K. *Sci. Rep.* **2014**, *4*, 5452.

(2)   This work. Unpublished results.

(3)   Sharma, D.; Gupta, V.K.; Brahmachari, G.; Mondal, S. and Gangopadhyay, A. *Bull. Mater. Sci.* **2007**, *30*, 469.

(4)   (a) Sowa, M.; Slepokura, K. and Matczak-Jon, E. *Acta Crystallogr. Sect. C-Cryst. Struct. Commun.* **2012**, *68*, o262. (b) Hibbs, D.E.; Overgaard, J.; Gatti, C. and Hambley, T.W. *New J. Chem.* **2003**, *27*, 1392. (c) Rossi, M.; Meyer, R.; Constantinou, P.; Caruso, F.; Castelbuono, D.; O'Brien, M. and Narasimhan, V. *J. Nat. Prod.* **2001**, *64*, 26.

(5)   Mou, M-Y. ; Pi, K. ; Zhang, Q-L.; Zhang, Y-Q. and Zhang, Q-J. *Acta Cryst. E*. **2008**, *E64*, o71.

(6)   Chou, N. H-H.; Parvez, M.; Ali, M.S.; Ahmed, S. and Ahmed, W. *Acta Cryst. E*. **2002**, *E58*, o285-o287.

(7)   Parvez, M.; Riaz, M. and Malik, A. *Acta Cryst. E*. **2001**, *E57*, o289-o291.

(8)   Adizov, S.M.; Mukhamathanova, R.F.; Turgunov, K.K.; Sham'yanov, I.D. and Tashkhodjaev, B. *Acta Cryst.* E. **2013**, *E69*, o578.

(9)   Li, H-J.; Zhou, D-L.; Xu, T-J.; Lam, C-K. and Lan, W-J. *Acta Cryst. E*, **2012**, *E68*, o1390.

(10)   (a) Rossi, M.; Rickles, L.F.; Halpin, W.A. *Bioorg. Chem.* **1988**, *14*, 55. (b) Rossi, M.; Cantrell, J.S.; Farber, A.J.; Dyott, T.; Carrell, H.L.; Glusker, J.P. *Cancer Res.* **1980**, *40*, 2774.

(11)   Hall, B.J.; Hanrahan, J.R.; Johnston, G.A.R.; Hambley, T.W. and Hibbs, D.E. *Acta Crystallogr. Sect. E.* **2001**, 57, o592 and references therein.

(12)   Wolniak, M.; Oszmianskib, J. and Wawera, I. *Magn. Reson. Chem.* **2008**, *46*, 215.

(13)   HYPERCHEM, version 7.52 for windows, Hypercube Trademarks, Inc., 2005, Gainesville, USA.

(14)   Jurd, L. ,*The Chemistry of Flavonoid Compounds*, Geissman, T.A., Ed. Pergamon Press, New-York, 1962, 107-155.

(15)   Cornard, J.P.; Merlin, J.C.; Boudet, A.C. and Vrielynck, L. *Biospectroscopy* **1997**, *3*, 183.

(16)   Cornard, J.P. and Merlin, J.C. *J. Mol. Struc.* **2001**, *569*, 129.

(17)   Vrielynck, L.; Cornard, J.P.; Merlin, J.C. and Bopp, P. *J. Mol. Struc.* **1993**, *297*, 227.

(18)   Cornard, J.P.; Boudet, A.C. and Merlin, J.C. *J. Mol. Struc.* **1999**, *508*, 37.

(19)   Sancho, M.; Almandoz, M.C.; Blanco, S.E. and Castro, E.A. *Int. J. Mol. Sci.* **2011**, *12*, 8895.

(20)   Carrër, C. "Chélation de métaux de transition par des polyphénols du régime alimentaire", Thèse de Doctorat de l'Université Louis Pasteur de Strasbourg, January 28th, 2005

(21)   McDaniel, D.H. and Brown, H.C. *J. Org. Chem.* **1958**, *23*, 420.

(22)   Hammett, L. P. *J. Am. Chem. Soc.* 1937, *59*, 96.

(23)   Hansch, C.; Leo, A. and Taft, R.W. *Chem. Rev.* **1991**, *91*, 165.

(24)   (a) Gampp, H.; M. Maeder, Meyer, C. J.; Zuberbühler, A. D. *Talanta* **1985**, 32, 95. (b) Gampp, H.; Maeder, M.; Meyer, C. J.; Zuberbühler, A. D. *Talanta* 1985, *32*, 251. (c) Gampp, H.; Maeder, M.; Meyer, C. J.; Zuberbühler, A. D. *Talanta* **1985**, *32*, 1133.

(25)   Thompson, M.; Williams, G.R. and Elliot, G.E.P. *Anal. Chim. Acta* **1976**, *85*, 375.

(26)   Murata, A.; Tominaga, M.; Inoue, H. and Suzuki, T. *Jpn. Analyst* **1973**, *22*, 179.

(27)   Slabbert, N.P.; *Tetrahedron*, **1977**, *33*, 821.

(28)   Varenikov, A.S.; Serdiuk, I.E. and Roshal, A.D. *Fr.Ukr. J. Chem*. **2013**, *1*, 153.

(29)   Aoi, W. and Marunaka, Y. *BioMed. Res. Int.* **2014**, article ID 598986.

(30)   Borsari, M.; Ferrari, E.; Grandi, R. and Saladini, M. *Inorg. Chim. Acta* **2002**, *328*, 61.

(31)   Inoue, M.; Fernando, Q. and Valcic, S.J. *Inorg. Biochem.* **2002**, *88*, 7.

(32)   (a) Ding, K.; Wang, Y.; Zhang, L. and Wu, Y. *Tetrahedron* **1996**, *52*, 1005. (b) Toda, F.; Tanaka, K. and Iwata, S. *J. Org. Chem.* **1989**, *54*, 3007.

(33)   Brussee, J.; Groenendijk, J.L.G.; Koppele, J.M. and Jansen, A.C.A. *Tetrahedron* **1985**, *41*, 3313.

(34)   Kantam, M.L.; Kavita, B. and Figueras, F. *Catal. Lett.* **1998**, *51*, 113.

(35)   Bozell, J.J. and Hames, B.R. *J. Org. Chem.* **1995**, *60*, 2398.

(36)   (a) Bailey, S.I.; Ritchie, I.M. and Hewgill, F.R. *J. Chem. Soc. Perkin Trans. II* **1983**, *5*, 645. (b) Laviron, E. *J. Electroanal. Chem.* **1984**, *164*, 213. (c) Sokolová, R.; Degano, I.; Hromadová, M.; Bulíčková, J.; Gál, M. and Valášek, M. *Collect. Czech. Chem. Commun.* **2010**, *75*, 1097. (d) Costentin, C.; Louault, C.; Robert, M. and Savéant, J-M. *J. Am. Chem. Soc.* **2008**, *130*, 15817. (e) Musialik, M.; Kuzmicz, R.; Pawlowski, T.S. and Litwinienko, G. *J. Org. Chem.* **2009**, *74*, 2699.

(37)   (a) Makris, D.P. and Rossiter, J.T. (2002) *J. Food Composition Anal.* **2002**, *15(1)*, 103. (b) Tournaire, C.; Hocquaux, M.; Beck, I.; Oliveros, E. and Maurette, M-T. *Tetrahedron* **1994**, *50(31)*, 9303. (c) Jungbluth, G.; Ruhling, I. and Ternes, W. *Chem. Soc. Perkin Trans.* **2000**, *2(9)*, 1946. (d) Jorgensen, L.V.; Cornett, C.; Justesen, U.; Skibsted, L.H. and Dragsted, L.O. *Free Rad. Res.* **1998**, *29(4)*, 339. (e) Timbola, A.K.; De Souza, C.D.; Giacomelli, C.; Spinelli, A. and Braz, J. *Chem. Soc.* **2006**, *17(1)*, 139. (f) Sokolová, R.; Degano, I.; Ramešová, Š.; Bulíčková, J.; Hromadová, M.; Gál, M.; Fiedler, J. and Valášek, M. (2011) *Electrochim. Acta* **2011**, *56(21)*, 7421. (g) Hendrickson, H.P.; Kaufman, A.D. and Lunte, C.E. (1994) *J. Pharm. Biomed. Anal.* **1994**, *12(3)*, 325.

(38)   Makris, D.P. and Rossiter, J.T. *J. Food Composition Anal.* **2002**, *15*, 103.

(39)   Zenkevich, I.G.; Eshchenko, A.Y.; Makarova, S.V.; Vitenberg, A.G.; Dobryakov, Y.G. and Utsal, V.A. *Molecules* **2007**, *12*, 654.

(40)   Zhou, A.; Kikandi, S. and Sadik, O.A. *Electrochem. Commun.* **2007**, *9(9)*, 2246.

(41)   Lei, R.; Xu, X.; Yu, F.; Li, N.; Liu, H.W. and Li, K. *Talanta* **2008**, *75(4)*, 1068.

(42)   Ramešová, S.; Sokolová, R.; Degano, I.; Bulíčková, J.; Žabka, J. and Gál, M. *Anal. Bioanal. Chem.* **2012**, *402*, 975.

(43)   Krishnamachari, V.; Levine, L.H. and Paré, P.W. *J. Agric. Food Chem.* **2002**, *50*, 4357.

(44)   Xing, J.; Chen, X. and Zhong, D. *J. Pharm. Biomed. Anal.* **2005**, *39*, 593.

(45)   Raymond, K.N. *Chem. Eng. News* **1983**, *61*, 4.

(46)   Gans, P. and O'Sullivan, B. *Talanta* **2000**, *51*, 33.

(47)   (a) Gampp, H.; Maeder, M.; Meyer, C.J. and Zuberbühler, A.D. *Talanta* **1985**, *32*, 95. (b) Rossotti, F.J.C.; Rossotti, H.S. and Whewell, R.J. *J. Inorg. Nucl. Chem.* **1971**, *33*, 2051. (c) Gampp, H.; Maeder, M.; Meyer, C.J. and Zuberbühler, A.D. *Talanta* **1985**, *32*, 257. (d) Gampp, H.; Maeder, M.; Meyer, C.J. and Zuberbühler, A.D. *Talanta* **1986**, *33*, 943.

(48)   Marquardt, D.W. *J. Soc. Indust. Appl. Math.* **1963**, *11*, 431.

(49)   Maeder, M. and Zuberbühler, A.D. *Anal. Chem.* **1990**, *62*, 2220.

Chapter IV. Electrochemical Study of the Flavones

In this chapter, we will describe the electrochemical results obtained for ladanein and its synthetic analogues (Figure 1) using cyclic voltammetry. This approach allowed us to gain insight into the redox behavior of this class of compounds for which very scarce data has been reported in the literature until now. For the sake of comparison and to evaluate the role of the carbonyl unit borne by the C-ring, 2-phenyl-chromone (flavone **F**) was studied as well and has been used as a model. Epicatechin, epigallocatechin gallate (EGCG) and curcumin will also be included in the discussion, since they display anti-HCV properties with a similar mode of action (prevention of the viral infection at the cellular entry level) (Figure 2).

First, the electrochemical behavior of flavonoids will be described. Furthermore, the importance of hydroxylation pattern on the redox behavior will be evaluated. Particular emphasis will be focused on the very limited electrochemical studies performed on flavonoids bearing the 5,6,7-trihydroxylation motif on the A-ring The electrochemical data for epicatechin, EGCG and curcumin will be also described. In the next section, the electrochemical data obtained for ladanein **FOMe** and its analogues will be presented and discussed.

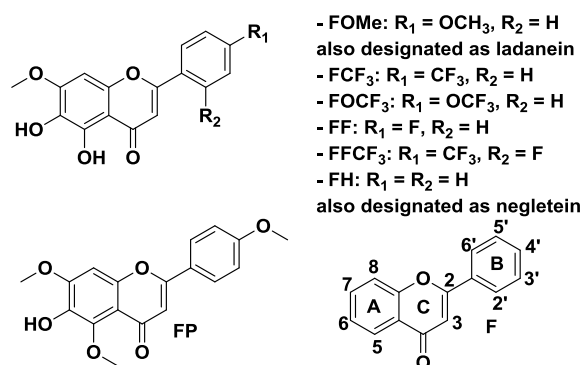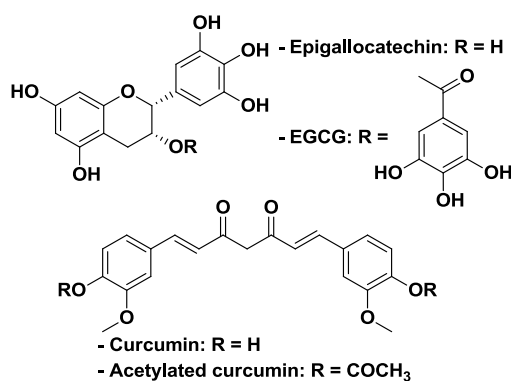**Figure 1.** Chemical structures of the flavones considered in this work.

Figure 2. Chemical structures of curcumin (and its acetylated derivative) and of epigallocatechin gallate EGCG (and of the deacylated analogue epigallocatechin EGC).

4.1. Introduction

The electrochemical profile of flavonoids is mainly driven by the stability of electro-generated phenoxyl radicals which determines the overall electrode reactions.[1,2] Furthermore, the redox behavior of flavonoids is influenced by proton-electron transfer mechanisms (in a wide range of pH), which are closely related to their physico-chemical properties, such as the acido-basic (see the previous chapter). The experimental conditions and these intrinsic physico-chemical properties have therefore an interdependent role on the stability of radical intermediates as well as on the course of electrochemical reactions. These latter aspects closely rely on structural characteristics, especially the number and the position of the hydroxyl substituents. If the influence of the C-ring on the global redox behavior of flavonoids can be neglected, the phenolic groups on rings A and B impose the electro-activity of the flavonoids and thereby their corresponding electrochemical profiles.[3]

Substituents such as methoxyl, acetylesters, glucosides, and keto groups have a secondary influence on the redox behavior and formation of oxidation products.[4,5] For instance, the phenol groups present in the A-ring and, especially, in the B-ring, exert a significant influence not only on the electrochemical profile but also on the electron/proton donor ability and the resulting antioxidant capacity. Another important feature is that the phenol pattern (*ortho/para* directing groups) influences the electron delocalization, affecting the stability of radical intermediates, which may even lead to different electrode reaction pathways and electrochemical profile. For example, the electrochemical oxidation of phenol is an irreversible process, occurring in one step, whereas the catechol oxidation occurs through a two electrons/two protons reversible mechanism. Phenol is oxidized in a one-electron and one proton step, to a phenoxyl radical which is thermodynamically unstable and coexists in three resonance forms. The highest spin density of this radical is in the *ortho-* and *para*-positions, whereas the *meta*-position is not favored for any kind of chemical reaction.[5] Therefore, the stabilization of the phenoxyl radical is followed by hydrolysis at a high potential mainly at *ortho-* and *para*-positions (Figure 3a).
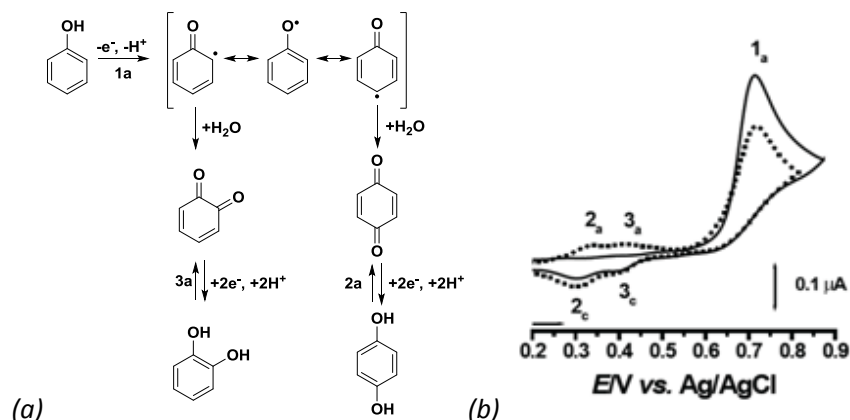
Figure 3. (a) Oxidation mechanism of phenol. (b) Voltammetric profile for phenol reduction and oxidation.

4.1.1. Flavonoids with Monophenol Pattern

As discussed previously, the oxidation of monophenols is always irreversible on the whole pH range.[5] It is generally accompanied by electro-deposition of oxidation products (*e.g.* hydroquinone and catechol) that undergoes reversible oxidation at lower potentials.[5,6] Figure 3b shows a typical voltammetric profile of phenol. The irreversible anodic peak 1a is followed on the reverse scan by two reversible redox pairs at low potentials corresponding to the oxidation products (Figure 1A). In flavonoids, the monophenol pattern can occur on ring B, where there are many examples, *i.e.* kaempferol[7], naringenin,[8] apigenin,[8,9,10] genistein,[11] pelargonidin,[12] as well as on ring A, exemplified by fisetin[13], or on both aromatic rings, (naringin,[14] diosmin,[15] daidzein[16]) (Figure 4).
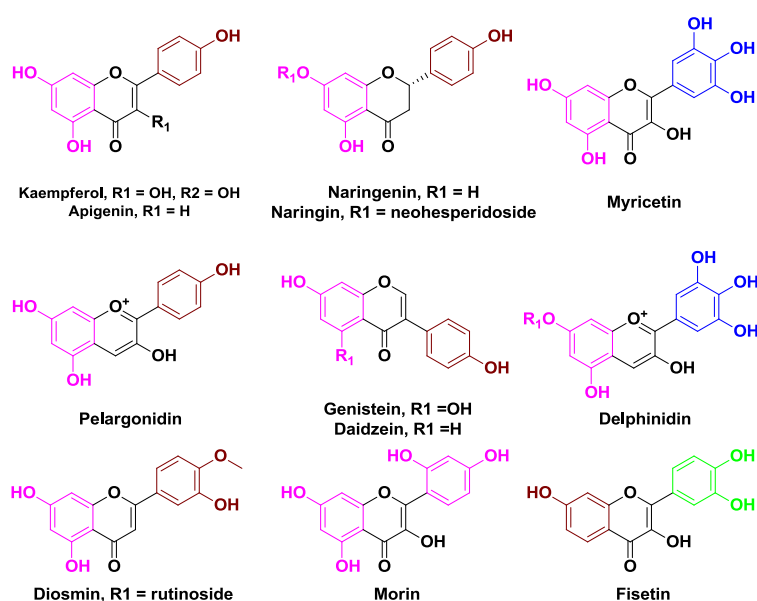

Figure 4. Chemical structures of selected flavonoids of particular electrochemical interest. Depicted in pink are the resorcinol groups, in red the phenol groups, in blue the pyrogallol groups and in green the catechol groups.

Resorcinol is probably the most frequent pattern in flavonoid chemistry and is almost ubiquitous in A-ring. However, its occurrence in cycle B is rare. Since this *meta* substitution does not allow stabilization of the radical intermediates, the resorcinol group is oxidized at higher positive potentials (> 0.7 V at neutral pH).[5,8] As for monophenols, such oxidation mechanism occurs *via* an EC mechanism involving a one electron/one proton transfer and the formation of an electroactive product. Although the first step is irreversible in the whole acidity range, the electroactive product may undergo reversible processes in non-alkaline medium.[5] The electrochemical profile of flavonoids displaying resorcinol or monophenol moiety is similar. For example, morin and other representative examples of non-catechol aglycones (Figure 4) share a similar electrochemical profile.[8,15,17,18] All these compounds undergo an irreversible anodic process at potentials higher than 0.8 V under mild acidic pH, while on successive scans the reversible redox pair corresponding to catechol like products may appear at lower peak potentials.

4.1.2. Flavonoids with Catechol Pattern

Para- and *ortho-* benzenediols derived flavonoids are much more easily oxidized than resorcinol or monophenols.[5] Besides, unlike phenol and resorcinol moieties, catechol-containing compounds undergo a two electron/two proton reversible oxidation process.[5-7,19] The reversibility is explained by means of electron delocalization in the *para* and *ortho* positions, which leads to the stabilization of phenoxyl radicals and reduces the overpotential required to achieve oxidation.[5,20] Hence, oxidation of such phenolic patterns takes place at very low positive potentials (*e.g.* E_{pa} ~0.2 V for the catechol model and 0.15 V for its hydroquinone state at pH 7.0). At higher pH, the phenol oxidation undergoes a non-proton coupled electron transfer mechanism, which often includes irreversible bond breaking followed by chemical reactions (*i.e.* dimerization and fall of peak currents).[16,17] The B ring catechol moiety is widely present among the strongest antioxidants. The redox reversibility and the low anodic potentials of 3',4'-dihydroxyl agree with the higher electron-donating properties of catechol B ring flavonoids.

To the best of our knowledge, only scarce examples of flavonoids bearing a catechol group on the A-ring have been described until now. In a first study, the effect of pH on the electrochemical CV response of the DM-β-CD-GNs/GCE (DM-β-CD = 2,6-dimethyl-β-cyclodextrin and GCE = Glassy Carbon Electrode) towards the detection of baicalin has been reported.[21] The electrochemical behavior was shown to be a two electrons/two protons process (Figure 5) and the oxidation and reduction processes were found to vary linearly with the pH (E_{pa} (V) = - 0.064pH + 0.598 and E_{pc} (V) = -0.056pH + 0.470). It has also been reported that the voltammetric behavior of a scutellarin analogue (5,6,4'-trihydroxy-7-O-glucuronide-flavone) also involves two electrons/two protons quasi-reversible redox

peaks with E_{pa} = 0.154 V and E_{pc} = 0.073 V at pH 7.4) on a graphite electrode.[22] The oxidation process was an adsorption-controlled process at low scan rates while at higher scan rates a diffusion-controlled process is suggested.
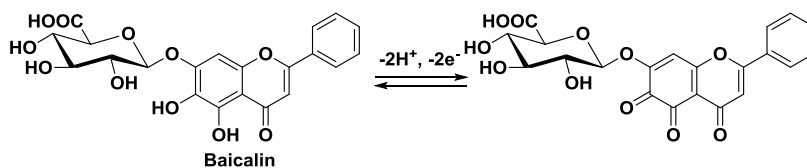

Figure 5. The redox mechanism of baicalin in DM-β-CD-GNs/GCE.

The CV of baicalein (5,6,7-trihydroxyflavone) has been studied as well and shows two different anodic peaks, I and II, with E_{pa1} = 0.118 V and E_{pa2} = 0.645 V (at pH 7.4), respectively in water with a thermally reduced graphene oxide (TRGO) modified GCE and GCE systems.[23] The first anodic peak at 0.118 V is reversible and may correspond to the oxidation of baicalein at the 6- and 7- phenolic hydroxyl positions. For the second anodic peak at 0.645 V, which is irreversible, it has been suggested that the electrochemical oxidation occurs at the third residue phenolic hydroxyl. The effect of pH on the voltammetric response of baicalein at the TRGO/GCE electrode was investigated and showed that both the oxidation and the reduction peak potentials shifted to the positive direction with decreasing pH from 7.40 to 2.40 further indicating that protons play an important role in the electrochemical reaction of baicalein.
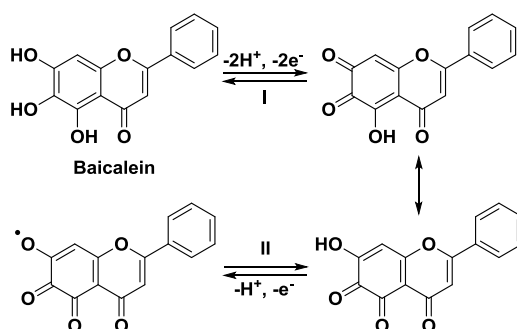
Figure 6. Postulated redox mechanism of baicalein.

4.1.3. Flavonoids with other Substitution Patterns

Besides the aforementioned mono- and diphenol (catechol and resorcinol) patterns, the pyrogallol pattern can be also found (third hydroxyl adjacent to a catechol moiety), for example in myricetin, delphinidin, gallocatechins and gallocatechin gallates (Figure 2 and Figure 4). Similarly to catechol, the pyrogallol moiety is reversibly oxidized at low potential thus conferring to the corresponding

compounds high electron donor ability. The voltammetric profile of such flavonoids is slightly altered with respect to analogous catechol-based compounds.[24,25]

Table 1. Anodic or half-wave peak potentials for various flavonoids of interest.

| Compound	E_{pa1} (V)	E_{pa2} (V)	pH	Substitution Pattern A/B rings	Ref.
5-OH	0.807^c		7.4	Phenol/-	3
7-OH Flavone	0.797^c		7.4	Phenol/-	3
6-OH	0.85^b		6.04	Phenol/-	26
Chrysin	0.767^c		7.4	Resorcinol/-	3
Baicalein	0.16^b	0.645^b	7.2	Pyrogallol/-	25
	0.118^b		7.4		23
Baicalin	$E_{1/2} = 0.27^{b,d}$		5.0	Pyrogallol/-	27
	$E_{1/2} = 0.09^{b,e}$		7.4		21
Diosmin	0.70^a	1.08^a	4.0	Phenol/Phenol	15,28
Daidzein	0.68^a	0.90^a	4.0	Phenol/Phenol	24,29,30
Fisetin	0.39^a	1.00^a	4.0	Phenol/Catechol	13,14
	0.12^b		7.2		25
	$E_{1/2} = 0.14^b$		7.5		1
Naringenin	0.45^b	nd	3.6	Resorcinol/Phenol	8,17,31
Kaempferol	0.45^a	nd	3.6	Resorcinol/Phenol	7,32
	0.17^b		7.2		25
	$E_{1/2} = 0.17^b$		7.5		1
Genistein	0.72^a	1.03^a	4.0	Resorcinol/Phenol	7,30,33
Quercetin	0.33^a	1.03^a	4.0	Resorcinol/Catechol	32,34
	0.11^b		7.2		25
	$E_{1/2} = 0.06^b$	$E_{1/2} = -0.03^b$	7.5		1
Catechin	0.33^a	0.74^a	4.0	Resorcinol/Catechol	32,35,36,1
	$E_{1/2} = 0.15^b$		7.5		
Epicatechin	0.33^a	0.74^a	4.0	Resorcinol/Catechol	17,20,25,25
	0.20^b		7.2		
ECG	0.20^b		7.2	Resorcinol/Catechol	25
Luteolin	$E_{1/2} = 0.336^b$	$E^{1/2} = 1.06^b$	6.1	Resorcinol/Catechol	37
	0.24^b		7.2		25
	0.223^c		7.4		3
EGC	0.08^b		7.2	Resorcinol/pyrogallol	25
EGCG	0.08^b		7.2	Resorcinol/pyrogallol	25
Scutellarin	0.154^f		7.4	Pyrogallol/Phenol	22

Solvent: water. nd = Not determined. a *versus* ENH. b *versus* CSE. c Ag/AgCl(KCl 3M). d Pyrolytic graphite (PG) disk electrode. e DM-β-CD-GNs/GCE and GCE. f reference electrode not mentioned. ECG = epicatechin gallate.

EGCG = epigallocatechin gallate. EGC = epigallocatechin. In italics, comparable data.

The 3-OH non-phenolic hydroxyl group of flavonols can be also electrochemically oxidized at potential close to those observed for A-ring phenolic moiety.[24] However, for flavanonols and flavanols, which lack the 2,3-double bond influences this oxidation process, shifting the expected peak potential to very positive values.[17] Table 1 gathers oxidation potentials measured for a wide range of flavonoids displaying either a phenol, catechol, pyrogallol substitution on either cycle A or B.

### 4.1.4. Redox Behavior of Curcumin and its Derivatives

Curcumin derivatives share similar electrochemical features with monophenolic flavonoids. It has been shown that the oxidation of curcumin is a two-step irreversible process (Pt electrode in 0.1 M n-Bu$_4$NClO$_4$ in acetonitrile).[38] The anodic potentials of the first and second steps of curcumin oxidation are 0.88 V/(Fc/Fc^+) (1.26 V/CSE) and 1.38 V/(Fc/Fc^+) (1.76 V/CSE)[39], respectively. An oxidation mechanism of curcumin has been proposed in CH$_3$CN and is depicted in Scheme 1.
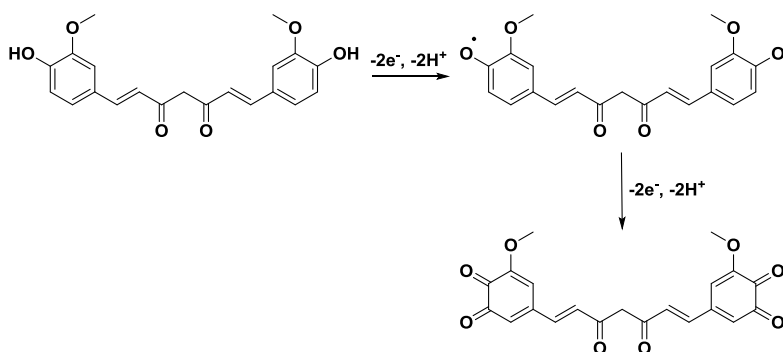
Scheme 1. Proposed oxidation mechanism of curcumin in CH$_3$CN at a Pt electrode.

The electrochemical behavior of curcumin in water has been described as well (Scheme 2).[40] The oxidation was found to be pH-dependent and it occurs in two consecutive oxidative steps. The closely-related compounds ferulic acid, capsaicin and dihydrocapsaicin were also investigated. Electrochemical behavior of ferulic acid is similar to that of curcumin involving two consecutive oxidation steps, whereas the oxidation of capsaicin and dihydrocapsaicin only involves one oxidation step. At pH 4.3, the first oxidation peak of curcumin (E_{p1a} = 0.57 V/Ag/AgCl (3 M KCl)) was suggested to arise from the formation of the phenoxyl radical, which can then be hydrolyzed at the *ortho*-position. This new species (sharing a common feature with ladanein) is then characterized by a reversible redox signal (E_{p3a} = 0.38 V and E_{p3c} = 0.34 V, E_{p3a}–$E_{p3c} \sim$ 30 mV, $i_{p3a}/i_{p3c} \sim$ 1). Curcumin and ferulic acid also displayed on the first voltammetric scan a second oxidation signal (E_{pa2} = 0.67 V) that is seemingly related to the hydroxylation at position 1 (and/or 7) of the double bond of their

hydrocarbon chain. Changing the scan direction, a cathodic appears at E_{p2c} = 0.62 V that correspond to the reduction of the second curcumin oxidation product.
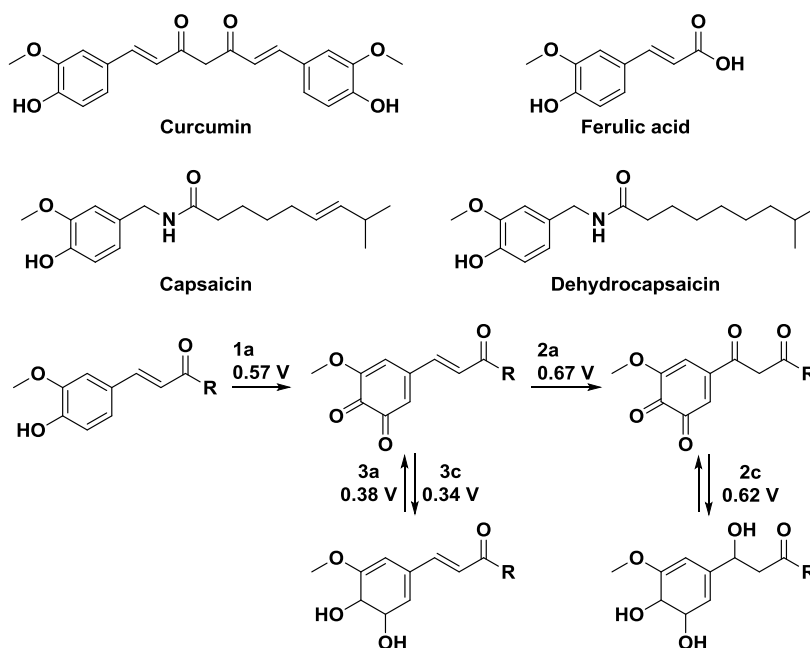
Scheme 2. Proposed oxidation mechanism of curcumin in water at a GC electrode.

4.2. Electrochemical Properties of Ladanein and its Analogues in DMSO

For solubility reasons, the electrochemical behavior of **FOMe** was examined by cyclic voltammetry (CV) in DMSO (containing 0.1 M NBu$_4$PF$_6$ as supporting electrolyte) using a planar glassy carbon electrode (GCE) of 0.07 cm^2 area, a Pt wire as the counter-electrode and a Ag/AgCl(3M KCl) as the reference electrode (+0.210 V/NHE). Figure 7 displays the CV profile of ladanein **FOMe** in the potential range from -0.8 V to 1.2 V. The repetitive scans were found to be fairly reproducible thus suggesting the absence of adsorption processes or degradation products under these experimental conditions. The scan rate was varied from 50 mV s^{-1} up to 6 V s^{-1}, and regardless of the sweep rate, the electrochemical behavior of **FOMe** showed a chemically irreversible oxidation (wave (I)) and a broadened reduction (wave (II)) in the reverse scan, which are seemingly typical of catechol-derived compounds with ECE type mechanism (see below).[41]
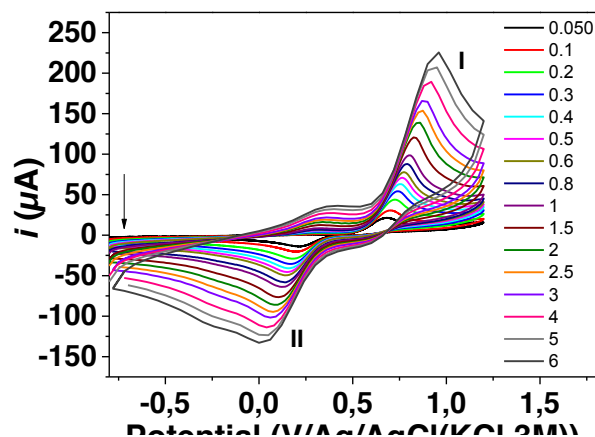
Figure 7. CV profiles of **FOMe** (2.32 mM) *versus* the sweep rate measured in DMSO with 0.1 M n-Bu$_4$NPF$_6$ electrolyte support at 25°C and showing the irreversible oxidation/reduction signals of the flavone. v = 200 mV s^{-1}; reference electrode = KCl(3M)/Ag/AgCl; working electrode = glassy carbon disk of 0.07 cm^2 area; counter-electrode = Pt wire.

Figure 8 depicts the CV profile of **FOMe** compared to that of DMSO and **F** (2-phenyl-chromone) used as a reference flavone (lacking substitution on A- and B-rings) at a sweep rate of 200 mV s^{-1}. It clearly demonstrates that the oxidation and reduction signals observed within the potential range from -0.8 V to 1.2 V clearly originate from the A-ring of the flavone **FOMe** containing the catechol moiety.
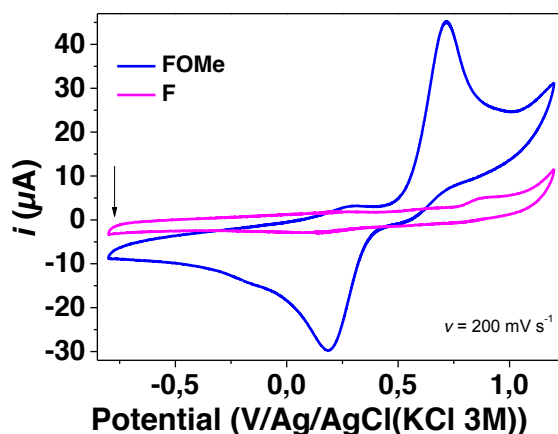
Figure 8. CV profiles of **FOMe** (2.32 mM) and the 2-phenyl-chromone (2.97 mM) measured in DMSO at a sweep rate of 200 mV s^{-1} with 0.1 M n-Bu$_4$NPF$_6$ electrolyte support at 25°C. Reference electrode = KCl(3 M)/Ag/AgCl; working electrode = glassy carbon disk of 0.07 cm^2 area; counter-electrode = Pt wire.

The comparison of the CV profile of ladanein **FOMe** with those measured for its analogues suggests that the same electrochemical behavior dominates within this series of compounds whatever the substitution on the B-ring as already demonstrated for their acido-basic properties.

Figure 9. CV profiles of **FOMe** compared to its synthetic analogues. Cyclic voltammograms measured for ~ 2-2.5 mM of the flavone in DMSO at a sweep rate of 200 mV s^{-1} with 0.1 M n-Bu$_4$NPF$_6$ electrolyte support at 25°C. Reference electrode = KCl(3 M)/Ag/AgCl; working electrode = glassy carbon disk of 0.07 cm^2 area; counter-electrode = Pt wire.
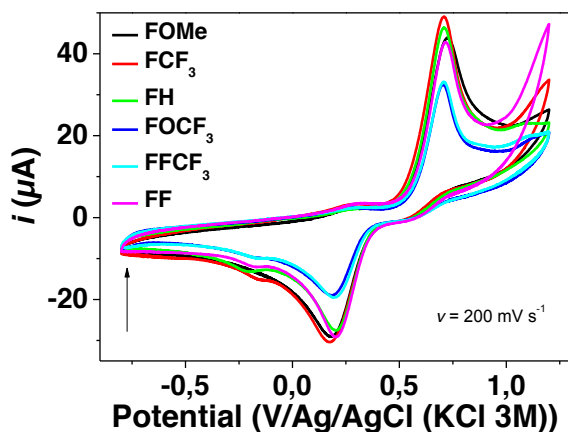
As it can be seen next on Figure 10 for ladanein **FOMe**, the linear dependence of log (i_p) *versus* log (v) indicates that the oxidation and reduction processes of the flavone are diffusion-controlled in DMSO. The same feature can be deduced for the analogues for which the slope of the log(i_p) = f(log(v)) relationship is ranging from 0.48 to 0.68 (Table 2). A slope value close to 0.5 reflects a diffusion-controlled electrode process, while a slope value close to 1.0 is expected for adsorption-controlled processes.[42] Therefore, ladanein **FOMe** and its analogues participate to the electrode reaction especially like a diffusional species.
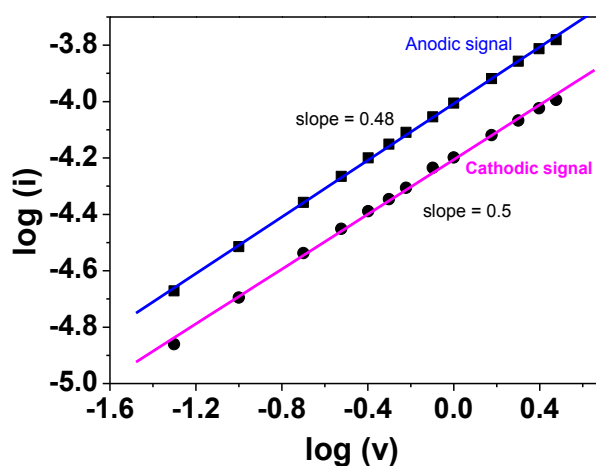

Figure 10. Variation of the log (i_p) of the diffusion-controlled oxidation/reduction processes as a function of log (v) (v = sweep rate in V s^{-1}) form ladanein **FOMe** (2.32 mM). I = 0.1 M n-Bu$_4$NPF$_6$ electrolyte support; T = 25°C; Reference electrode = KCl(3 M)/Ag/AgCl; working electrode = glassy carbon disk of 0.07 cm^2 area; counter-electrode = Pt wire.

The anodic (E_{pa}) to cathodic (E_{pc}) peak separation (ΔE_p) obtained for the compounds considered in this work was found to be several hundred mV (Figure 11) higher than that expected for a one (~ 60 mV at 298 K) or two-electron (~ 30 mV at 298 K) electrochemically reversible processes. The ΔE_p increases with the scan sweep (Figure 11) which confirms that the electrode process is diffusion controlled in DMSO and that once again it corresponds to the signature of an irreversible system.
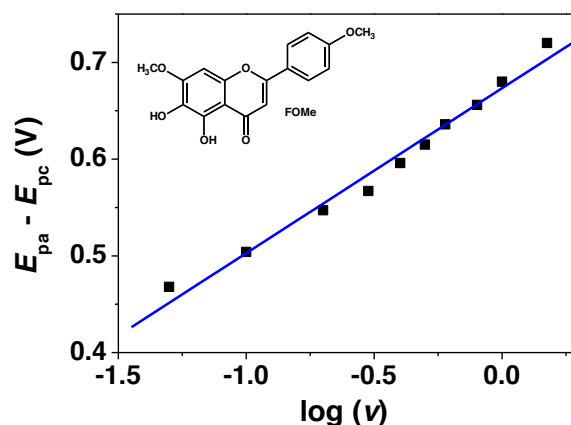

Figure 11. Variation of ΔE_p as a function of the sweep rate (log (v)) (v = sweep rate in V s^{-1}) for **FOMe** (2.32 mM). I = 0.1 M n-Bu$_4$NPF$_6$ electrolyte support; T = 25°C; Reference electrode = KCl(3 M)/Ag/AgCl; working electrode = glassy carbon disk of 0.07 cm^2 area; counter-electrode = Pt wire.

Table 2. Electrochemical parameters calculated on the oxidation and reduction peaks within the -0.8 V to 1.2 V.

Compounds	log (i_{pa}) = f(log(v))	log (i_{pc}) = f(log(v))	$\|E_{pa}\|$ = f(log(v)) (mV/log unit)	$\|E_{pc}\|$ = f(log(v)) (mV/log unit)	$\|E_{pa}-E_{pa/2}\|$ (mV)	$\|E_{pc}-E_{pc/2}\|$ (mV)	βn_β (pa)	βn_β (pc)
F/Flavone	na	na	na	na	na	na	na	na
FOMe/ Ladanein	0.48	0.50	84	68	109	118	0.36/0.44	0.42/0.40
FH/ Negletein	0.53	0.50	121	67	98	106	0.23/0.49	0.45/0.45
FP	0.68	0.64	115	77	95	98	0.26/0.50	0.39/0.49
FCF$_3$	0.54	0.54	121	72	107	124	0.25/0.42	0.44/0.38
FF	0.57	0.57	108	85	94	107	0.28/0.51	0.35/0.45
FFCF$_3$	0.59	0.57	97	57	82	88	0.31/0.58	0.57/0.54
FOCF$_3$	0.55	0.52	102	70	86	105	0.29/0.55	0.43/0.45
na = not applicable								

Figure 12 exemplifies the variation of E_{pa} (or E_{pc}) as a function of log (v) for **FFCF$_3$**. The same observations can be made for the other compounds. A linear variation can be observed for both the anodic and cathodic signals and suggests a mixed kinetic control by the electron transfer and the

chemical reaction. In most of the cases, a kinetic control by a slow electron transfer (explained by an overpotential process; *i.e.* potential that is developed because of limited reaction kinetic) can be evidenced at higher sweep rates.[43] A mixed kinetic control of the first electron transfer and the subsequent deprotonation on the global reaction was also observed for catechol, caffeic acid, dihydrocaffeic acid and caffeic acid phenethyl ester in DMSO.[41] This feature is seemingly not affected by the structural differences among these four compounds and is a consequence of the competition between deprotonation and radical cation delocalization, being the first process the most favored one. Considering the close redox shape (Figure 9) observed for our flavone derivatives, we also suggest the same property.
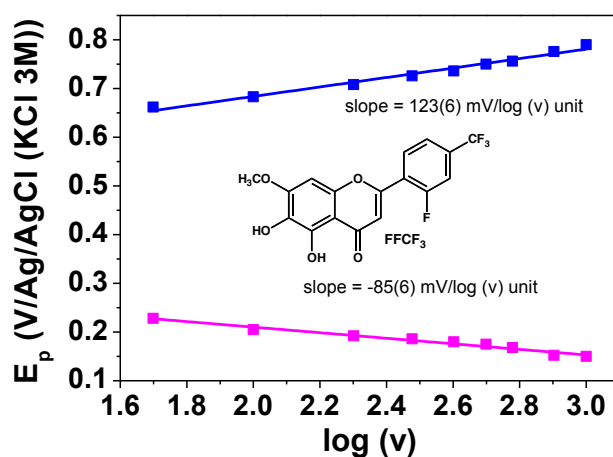

Figure 12. Variation of E_{pa} and E_{pc} as a function of log (v) (v = sweep rate in mV s^{-1}) for **FFCF$_3$** (2.44 mM). I = 0.1 M n-Bu$_4$NPF$_6$ electrolyte support; T = 25°C; Reference electrode = KCl(3 M)/Ag/AgCl; working electrode = glassy carbon disk of 0.07 cm^2 area; counter-electrode = Pt wire. Only the sweet rates ranging from 50 mV s^{-1} to 1 V s^{-1} have been considered (mixed kinetic process). At sweep rates higher than 1 V, the overpotential process dominates.

To further investigate this feature, we have examined the dependence of the current function ($i_p/v^{1/2}$) with the sweep rate v, which is another diagnostic criterion to the mechanism of electron transfer.[45] For uncomplicated charge transfer reaction (reversible and irreversible), horizontal straight lines are obtained, while other dependences (increase of decrease) are related to coupled charge transfers with chemical reactions.[45] Figure 13 displays the variation of ($i_{pa}/v^{1/2}$) and ($i_{pc}/v^{1/2}$) as a function of v for **FF** and **FH**. The $i_{pa}/v^{1/2}$ and $i_{pc}/v^{1/2}$ ratios vary with the sweep rate for values of v lower than ~ 1 V s^{-1}. This is likely a characteristic of a coupled chemical reaction following the electron transfer (EC mechanism, see below). For sweep rates higher than 1 V, the electrochemical behavior is altered and no significant variation of ($i_{pa}/v^{1/2}$) and ($i_{pc}/v^{1/2}$) with v can be then observed (Figure 13). This indicates a mechanism transition and suggests that the slow chemical reaction (likely

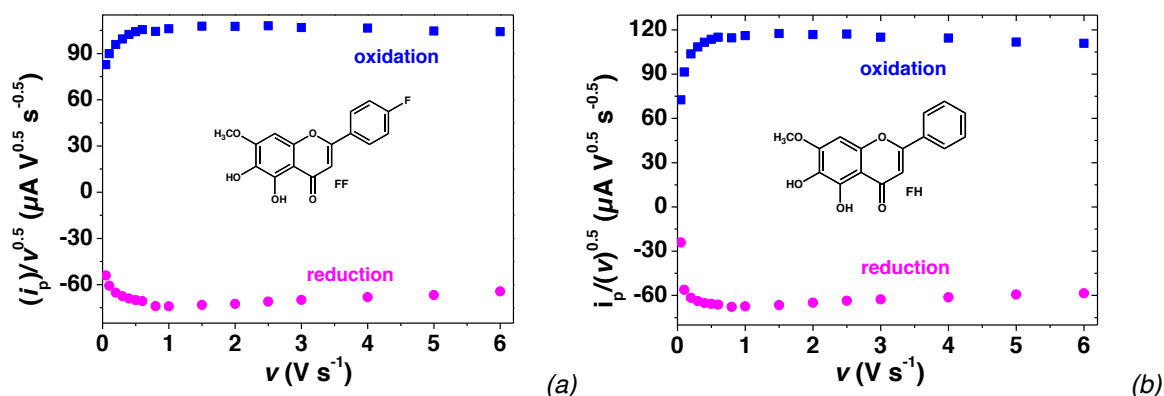a deprotonation step) significantly influences the electron transfer kinetic process (reaction overpotential).

Figure 13. Variation of $i_{pc}/v^{1/2}$ (a) and $i_{pa}/v^{1/2}$ (b) as a function of the sweep rate v (mV s^{-1}) for (a) **FF** (2.18 mM) and (b) **FH** (2.25 mM). I = 0.1 M n-Bu$_4$NPF$_6$ electrolyte support; T = 25°C; Reference electrode = KCl(3 M)/Ag/AgCl; working electrode = glassy carbon disk of 0.07 cm^2 area; counter-electrode = Pt wire.

In order to gain further insight on the rate determining step, a Tafel parameter (noted b) was determined using the following equation[44] valid for a totally irreversible diffusion controlled process.

$$E_p = \frac{b}{2} \times log(v) + Const. \quad with \ b = \frac{2.303RT}{\beta n_\beta F}$$

with βn_β (charge transfer coefficient) being the product of the symmetry factor β by the total number of electrons n_β transferred in the corresponding charge transfer step, F the Faraday constant (96 485 C); R the gas constant (8.32 J mol^{-1} K^{-1}) and T the temperature (298 K). As mentioned previously (Figure 12), the irreversible character of both signals in the anodic and reverse scans can be assessed by the anodic (or cathodic) shift of the oxidation (or reduction) potential with log (v). As an example, Figure 14 shows the variation of E_{pa} (or E_{pc}) as a function of log (v) for ladanein **FOMe**. Two straight lines can be observed for both the anodic and cathodic processes. As mentioned previously, this would suggest a kinetic control by a slow electron transfer at high sweep rates and a mixed kinetic control by electron transfer and chemical reaction at lower scan rates. The rate constant of the chemical reaction (*i.e.* the deprotonation) following the electron transfer can be deduced (k_H = 0.1(Fv_i/RT)) where v_i is the scan rate at the intercept of the two straight lines. The rates of the chemical reactions (deprotonation of the phenolic units) are comparable and were estimated to be at ~ 2.8 s^{-1} and 3.0 s^{-1} for the anodic and cathodic processes, respectively.
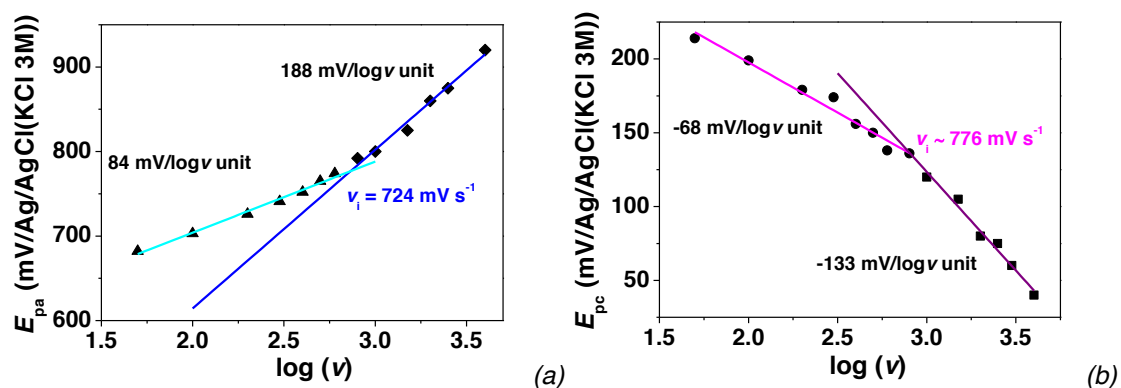
Figure 14. Variation of E_{pa} (a) and E_{pc} (b) as a function of log v (v = sweep rate in mV s^{-1}) for ladanein **FOMe** (2.32 mM). I = 0.1 M n-Bu$_4$NPF$_6$ electrolyte support; T = 25°C; Reference electrode = KCl(3 M)/Ag/AgCl; working electrode = glassy carbon disk of 0.07 cm^2 area; counter-electrode = Pt wire.

For a totally irreversible wave and using the previous equation, it is expected that the cathodic (or anodic) shift in peak potential (or half-peak potential) is ~ 30 mV/βn_β. Using this approach and considering only sweep rates ranging from 50 mV s^{-1} to 1 V s^{-1}, the βn_β values for the cathodic signals were calculated and found to be in close agreement with the theoretical value of βn_β = 0.5 (*i.e.* for an elementary 1 e$^-$ transfer with n_β = 1 and β = 0.5),[45] while the βn_β values for the anodic signals are seemingly close to a theoretical value of βn_β = 0.25. It is noteworthy that this approach is formally correct only if the electrode process consists of a single elementary step involving the simultaneous release of electrons from the electrode to the reactant. In many cases, an electrode process consists of a sequence of consecutive (or even parallel) elementary electron-transfer steps and chemical steps. Under these conditions, the above approach can still be regarded as formally correct only if the first elementary step of the sequence determines the rate of the whole process and involves the simultaneous release of n electrons from the electrode.[46]

To go a step further, the following equation[47] was used for also diagnosing the irreversibility of our systems and determine the charge transfer coefficients:[45]

$$E_p - \frac{E_p}{2} = 1.857 \frac{RT}{\beta n \beta}$$

With E_p = E_{pa} (or E_{pc}), $E_{p/2}$ = the potential determined at $i_{p/2}$ and βn_β the charge transfer coefficient. In a multistep electrode process consisting of a series of consecutive elementary steps, the electrode kinetics is indeed only affected by the rate determining step and by the steps that precede it, while it is not influenced by the subsequent steps, which may well involve further electron transfers (which is

seemingly the case herein). Figure 15 displays the variation of E_p - $E_{p/2}$ measured for ladanein **FOMe** for both the anodic and cathodic waves as a function of the sweep rate. The charge transfer coefficients βn_β was thus calculated to be 0.44 (ordinate at the origin = 0.109) for the anodic signal and 0.40 (ordinate at the origin = 0.118) for the cathodic one (Table 2). Assuming a 1 electron transfer in the limiting charge transfer process, the factor coefficient was estimated to be close in that case to 0.5 for both the cathodic and anodic process in good agreement with the previously measured data. In addition, the fact that βn_β has a fractional value confirms irreversible electron transfers for both the anodic and cathodic signals.
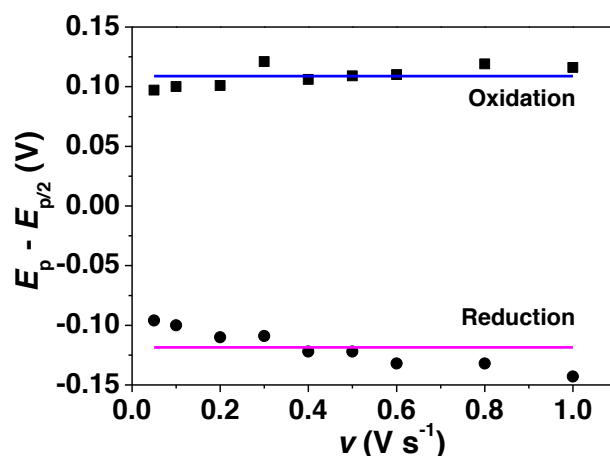

Figure 15. Variation of E_{pa} and E_{pc} as a function of v (v = sweep rate in V s^{-1}) for ladanein **FOMe** (2.32 mM). I = 0.1 M n-Bu$_4$NPF$_6$ electrolyte support; T = 25°C; Reference electrode = KCl(3 M)/Ag/AgCl; working electrode = glassy carbon disk of 0.07 cm^2 area; counter-electrode = Pt wire.

The maximum of the current intensity i_p for an irreversible system can be also expressed as follows:

$$i_p = 2.99 \times 10^5 n (\beta n\beta)^{0.5} A C_0 D^{0.5} v^{0.5}$$

Where A = area of the working electrode (0.07 cm^2), n = total number of electrons exchanged, βn_β = charge transfer coefficient, D$_0$ = diffusion coefficient (cm^2 s^{-1}), C$_0$ = concentration of the electroactive species (mol cm^{-3}) and v = sweep rate (V s^{-1}). Figure 16 depicts the variation of i_{pa} and i_{pc} as a function of $v^{0.5}$. It can be concluded that no adsorption processes are expected since i_{pa} and i_{pc} experience linear dependence with the ordinate at the origin being equal to 0. Both processes are also diffusion-controlled reactions.
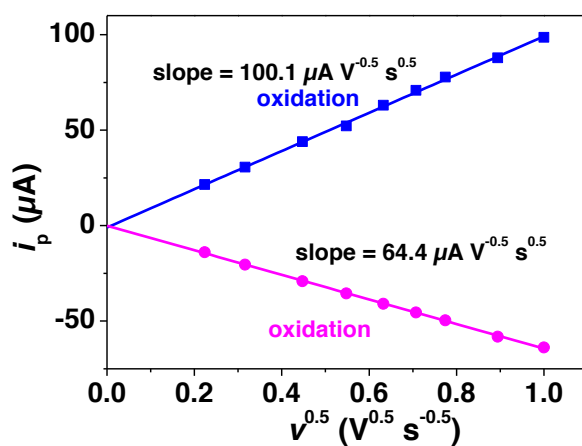
Figure 16. Variation of i_{pa} and i_{pc} as a function of the square root of v (v = sweep rate in mV s^{-1}) for ladanein **FOMe** (2.32 mM). I = 0.1 M n-Bu$_4$NPF$_6$ electrolyte support; T = 25°C; Reference electrode = KCl(3 M)/Ag/AgCl; working electrode = glassy carbon disk of 0.07 cm^2 area; counter-electrode = Pt wire.

^{1}H DOSY NMR measurement on **FOMe** in DMSO-d_6 was performed and allowed the determination of the diffusion coefficient D$_0$ (Figure 17) which was found to be 2.34 x 10^{-6} cm^2 s^{-1}.
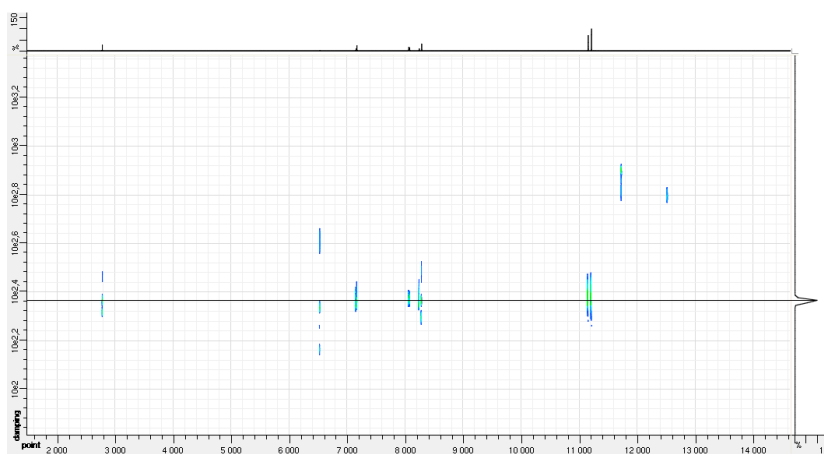
Figure 17. DOSY ^{1}H NMR spectrum of the flavone **FOMe** in DMSO-d_6. T = 298 K. Frequency = 600 MHz.

Therefore, assuming βn$_β$ values for the anodic for the cathodic processes provided in Table 2 and using the determined D$_0$ value, the total number of electron involved in the anodic and cathodic process can be evaluated (Table 3). For most of the flavones, the total number of electrons involved was estimated to be close to 2 for both the oxidation and the cathodic processes. The differences observed is rather explained by the rough estimations of the n(βn$_β$) and of the D$_0$ values than a different electrochemical behavior.

Table 3. Evaluation of the numbers of electron exchanged during the oxidation and reduction processes within the potential range from -0.8 V to 1.2 V.

Compounds	$\lvert i_{pa}\rvert = f(0v^{0.5})$ $\mu A\ V^{-0.5}\ s^{0.5}$	$\lvert i_{pa}\rvert = f(0v^{0.5})$ $\mu A\ V^{-0.5}\ s^{0.5}$	C (mM)	$n(\beta n_{\beta})^{0.5}$ pa	$n(\beta n_{\beta})^{0.5}$ pc	n pa	n pc
F/Flavone	na	na	2.97				
FOMe/Ladanein	100.1	64.4	2.32	1.5	1.0	2.3	1.6
FH/Negletein	128.5	77.1	2.25	2.0	1.2	2.9	1.8
FP	111.1	76.0	2.19	1.8	1.2	2.6	1.8
FCF$_3$	120.8	74.6	2.44	1.8	1.1	2.8	1.8
FF	113.3	80.5	2.18	1.9	1.3	2.6	2.0
FFCF$_3$	89.7	50.3	2.05	1.6	0.9	2.1	1.2
FOCF$_3$	85.7	44.5	2.34	1.3	0.7	1.8	1.0
na = not applicable. The diffusion coefficient of the flavones have been estimated to be close to that of FOMe							

Taken all together, our data are in agreement with a successive ECE 2e- oxidation/deprotonation for which the first electron transfer is the rate limiting step. The electrochemical response of **FOMe** in DMSO is indeed similar to that measured for catechol, caffeic acid,[48] dihydrocaffeic acid or caffeic acid phenethyl ester under comparable conditions.[41] The catechol unit borne by A-cycle likely experiences an anodic oxidation to *ortho*-quinone due to an ECE mechanism that involves the loss of one electron in the system coupled to a slow deprotonation reaction and, finally, the fast loss of a second electron. Scheme 3 depicts the general electrochemical mechanism which can be proposed for our series of flavones. A deprotonation reaction may also occur as the last step.
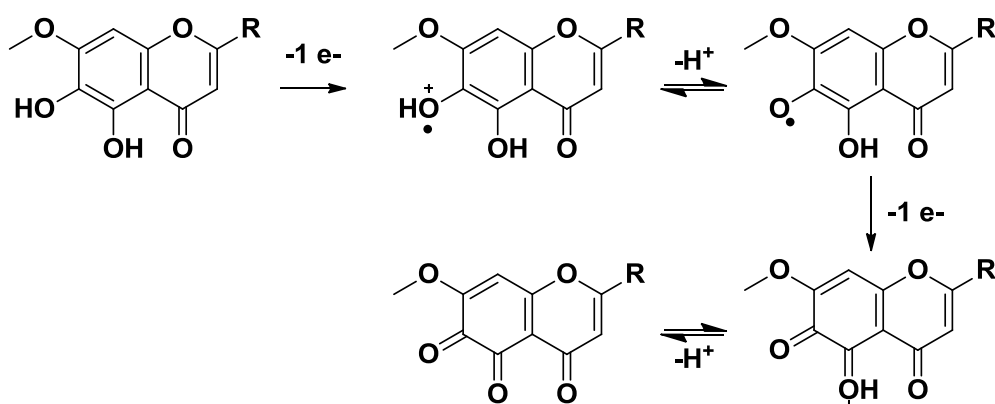
Scheme 3. Suggested electrochemical behavior of ladanein and its analogues within the potential range considered (from -1.2 V to 0.8 V) in DMSO.

The electrochemical behavior of ladanein **FOMe** and its analogues in the potential range from -2.35 V to -1.2 V was then investigated. No electrochemical signal was observed when examining the intermediate potential range from -0.5 V to -1.5 V (Figure 18a). From -2.35 V to -1.2 V, a quasi-reversible electrochemical signal was observed (Figure 18b) and attributed to the C-ring enone moiety as demonstrated with the 2-phenyl-chromone (flavone **F**) model. Figure 19 displays the influence of the sweep rate on this quasi-reversible redox signal.
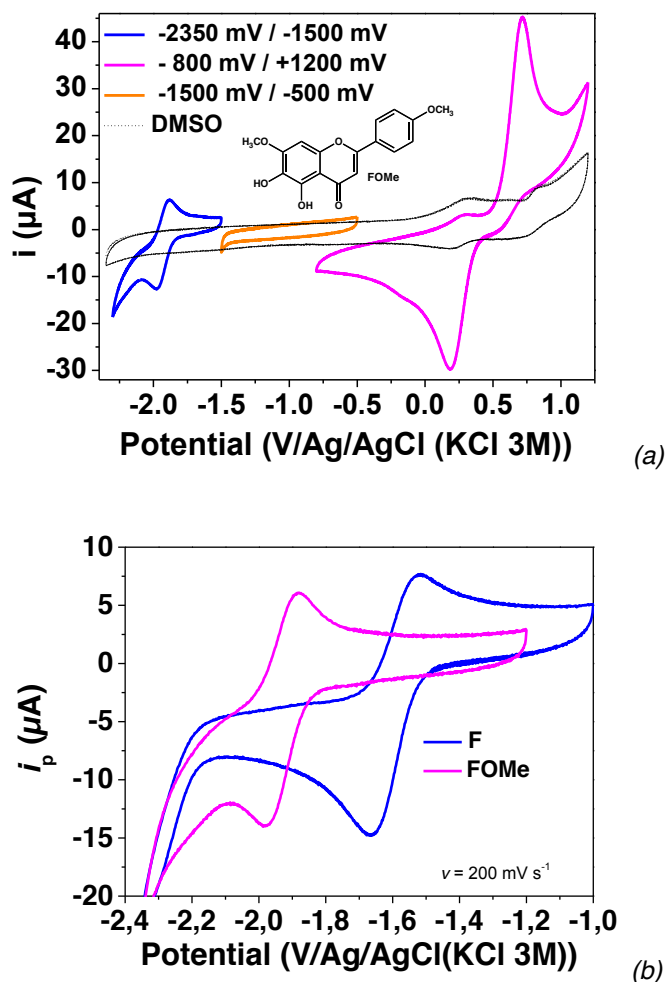

(a)

(b)

Figure 18. CV profiles of **FOMe** (2.32 mM, (*a*) and (*b*)), 2-phenyl-chromone (**F**, 2.97 mM, (*b*)) and DMSO (*b*) measured at a sweep rate of 200 mV s^{-1} with 0.1 M *n*-Bu$_4$NPF$_6$ electrolyte support at 25°C. Reference electrode = KCl(3 M)/Ag/AgCl; working electrode = glassy carbon disk of 0.07 cm^2 area; counter-electrode = Pt wire.
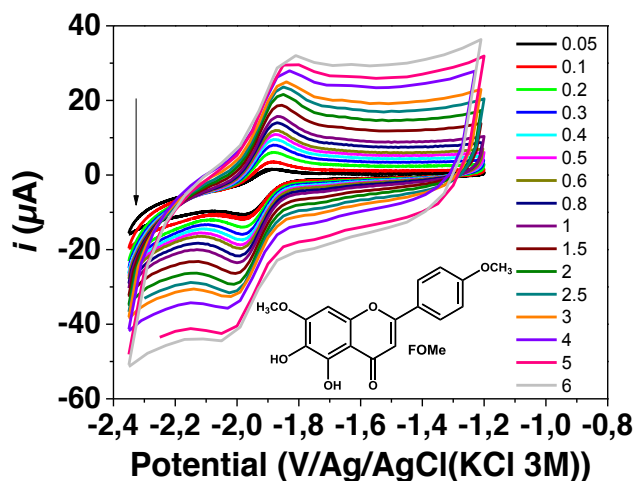
Figure 19. CV profiles of **FOMe** (2.32 mM) as a function of the sweep rate measured in DMSO with 0.1 M *n*-Bu$_4$PF$_6$ electrolyte support at 25°C and showing the reversible electrochemical process centered on the flavone core. Reference electrode = KCl(3 M)/Ag/AgCl; working electrode = glassy carbon disk of 0.07 cm^2 area; counter-electrode = Pt wire.

In contrast to the irreversible anodic and cathodic waves discussed previously, the position of this quasi-reversible signal is influenced by the substitution pattern of the B-ring. The enone type function belonging to the C-ring is indeed conjugated with the B-ring and is therefore sensitive to any electron-withdrawing or -donating effects arising from substituents in appropriate positions on the B-ring. In addition, the characteristic A-ring substitution (**FH**) shifted by more than 280 mV this redox signal with respect to 2-phenyl-chromone (flavone **F**) which lacks any substituent. Interestingly, **FH** seems to display a 2 e$^-$ reduction. This may be due to electronic effects exerted by the substituents on the A-ring and also to the strong intramolecular hydrogen bond between 5-OH and the adjacent carbonyl unit. Methoxylation of the 4'-position (**FOMe**, mesomeric effect +M) and methylation of the 5-position (**FP**, absence of hydrogen bonding and strong steric interactions) further shifted this redox signal by ~ 50 mV and ~ 150 mV, respectively.
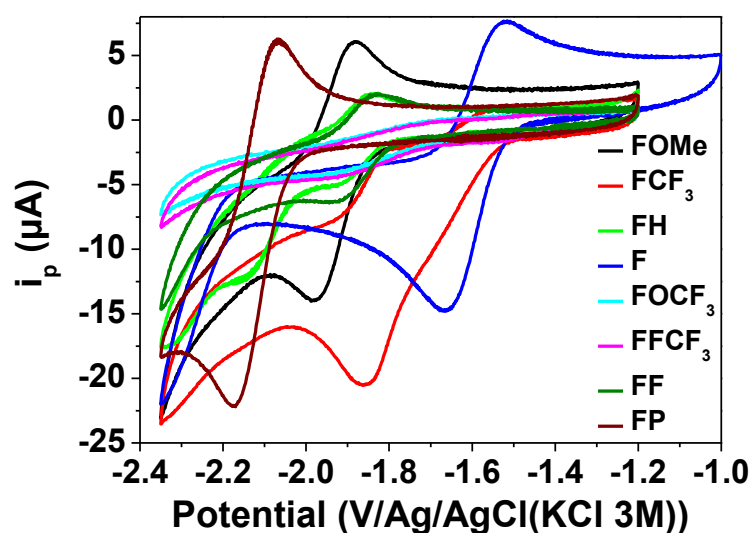
Figure 20. CV profiles of the different flavones considered in this work that demonstrate the effect of the substitution of the B-ring on the quasi-reversible signal arising from the carbonyl unit. Solvent: DMSO with 0.1 M *n*-Bu₄NPF₆ electrolyte support; T = 25°C and. v = 200 mV s⁻¹; reference electrode = KCl(3 M)/Ag/AgCl; working electrode = glassy carbon disk of 0.07 cm² area; counter-electrode = Pt wire.

The E_{pa} and E_{pc} values slightly increase with increasing the sweep rate in agreement with a quasi-reversible reaction (Figure 21). The half-wave potential $E_{1/2}$ values were estimated according to the following equation:

$$E_{1/2} = \frac{(E_{pa} + E_{pc})}{2}$$
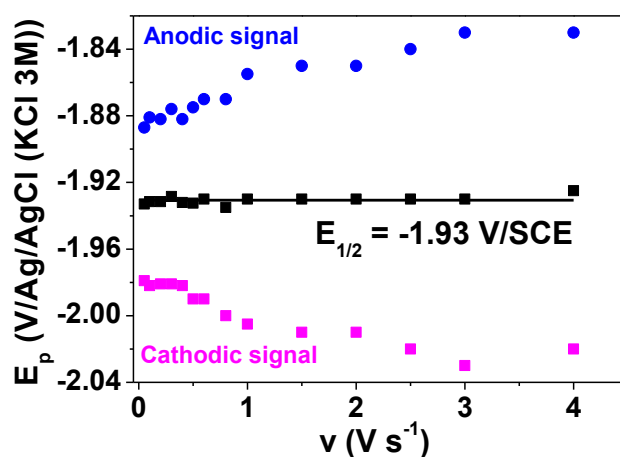
Figure 21. Variation of E_{pa} and E_{pc} (V) as a function of v (v = sweep rate in mV s⁻¹) of ladanein **FOMe** (2.32 mM). I = 0.1 M *n*-Bu₄NPF₆ electrolyte support; T = 25°C; Reference electrode = KCl (3 M)/Ag/AgCl; working electrode = glassy carbon disk of 0.07 cm² area; counter-electrode = Pt wire.

Table 4 gathers the half-wave potentials $E_{1/2}$ of the flavones considered in this work which were determined using this approach (Figure 21). The anodic (E_{pa}) to cathodic (E_{pc}) peak separations (ΔE_p) measured were found to be much higher than expected for a reversible one electron transfer (~ 60 mV at 298 K) thus confirming the quasi-reversibility of the corresponding redox signals. In addition, the i_{pa} to i_{pc} ratios were found to be lower than 1 once again indicating quasi-reversible processes (Table 4). This may arise from a disproportionation reaction or a side reaction such as dimerization (see below, Scheme 4). On the other hand, with the exception of the final precursor (**FP**), the sequence of the half-wave potentials follows the λ_{max} sequence of either band I or band II (see previous chapter, Figure 22) thus confirming the key role of the carbonyl group in each of these processes.
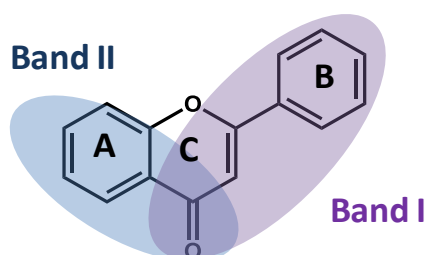
Figure 22. Main chromophores assumed to be responsible for the absorptions I and II.

Table 4. Electrochemical parameters measured for the quasi-reversible redox signal of our series of flavones.

Compounds	C (mM)	$E_{1/2}$ (V)	ΔE_p (200 mV)	i_{pa}/i_{pc} (200 mV)	λ_{max} Band I	λ_{max} Band II
F/Flavone	2.97	-1.59	144	0.82	295	252
FOMe/Ladanein	2.32	-1.93	101	0.72	335	286
FH/Negletein	2.25	-1.87	91	0.45	321	277
FP	2.19	-2.12	104	0.58	325	277
FCF$_3$	2.44	-1.84	56	0.55	322	277
FF	2.18	-1.88	100	0.53	321	278
FFCF$_3$	2.05	-1.83	190	0.29	320	273
FOCF$_3$	2.34	-1.82	215	0.41	321	277

Finally, Figure 23 further displays the variation of i_{pa} and i_{pc} as a function of $v^{1/2}$. No matter the flavone considered, the intensities of the cathodic and anodic signals vary linearly with the square root of the sweep rate in agreement with a (quasi)reversible system as shown by the following equation:

$$i_p = 2.99 \times 10^5 \, n^{2/3} A C_0 D^{1/2} v^{1/2}$$

These features indicate diffusion-controlled processes and once again suggest the absence of adsorption processes since the ordinate at the origin is close to 0 for every flavone considered.

Figure 23. Variation of i_{pa} and i_{pc} as a function of the square root of v (v = sweep rate in mV s^{-1}) measured for ladanein **FOMe** (2.32 mM). I = 0.1 M n-Bu$_4$PF$_6$ electrolyte support;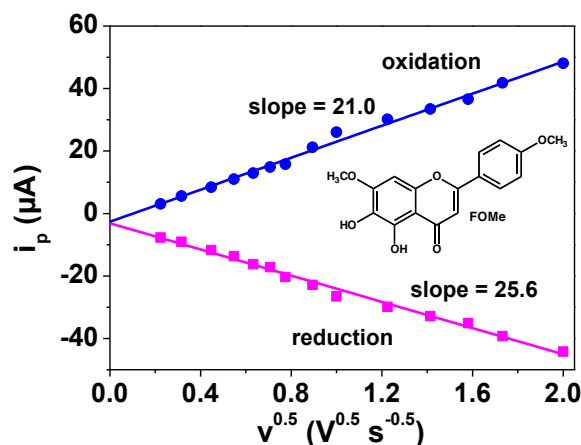 T = 25°C; Reference electrode = KCl(3 M)/Ag/AgCl; working electrode = glassy carbon disk of 0.07 cm^2 area; counter-electrode = Pt wire.

It has been shown that the carbonyl group might be the reduction centre both in flavone and flavanone derivatives. For instance, literature data showed that the 2-phenyl-chromone displays a one electron reversible diffusion wave $E_{1/2}$ at -2.28 V and a two electrons diffusion wave $E_{1/2}$ at -2.85 V in DMF at 298 K (*versus* Ag/Ag$^+$).[49] Electrochemical reduction of 7-acetoxyflavone and 7-hydroxyfavone on GCE in DMF showed a 2 electrons irreversible reduction (E_{pc} = -1.77 V/CSE for 7-hydroxyflavone and -1.44 V/CSE for 7-acetoxyflavone at v = 200 mV s^{-1}).[50] This electrode process was found to be diffusion controlled and the effect of the substituents was observed due to extended conjugation as observed for our flavone derivatives. Under our experimental conditions (DMSO, 0.1 M n-Bu$_4$NPF$_6$), a single quasi-reversible signal whose half wave potential is equal to $E_{1/2}$ = -1.59 V was evidenced for the model flavone. This apparent 1 electron quasi-reversible diffusion signal is suggested to lead to monoradical species which was confirmed in previous studies by EPR spectroscopy. No further redox signal was evidenced when extending the potential range toward more negative values under our experimental conditions. Therefore, we anticipate that the reversible redox wave observed at $E_{1/2}$ = -1.93 V/SCE for ladanein **FOMe** is also associated with the reduction of the carbonyl group as shown in Scheme 2. A cathodic shift of ~ 340 mV is indeed observed between **FOMe** and the unsubstituted 2-phenyl-chromone **F**. This property is mainly due to the substitution pattern of the A- and B-rings (electronic effects) of **FOMe** as well as the intramolecular hydrogen bonding between the carbonyl unit and 5-hydroxyl group. The comparison of **FH** and **F** indeed shows a cathodic shift of 280 mV of the carbonyl redox wave thus demonstrating

that the substitution pattern of A-ring induces the larger shift, while the methoxylation of the B-ring only shifts the $E_{1/2}$ value of about 60 mV with respect to **FH**. Methylation of the 5-OH position and therefore inhibition of the hydrogen bond with the β-carbonyl (final precursor, **FP**) induces a cathodic shift of this quasi-reversible signal of 190 mV with respect to the parent ladanein **FOMe**. This indicates that **FP** is electrochemically more inert with respect to carbonyl reduction and clearly emphasizes the key role of this hydrogen bond in the electrochemical activation/behavior of the flavone.
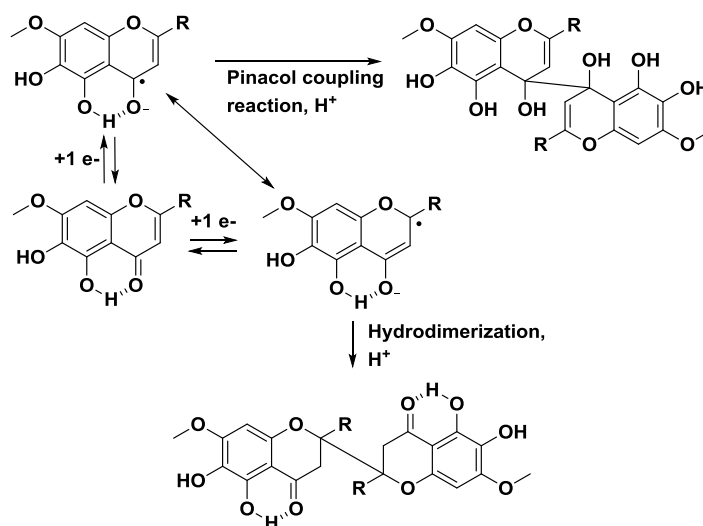
Scheme 4. Suggested electrochemical behaviour of the flavone derivatives upon 1 electron reduction of the enone unit. The reduction of the carbonyl unit is likely the plausible redox pathway.

We demonstrated that the flavones exhibit peculiar redox properties in the potential range from -0.8 V to 1.2 V (2 electrons oxidation of the A-ring catechol *via* an ECE mechanism) and from -2.35 V to -1.2 V (1 electron reduction of the carbonyl unit). However, scanning the potential from -2.35 V to 1.2 V markedly alters the CV profile of ladanein **FOMe** (as well as the other flavones examined in this work) as shown in Figure 24 with the formation of additional reduction and oxidation signals. New anodic peaks appear at -0.11 and 0.17 V whereas the anodic peak corresponding to the catechol oxidation is shifted from 0.72 to 0.64 V. For the reduction process, three new cathodic peaks appear at -0.30, -1.07 and -1.62 V. In addition, the reduction peak corresponding to the A-ring process is also shifted from 0.18 to 0.23 V. This can be related to the formation of degradation products (pinacol coupling reaction[51] or hydrodimerization[52]) of two radicals formed upon reduction of the enone unit as shown in Scheme 4. This would explain the low i_{pa} to i_{pc} ratios which were found to be lower than 1.
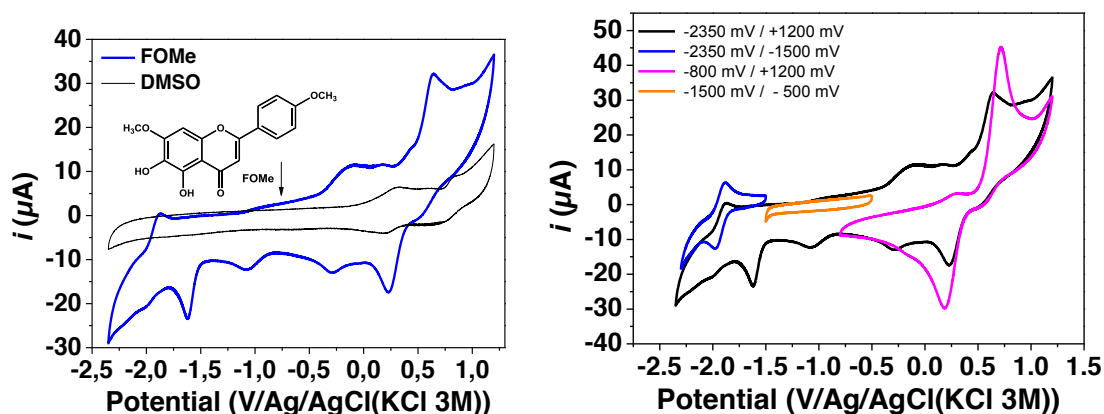
Figure 24. CV profiles of **FOMe** (2.32 mM) in DMSO with 0.1 M n-Bu$_4$NPF$_6$ electrolyte support at 25°C showing the formation of additional electrochemical signals when scanning the potential from -2.35 V to 1.2 V. v = 200 mV s^{-1}; reference electrode = KCl(3 M)/Ag/AgCl; working electrode = glassy carbon disk of 0.07 cm^2 area; counter-electrode = Pt wire.

4.3. Conclusion

We have described in this chapter the electrochemical behavior of the synthesized flavones as well as that of other polyphenols and flavonoids with different substitution patterns. It was decided to study their electrochemical behavior because it is likely that their antiviral activity is related to their redox properties. It is possible that the active compounds are not the flavones themselves but coupling products that may be formed *in vivo*. It has been suggested that both C,C and C,O coupling products may be formed and they may be directed by metal chelation. Furthermore, very scarce data can be found in the literature about the electrochemical properties of 5,6,7-trihydroxylated flavonoid compounds.

The measurements were performed in DMSO for the sake of solubility. It was found that between -0.8 and 1.2 V, the flavones display an anodic peak corresponding to a 2 electron oxidation and a broad cathodic peak, corresponding to a 2 electron reduction process as well. It is suggested that an ECE process takes place and it is related to cycle A, especially the positions 5 and 6. This ECE process is irreversible for both the oxidation and reduction, displays no adsorption and is limited by diffusion. This process may result from an electron transfer limited by a slow deprotonation step. No degradation products appeared under these conditions. Furthermore, the substituents present in cycle B were found to exert little influence on this electrochemical behavior of the flavones within this potential range as already observed for the acido-basic properties.

When studying the electrochemical behavior of the compounds between -2.35 and -1.5 V, (quasi)reversible oxidation and reduction processes were observed. This is a 1 electron process much

likely based on the enone moiety in the C-ring and is limited by diffusion with no adsorption observed. Contrarily to the reduction/oxidation on the A-ring, the substituents present in cycle B have a much stronger influence on the electrochemical behavior of the flavones in this potential range, because the enone moiety and the aromatic B-ring are conjugated. The fact that the i_{pc}/i_{pa} ratio was not close to 1 suggests that there are parasite reactions (dismutation, coupling) that take place and may lead to the formation of degradation compounds. This may explain that, when the behavior of the flavones is examined between -2.35 and 1.2 V, new peaks appear, probably due to the formation of these products resulting from coupling reactions. In the future, efforts will be directed toward the identification and mechanism of formation.

EXPERIMENTAL SECTION

Solvents and Materials

Ladanein **FOMe** and its analogues were synthesized according the procedures described in this report. The electrochemical behaviour of **FOMe** and its analogues were examined in spectroscopic grade dimethylsulfoxide (DMSO, Bioreagent for molecular biology, >> 99.9%, Sigma). All the stock solutions were prepared by weighting solid products using a Mettler Toledo XA105 Dual Range (0.01/0.1 mg - 41/120 g). The complete dissolution of the ligands was obtained with the help of ultrasonic bath (Bandelin Sonorex RK102). All the physico-chemical measurements were carried out at room temperature.

Electrochemistry

The electrochemical properties of ladanein and its analogues were measured by cyclic voltammetry (CV) in DMSO solvent. Even though DMSO is an amphiprotic solvent because its autoprotolysis occurs slightly ($pK_{SH} \sim 33$) and the lyate ion ($CH_3SOCH_2^-$) is somewhat stable, DMSO has been, however, classified as a dipolar aprotic protophilic solvent and is assumed as an suitable solvent[53-55] to characterize the electrochemical properties of our flavones (measurable potential limits of +0.9 V to -3.9 V with respect to *Fc/Fc*$^+$, E = +0.524 V/Ag/AgCl[54]). Cyclic voltammetry of ladanein **FOMe** and derivatives ($\sim 10^{-3}$ M) was first performed using a Voltalab 50 potentiostat/galvanostat (Radiometer Analytical MDE15 polarographic stand, PST050 analytical voltammetry and CTV101 speed control unit) controlled by the Voltamaster 4 electrochemical software. A conventional three-electrode cell (10 mL) was employed in our experiments with a glassy carbon disk (GC, s = 0.07 cm^2) set into a Teflon rotating tube as a working electrode, a Pt wire as a counter electrode, and KCl(3 M)/Ag/AgCl reference electrode (+210 mV *versus* NHE).[56] Prior to each measurement, the surface of the GC electrode was carefully polished with 0.3 μm aluminium oxide suspension (Escil) on a silicon carbide abrasive sheet of grit 800/2400. Thereafter, the GC electrode was copiously washed with water and dried with paper towel and argon. The electrode was installed into the voltammetry cell along with a platinum wire counter electrode and the reference. The solutions containing *ca.* 10^{-3} M of the flavones were vigorously stirred and purged with O_2-free (Sigma Oxiclear cartridge) argon for 15 minutes before the voltammetry experiment was initiated, and maintained under an argon atmosphere during the measurement procedure. The voltammograms were recorded at room temperature (25 ± 1°C) in DMSO with 100 mM tetra-*n*-butylammonium hexafluorophosphate (*n*-Bu$_4$PF$_6$) as supporting and inert electrolyte.[57] For the CV measurements, the voltage sweep rate was varied from 50 mV s^{-1} to 6 V s^{-1} and several cyclic voltammograms were recorded from +1.2 V to -2.3

V. Peak potentials were measured at a scan rate of 200 mV s^{-1} unless otherwise indicated. Redox potentials were determined from oxidation and reduction potentials.

References

(1)   Hodnick, W.F.; Milosavlejvi, E.B.; Nelson, J.H. and Pardini, R.S. *Biochim. Pharmacol.* **1988**, *37*, 2607.

(2)   Seyoum, A.; Asres, K. and El-Fiky, F.K. *Phytochemistry* **2006**, *67*, 2058.

(3)   Gomes, A.; Fernandes, E.; Beatriz, M.; Garcia, Q.; Silva, A.M.S.; Pinto, D.C.G.A.; Santos, C.M.M.; Cavaleiro, J.A.S. and Lima, J.L.F.C. *Bioorg. & Med. Chem.* **2008**, *16*, 7939.

(4)   Abdel-Hamid R. and Newair, E.F. *J. Electroanal. Chem.* **2011**, *657*, 107.

(5)   Enache, T.A. and Oliveira-Brett, A.M. *J. Electroanal. Chem.* **2011**, *655*, 9.

(6)   Nasr, B.; Abdellatif, G.; Cañizares, P.; Sáez, C.; Lobato, J. and Rodrigo, M.A. *Environ. Sci. Technol.* **2005**, *39*, 7234.

(7)   (a) Volikakis, G.J. and Efstathiou, C.E. *Anal. Chim. Acta* **2005**, *551*, 124. (b) Jorgensen, L.V.; Cornett, C.; Justesen, U.; Skibsted, L.H. and Dragsted, L.O. *Free Rad. Res.* **1998**, *29*, 339.

(8)   Mülazimoğlu, I.E.; Özkan, E. and Solak, A.O. *Anal. Bioanal. Electrochem.* **2011**, *3,* 102.

(9)   Masek, A.; Zaborski, M. and Chrzescijanska, E. *Food Chem.* **2011**, *127,* 699.

(10)   Xing, T.L.; Wang, F.; Mao, Y.Y.; Wang, L.P. and Ye, B.X. *J. Chin. Chem. Soc.* **2009**, *56*, 303.

(11)   Fogliatto, D.K.; Barbosa, A.M.J. and Ferreira, V.S. *Colloid Surf. B: Biointerfaces* **2010**, *78,* 243.

(12)   Lima, A.A.; Sussuchi, E.M. and De Giovani, W.F. *Croatica Chem. Acta* **2007**, *80,* 29.

(13)   (a) Brondani, D.; Vieira, I.C.; Piovezan, C.; Silva, J.M.R.; Neves, A.; Dupont, J. and Scheeren, C.W. *Analyst* **2010**, *135,* 1015. (b) Markovic, Z.S.; Mentus, S.V. and Dimitric, M.J.M. *J. Phy. Chem. A* 2009, *113,* 14170.

(14)   Volikakis, G.J. and Efstathiou, C.E. *Talanta* **2000**, *51,* 775.

(15)   Diculescu, V.; Santana, H.E.; Gil, E.S. and Oliveira-Brett, A.M. *Electroanal.* **2012**, *24,* 1019.

(16)   Fernandes, I.P.G.; Oliveira, S.C.B.; Ghalkhani, M.; Shahrokhian, S. and Oliveira-Brett, A.M. *Anal. Chim. Acta* **2010**, *22,* 1.

(17)   Zhang, D.; Chu, L.; Liu, Y.; Wang, A.; Ji, B.; Wu, W.; Zhou, F.; Wei, Y.; Cheng, Q.; Cai, S.; Xie, L. and Jia, G. *J. Agric. Food Chem.* **2010** *59,* 10277.

(18)   Gil, E.S.; Enache, A.T. and Oliveira-Brett A.M. *Electroanal.* **2012**, *24,* 1576.

(19)   Oliveira-Brett, A.M. and Ghica, M-E. *Electroanal.* **2003**, *15 (22)*, 1745.

(20)   Dueñas, M.; González-Manzano, S.; González-Paramás, A. and Santos-Buelga, C. *J. Pharmaceut. Biomed* **2010**, *51,* 443.

(21)   Liu, Z.; Zhang, A.; Guo, Y. and Dong, C. *Biosens. Bioelectron.* **2014**, *58*, 242.

(22)   Liu, H.; He, F-Y. and Huang, F. *Fenxi Ceshi Xuebao* **2013**, *32*, 494.

(23)   Zhang, D.; Zhang, Y. and He, L. *Electroanal.* **2013**, *25*, 2136.

(24)   (a) Volikakis, G.J. and Efstathiou, C.E. *Talanta* **2000**, *51,* 775. (b) Sims, M.J.; Li, Q.; Kachoosangi, R.T.; Wildgoose, G.G. and Compton, R.G. *Electrochim. Acta* **2009**, *54,* 5030.

(25)   Furuno, K.; Akasako, T. and Sugihara, N. *Biol. Pharm. Bull.* **2002**, *25(1)*, 19.

(26)   Gomez-Pineda, L.E.; Oropeza-Guzman, M.T. and Pina-Luis, G.E. *ECS Trans.* **2009**, *20(1)*, 141.

(27)   Sun, Z.; Ma, Z.; Zhang, W.; Wang, X.; Fan, C.and Li, G. *Anal. Bioanal. Chem.* **2004**, *379,* 283.

(28)   El-Shahaw, M.S. *Anal. Sci.* **2006**, *22,* 1351.

(29)   Liang, J.; Tian, Y.X.; Fu, L.M.; Wang, T.H.; Li, H.J.; Wang, P.; Han, R.M.; Zhang, J.P. and Skibsted, L.H. *J. Agric. Food Chem.* **2008**, *56,* 10376.

(30)   Han, R.M.; Tian, Y.X.; Liu, Y.; Chen, C.H.; Ai, X.C.; Zhang, J.P. and Skibsted, L.H. *J. Agric. Food Chem.* **2009**, *57,* 3780.

(31)   He, J.B.; Yuan S.J.; Du; J.Q.; Hu, X.R. and Wang, Y. *Bioelectrochem* **2009**, *75,* 110.

(32)   Zoulis, N.E. and Efstathiou, C.E. *Anal. Chim. Acta* **1996**, *320,* 255.

(33)   Wu, L.; Laughlin-Jr, J.B. and Dewald, H.D. *Electroanal.* **1997**, *9,* 796.

(34)   Oliveira-Brett, A.M. and Ghica, M.E. *Electroanal.* **2003**, *15,* 1745.

(35)   Martinez, S.; Valek, L.; Petrovic, Z.; Metikos-Hukovic, M. and Piljac, J. *J. Electroanal. Chem.* **2005**, *584,* 92.

(36)   Medvidovic-Kosanovic, M.; Šeruga, M.; Jakobek, L. and Novak, I. *Croatica Chem. Acta* **2010**, *83,* 197.

(37)   Ramesová, S.; Sokolová, R.; Tarábekb, J. and Degano, I. *Electrochim. Acta* **2013**, *110,* 646.

(38)   Masek, A.; Chrzescijansk, E. and Zaborski, M. *Electrochim. Acta* **2013**, *107*, 441.

(39)   Pavlishchuk, V.V. and Addison, A.W. *Inorg. Chim. Acta* **2000**, *298*, 97.

(40)   Manaia, M.A.N.; Diculescu, V.C.; Gil, E.S. and Oliveira-Brett, A.N. *J. Electroanal. Chem.* **2012**, *682*, 83.

(41)   Salas-Reyes, M.; Hernández, J.; Domínguez, Z.; González, F.J.; Astudillo, P.D.; Navarro, R.E.; Martínez-Benavidez, E.; Velázquez-Contreras, C. and Cruz-Sánchez, S. *J. Braz. Chem. Soc.* **2011**, *22(4)*, 693.

(42)   Bard, A.J. and Faulkner, L.R. *Electrochemical Methods, Fundamentals and Applications*, 2nd ed., John Wiley & Sons, New York, 2001, pp. 236, 503, 709.

(43)   Harrison, J.A. and Khan, Z.A. *J. Electroanal. Chem.* **1970**, *28*, 153.

(44)   Andrieux, C.P. and Saveant, J.M. *J. Electroanal. Chem*. **1978**, *93*, 163.

(45)   Nicholson, R.S. and Shain, I. *Anal. Chem.* **1964**, *36*, 706.

(46)   Guidelli, R.; Compton, R.G.; Feliu-Martinez, J.M.; Gileadi, E.; Lipkowski, J.; Schmickler, W. and Trasatti, S. Definition of the Transfer Coefficient, IUPAC 2013.

(47)   Bard, A.J. and Faulkner, R. *Electrochemical Methods*; John Wiley: New York, 1980.

(48)   Petrucci, R.; Astolfi, P.; Greci, L.; Firuzi, O.; Saso, L. and Marrosu, G. *Electrochim. Acta* **2007**, *52 (7)*, 2461.

(49)   (a) Vakulskaya, T.I.; Larina, L.I. and Vashchenko, A.V. *Magn. Reson. Chem.* **2011**, *49*, 508. (b) Senboku, H.; Yamauchi, Y.; Kobayashi, N.; Fukui, A. and Hara, S. *Electrochim. Acta* **2012**, *82*, 450.

(50)   Nagarajan, P.; Sulochana, N. and Muralidharan, V.S. *Bull. Electrochem.* **2004**, *20(2)*, 93.

(51)   (a) Nakayama, T.; Shimizu, T.; Torii, Y.; Miki, S.; and Hamanoue, K. *J. Photochem. Photobiol., A* **1997**, *111(1-3)*, 35. (b) Kawata, H.; Kumagai, T.; Suzuki, E. and Niizuma, S. *J. Photochem. Photobiol., A* **1996**, *101(2-3)*, 201.

(52)   (a) Chen, A-W.; Kuo, W-B. and Chen, C-W. *J. Chin. Chem. Soc.* **2003**, *50*, 123. (b) Handy, S.T. and Omune, D. *Org. Lett.* **2005**, *7(8)*, 1553. (c) Berthelot, J.; Guette, C.; Fournier, F. and Davoust, D. *Tetrahedron Lett.* **1987**, *28(17)*, 1881.

(53)   Kolthoff, I.M. *Treatise on analytical chemistry. Part 1, Theory and practice. Thermal methods*, John Wiley & Sons, **1993**.

(54)   Ashnagar, A.; Bruce, J.M.; Dutton, P.L. and Prince, R.C. *Biochim. Biophys. Acta* **1984**, *801*, 351.

(55)   Tsierkezos, N.G. *J. Sol. Chem.* **2007**, *36*, 289.

(56)   Sawyer, D.T.; Sobkowiak, A. and Roberts, J.L. *Electrochemistry for Chemists*, Wiley, **1995**.

(57)   Izutsu, K. *Electrochemistry in Nonaqueous Solutions*, Wiley, **2002**.

Chapter V. Iron(III) coordination properties of the flavones

We will herein describe the Fe(III) coordination properties of ladanein **FOMe** and its synthetic analogues (Figure 1). It is suggested that iron(III) plays a critical role in the bioactivation of ladanein to form an efficient antiviral species. Absorption spectrophotometric, potentiometric and spectrometric (ESI-MS) methods were used to characterize the metal complexes and quantify the strength of the interaction with the redox active ferric metal cation. Fast kinetic techniques were also employed to unravel the mechanism of formation of the ferric complexes with ladanein under acidic pH and at physiological pH (*i.e.* use of an exogenous ligand such as nitrilotriacetic acid to avoid Fe(III) hydrolysis and precipitation). Either with an excess of iron(III) at acidic pH or with a stoichiometric ratio at neutral pH in the absence of NTA, the complex formation reaction between Fe(III) and ladanein was followed by a redox reaction giving iron(II) and an oxidation product of ladanein. Even though flavonoids are very often reported to exert their biological activities by metal complexation, relatively scarce physico-chemical approaches have been published until now. In addition to our data, literature data about epicatechin, epigallocatechin gallate (EGCG) and curcumin (which may share a similar same mode of action blocking viral entry) will be discussed (Figure 2).
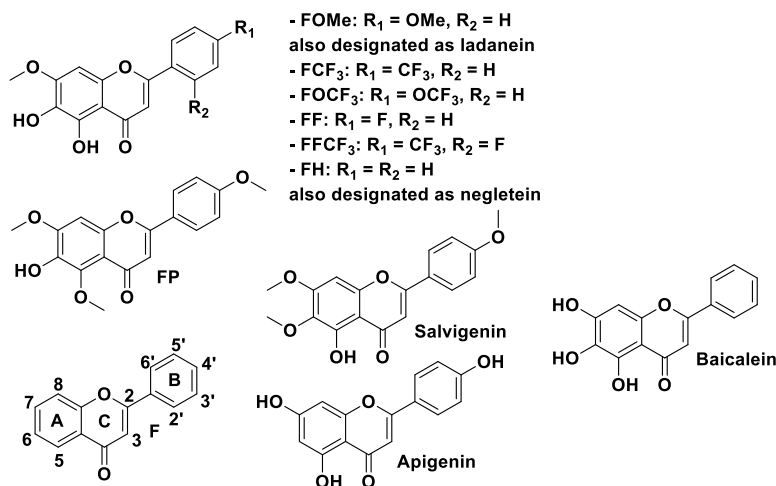

Figure 1. Chemical structures of the flavones considered in this work together with some model flavonoid compounds.
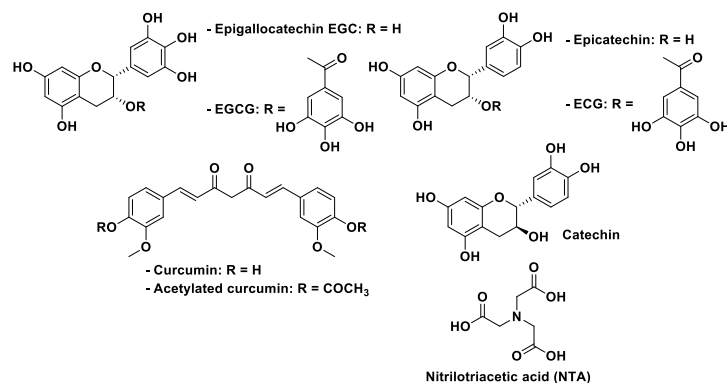
Figure 2. Chemical structures of curcumin (and its acetylated derivative), epigallocatechin gallate EGCG, epigallocatechin and catechin.

5.1. Biological Importance of Iron

Iron is the second most abundant metal after aluminium and the fourth most abundant element in the terrestrial crust. The earth's core is believed to consist mainly of iron and nickel, and occurrence of iron in meteorites suggests that it is abundant throughout the solar system as well.[1] Although the oxidation states of iron can range from –II to +VI, the most important oxidation states of iron in aqueous chemistry are +II and +III. Aqueous solutions of Fe^{II} in the absence of complexing anions contain the pale blue-green ion $Fe(H_2O)_6^{2+}$, which is oxidized in acidic solutions according to the following equation:

$$2\,Fe^{2+} + \tfrac{1}{2}\,O_2 + 2\,H^+ \longrightarrow 2\,Fe^{3+} + H_2O \quad E° = 0.46\,V$$
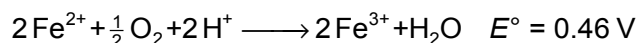
Ferric ion exists in the form of pale purple $Fe(H_2O)_6^{3+}$ only in a non-complexing medium at pH < 1. Above this pH, a stepwise hydrolysis occurs, giving rise to two different species, $Fe(H_2O)_5(OH)^{2+}$ and the dimer $Fe_2(H_2O)_8(OH)_2^{4+}$. Furthermore, a small amount of $Fe(H_2O)_4(OH)_2^{+}$ is also formed. At pH > 2, condensed species and colloidal gels are formed leading to the precipitation of the red brown gelatinous hydrous oxide $Fe_2O_3\cdot nH_2O$. The ferric hydroxo species are yellow because of charge transfer bands in the UV region that have tails in the visible. The hydrolysis of iron(III) is complicated and conditions dependent process (log $K_{Fe(OH)2+}$ = -1.39 in CH_3OH/H_2O 80/20 *w/w*).[79]

All living cells, whether they are microbial, vegetal or animal require iron as an essential nutrient. The only known possible exceptions are certain strains of bacterium *Lactobacillus*, where iron is replaced by manganese and cobalt.[2] Iron is found in a wide variety of cellular enzymes, with functions ranging from electron and oxygen transport to free radical induced coupling reactions.[3,4]

Healthy people in industrialized countries have in average 4 to 5 grams of iron in their bodies. In the human body, Fe(III) is mainly present at neutral pH (pH = 7.4). Therefore, to assure its solubility under physiological conditions, iron is constantly and mostly bound to proteins such as hemoglobin (~ 2.5 g) and transferrin (iron carrier), to ferritin complexes (~ 2 g in adult men) that are present in all cells as well as to low molecular weight moderate chelators such as citrates. The non-protein bound iron is called "*labile iron pool*" or "*chelatable iron pool*", and could be the target of exogenous chelators such as polyphenols. The ferritin complexes are commonly found in bone marrow, liver, and spleen. Ferritins, which are located in the liver, are the primary physiologic source of reserve iron in the body.[5]

In mammals, and particularly in humans, both low and high levels of iron can cause serious problems. Iron deficiency results in anaemia as its most common consequence. There is increasing evidence that iron deficiency affects other metabolic processes, including electron transport, DNA synthesis, catecholamine metabolism and several enzyme systems.[6] Adverse effects on work performance, neurological function, immune response and epithelial tissues have also been attributed to iron deficiency.[6] On the other hand, increased levels of iron in the human organism (also known as iron overload) have a negative effect on the liver, pancreas, heart and other tissues. It is believed that iron-derived oxidative stress is the cause of these effects. Indeed, iron, even in tiny amounts, can catalyze hydroxyl radical production by the redox cycling indicated in the following reactions, known as Fenton cycle.[7]

$$Fe^{III} + O_2^{\cdot-} \longrightarrow Fe^{II} + O_2 \text{ and } Fe^{II} + H_2O_2 \longrightarrow Fe^{III} + OH^- + OH^{\cdot}$$
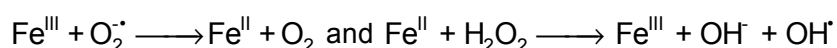
The generation of reactive oxygen species (ROS) is an inevitable by-product of aerobic metabolism. In consequence, organisms have developed not only antioxidant defensive systems, but also repair systems that prevent the accumulation of oxidatively damaged molecules. However, hydroxyl radical, being more reactive than physiological reactive oxygen species (hydrogen peroxide or superoxide anion), can cause all sorts of oxidative damage to proteins, lipids and nucleic acids.[7]

5.2. Iron Chelation by Baicalein Derived Flavones.

Baicalein displays three potential binding sites for metal ions, namely the 5-hydroxy-4-carbonyl, the 5,6-dihydroxy or the 6,7-dihydroxy binding sites. Similarly, flavonols such as quercetin also possess several potential binding sites such the 3-hydroxy-4-carbonyl, the 5-hydroxy-4-carbonyl and the 3',4'-dihdroxy. Numerous experimental and theoretical investigations have been performed on flavonols such as quercetin or myricetin to characterize the binding involved in the metal chelation,[8-14]

however, there are still controversies on mechanisms, chelation sites, structures, stoichiometries and stabilities of the complexes formed, especially in acidic aqueous solutions.
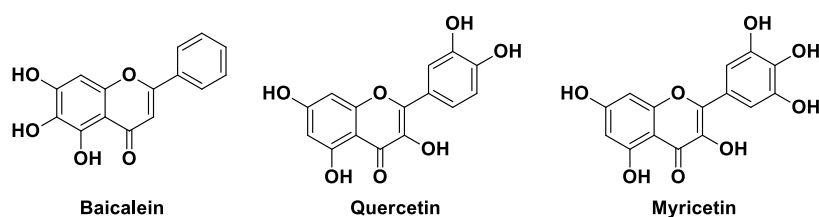

Figure 3. Chemical structures of Baicalein, Quercetin and Myricetin.

However, physico-chemical reports to assess the metal ions binding sites of baicalein derived flavones are much scarcer. For instance, in a first study,[15] the iron(II) binding characteristics of baicalein and baicalin under physiologically relevant conditions (20 mM phosphate buffer, pH 7.2) were described. Using absorption spectrophotometry and ESI-MS, a 2:1 baicalein–ferrous complex was characterized with a binding constant of β_{21} = 2–9 × 10^{11} M^{-2}, whereas a 1:1 baicalein–ferric complex was proposed with an apparent binding constant of β_{21} = 1–3 × 10^{6} M^{-1}. Using ^{1}H NMR as well as Zn^{2+} and Ga^{3+} as metallic probes, the iron-binding site of iron to baicalein was suggested to be the O6/O7 oxygen atoms present on the A-ring. Furthermore, baicalein was shown to strongly inhibit the Fe-promoted Fenton chemistry *via* a combination of chelation and radical scavenging mechanism while baicalin provided only partial protection against radical damage. These results indicate that baicalein is a strong iron chelator under physiological conditions. Modulation of metal homeostasis and inhibition of Fenton chemistry were suggested to be possible mechanisms of its known biological activity. The physico-chemical study of baicalin was not possible because of its instability in aqueous solution. Indeed, baicalin degrades rapidly at neutral or basic pH, *via* phenoxyl radical formation and subsequent hydrolysis, leading to the corresponding quinone form of baicalein, accompanied by the dissociation of the sugar group.[16] The mixture of baicalin, its degraded species and, possibly, their iron-adducts prevent reliable quantification of the ferrous/ferric complexes with baicalin. In the same study, the authors stated that baicalein binds Fe^{2+} one order of magnitude higher than quercetin does (5 × 10^{10} M^{-2}, 2:1 complex),[17] suggesting that baicalein may be more effective than quercetin in modulating iron homeostasis under physiological conditions.

A mechanistic study[18] performed on five flavonoids (baicalin, hesperidin, naringin, quercetin and rutin) selected according to their structural characteristics revealed that flavonoids exert their antioxidant activity mainly by chelating iron ions and scavenging peroxyl radicals rather than by their OH radical scavenging effect, which is suggested to be much less important.

In an *in vitro* analysis,[19] 26 flavonoids from different subclasses were analyzed for their iron(II) chelating activity and the stability of the formed complexes in four patho/physiologically relevant pH conditions (pH values of 4.5, 5.5, 6.8, and 7.5; pH 4.5 is found in lysosomes, which are organelles important in iron traffic[20] while the two acidic pHs - 5.5 and 6.8 - were chosen to mimic severe or moderate ischemia, where iron is known to participate in tissue damage)[21] and compared with the clinically and broadly used iron chelator ferrioxamine B (DFO, Figure 4). As in the previous study,[15] it was suggested that the most effective iron(II) binding site of flavonoids represents the 6,7-dihydroxy bidentate unit present in baicalein. A ferrous baicalein complex with a 1:1 stoichiometry was suggested and binding of Fe(II) by baicalein was shown to be not inferior in all tested pH to DFO. The 3-hydroxy-4-keto conformation together with 2,3-double bond and the B catechol ring (*e.g.* quercetin, myricetin) were associated with a substantial iron chelation under neutral conditions (similarly active to baicalein or ferrioxamine at the neutral conditions but shown to be not as effective at more acidic conditions). The 5-hydroxy-4-carbonyl bidentate site was shown to be less efficient (*e.g.* naringenin, naringin, hesperetin, hesperidin) and the ferrous complexes were not stable in acidic conditions.
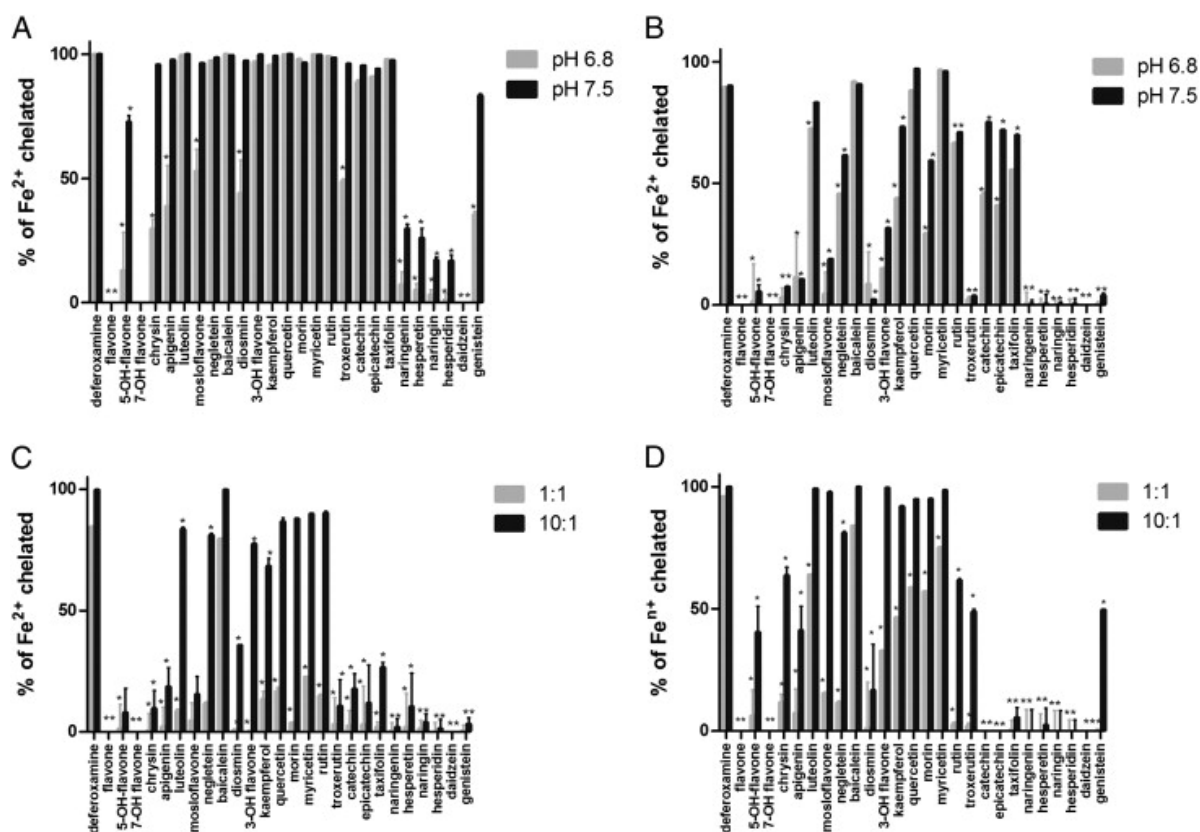

Figure 4. Iron chelation by flavonoids. Ferrous chelation at pH 6.8 and 7.5 (A):, the concentration ratio 10:1 (B):, the ratio 1:1 flavonoid:iron, respectively, at pH 5.5 (C), and total iron chelation at pH 4.5 (D). The efficiency of iron chelation was compared to DFO: * $p < 0.05$ (taken from ref. 19).

Binding of baicalein to bovine serum albumin (BSA) in the absence and presence of Cu^{2+} or Fe^{3+} in aqueous solution has also been investigated[22] by spectrophotometric methods (fluorescence, synchronous fluorescence, absorption and circular dichroism). A significant decrease of the binding constant of baicalein to BSA in the presence of Cu^{2+} or Fe^{3+} was shown and suggested to result from the competition of the metal ions and baicalein binding to BSA.

In a last report,[23] spectroscopic (UV/visible, Raman), spectrometric (ESMS) and theoretical approaches were used to evaluate the interaction of iron(III) with quercetin and baicalein in aqueous buffered solutions. Formation of two ferric quercetin complexes, with pH-dependent stoichiometries of 1:2 and 1:1, and one iron baicalein species with 1:1 stoichiometry were proposed. Vibrational analysis and theoretical calculations suggested that the 3-hydroxy-4-carbonyl and the 3′-hydroxy-4′-hydroxy group of catechol as the main chelating sites for quercetin. For baicalein, the 5-hydroxy-6-hydroxy group was found to be the most energetically favourable site, although 5-hydroxy-4-carbonyl and 6-hydroxy-7-hydroxy chelating sites are energetically similar.

## 5.3. Is Iron Chelation Essential for Ladanein Bioactivation?

An ICP-MS analysis showed that the most active fractions of extracted ladanein (S3F4) were significantly enriched in Cu(II) and Fe(III), whereas the levels of these two redox active cations were found to be significantly lower in the less active fractions. This finding raised the question whether higher activity of natural ladanein (compared to the synthetic flavone) is due to metal complexation or another process.

Table 1. ICP-MS data from the most active and the most inactive fractions along **FOMe** extraction.

	DE-1	DE-2	DE-1	DE-2	
Mg/kg	**LF-HPE1**	**LF-HP S2F1**	**S3F3**	**S3F4**	
Mg	508	212	111	76	
Al	23	12	11	21	
Cr	<5	<5	<5	25	
Mn	<25	<25	<25	<25	
Fe	6	4	34	**158**	← **Fe-enriched active fraction**
Co	<5	<5	<5	<5	
Ni	<2	<2	7	15	
Cu	5	14	**49**	**24**	← **Cu-enriched active fraction**
Zn	42	305	55	**87**	← **Zn-enriched active fraction**

As	<5	<5	<5	<5
Se	<5	<5	<5	<5
Sr	<2	<2	<2	<2
Zr	<25	<25	<25	<25
Cd	<2	<2	<2	<2
Sn	<2	<2	<2	<2
Ba	2	<5	<5	<5
Hg	<5	<5	693	<5
Pb	<2	<2	10	18
I	<60	<60	773	<60

Iron(III) complexation might indeed play a critical role by preventing flavone degradation through the unspecific polymerization upon 2e⁻ oxidation and subsequent quinone formation (see previous chapter). Metal chelation favours oligomerization *via* 1e⁻ oxidative coupling reactions. Oligomerization (either by *C,C-* or *C,O-* coupling) through oxidative phenolic coupling reactions is indeed a common feature of many naturally occurring flavones (Scheme 1). We therefore anticipated that the antiviral activity of ladanein, which was shown to be both iron- and pH-dependent, strongly relies on the physico-chemical properties of the flavone.
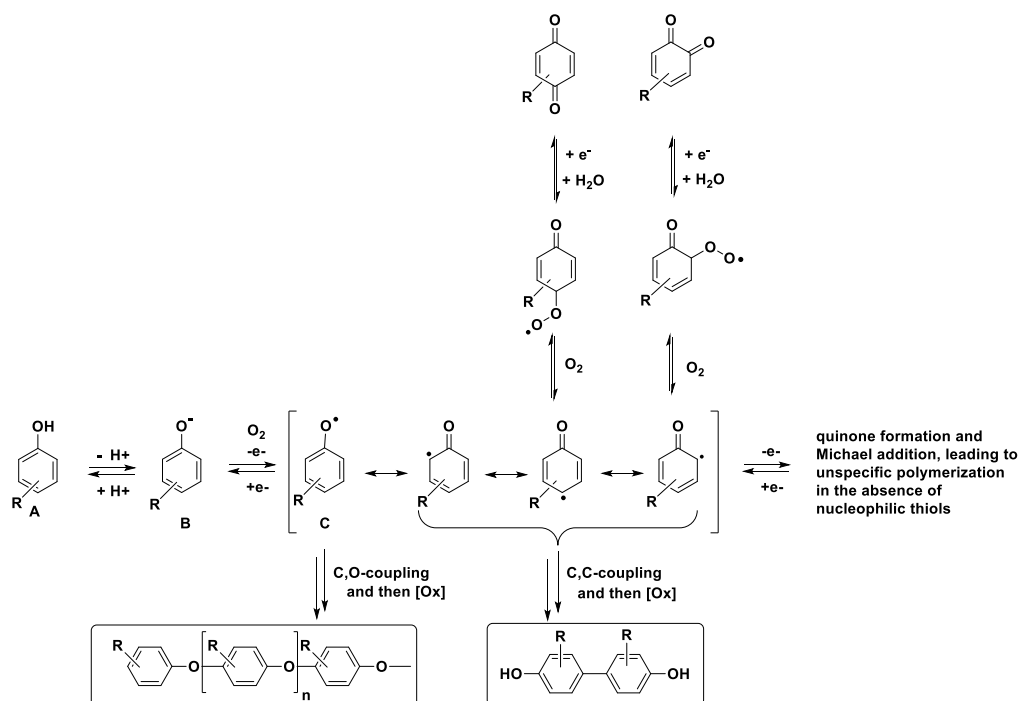
Scheme 1. Potential pathways for oxidative coupling reactions with ladanein.

To further confirm the hypothesis that the antiviral activity of ladanein originates from Fe(III) chelation (and bioactivation), my previous colleagues studied the influence of a strong iron(III) chelator ferrioxamine B (noted DFO) on the antiviral activity of ladanein. Clearly, the antiviral activity

of ladanein was abolished after addition of an equimolar amount of the exogenous iron(III) chelator (Figure 5). The anti-HIV and anti-HCV activity of ladanein **FOMe** is hence Fe(III) and pH-dependent which suggests that the flavone, by still unidentified mechanisms, severely alters the physico-chemical properties of the viral particles and inhibits their infectivity. All this evidence then prompted us to further investigate the Fe(III) coordination properties of ladanein. Due to the low solubility of ladanein and its synthetic analogues in water, a detailed physico-chemical study was carried out in a mixed solvent made of 80% of CH_3OH and 20 % of H_2O (*w/w*).
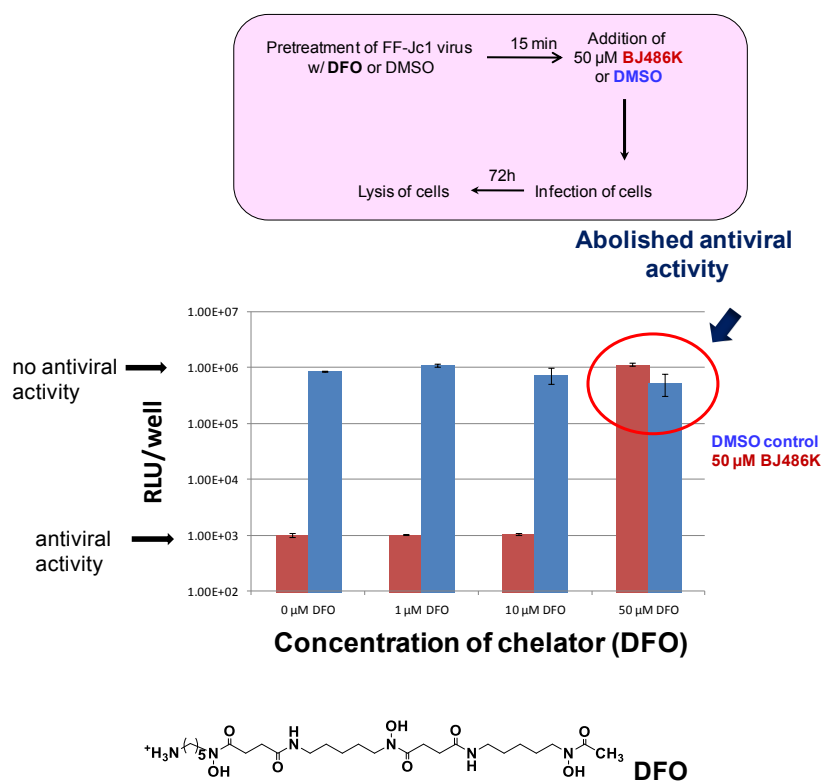

Figure 5. Influence of iron chelator DFO on antiviral activity of **BJ486K**.

First, the results obtained on ladanein by my previous colleague, Alexandra Novodomska will be presented and then will be completed with the data that I have obtained for ladanein and its analogues during my PhD work. As shown in Figure 6, ladanein has two potential binding sites (the 5-hydroxy-4-carbonyl and the 5,6-dihydroxy) for iron(III). This "so-called" catechol unit borne by ladanein (*i.e.* the 5-hydroxy group forms a strong hydrogen bond with the 4-carbonyl and alters the properties of the 6-hydroxy unit which may be regarded as a "simple" phenol) is known to firmly bind iron(III) and constitutes the molecular basis of numerous natural metal chelators (*e.g.* siderophores, flavonoids...). By contrast, the β-hydroxy-ketone binder is supposed to be less reactive than the catechol group. No matter which binding site is concerned, it is noteworthy that the 5-hydroxy group

will be involved in the chelation of iron(III) (unit shared by the 5,6-dihdroxy and 5-hydroxy-4-carbonyls groups).

To unravel which binding site is involved in the chelation of Fe(III), an absorption spectrophotometry titration of ladanein under acidic conditions (pH 1 and 2) (Figure 7) was first performed and the results compared to those obtained for salvigenin, the 6-methylated ladanein analogue (Figure 8).
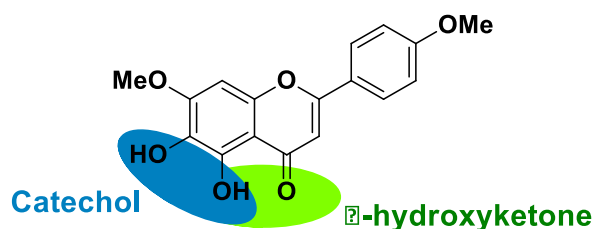

Figure 6. Potential binding sites of ladanein **FOMe** for chelation of the oxophilic trivalent cation Fe(III).
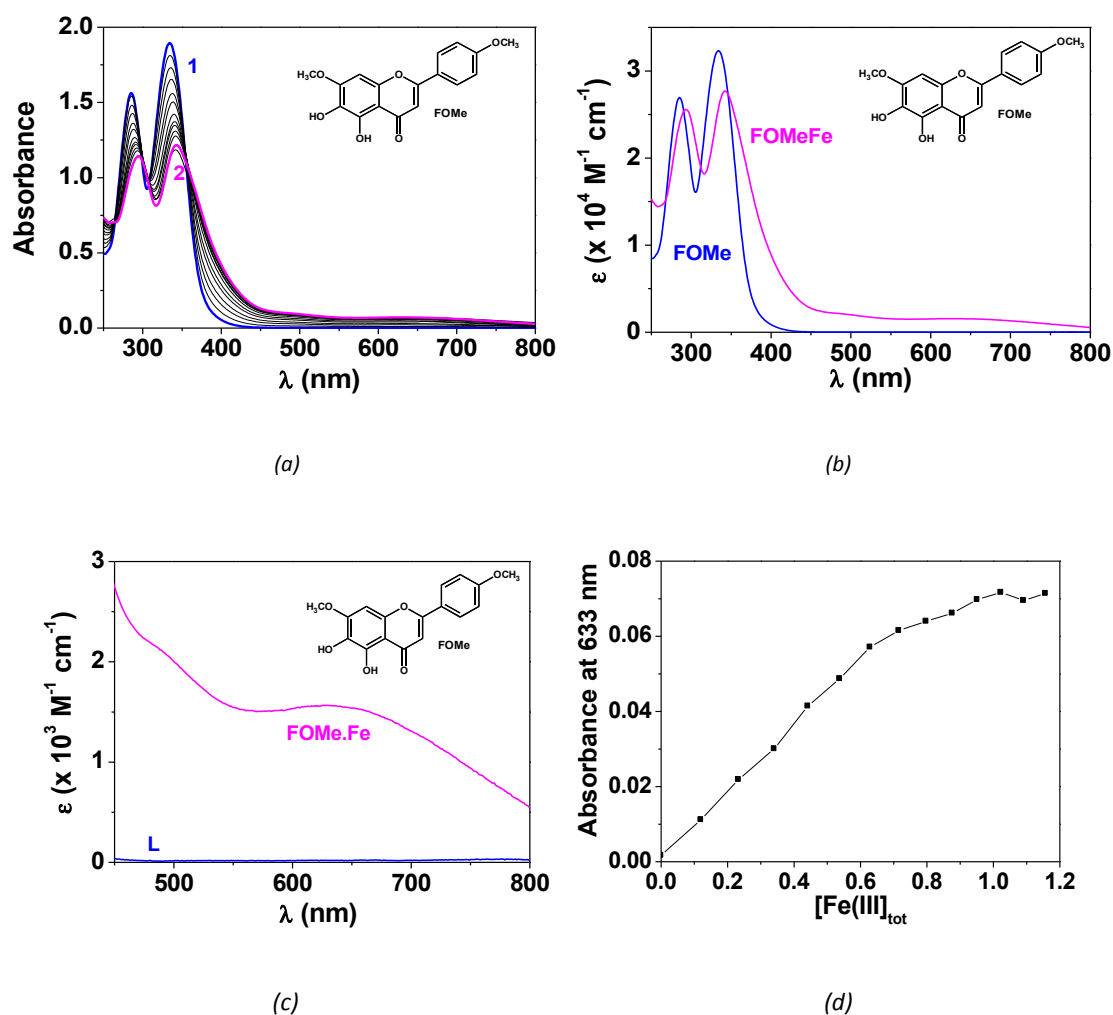

(a)

(b)

(c)

(d)

Figure 7. Absorption spectrophotometric titration of ladanein **FOMe** with Fe(III) at pH 2.0. (*a*) Absorption spectra versus [Fe(III)]$_{tot}$, (*b*) and (*c*) absorption electronic spectra of ladanein **FOMe** and its ferric complexes and (*d*) variation of the absorbance at 633 nm (LMCT) as a function of [Fe(III)]$_{tot}$. Solvent: CH$_3$OH/H$_2$O (80/20 by weight); *I* = 0.1 M (NEt$_4$ClO$_4$); *T* = 25.0(2) °C; pH = 2.0; *l* = 1 cm; (1) [**FOMe**]$_{tot}$ = 5.92 × 10^{-5} M; (2) [Fe(III)]$_{tot}$/[**FOMe**]$_{tot}$ = 1.60.
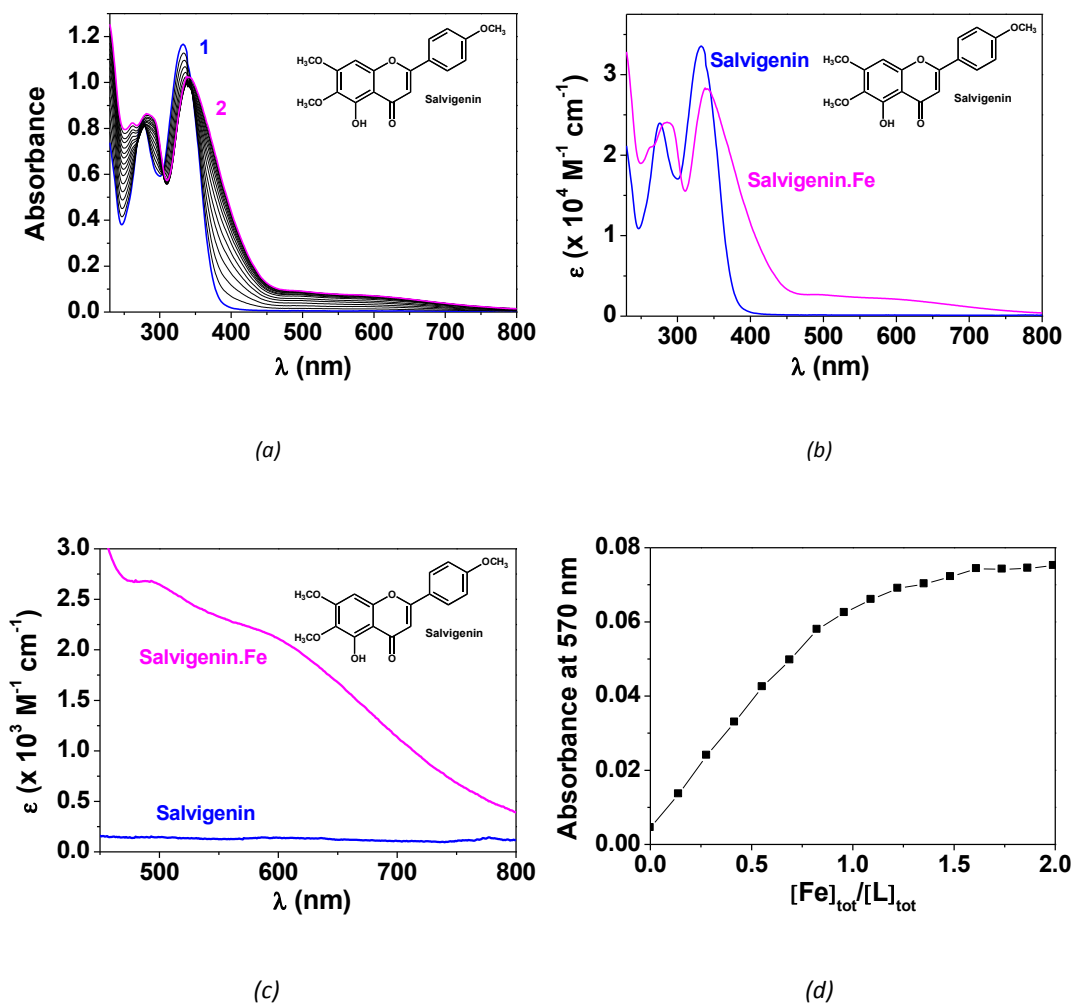

(a)

(b)

(c)

(d)

Figure 8. Absorption spectrophotometric titration of salvigenin with Fe(III) at pH 2.0. (*a*) Absorption spectra *versus* [Fe(III)]$_{tot}$, (*b*) and (*c*) absorption electronic spectra of salvigenin and its ferric complexes and (*d*) variation of the absorbance at 570 nm (LMCT) as a function of [Fe(III)]$_{tot}$. Solvent: CH$_3$OH/H$_2$O (80/20 by weight); *I* = 0.1 M (NEt$_4$ClO$_4$); *T* = 25.0(2) °C; pH = 2.0; *l* = 1 cm; (1) [salvigenin]$_{tot}$ = 3.48 × 10^{-5} M; (2) [Fe(III)]$_{tot}$/[salvigenin]$_{tot}$ = 2.0.

The absorption spectrophotometric titrations of ladanein and salvigenin by Fe(III) at pH 2.0 clearly show the ability of these flavones to firmly bind Fe(III) through its β-hydroxy-ketone chelating unit. Indeed, ladanein and salvigenin share similar spectral variations upon addition of ferric ions. Fe(III) coordination is evidenced by the formation of a Ligand-to-Fe(III) Charge Transfer (LMCT) absorption band in the visible region at 633 nm (ε^{633} = 1560 M^{-1} cm^{-1}) and 600 nm (ε^{600} = 2100 M^{-1} cm^{-1}) for ladanein and salvigenin, respectively, as typically observed for phenolate or catecholate Fe(III)

binders.[24,25] The spectral shift of 33 nm observed between the LMCT absorption maxima of the ferric complexes of ladanein and salvigenin may be due to the 6-methoxy present for salvigenin which affects the electronic distribution of the A-ring (see the acido-basic properties chapter). Even though it can be anticipated that the 5-O-methylation would not lead to a potential metal chelator, a negative test has been performed using the final precursor of ladanein **FP** as a model, confirming the essential role of the 5-hydroxy position.

Before we proceed any further, it is important to highlight that iron(III) has a $3d^5$ electronic configuration and that the application of a strong crystal field induces, in a octahedral symmetry, a splitting of the five d orbitals into two groups e_g (d_{z^2} and $d_{x^2-y^2}$) and t_{2g} (d_{xy}, d_{xz} and d_{yz}). The energy difference between the two orbital groups is noted Δ_0 (= 10 Dq) and usually lies between 10000 and 16000 cm^{-1} for most of the high spin iron(III) biological systems.[26] The Δ_0 of **FOMe.**Fe (5100 cm^{-1}) is close to the values determined for ferric complexes with phenolate-based ligands[27] and is lower than the values measured for catecholate-based ligands (*e.g.* Δ_0 = 8080 cm^{-1} for tris(catecholate)-iron complex). These Δ_0 values are however significantly different from the value calculated for Fe(OH)$_6^{3-}$ (Δ_0 = 13000 cm^{-1}).[28] For phenolate and catecholate based ligands, the difference with respect to Fe(H$_2$O)$_6^{3+}$ can be explained by the partly oxidized character of the ligand (*i.e.* semi-quinone) and the partly reduced character of iron (*i.e.* Fe^{II}) in the excited state during the charge transfer process.

The spectral data has been processed by statistical methods allowing us to unambiguously confirm the presence of monoferric monochelates under these experimental conditions. The **FOMe**.Fe(III) complex was characterized and quantified (log $K^*_{\textbf{FOMe}.Fe}$ = 6.0(3) at pH 2.0; K_D = 1 µM). This ferric complex displays comparable affinity for ferric cation as that determined for salvigenin.Fe(III) under identical experimental conditions (log $K^*_{salvigenin.Fe}$ = 5.8(2) at pH 2.0; K_D = 1.6 µM). Interestingly, our data is also in excellent agreement with those measured for baicalein at pH 7.2 (log $K^*_{baicalein.Fe}$ ranging from 6.0 to 6.5; K_D from 0.33 to 1 µM).[15] However, the authors attributed the 6,7-dihydroxy unit as the preferential chelation site which is not present for ladanein and salvigenin. Furthermore, we compared our physico-chemical data obtained on ladanein and salvigenin to those previously measured for apigenin (5,7-dihydroxyflavone, Figure 9) which only displays the 5-hydroxy-4-carbonyl binding site.[29] Apigenin was also found to afford a monoferric monochelate with an apparent stability constant (log $K^*_{apigenin.Fe}$ = 5.5(1) at pH 2.0; K_D 3.16 µM) and a LMCT absorption band (λ^{max} = 520, ε^{520} = 2080 M^{-1} cm^{-1}), which is in agreement with our data on ladanein and salvigenin thus supporting our initial hypothesis.
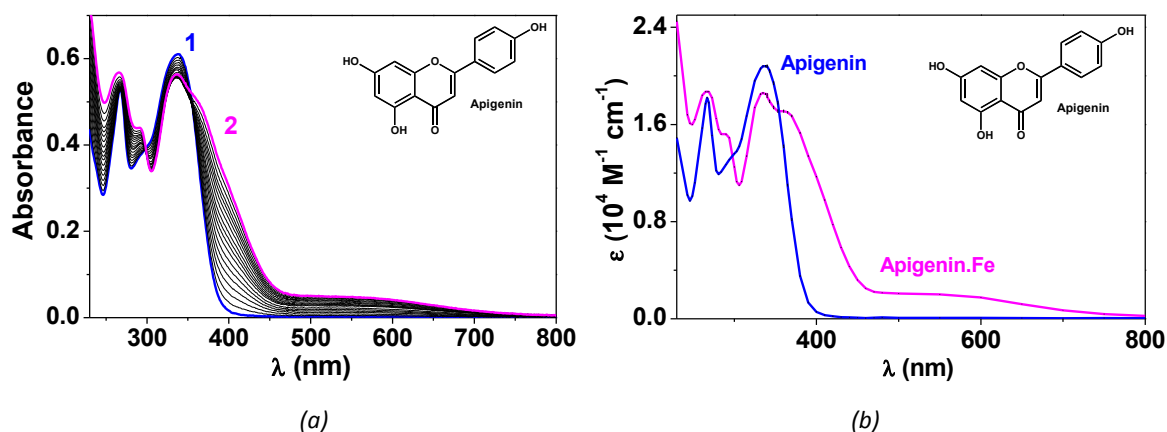
Figure 9. Absorption spectrophotometric titration of apigenin with Fe(III) at pH 2.0. (*a*) Absorption spectra *versus* $[Fe(III)]_{tot}$ and (*b*) absorption electronic spectra of apigenin and its ferric complexes. Solvent: CH_3OH/H_2O (80/20 by weight); I = 0.1 M $(NaClO_4)$; T = 25.0(2) °C; pH = 2.0; l = 1 cm; (1) $[apigenin]_{tot}$ = 2.91 × 10^{-5} M; (2) $[Fe(III)]_{tot}/[apigenin]_{tot}$ = 1.6. From ref 29.

Efforts to characterize the ferric complexes of ladanein by ESI-MS were unsuccessful due to the high voltages necessary to desolvate/ionize the metal complexes, which consequently lead to the complex dissociation. For that reason, we confirmed the stoichiometry of the ladanein.Fe(III) and salvigenin.Fe(III) complexes with the method of continuous variations (Figure 10). Solutions of the flavones and iron(III) at pH 2.0, subject to the condition that the sum of the total flavone and Fe(III) concentrations is constant, were prepared. Absorption spectra were measured for each of the solutions and the maximum x_{max} value (~ 0.43 for ladanein and ~ 0.47 for salvigenin) indicates the predominant formation of 1:1 stoichiometry ferric complexes. The binding site is assumed to be the β-hydroxy-ketone unit as evidenced by a comparative study with apigenin (Figure 10).

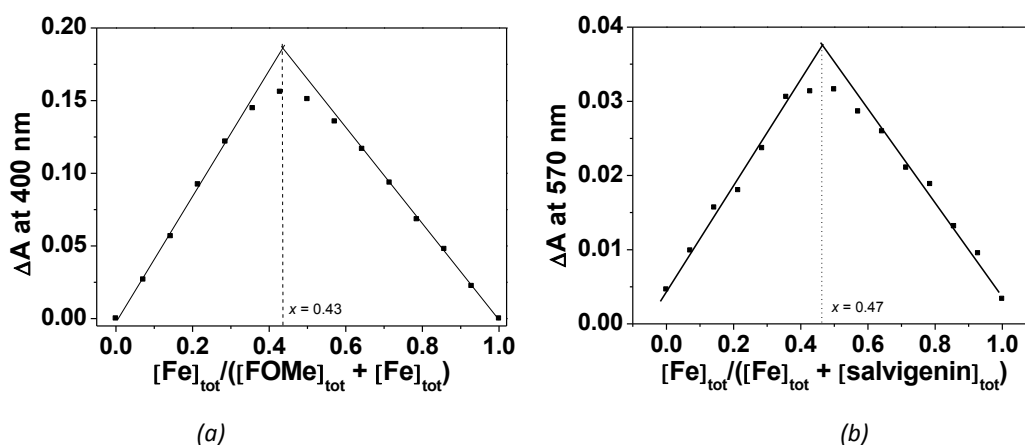**Figure 10.** Job plots obtained upon mixing (a) ladanein and Fe^{3+} ($\Delta A/\Delta A_{max}$ at 400 nm) and (a) salvigenin and Fe^{3+} ($\Delta A/\Delta A_{max}$ at 570 nm). Solvent: CH_3OH/H_2O (80/20 by weight); I = 0.1 M (NEt_4ClO_4); T = 25.0(2) °C; pH = 2.0; ($[\mathbf{FOMe}]_{tot}$ + $[Fe(III)]_{tot}$) = 4.94 × 10^{-5} M; ($[salvigenin]_{tot}$ + $[Fe(III)]_{tot}$) = 3.48 × 10^{-5} M; l = 1 cm.

We then examined the Fe(III) binding properties of the synthetic ladanein analogues at pH 2.0. Table 2 gathers the spectroscopic properties of the metal complexes as well as the apparent stability constants which were evaluated. With the exception of the 4'-fluoroflavone **FF**, the ladanein analogues display binding affinities for Fe(III) comparable to that of ladanein. Interestingly, for the synthetic analogues displaying an electron-withdrawing substituent on the B-ring (**FFCF₃**, **FCF₃**, **FF** and **FOCF₃**), the LMCT is bathochromically shifted of about 20 nm with respect to **FOMe** or **FH** which may be explained by the electronic effects on the carbonyl unit induced by these substituents which affect the LMCT transitions. This feature confirmed the essential role of the carbonyl group in the Fe(III) binding and support the fact that the bidentate binding site is the β-hydroxy-carbonyl unit.

Table 2. Apparent stability constants of the Fe(III) complexes of ladanein and its analogues.[a]

Complex	log K*FFe	λ_{max} LMCT (nm) $\varepsilon^{\lambda max}$ (M⁻¹ cm⁻¹)
FOMe.Fe	6.0(3)	633(1560)
FH.Fe	5.4(6)	635(1200)
FFCF₃.Fe	5.8(4)	651(1050)
FCF₃.Fe	5.3(6)	650(1230)
FF.Fe	4.7(3)	655(910)
FOCF₃.Fe	5.8(3)	649(1040)
[a] Solvent: CH₃OH/H₂O (80/20 by weight); *I* = 0.1 M (NEt₄ClO₄); *T* = 25.0(2) °C; [H⁺] = 10⁻² M. Error = 3σ with σ = standard deviation.		

The monoferric complex of ladanein displays a Phenolate-to-Fe(III) Charge Transfer absorption band centered at 633 nm (ε^{633} = 1560 M⁻¹ cm⁻¹) under more acidic pH. Decreasing the acidity of the medium to pH 1.0 does not significantly alter the spectral properties of the complex (λ^{max} = 635, ε^{635} = 1680 M⁻¹ cm⁻¹). However, the stability decreases (log $K^{*}_{ladanein.Fe}$ = 5.6(3) at pH 1.0; K_D = 2.5 μM) due to a proton/metal competition in favor to protonation under acidic conditions. We then performed a spectrophotometric absorption titration of the ferric complexes with ladanein as a function of pH. Figure 11 clearly shows that the decrease of pH influences mainly the absorptivity of the LMCT band without altering its position, while raising the pH leads to both hypochromic and hypsochromic shifts of the latter absorption. The statistical processing of the spectral and potentiometric data sets allowed us to evidence a protonated ferric complex (log $K_{FOMeH.Fe}$ = 3.6(3)) under acidic conditions and a hydroxylated ferric species (log $K_{FOMe.Fe(OH)}$ = -4.4(4)) under more basic conditions.
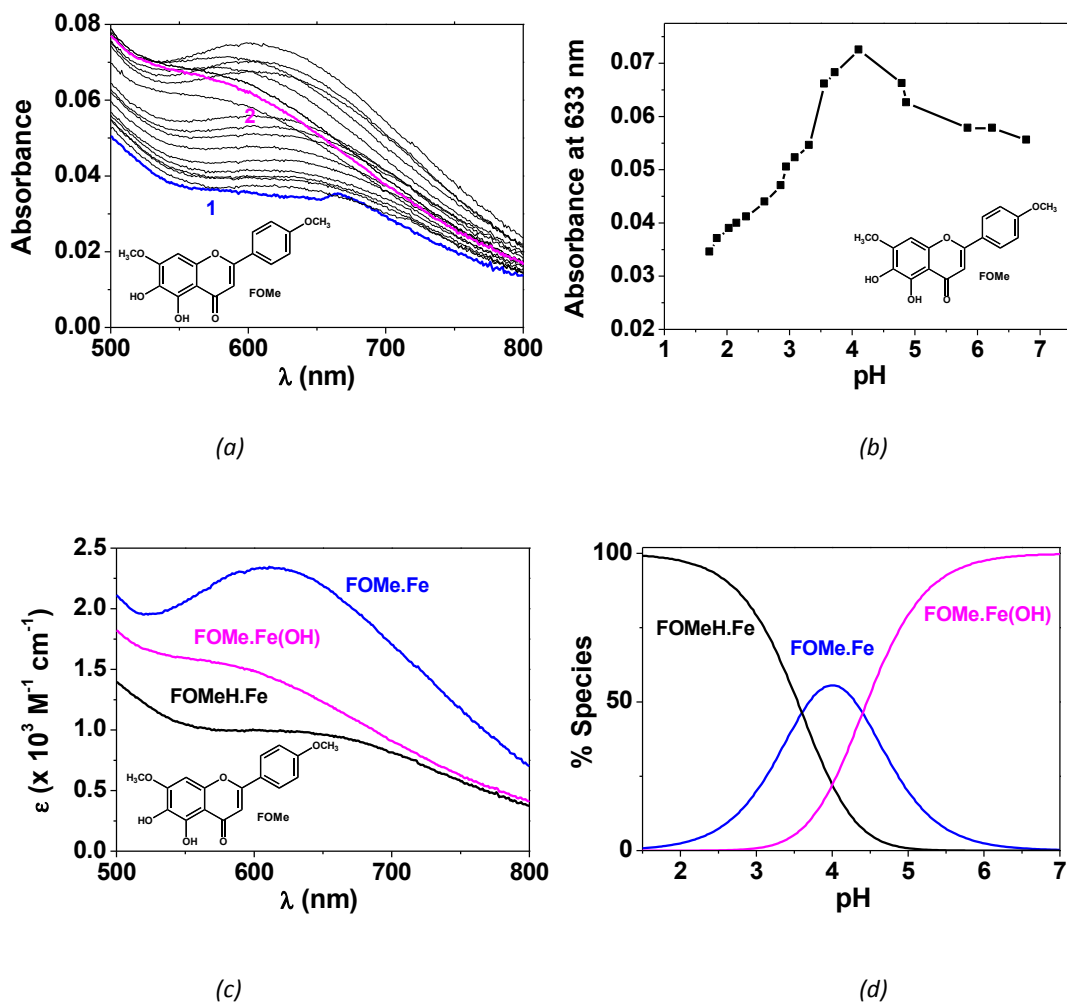
Figure 11. Absorption spectrophotometric titration of the ferric complexes of ladanein as a function of pH. (a) spectral variation of the LMCT recorded, (b) variation of the absorbance at 633 nm as a function of pH, (c) electronic spectra of the ferric complexes and (d) distribution diagrams of the ferric complexes of ladanein. Solvent: CH_3OH/H_2O (80/20 by weight); I = 0.1 M (NEt_4ClO_4); T = 25.0(2) °C; l = 1 cm; $[FOMe]_{tot}$ = 4.55 x 10^{-5} M; $[Fe(III)]_{tot}$ = 4.14 × 10^{-5} M;.(1) pH = 1.72; (2) pH = 6.79.

The low pK_a value (log $K_{FOMeH.Fe}$ = 3.6(3)) can be related to the 6-OH deprotonation which is anticipated to not strongly participate to the Fe(III) binding. The significant decrease of about 6.7 orders of magnitude with respect to the free ligand (log K_H = 10.33(5)) may be explained by electronic effects and altered hydrogen pattern upon complexation to the ferric cation.[30] On the other hand, hydrolysis is a common feature of the oxophilic Fe(III) which acts as a hard Lewis acid. The hydrolysis constant of the ferric complex with ladanein is significantly increased (log $K_{FOMe.Fe(OH)}$ = -4.4(4)) with respect to free iron(III) (log $K_{Fe(OH)}$ = -1.39). Taken together, these data support the fact that ladanein binds Fe(III) through its hydroxy-ketone chelating unit. Contrarily to catecholate-derived systems,[26,28] the spectrophotometric and potentiometric titration conducted in excess of ladanein did not reveal the formation of bischelate or trischelate. This feature clearly indicates that only monoferric

monochelates are formed with our flavones and that increasing the pH predominantly favours the hydrolysis of the ferric complex and its subsequent dissociation. Indeed, further increase of the pH above pH 7-8 for the ferric ladanein complexes resulted in the release of the trivalent metal cation and its subsequent precipitation due to formation of polyhydroxo ferric complexes.

Table 3. Stability constants of Ladanein.Fe(III) complexes.[a]

Equilibrium	log K (± 3σ)
$L^{2-} + Fe^{3+} \xrightleftharpoons{K_{LFe}} LFe^+$	log K_{LFe} = 23.8(2)
$LFe^+ + H^+ \xrightleftharpoons{K_{LHFe}} LHFe^{2+}$	log K_{LHFe} = 3.6(3)
$LFe^+ \xrightleftharpoons{K_{LFeOH}} LFe(OH)$	log K_{LFeOH} = -4.4(4)
[a] **Solvent: CH_3OH/H_2O (80/20 by weight); I = 0.1 M (NEt_4ClO_4); T = 25.0(2) °C; the first protonation constant of free ladanein FOMe (related to the 5-OH unit has been estimated to be 13.**	

To compare the Fe(III) chelating properties of ladanein with other systems of interest, we calculated the pFe values. The notion of pM was first introduced by K. Raymond for Fe(III)[31] and can be applied to any metal ion. The pM corresponds to the logarithm of the reciprocal of the concentration of the free metal ion (pM = -log $[M]_{free}$) under given conditions of acidity of the medium (physiological pH) and of analytical concentrations of the ligand and metal. This value, therefore, takes into account the diverse characteristics of the ligands which are compared (acido-basic properties of the free ligand and of the metal complexes, stoichiometry of metal complexes, etc) and thus allows for a direct comparison of their chelating affinity for a given cation. High pM values will reflect a strong binding affinity of the ligand toward the studied metal ion. For our calculations, we have chosen to use a concentration of 10^{-6} M for iron(III) which corresponds to the homeostatic concentration in the human body, and we used a ten-fold excess of ladanein (*i.e.* not biological relevant concentration). Table 4 gathers the pFe value for ladanein together with those calculated for various Fe(III) chelators (siderophores and polyphenols) including curcumin and EGCG for which antiviral activities towards HCV have been reported.

Even though there are numerous reports focusing on the biological activities of curcumin, physico-chemical investigations of its Fe(III) coordination properties are extremely scarce. To the best of our knowledge, only the group of M. Saladini[32] thoroughly evaluated the acido-basic and Fe(III) coordination properties of curcumin (noted CU) and its diacetylated analogue (noted DCU) in a CH_3OH/H_2O (50/50 by weight) solvent mixture. The enolic proton was shown to be the more acidic

ionizable site (log K_H = 8.54(3)) and the β-diketonate unit was demonstrated to be the coordination moiety. Similarly to ladanein and its synthetic analogues, only monoferric monochelates with curcumin and diacetylcurcumin were characterized and quantified. It is also noteworthy that these species are characterized by a LMCT absorption band lying at ~ 500 nm. It has been suggested that the binding of a second (or third) curcumin ligand is prevented due to strong steric interactions. Furthermore, the increase of the pH (pH ≥ 7) was shown to lead to dihydroxylated and trihydroxylated species ($[FeH_2CU(OH)_2]/[FeH_2CU(OH)_3]^-$ and $[FeDCU(OH)_2]/[FeDCU(OH)_3]^-$ with CU = fully deprotonated curcumin and DCU = fully deprotonated diacetylated curcumin). By comparing their stability constants, it was concluded that curcumin was as effective to chelate iron(III) as DFO does. Using the pFe values, we however clearly demonstrate that curcumin (pFe = 16.66) is by far a worse Fe(III) binder than DFO (pFe = 26.6).

By contrast with curcumin or ladanein (*i.e.* only monochelates have been evidenced), catechol-based chelators such as catechol, tiron, flavanols (catechin, epicatechin, EGC, ECG, EGCG, Figure 2) or flavonols (rutin, quercetin) can form, depending on the pH, monoferric monochelate, bischelate or trischelate. Increasing pH favours the successive binding of the catecholate binding unit (Figure 13).
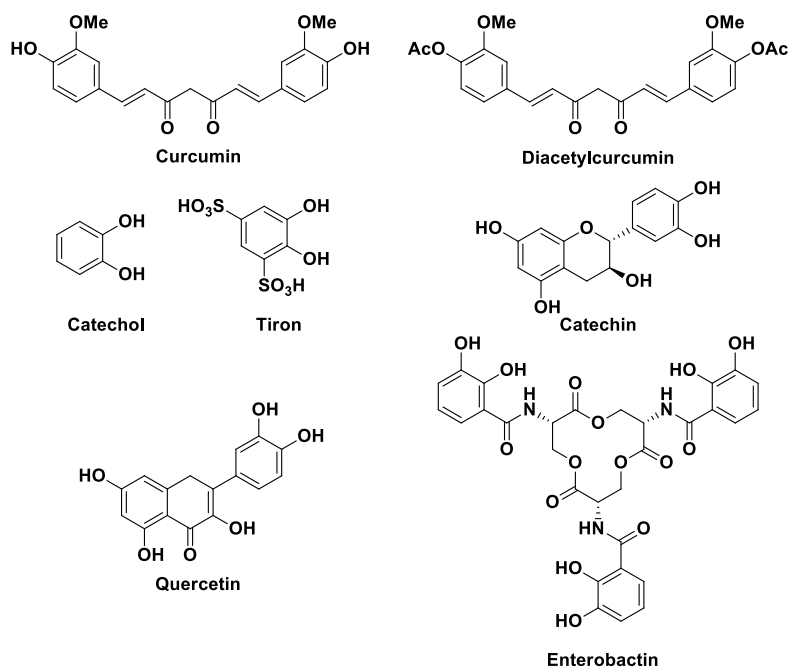

Figure 12. Chemical structures of various iron(III) chelators mentioned in Table 4.

As a consequence, the ferric bischelate was found to be the major species at physiological pH. (Epi)catechin derived chelators can be considered as strong Fe(III) binders even though they do not display a chelating ability as good as that of DFO (Table 4).[25,40] The pyrogallol unit of epigallocatechin

or the galloyl ester of ECG or EGCG help stabilize the ferric complexes with respect to catechin (Table 4). By contrast, quercetin (pFe = 27.04) and rutin (pFe = 27.26) can be considered as efficient as DFO.[42] Indeed, the high pFe values are the result of the ability of quercetin and rutin to chelate two ferric cations thanks to the various bidentate units available (3',4'-catechol, α-hydroxy-ketone or β-hydroxy-ketone). Table 4 also clearly shows that the affinity of ladanein (displaying a single bidentate unit, pFe = 19.22) for Fe(III) is much higher than that of 5-hydroxy-flavone (pFe = 11.13), 5-hydroxy-isoflavone (pFe = 10.42)[41] or baicalein (pFe = 7-7.5,[15] this rather low pFe value measured for baicalein may have been underestimated by the authors of the corresponding study). The substitution pattern and electronic effects may explain this stabilization of the ladanein ferric species. However, ladanein can be regarded as a moderate ferric chelator when compared to natural siderophores such as ferrioxamine B (trishydroxamate) or enterobactin (triscatecholate), which are hexadentate and pre-organized ligands. These physico-chemical data agree very well with the inhibition of the antiviral activity of ladanein upon addition of an equimolar amount of DFO (Figure 5 and Figure 14).
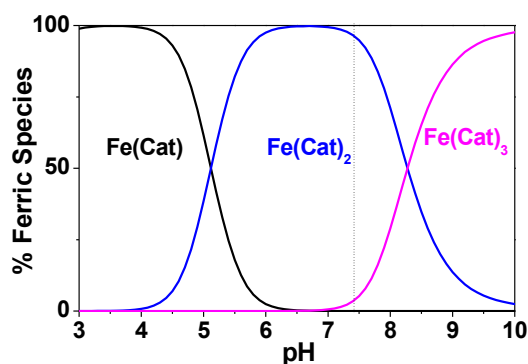
Figure 13. Distribution diagrams of the ferric complexes with catechin (noted Cat). Solvent: H_2O; I = 0.1 M (NaClO$_4$); T = 25.0(2) °C; [Cat]$_{tot}$ = 1.5 x 10^{-4} M; [Fe(III)]$_{tot}$ = 5 × 10^{-5} M.

Figure 14. Distribution diagrams of the ferric complexes with ladanein **FOMe** and DFO showing the competition between these two chelators for Fe(III). Solvent: H_2O; I = 0.1 M; T = 25.0(2) °C; [**FOMe**]$_{tot}$ = 5 x 10^{-5} M; [Fe(III)]$_{tot}$ = 5 × 10^{-5} M.

Table 4. pFe values for various Ferric complexes.[*a*]

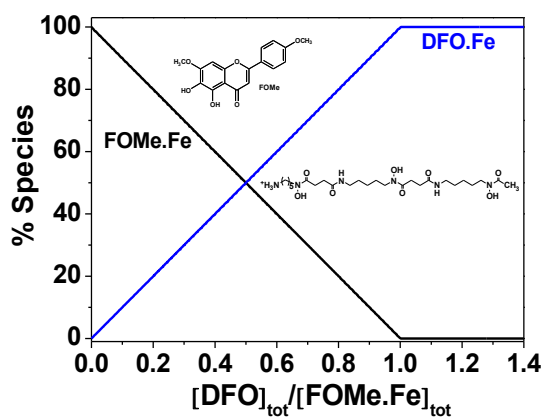| Chelator	pFe
Enterobactin[33]	35.5[a]
Ferrioxamine B[34]	26.6[b]
Catechol[35-38]	16.6[b]
Tiron[39]	20.0[b]
Tiron + NTA[25]	20.3[b]
Catechin[25]	17.6[b]
Catechin +NTA	18.9[b]
EGCG[40]	23.4[e]
EGC[40]	23.1[e]
ECG[40]	23.2[e]
Ladanein	19.22[c]
Ladanein + NTA	na
Baicalein[15]	7-7.5[b]
Curcumin[32]	16.66[d]
Diacetylated curcumin[32]	17.53[d]
5-hydroxy-flavone[41]	11.13[b]
5-hydroxy-isoflavone[41]	10.42[b]
Rutin[42]	27.26[b]
Quercetin[42]	27.04[b]

[a] pFe = -log $[Fe]_{free}$ with $[L]_{tot} = 10^{-5}$ M and $[Fe]_{tot} = 10^{-6}$ M at p[H] = 7.4. [b] water. [c] CH_3OH/H_2O (80/20 by weight). d CH_3OH/H_2O (50/50 by weight). [e] water pH 7.0; EGCG = epigallocatechin gallate; EGC = epigallocatechin; ECG = epicatechin gallate.na = not applicable.

5.4. Uptake of Fe(III) by Ladanein under Acidic Conditions.

Kinetic studies of the ferric complexes with ladanein were carried out using stopped flow spectrophotometry under acidic conditions (5.88×10^{-3} M < $[H^+]^{tot}$ < 9.4×10^{-2} M). The **L**HFe^{2+} complex (**L** being the fully deprotonated form of ladanein **FOMe**) is the major ferric complex, while Fe^{3+} and Fe(OH)$^{2+}$ are the predominant free iron(III) species under these experimental conditions of acidity ($K_{Fe(OH)2+} = 10^{-1.39}$).[79] It was chosen to monitor the formation kinetics under pseudo-first order conditions ($[Fe^{3+}]_{tot} > 10 \times [FOMe]_{tot}$) at λ = 650 nm (corresponding to the ladanein→Fe(III) CT absorptions), which corresponds to the largest spectrophotometric amplitude between the absorptions of the reactants (Fe^{3+} + **L**H$_2$) and of the product **L**HFe^{2+}. The absorbance always followed an exponential growth *versus* time indicating a first order kinetics ($v = -d[L]/dt = k_{obs}[L]$) with respect to the ligand. The kinetic recordings revealed a single rate limiting step in the second time span. Importantly, no loss of the spectral signal during the dead time of the stopped-flow device (~ 3 ms) was observed (Figure 15a). In addition, the absorbances at the end of the rate limiting step satisfactorily correspond to the expected values for the **L**HFe^{2+} complex. Interestingly, a slower

biphasic kinetic oxidation of ladanein mediated by iron(III) complexation is observed in the minute time span (Figure 15c). This clearly indicates that metal chelation by ladanein triggers oxidation of the flavone even under acidic conditions, whereas the ligand is stable over a long period in the absence of the ferric cation. This supports the fact that metal chelation might favour specific C,C- or C,O-oxidative coupling reactions or intramolecular redox processes (auto-oxidation).[43]

(a)

(b)

(c)
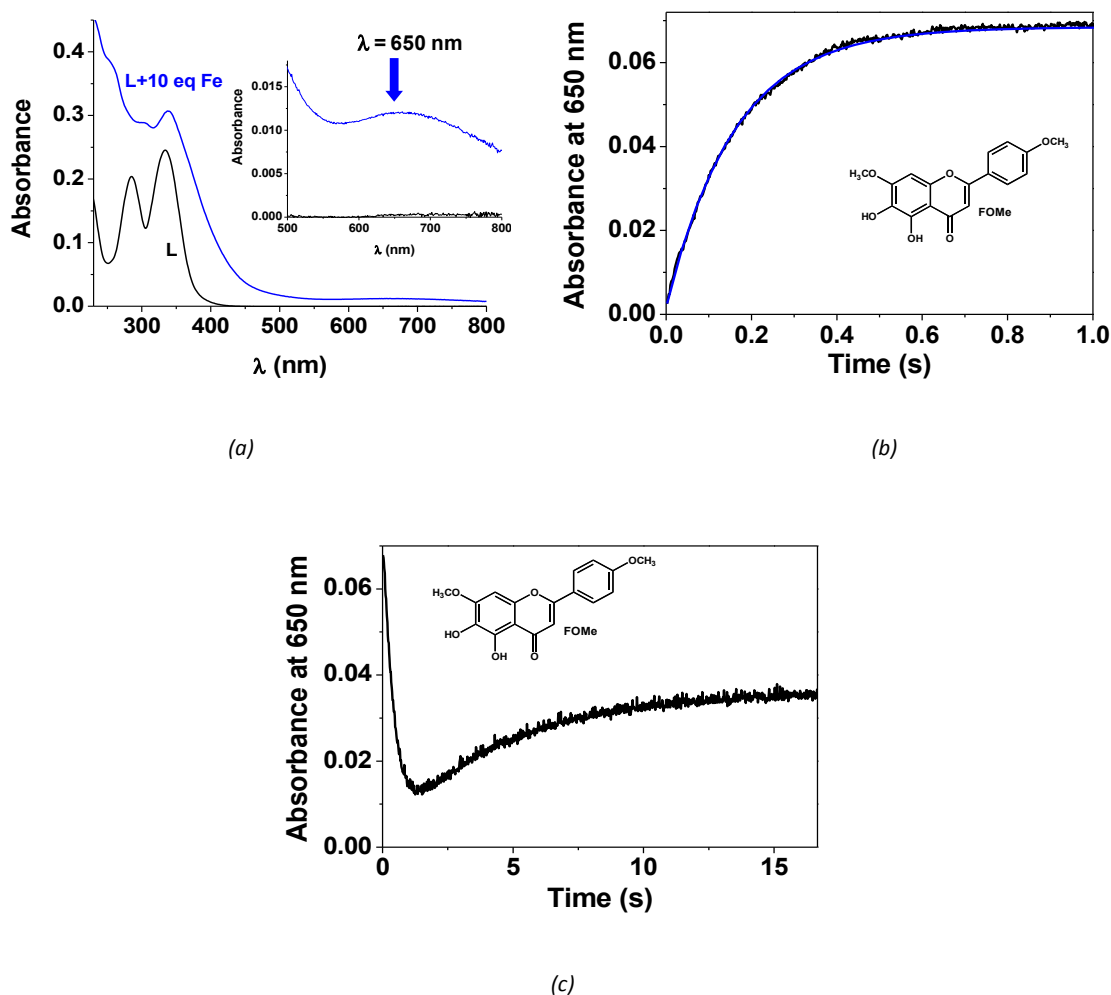
Figure 15. (*a*) UV-visible absorption spectra of ladanein **FOMe** with and without an excess of ~ 10-fold of iron(III) (*l* = 0.2 cm). (*b*) Variation of the absorbance at 650 nm (LMCT) for the formation of the ferric complexes with ladanein. (*c*) Variation of the absorbance at 650 nm showing the slower oxidation of ladanein mediated by iron(III) complexation. Solvent: CH$_3$OH/H$_2$O (80/20 by weight); *l* = 0.1 M (NEt$_4$ClO$_4$); *T* = 25.0 ± 2 °C; [H$^+$]$_{tot}$ = 0.032 M; [**FOMe**]$_{tot}$ = 3.83 x 10^{-5} M ; [Fe]$_{tot}$ = 3.09 x 10^{-4} M.

For [H$^+$]$_{tot}$ ranging from 9.4 x 10^{-3} to 0.032 M, the iron(III) concentration used in excess (*i.e.* [Fe$^+$]$_{tot}$ ≥ 10 x [**FOMe**]$_{tot}$ to impose pseudo-first order conditions) was varied and the pseudo-first order rate constants (k_{obs}) were determined. The variation of the pseudo-first-order rate constant (k_{obs}) with Fe(III) and H$^+$ concentrations are presented in Figure 16.

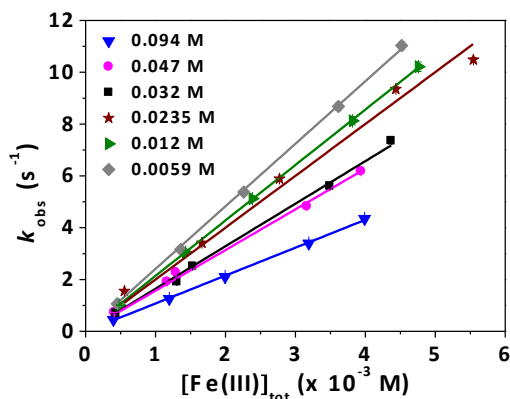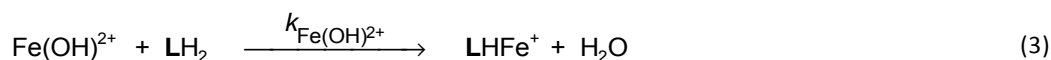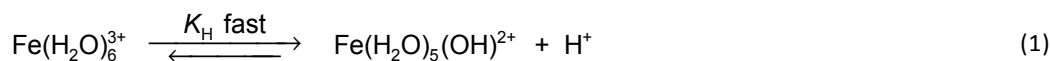**Figure 16.** Formation kinetics of the ladanein ferric complex - Variation of the pseudo-first-order rate constant as a function of Fe(III) and H^+ concentrations. [**FOMe**]$_{tot}$ = 3-5 $\times$ 10^{-5} M; solvent: CH_3OH/H_2O (80/20 by weight); I = 0.1 M (NEt$_4$ClO$_4$); T = 25.0(2) °C. Uncertainties are given as 3σ.

Over the [H^+] range considered in this work (0.0059 M $\leq$ [H^+]tot < 0.094 M), k$_{obs}$ (s^{-1}) vary linearly with the Fe(III) concentration with no significant ordinate at the origin. Under our experimental conditions, the major Fe(III) species in solution are Fe^{3+} and $Fe(OH)^{2+}$ and ladanein is fully protonated (LH$_2$, with L standing for the fully deprotonated ladanein FOMe). With respect to these observations, the following mechanism can thus be suggested:

$$Fe(H_2O)_6^{3+} \xrightleftharpoons{\quad K_H \text{ fast} \quad} Fe(H_2O)_5(OH)^{2+} + H^+ \tag{1}$$

$$Fe^{3+} + \mathbf{L}H_2 \xrightarrow{\quad k_{Fe^{3+}} \quad} \mathbf{L}HFe^+ + H^+ \tag{2}$$

$$Fe(OH)^{2+} + \mathbf{L}H_2 \xrightarrow{\quad k_{Fe(OH)2+} \quad} \mathbf{L}HFe^+ + H_2O \tag{3}$$

The rate law relative to LH$_2$ is hence:

$$v = -\frac{d[\mathbf{L}H_2]}{dt} = k_{Fe^{3+}} [Fe^{3+}] [\mathbf{L}H_2] + k_{Fe(OH)^{2+}} [Fe(OH)^{2+}] [\mathbf{L}H_2]$$

$$v = -\frac{d[\mathbf{L}H_2]}{dt} = = k_{obs} [\mathbf{L}H_2] \tag{4}$$

which becomes eqn (5) if [Fe^{3+}] and [$Fe(OH)^{2+}$] are expressed as a function of K_H and [Fe(III)]$_{tot}$.

$$v = \left(\frac{k_{Fe^{3+}} [H^+] + k_{Fe(OH)^{2+}} K_H}{[H^+] + K_H} \right) [Fe(III)]_{tot} [\mathbf{L}H_2]$$

$$v = k_a [Fe(III)_{tot}] \times [\mathbf{L}H_2] \tag{5}$$

Figure 17 presents the variation of k_a versus the total proton concentration according to eqn. (5). The K_H value was taken from the literature ($K_H = 4.07 \times 10^{-2}$ M),[79] and we were able to calculate the bimolecular rate constants k_{Fe3+} ($4.3(1.6) \times 10^2$ M^{-1} s^{-1}) and $k_{Fe(OH)2+}$ ($2.7(2) \times 10^3$ M^{-1} s^{-1}) related to the reactivity of Fe^{3+} and $Fe(OH)^{2+}$, respectively.
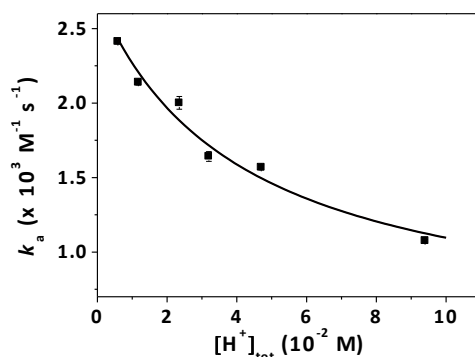
Figure 17. Variation of k_a (see eqn. (5) for definition) versus $[H^+]_{tot}$. Solvent: CH_3OH/H_2O (80/20 by weight); I = 0.1 M; T = 25.0(2) °C. Uncertainties are given as 3σ.

We have showed that, at acidic pH, the formation of **L**HFe occurs *via* two parallel pathways involving the two Fe(III) species Fe^{3+} and $Fe(OH)^{2+}$. Table 5 summarizes the reactivity of the two ferric species considered in this study (Fe^{3+}, $Fe(OH)^{2+}$) with ladanein FOMe and various bidentate ligands.

Table 5. Reactivity of various ferric species with catecholate, hydroxamate, hydroxy-carboxylate and phosphate-based ligands.

Ligands	$k_{Fe^{3+}}$ (M^{-1} s^{-1})	$k_{Fe(OH)}{}^{2+}$ (10^3 M^{-1} s^{-1})	$k_{FeNTA(OH)}$ (10^4 M^{-1} s^{-1})
Ferrioxamine B		3.6	-
Pyoverdine *PaA*	<80	7.7(4)	6.2(3)
Ladanein	430(160)	2.72(2)	0.84(3)
Apigenin	800(200)	2.0(3)	-
Catechin[29,44]	90(4)	3.1(2)	2.05(5)
	-	3.3(2)	-
Catechol[45]	-	3.1(2)	-
Phenol[46]		1.5	-
Tiron[47]	-	3.08(0.48)	2.7(2)[a]
Salicylic acid[48]	-	3.5	-
2,3-Dihydroxybenzoic acid	-	4.8	-
Phosphate[49]	-		2.4(4)
Tartaric acid	-	5.1	
Citric acid	-	3.1	
Acetohydroxamic acid[49,50]		5.65(0.864)	3.8(3)

Under acidic conditions, two Fe(III) species are involved in the formation kinetics of the complexes; Fe^{3+} and $Fe(OH)^{2+}$. The rate constant $k_{Fe^{3+}}$ is consistent with an associative ligand interchange mechanism (I_a) and is sensitive to the nature of the entering ligand substituting the first water molecule (Table 5).[51,52] In contrast to Fe^{3+}, $Fe(OH)^{2+}$ has been reported to undergo a dissociative ligand interchange pathway (I_d) for which the rate-limiting step is the loss of the first water molecule and which does not depend on the nature of the entering ligand (Table 5, Figure 18).[53,54]
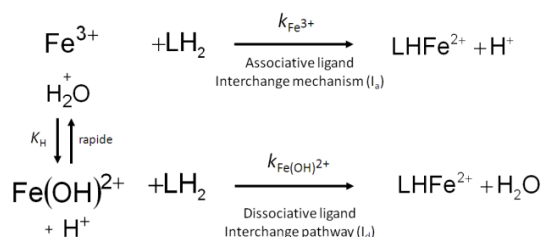

Figure 18. Suggested formation mechanism for the ferric complexes with ladanein **FOMe**.

The rate constants ($k_{Fe(OH)2+}$, Table 5) related to the ladanein ferric complex formation with $Fe(OH)^{2+}$ are in agreement with those reported in literature for siderophore, polyphenol or hydroxycarboxylate chelators (Table 4).[51] This mechanism is also known as the Eigen-Wilkins mechanism, with a fast formation of an outer-sphere complex (defined by K_{os}) followed by a metal desolvation rate-limiting step (k_{ex}).[55]

$$k_{Fe(OH)} = K_{os} \times k_{ex} \qquad (6)$$

The value of K_{os} can be evaluated using the water exchange rate constant k_{ex} determined by NMR methods[52] (1.2×10^5 s^{-1}) giving rise to the following expressions:[51]

$$K_{os} = 2.72 \times 10^3 / 1.2 \times 10^5 = 0.023 \text{ M}^{-1} \text{ for ladanein } \textbf{FOMe}.$$

These values are similar to the K_{os} determined for the binding of Fe(III) by various siderophores such as ferrioxamine B (0.03 M^{-1}),[56,57] azotobactin-δ (0.05 M^{-1})[58] or chrysobactin (0.0175 M^{-1}).[59]

5.5. Ternary Ferric Complexes with Ladanein and NTA.

The kinetic approaches of Fe(III) binding by polyphenols, siderophores or synthetic analogues have been up to now mainly studied under acidic conditions to limit the precipitation of the hydroxo-ferric species.[53,54] Such conditions are convenient but far from being physiological. Indeed, in the human body, Fe(III) is mainly exposed to neutral pH (pH = 7.4). To maintain its solubility under physiological conditions, iron is therefore constantly bound to proteins (hemoglobin, transferrin) and to low

molecular weight moderate chelators such as citrates. The non-protein bound iron is called "*labile iron pool*" or "*chelatable iron pool*", and could be the target of exogenous chelators such as polyphenols.[60] Polyaminocarboxylate-type ligands such as citrate and nitrilotriacetic acid (**NTA**) are currently used in model systems to ensure iron solubility.[61-64] For instance, they have been used to study Fe(III) uptake processes by siderophores[65], hydroxamic acids[66] or transferrin[63,64] at physiological pH. The aminotricarboxylate chelator **NTA** can be considered as a model of citric acid and is one of the most studied organic chelators. The speciation of its ferric complexes is well known.[67,68] However, kinetic approaches are relatively scarce. For instance, Bates *et al.*[61] have reported the exchange mechanism of Fe(III) from ferricitrate or ferrinitrilotriacetate to transferrin and have found that the rate limiting step is the disentanglement of the Fe-citrate polymer into reactive monomer. They have concluded that in the case of Fe-nitrilotriacetate, the reaction was rapid because of its particularly favourable configuration but also because of its inability to form polynuclear species. Faller and Nick[65] have studied the exchange of Fe(III) with smaller molecules such as ferrioxamine B and 3-hydroxy-1,2-dimethyl-4-pyridone which are both supplied in Fe(III) overload treatment. They have observed a different mechanism with the rapid formation of a stable ternary complex L.Fecitrate followed by a limiting dissociation of the citrate and have thus proposed a ligand size effect to explain these differences. To mimic physiological conditions of iron chelation by polyphenols, we have thus examined the influence of an exogenous ligand such as **NTA** on the Fe(III) coordination properties of ladanein. For the sake of comparison, salvigenin has been also used as a model.

As the conditions used in our study are different from those employed in the literature, we first examined the Fe(III) coordination properties of **NTA** at pH 7.4 in a CH_3OH/H_2O solvent (80/20 by weight). Figure 19 displays the UV-visible absorption spectrophotometric titration of **NTA** by Fe(III) as well as the electronic spectra of the corresponding ferric complexes. A monoferric **NTA** complex has been characterized and quantified (log K^*_{FeNTA} = 6.0(3) at pH 7.4).

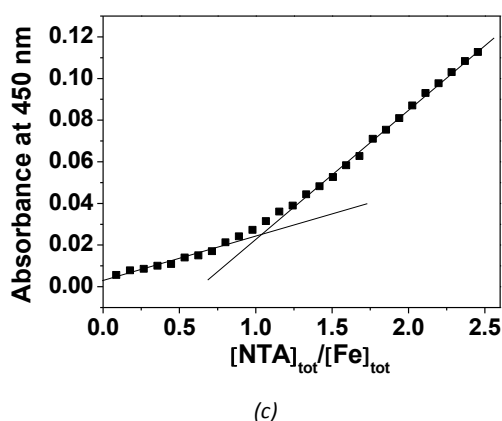*(a)*   *(b)*

(c)
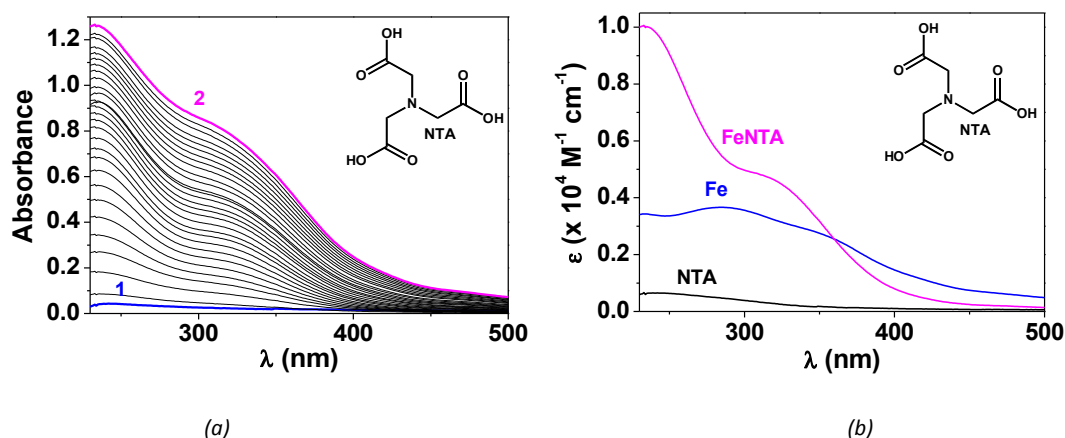
Figure 19. (*a*) Absorption spectrophotometric titration of **NTA** with Fe(III) at pH 7.4, (*b*) electronic spectra of the ferric **NTA** complexes and (c) variation of the absorbance at 450 nm suggesting the formation of the monoferric monochelate Fe**NTA** complex.. Solvent: CH_3OH/H_2O (80/20 by weight); I = 0.1 M (Hepes); pH 7.4; T = 25.0(2) °C; l = 1 cm; (1) $[\textbf{NTA}]_{tot}$ = 8.37 x 10^{-5} M; (2) $[Fe(III)]_{tot}/[\textbf{NTA}]_{tot}$ = 2.52.

Figure 20 shows the results of UV-visible absorption spectrophotometric titrations of the flavone ladanein **FOMe** by Fe**NTA** at pH 7.4. The stepwise addition of Fe**NTA** to a solution of ladanein induces significant alterations of the π-π* transitions centered on the flavone core. The absorption band lying at higher energies (Band II, A-C rings) experiences bathochromic and hyperchromic shifts while the intensity of band I (C-B rings) decreases without a noticeable shift of its position. Similarly to the binding of free iron by ladanein, a broad absorption (LMCT transitions) emerges in the visible region and clearly supports the involvement of the β-hydroxy-ketone unit as the binding site. As for catecholate-type ligands,[25] the LMCT absorption band of ternary **FOMe.**Fe**NTA** complexes lies at much higher energies (λ^{max} = 571 nm, ε^{571} = 2110 M^{-1} cm^{-1}) than the corresponding **FOMe.**Fe complexes (λ^{max} = 633 nm, ε^{633} = 1560 M^{-1} cm^{-1}). The presence of the **NTA** binder thus induces a hypsochromic shift of the charge-transfer band of about 52 nm with respect to the **FOMe.**Fe complex. When the water molecules of the first coordination shell of Fe(III) in **FOMe.**Fe are displaced by the trianionic **NTA** molecule, the Lewis acidity of the metallic centre decreased and its *d* orbitals are then destabilized by the negative charges of **NTA**. For the same reasons, the LMCT band shifts to lower wavelengths when the number of negatively charged phenolate or catecholate units increases around the ferric centre.

(a)

(b)

(c)

(d)

(e)
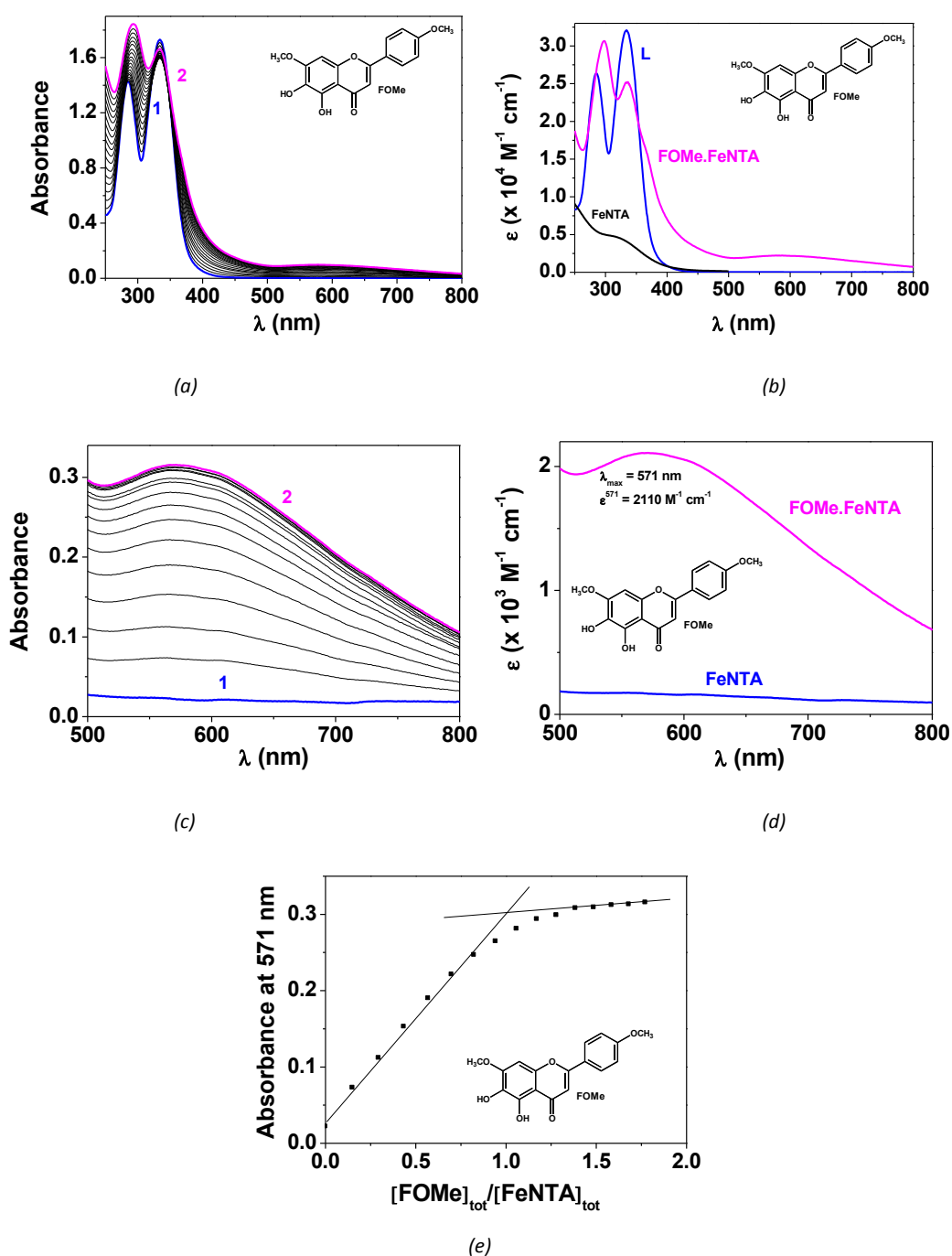
Figure 20. Absorption spectrophotometric titration of ladanein **FOMe** with Fe**NTA** at pH 7.4. (*a* and *c*) Absorption spectra *versus* [Fe**NTA**]$_{tot}$, (*b* and *d*) absorption electronic spectra of ladanein and its ferric ternary complexes with **NTA** and (*e*) variation of the absorbance at 571 nm (LMCT) as a function of the [**FOMe**]$_{tot}$/[Fe**NTA**]$_{tot}$ ratio. Solvent: CH$_3$OH/H$_2$O (80/20 by weight); pH = 7.4 (Hepes buffer); I = 0.1 M (Hepes); T = 25.0(2) °C; l = 1 cm; (a) (1) [**FOMe**]$_{tot}$ = 5.41 × 10^{-5} M; (2) [Fe**NTA**]$_{tot}$/[**FOMe**]$_{tot}$ = 2.0; (b) (1) [Fe**NTA**]$_{tot}$ = 2.30 × 10^{-4} M; (2) [**FOMe**]$_{tot}$/[Fe**NTA**]$_{tot}$ = 1.51.

A ternary **FOMe**.Fe**NTA** complex was characterized and quantified (log $\beta^*_{FOMe:FeNTA}$ = 10.7(4) at pH 7.4). It is noteworthy that NTA completes the Fe(III) sphere and prevents hydrolysis of the metal

cation, the degradation by auto-oxidation does not take place (see below) and the titration can be performed continuously. We also carried out an absorption spectrophotometric titration of salvigenin by Fe**NTA** under comparable experimental conditions (Figure 21). Similarly to ladanein, a single ternary complex salvigenin.Fe**NTA** was identified (λ^{max} = 571 nm, ε^{571} = 2110 M^{-1} cm^{-1}) and quantified (log $\beta^*_{\text{FOMe.FeNTA}}$ = 10.7(4) at pH 7.4). These conditional binding constants obtained on ladanein and salvigenin are in excellent agreement with those determined for catechin (noted Cat) or tiron (3,5-disulfonate catechol, noted Tir) at pH 7.4 in water (log $\beta^*_{\text{Tir:FeNTA}}$ = 12,4(2) and log $\beta^*_{\text{Cat:FeNTA}}$ = 10.86(3)).[25,29]

(a)

(b)

(c)
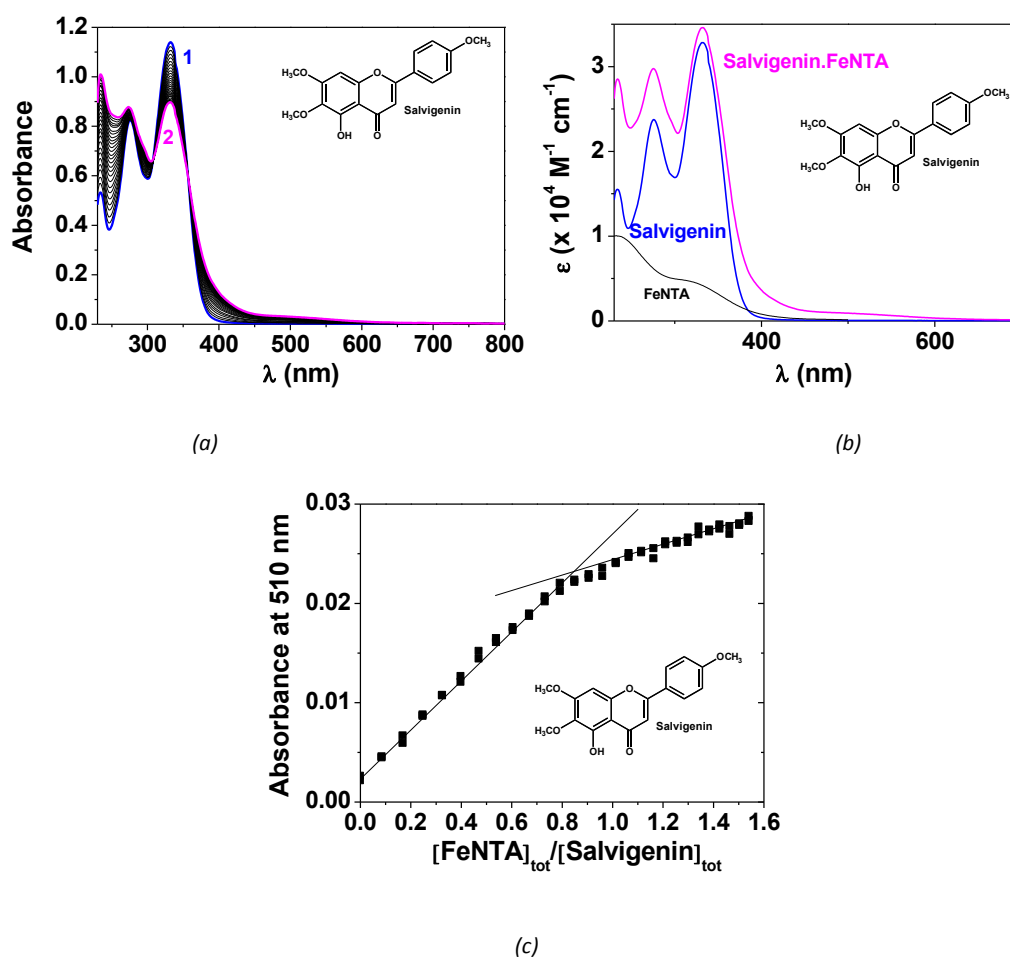
Figure 21. Absorption spectrophotometric titration of salvigenin with FeNTA at pH 7.4. (*a*) Absorption spectra *versus* [FeNTA]$_{tot}$, (*b*) absorption electronic spectra of salvigenin and its ferric ternary complexes with NTA and (*c*) variation of the absorbance at 510 nm (LMCT) as a function of the [Fe**NTA**]$_{tot}$/[salvigenin]$_{tot}$ ratio. Solvent: CH$_3$OH/H$_2$O (80/20 by weight); pH = 7.4 (Hepes buffer); I = 0.1 M (Hepes); T = 25.0(2) °C; l = 1 cm; (a) (1) [**FOMe**]$_{tot}$ = 3.48 × 10^{-5} M; (2) [Fe**NTA**]$_{tot}$/[salvigenin]$_{tot}$ = 1.54.

To further confirm the stoichiometry of the ternary ferric complexes with ladanein and its synthetic analogues, electrospray mass spectra were recorded (Figure 22) in negative mode. No matter the flavone considered, a ternary ferric complex was constantly characterized (Table 6) thus confirming the data obtained by absorption spectrophotometry. Interestingly, for **FH**, **FOCF₃** and **FF**, additional species involving an extra Fe**NTA** subunit were observed and most likely correspond to adducts induced by the ESI-MS conditions.

(a)   *(b)*
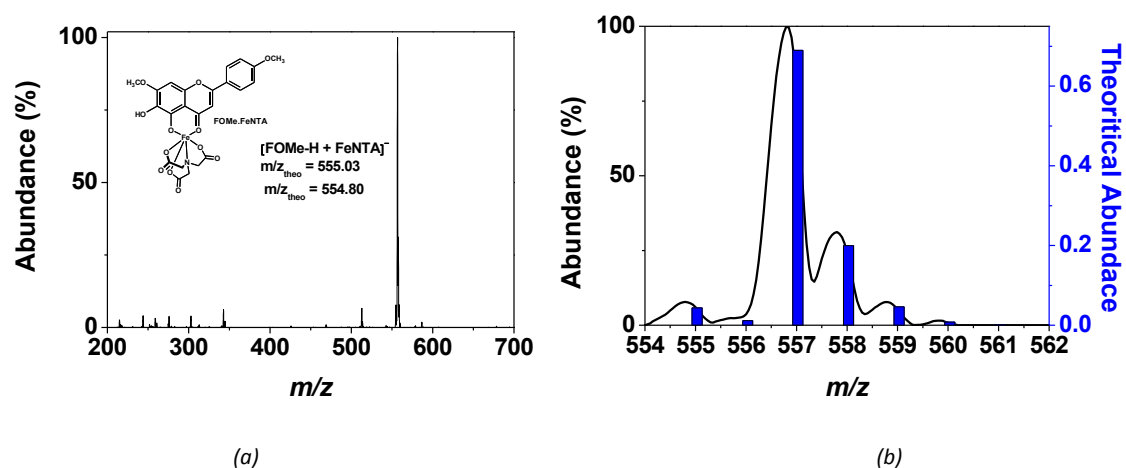
Figure 22. Electrospray mass spectra of ladanein ferric complex in the presence of **NTA**. Solvent: CH_3OH/H_2O, capillary voltage = 4000 V. [**FOMe.FeNTA**]$_{tot}$ = 10^{-4} M; negative mode; Fragmentor = 150 V.

Table 6. Intensity maxima of the ESI-MS monoisotopic ions of the metallic ternary complexes formed with ladanein **FOMe** and its analogues.

Species	m/z experimental	m/z theoretical
[FeNTA-H]$^-$	nd	240.95
[FOMe-H+FeNTA]$^-$	554.80	555.03
[FH-H+FeNTA]$^-$	524.75	525.02
[FH-H+2FeNTA]$^-$	768.6	768.97
[FOCF$_3$-H+FeNTA]$^-$	608.75	609.00
[FOCF$_3$-H+2FeNTA]$^-$	852.50	852.95
[FFCF$_3$-H+FeNTA]$^-$	610.75	611.00
[FCF$_3$-H+FeNTA]$^-$	592.80	593.00
[FF-H+FeNTA]$^-$	542.75	543.01
[FF-H+2FeNTA]$^-$	786.60	786.96
nd = not determined		

A survey of the literature data on ternary ferric complexes containing **NTA** revealed that the X-ray structure data available are rather limited. To the best of our knowledge, only the solid state structures of di-*tBu*-catechol,[69] phenanthroline,[70] oxalate[71] or 3-carboxylato-1-cyclopropyl-6-fluoro-7-

tetrahydropyrazine-4-quinolone[72] Fe**NTA** complexes have been described. The structural arrangement of **FOMe.**Fe**NTA** complexes can then be proposed on the basis of the published X-ray crystal data obtained for a ternary ferric complex containing **NTA** and di-*tBu*-catechol[69], carboxylato-quinolone[72] and oxalate.[71] These complexes are characterized by a distorted octahedral geometry around the Fe(III) centre, where the NTA plays the role of a tetradentate binding unit, the three carboxylates and the tertiary amine being involved in the chelation process. The catecholate-type unit (di-*tBu*-catechol) or the carboxylato-quinolone act as bidentate coordination sites. We can thus suggest a similar structure in the case of the **L.**Fe**NTA** complex (Figure 23).

(a)   *(b)*   *(c)*   *(d)*

(e)
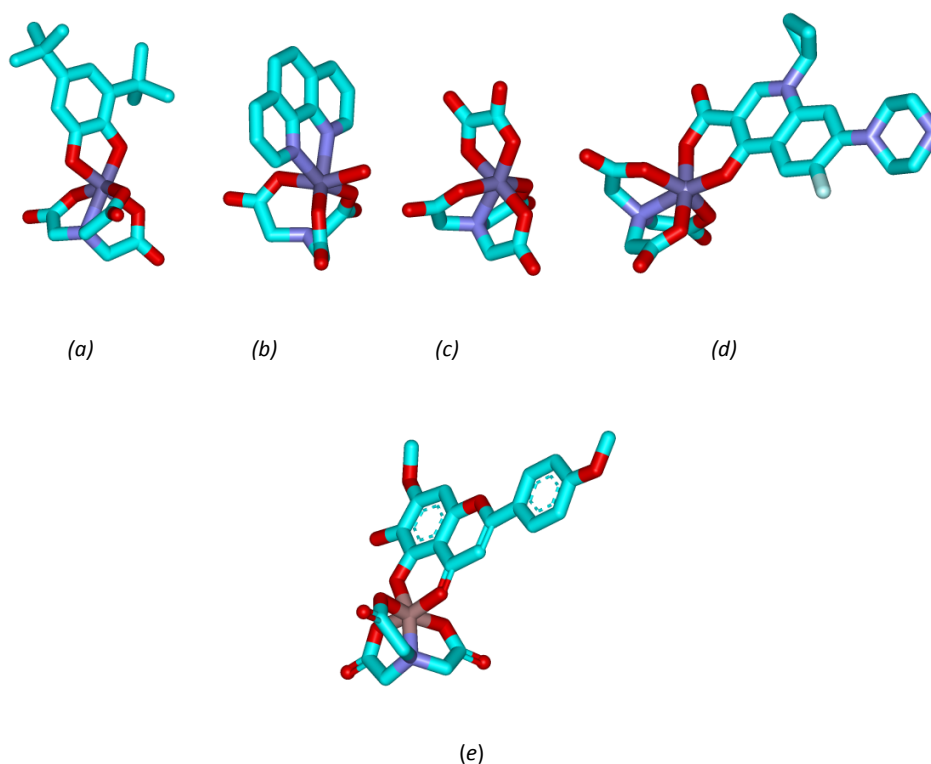
Figure 23. X-ray structures of ternary complexes containing the Fe**NTA** subunit (*a*) di-tBu-catechol, (*b*) phenanthroline, (*c*) oxalate and (*d*) 3-carboxylato-1-cyclopropyl-6-fluoro-7-tetrahydropyrazine-4-quinolone. (*e*) Modeled structure of ladanein NTA gallium(III) complex (hyperchem 7.5, semi-empirical PM3 method).

The uptake of Fe(III) by ladanein **FOMe** was then investigated under physiological conditions. In order to avoid precipitation of iron hydroxo-species at pH 7.40, we used **NTA** as iron chelator. The kinetic study was carried out in excess of ladanein (so as to ensure pseudo-first order conditions) and in the presence of one equivalent of **NTA** with respect to Fe(III). A single exponential signal was observed at 570 nm (Figure 24a) which corresponds to the maximum of absorption of the LMCT band. The initial absorbance could be extrapolated over the dead time of the fast mixing device (3 ms), and the value thus obtained was easily attributed to the absorbance of the reagents (**FOMe** +

Fe**NTA**). Therefore, no fast step is lost during the mixing of the reagents. Importantly, no oxidation of ladanein mediated by complexation to the Fe(III) metal ion (Figure 24b) was observed in contrast to the observations made for ladanein with Fe(III) in the absence of **NTA**. This suggests that the binding of **NTA** markedly alters the redox properties of the metal complex as suggested by the hypsochromic shift of the LMCT absorption. The presence of an auxiliary ligand seems to protect ladanein from spontaneous Fe-promoted oxidation and might constitute a smart way to improve its bioavailability and activity *in vivo*. Furthermore, the complex **FOMe**.Fe**NTA** displayed a similar antiviral activity as the free flavone. We therefore employed this strategy to increase the stability of ladanein by using a redox-inert and biocompatible metal cation such as Mg(II) and carboxylate-based exogenous ligands. This will be presented and discussed in the following chapter of my PhD manuscript.

(a)

(b)

(c)
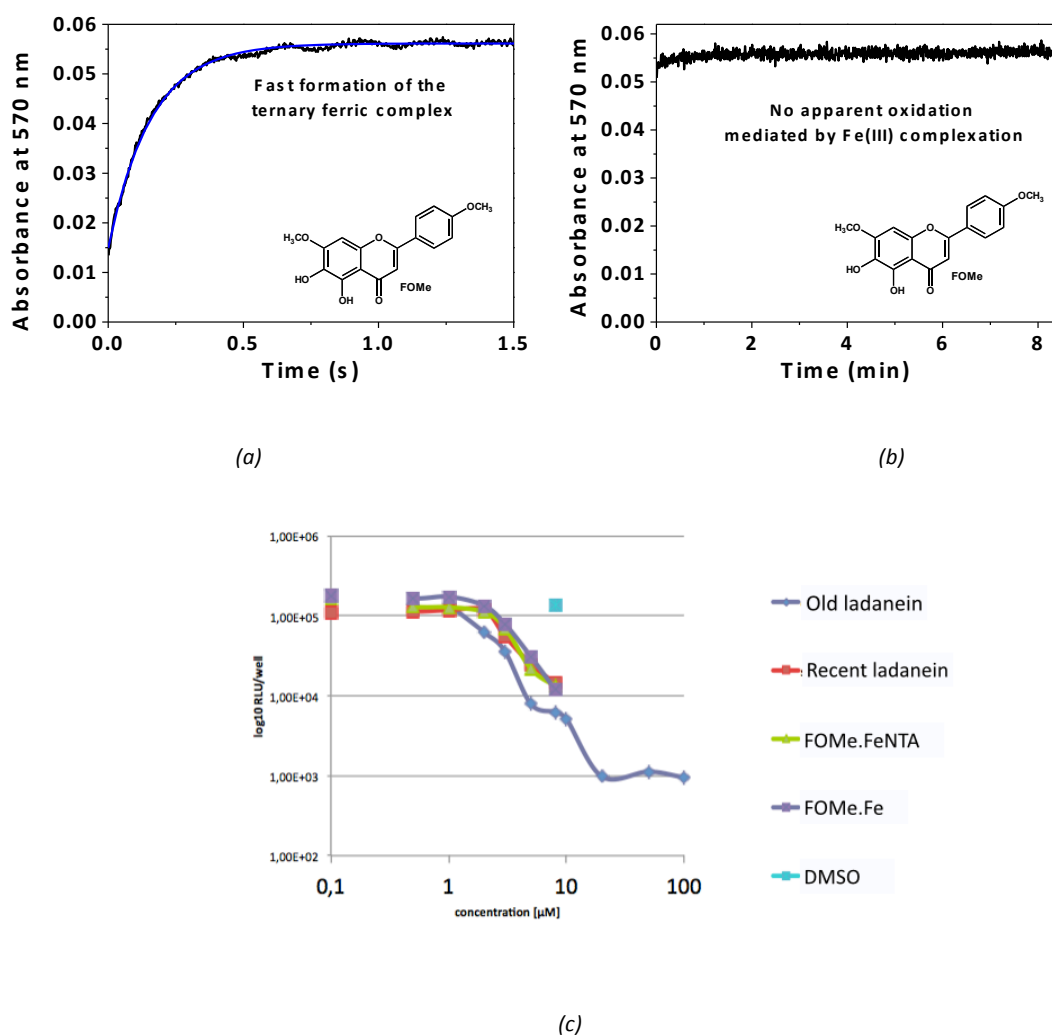
Figure 24. (*a*) Variation of the absorbance at 570 nm (LMCT) for the formation of the ternary ferric complex with ladanein and NTA. (*b*) Variation of the absorbance at 570 nm over a longer time showing the absence of oxidation of ladanein mediated by iron(III) complexation. Solvent: CH_3OH/H_2O (80/20 by weight); $I = 0.1$ M (NEt$_4$ClO$_4$); $T = 25.0 \pm 2$ °C; pH = 7.4 (0.1 M Hepes); [Fe**NTA**]$_{tot}$ = 2.30 x 10^{-5} M ; [**FOMe**]$_{tot}$ = 5.82 x 10^{-4} M. (c) Antiviral activity of the **FOMe**.Fe**NTA** complex

 The rate limiting step was observed in the second time range, and its amplitude does not vary significantly with the concentration of ladanein. The absorbance value reached at the end of this stage was found to be in excellent agreement with the value expected for the mixed ternary complex **FOMe**.Fe**NTA**. Therefore, we suggest that this kinetic step corresponds to the formation of this ternary complex according to the following equation:

$$\text{Fe}\textbf{NTA} + \textbf{FOMe} \underset{k_{-1}}{\overset{k_1}{\rightleftharpoons}} \textbf{FOMe}.\text{Fe}\textbf{NTA} \tag{7}$$

The pseudo-first-order rate constants k_{obs} vary linearly with the analytical concentration of ladanein **FOMe**, and a significant ordinate at the origin ($k_{-1} = 0.9(3)$ s^{-1}) could be determined (Figure 25). The linear least squares fits of these kinetic data (k_{obs} versus [**FOMe**]$_{tot}$) led to the determination of the bimolecular formation rate constant k_1 ($8.4(4) \times 10^3$ M^{-1} s^{-1}). In the absence of any other faster or slower steps, the ratio k_1/k_{-1} ($K^*_{\textbf{FOMe}.\text{Fe}\textbf{NTA}} = 1.0(3) \times 10^4$ M^{-1}) therefore accounts for the successive stability of the ferric ternary complex with ladanein **FOMe** and Fe**NTA** at pH 7.4. Using the successive stability constant previously determined for Fe**NTA** (log $K^*_{\text{Fe}\textbf{NTA}} = 6.0(3)$ at pH 7.4), the global stability constant of the **FOMe**.Fe**NTA** ternary complex can be recalculated to (log $\beta^*_{\textbf{FOMe}.\text{Fe}\textbf{NTA}} = 10$ at pH 7.4) which is in good agreement with the one evaluated from absorption spectrophotometry (log $\beta^*_{\textbf{FOMe}.\text{Fe}\textbf{NTA}} = 10.7(4)$ at pH 7.4).
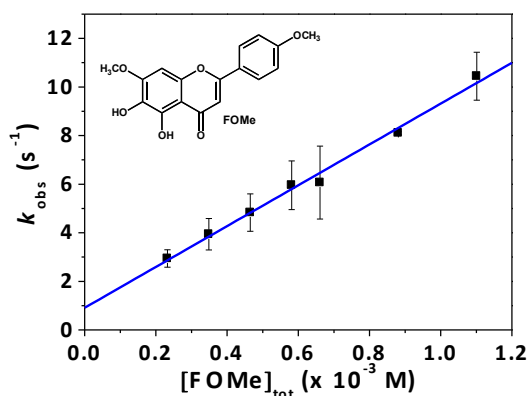
Figure 25. Formation kinetics of the ladanein ferric ternary complex with **NTA** - Variation of the pseudo-first-order rate constant as a function of **FOMe** concentrations. [Fe**NTA**]$_{tot}$ = 2.30×10^{-5} M; Solvent: CH_3OH/H_2O (80/20 by weight); I = 0.1 M (NEt$_4$ClO$_4$); T = 25.0(2) °C; pH = 7.4 (0.1 M Hepes). Uncertainties are given as 3σ.

We have up to now assumed a single Fe**NTA** species which corresponds under our experimental conditions (pH 7.4) to a mixture of two major hydroxylated species of Fe**NTA**: the *mono*- Fe**NTA**(OH) and *bis*-hydroxo Fe**NTA**(OH)$_2$ species. It has been reported that only the *mono*-hydroxo species is reactive.[49] Therefore, the k_1 value that has been determined corresponds to the reactivity of

Fe**NTA**(OH). Table 5 summarizes the reactivity of the three ferric species considered in this work (Fe^{3+}, $Fe(OH)^{2+}$ and FeNTA(OH)) with ladanein **FOMe,** catechol and various bidentate ligands. The difference observed for ladanein **FOMe** can be explained by the different experimental conditions (CH_3OH/H_2O *versus* H_2O). The reactivity of the FeNTA(OH)$^-$ species appears to be independent of the nature of the coordinating ligand. This suggests that this ferric species with **NTA** also follows a dissociative interchange mechanism of Eigen-Wilkins type as does $Fe(OH)^{2+}$. Moreover, the reactivity of FeNTA(OH) is four to ten times higher than that of $Fe(OH)^{2+}$, suggesting a strong labilizing effect of the water molecules by the trianionic and tetradentate NTA ligand in the first coordination shell of Fe(III). Indeed, an increase on the amount of negative charges around the iron centre will strongly destabilize the remaining bounded water molecules.

5.6. Conclusion

In conclusion, we have described the Fe(III) binding properties of ladanein and its analogues and discussed these data with respect to other relevant flavonoids. It was of importance to study these properties of the flavones because Fe(III) is believed to play a key role on the antiviral activity of our family of compounds. Indeed, when an exogenous iron chelator such as DFO is added, the antiviral activity of ladanein is abolished. It is then suggested that the flavones may be bioactivated thanks to iron-directed *C,C*- and/or *C,O*-couplings. Furthermore, scarce data can be found in the literature about the binding properties of 5-hydroxylated flavones.

Using absorption spectroscopic methods it was found that ladanein does form complexes with Fe(III) at acidic pH values (*i.e.* conditions used in order to avoid the formation of insoluble ferric species at higher pH values). Of the two possible binding sites, it was shown that ladanein binds Fe(III) through the 5-hydroxy-4-carbonyl group (*i.e.* β-hydroxyketone group) and not the 5,6-catechol group, which likely does not behave as one due to the strong hydrogen bonding between 5-OH and the adjacent carbonyl. The fact that salvigenin also forms complexes with Fe(III) and that the final precursor does not gives further proof of the binding site. The stoichiometry of the complexes was confirmed to be 1:1 (*i.e.* formation of a monoferric monochelate) by the method of continuous variations (Job's plot). With the exception of **FF**, all flavones show similar Fe(III) binding affinities. In addition the pFe value for ladanein was calculated and it is was found to be much higher than those calculated for more simple compounds, much likely due to the different substituents borne by the flavone core structure.

Kinetic studies of the ladanein ferric complexes were performed using stopped flow spectrophotometry (*i.e.* due to the fast formation) and they show first order kinetics with respect to the ligand. When a longer time span was used, an oxidation of ladanein caused by Fe(III)

complexation was observed. It was also shown that at acidic pH the formation of **L**HFe occurs *via* two parallel reactions involving either Fe^{3+} and $Fe(OH)^{2+}$.

Finally; it was decided to study the binding capabilities of ladanein under physiological conditions. To avoid the formation of insoluble ferric species, **NTA** was used as an exogenous ligand. It was found that at pH 7.4 a ternary **FOMe**.Fe**NTA** complex is formed. Furthermore, the stoichiometry of the complexes was studied by ESI-MS, allowing the identification of the ternary complexes for each of the analogues. Lastly but not the least, it was very interesting to find that the addition of **NTA** to the flavone-Fe(III) complex prevented the oxidation of the flavone, likely due to alteration of the redox behavior of Fe(III).

EXPERIMENTAL SECTION

Solvents and Materials

For solubility reasons (ladanein **FOMe** and its synthetic analogues are sparingly soluble in water), the physico-chemical properties of ladanein **FOMe**, its synthetic analogues and their corresponding ferric complexes were examined in a methanol/water (80/20 by weight) mixture. Distilled water was further purified by passing through a mixed bed of ion-exchanger (Bioblock Scientific R3-83002, M3-83006) and activated carbon (Bioblock Scientific ORC-83005). Both, distilled water and spectroscopic grade methanol (Merck, Uvasol®, p.a.) were de-oxygenated using CO_2- and O_2-free argon prior to use (Sigma Oxiclear cartridge). All the stock solutions were prepared by weighing solid products using an AG 245 Mettler Toledo analytical balance (precision 0.01 mg). The complete dissolution of the ligands was obtained with the help of ultrasonic bath. Each time, the concentration of ladanein was checked by measuring the absorbance value at 334 nm (ε^{334} = 3.2 × 10^4 M^{-1} cm^{-1}).The ionic strength was adjusted to 0.1 M with tetraethylammonium perchlorate ($NEt_4ClO_4.H_2O$, Fluka, puriss.) and all measurements were carried out at (25.0 ± 2) ° C. *CAUTION! Perchlorate salts combined with organic ligands are potentially explosive and should be handled in small quantities and with the adequate precautions.*[73]

Fe(III) perchlorate stock solutions (Fluka) were freshly prepared in water at acidic pH (pH < 1.5) immediately before use and their concentrations were ascertained by UV-visible absorption spectrophotometry (ε^{240}= 4.16 x 10^3 M^{-1} cm^{-1} et ε^{260}= 2.88 x 10^3 M^{-1} cm^{-1}).[74] The glassware used was rinsed after each experiment with a hydrochloric acid solution to remove all traces of iron.

The FeNTA solutions were freshly prepared by adding an aqueous solution of iron(III) (one equivalent) whose concentration (2.41 × 10^{-2} M) was previously determined to one equivalent of solid nitrilotriacetic acid (NTA, $C_6H_9NO_6$). Few drops of strong perchloric acid (70%) were then added for obtain a better solubility. The pH of the mixture was then raised to 7.4 with the help of a 0.1 M HEPES buffer (*i.e.* the final concentration of Fe(NTA) is 2.41 × 10^{-3} M). A slight excess of NTA with respect to iron(III) is always used to ensure complete complexation of iron(III) and avoid free ferric species in solution at pH = 7.4.

Characterization and Quantification of the Fe(III) Complexes with Ladanein and its Analogues

Determination of FOMe/Fe(III) Complex Stoichiometry – Job's Plots

For the characterization of the **BJ486K**.Fe(III) complexes (method of continuous variations, **BJ486K** corresponds to the ladanein prepared using the former synthesis), stock solutions of **BJ486K** and iron(III) were freshly prepared under acidic conditions ($[HClO_4]_{tot} = 10^{-2}$ M; pH ~ 2.0) and were diluted to obtain the same concentration for both solutions at 4.94×10^{-5} M. The ionic strength was kept constant at 0.1 M with tetraethylammonium perchlorate (NEt_4ClO_4, Fluka, puriss.). UV-Vis absorption spectra of mixtures with different $[\mathbf{BJ486K}]_{tot}/([\mathbf{BJ486K}]_{tot} +[Fe(III)]_{tot})$ ratios were measured in a 1 cm Hellma optical cell with a Cary 300 (Varian) spectrophotometer. The Job's plot was processed with Origin program.

Spectrophotometric Titrations of Ladanein and its Synthetic Analogues with Fe(III) at pH 2.0

Stock solution of the flavones was prepared in CH_3OH/H_2O (80/20 by weight) and then freshly diluted with $HClO_4$ (10^{-2} M) to obtain a ligand concentration of ~ 5.92×10^{-5} M for **FOMe** and $4\text{-}7 \times 10^{-5}$ for the other flavones. The ionic strength was kept constant at 0.1 M with tetraethylammonium perchlorate (NEt_4ClO_4, Fluka, puriss.). The spectrophotometric titrations of the flavones by Fe(III) were thus carried out on solutions at pH ~ 2 (10^{-2} M $HClO_4$). Microvolumes of a concentrated solution of Fe(III) freshly prepared just before use were added to an aliquot of 0.5 mL or 2.5 ml of the ligand solution in a 1 cm path length optical Hellma cell (*e.g.* the $[Fe(III)]_{tot}/[\mathbf{flavone}]_{tot}$ ratio varied from 0 to ~1.2-1.6). Special care was taken to ensure that complete equilibration was attained. The corresponding UV-Vis spectra were recorded from 230 nm to 800 nm on a Cary 50 (Varian) or 300 (Varian) spectrophotometer maintained at (25.0 ± 2) °C by the flow of a Lauda E200 thermostat.

Absorption Spectrophotometric Titration of the Ferric Complexes of Ladanein *versus* pH

Spectrophotometric titration of the Fe(III) complexes with ladanein as a function of pH was performed. Due to Fe(III)-catalyzed oxidation of ladanein under neutral conditions, a specific protocol was adopted. A stock solution of ladanein was freshly prepared by quantitative dissolution of a solid sample in CH_3OH/H_2O (80/20 by weight), which was further diluted to get a ligand concentration of 4.55×10^{-5} M. The ionic strength was adjusted to 0.1 M with NEt_4ClO_4 (Fluka, puriss). For each pH measurement, an aliquot of 2 mL of the solution was introduced into a 1 cm Hellma quartz optical cell and 37.0 μL of the Fe(III) stock solution (2.24×10^{-3} M) was added. After each addition of base (NEt_4OH) or acid ($HClO_4$), the solution was mixed and its corresponding pH value was measured using

a combined glass electrode (Metrohm 6.0234.500, Long Life) and an automatic titrator system 716 DMS (Metrohm). Special care was taken to ensure that complexation equilibration was attained. The absorption spectra *vs.* pH (1.72 < pH< 6.79) were thus recorded using a Cary 300 (Varian) spectrophotometer maintained at 25.0(2) °C by the flow of a Lauda E200 thermostat. The free hydrogen ion concentration was measured following the protocol described in the previous chapter dealing with the acido-basic properties of the flavones.

Fe(III) Coordination Properties of Ladanein in the Presence of an Exogenous NTA Ligand at pH 7.4

With respect to the biological tests of the antiviral activity of ladanein performed at pH 7.5-8, it was of importance to find appropriate conditions to study iron(III) complexation by ladanein under comparable conditions. Exogenous chelators such as citrates or nitrilotriacetic acid (**NTA**) have been usually used to ensure iron solubility at pH 7.4.[75] We therefore used **NTA** in combination with ladanein to characterize and quantify the corresponding ferric complexes. A stock solution of ladanein (5.41×10^{-5} M) was freshly prepared in HEPES aqueous buffer at pH 7.4 (0.1 M in CH_3OH/H_2O, 80/20 by weight). The ionic strength was adjusted to 0.1 M with tetraethylammonium perchlorate (NEt_4ClO_4, Fluka, puriss.). The absorption spectrophotometric titration of ladanein by Fe**NTA** was carried out in a Hellma quartz optical cell (*l* = 1 cm). Microvolumes of a concentrated solution of Fe**NTA** stock solution (2.41×10^{-3} M) were added to an aliquot of 2.0 mL of the ligand solution in a 1 cm path length optical Hellma cell (the [Fe**NTA**]$_{tot}$/[ladanein]$_{tot}$ ratio varied from 0 to 2.0). After each addition the solution was mixed and special care was taken to ensure that complete equilibration was reached. The corresponding UV-Visible spectra were recorded on a Cary 300 (Varian) spectrophotometer.

Electrospray Mass Spectrometric Measurements - Characterization of the Ternary Complexes

Electrospray mass spectra of the flavones ferric complexes in the absence and in the presence of NTA were carried out with an ion-trap instrument (Bruker Esquire 3000plus, Bruker Daltonic, Bremen, Germany) equipped with an Agilent Technologies 6120 quadrupole equipped with an electrospray (ESI) interface. The sample solutions were continuously introduced into the spectrometer source with a syringe pump (Kd Scientific) with a flow rate of 800 μL.h^{-1}. For electrospray ionization, the drying gas was heated at 250 °C and its flow was set at 6 L.min^{-1}. The capillary exit voltage was fixed at 5 kV and the skimmer voltage was varied from 50 to 200 V in order to optimize the signal responses. Scanning was performed from m/z = 100 to 1500. Different attempts to characterize the ferric complexes in the absence of NTA were unsuccessful either in the positive or negative mode. This can be due to the predominant presence of solvated monoferric monochelates which easily

fragmentate. By contrast, in the presence of NTA ($[Flavone]_{tot} = 10^{-5}$ M, $[Fe(III)]_{tot} = [NTA]_{tot} = 10^{-5}$ M), the complexes were observed in the negative mode.

Analysis and Processing of the Spectroscopic Data

The spectrophotometric data were analyzed with Specfit[76] programs which adjust the absorptivities and the stability constants of the species formed at equilibrium. Specfit uses factor analysis to reduce the absorbance matrix and to extract the eigenvalues prior to the multiwavelength fit of the reduced data set according to the Marquardt algorithm.[77,78]

Kinetic Measurements

Formation of the ferric complexes with ladanein was followed at 25.0(2) °C on a SX-18MV stopped-flow spectrophotometer from Applied Photophysics. The formation kinetics of the ladanein ferric complexes was studied in the $[H^+]$ range 5.88×10^{-3} M $- 9.4 \times 10^{-2}$ M in the presence of an excess of Fe(III) (5.54×10^{-3} M $< [Fe(III)] < 5.54 \times 10^{-4}$ M). The ladanein concentration was ~ 3-5 x 10^{-5} M. The reaction was monitored at 650 nm. The λ corresponds to the absorption maximum of the ladanein$\rightarrow$Fe(III) CT band and thereby to the maximum of absorbance difference between the reactants (ladanein and Fe(III)) and the products (ferric complexes of ladanein). Fe^{3+} and $Fe(OH)^{2+}$ are the predominant free ferric species (Figure 26) under these experimental conditions ($K_{Fe(OH)2+} = 10^{-1.39}$).[79] At least ten times more concentrated solutions of Fe^{3+} with respect to ladanein were used to impose pseudo-first order conditions.
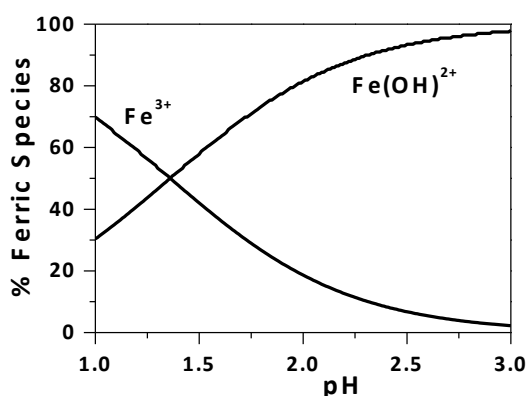
Figure 26. Speciation diagrams of free iron(III) (2×10^{-3} M) in methanol/water solvent (80/20 w/w; I = 0.1 M) as a function of pH. Fe^{3+} + H2O $\rightarrow$ $Fe(OH)^{2+}$ + H^+ with log $K_{Fe(OH)2+}$ = -1.39 (I = 0.1 M ; T = 25°C).

The uptake of Fe(III) by ladanein **FOMe** (*i.e.* **BJ486K**) was then investigated under physiological conditions (pH 7.4, HEPES buffer at 0.1 M). In order to avoid precipitation of iron hydroxo-species at

p[H] 7.40, we used NTA as iron(III) chelator. The uptake kinetics of Fe(III) by ladanein in the presence of NTA was followed at 570 nm. Kinetic experiments were performed in excess of ladanein and with a ratio [Fe(III)]/[NTA] ~ 1. The Fe**NTA** solution (2.3 x 10^{-5} M) was rapidly mixed with increasing concentrated solutions of ladanein (2.33 x 10^{-4} < [**BJ486K**]$_0$ < 1.10 x 10^{-3} M). At least ten times more concentrated solutions of ladanein with respect to Fe(**NTA**) were used to impose pseudo-first order conditions.

Analysis and Processing of the Kinetic Data

The data sets, averaged out of at least three replicates, were analyzed with the commercial software Biokine.[80] This program fits up to three exponential functions to the experimental curves with the Simplex algorithm[81] after initialization with a Padé-Laplace method.[82]

References

(1)   Cotton, F.A. and Wilkinson, G. *Advanced Inorganic Chemistry*, 5th ed., John Wiley & Sons, New York, **1988**.

(2)   Weinberg, E.D. *Quart. Rev. Biol.* **1989**, *64*, 261.

(3)   Neilands, J.B. *Struct. & Bond.* **1972**, *11*, 145.

(4)   Raymond., K.N.; Müller, G. and Matzanke, B.F. *Top. Curr. Chem.* **1984**, *123*, 49.

(5)   Wei Wang, W.; Knovich, M.A.; Coffman, L. G.; Torti, F.M.; Torti, S.V. *Biochim. Biophys. Acta* **2010**, 1800, 760.

(6)   Baynes, R.D. and Bothwell, T.H. *Ann. Rev. Nutr.* **1990**, *10*, 133.

(7)   Prousek, J. *Pure Appl. Chem.* **2007**, *79*, 2325.

(8)   Bodini, M.E.; Copia, G.; Tapia, R.; Leighton, F. and Herrera, L. *Polyhedron* **1999**, *18*, 2233.

(9)   Fernandez, M.; Lurdes, T.M.; Florencio, M.H. and Jennings; K.R. *J. Inorg. Biochem.* **2002**, *92*, 105.

(10)   Leopoldini, M.; Pitarch, I.P.; Russo, N. and Toscano, M. *J. Phys. Chem. A* **2004**, *108*, 92.

(11)   Leopoldini, M.; Russo, N.; Chiodo, S. and Toscano, M. *J. Agric. Food Chem.* **2006**, *54*, 6343.

(12)   Leopoldini, M.; Russo, N. and Toscano, M. *Food Chem.* **2011**, *125*, 288.

(13)   Mira, L.; Fernandez, M.T.; Santos, M.; Rocha, R.; Florencio, H. and Jennings, K.R. *Free Rad. Res.* **2002**, *36*, 1199.

(14)   Yoshino, M. and Murakami, K. *Anal. Biochem.* **1998**, *257*, 40.

(15)   Perez, C.A. Wei, Y. and Guo, M. *J. Inorg. Biochem.* **2009**, *103*, 326.

(16)   Xing, J.; Chen, X. and Zhong, D. *J. Pharmacol. Biomed. Anal.*, **2005**, *39*, 593.

(17)   Guo, M.; Perez, C.A.; Wei, Y.; Rapoza, E.; Su, G.; Bou-Abdallah, F. and Chasteen, N.D. *Dalton Trans.* **2007**, 4951.

(18)   Deng, W.; Fang, X. and Wu, J. *Radiat. Phys. Chem.* **1997**, *50*, 271.

(19)   Mladěnka, P.; Macáková, K.; Filipský, T.; Zatloukalová, L.; Jahodář, L.; Bovicelli, P.; Proietti Silvestri, I; Hrdina, R. and Saso, L. *J. Inorg. Biochem.* **2011**, *105*, 693.

(20)   (a) Zhao, Y.; Li, H.; Gao, Z. and Xu, H. *Eur. J. Pharmacol.* **2005**, *509*, 195. (b) Zhang, Y.; Li, H. and Gao, Z. *Eur. J. Pharmacol.* **2006**, *535*, 263.

(21)   Hamada, H.; Hiramatsu, M.; Edamatsu, R. and Mori, A. *Arch. Biochem. Biophys.* **1993**, *306*, 261.

(22)   Li, D.; Zhu, M.; Xu, C. and Ji, B. *Eur. J. Med. Chem.* **2011**, *46*, 588.

(23) Dimitric Markovic, J.M.; Markovic, Z.S.; Brdaric, T.P.; Pavelkic, V.M. and Jadranin, M.B. *Food Chem.* **2011**, *129*, 1567.

(24) (a) Cox, D.D.; Benkovic, S.J.; Bloom, L.M.; Bradley, F.C.; Nelson, M.J.; Que Jr., L. and Wallick, D.E. *J. Am. Chem. Soc.* **1988**, *110*, 2026. (b) Gaber, B.P.; Miskowski, V. and Spiro, T.G. J. *Am. Chem. Soc.* **1974**, *96*, 6868.

(25) Elhabiri, M.; Carrër, C.; Marmolle, F. and Traboulsi, H. *Inorg. Chim. Acta* **2007**, *360*, 353.

(26) Solomon, E.I.; Brunold, T.C.; Davis, M.I.; Kemsley, J.N.; Lee, S.K.; Lehnert, N.; Neese, F.; Skulan, A.J.; Yang, Y.S. and Zhou, J. *Chem. Rev.,* **2000**, *100***, 235.

(27) Palaniandavar, M.; Velusamy, M. and Mayilmurugan, R. *J. Chem. Sci.* **2006**, *118*, 601.

(28) Karpishin, T.B.; Gebhard, M.S.; Solomon, E.I. and Raymond, K.N. *J. Am. Chem. Soc.,* **1991**, *113*, 2977.

(29) Carrër, C. "Chélation de métaux de transition par des polyphénols du régime alimentaire", Thèse de Doctorat de l'Université Louis Pasteur de Strasbourg, January 28th, 2005

(30) Loginova, L.F.; Medyntsev, V.V. and Khomutov, B.I. *Zh. Obshch. Khim.* **1972**, 42, 739.

(31) Harris, W.R., Carrano, C.J. and Raymond, K.N. *J. Am. Chem. Soc.* **1979**, *101*, 2213.

(32) Borsari, M.; Ferrari, E.; Grandi, R. and Saladini, M. *Inorg. Chim. Acta* **2002**, *328*, 61.

(33) Loomis, L.D. and Raymond, K.N. *Inorg. Chem*. **1991**, *30*, 906.

(34) (a) Harris, W.R.; Raymond, K.N. and Weitl, F.L. *J. Am. Chem. Soc.* **1981**, *103*, 2667. (b) Evers, A.; Hancock, R.D.; Martell, A.E. and Motekaitis, R.J. *Inorg. Chem.* **1989**, *28*, 2189.

(35) Mentasti, E.; Pelizetti, E. and Saini, G. *J. Inorg. Nucl. Chem.* **1976**, *38*, 785.

(36) Powell, H.K.J. and Taylor, M.C. *Aust. J. Chem.* **1982**, *35*, 739.

(37) Jameson, R.F. and Wilson, M.F. *Dalton Trans.* **1972**, 2617.

(38) Avdeef, A.; Sofen, R.S.; Bregante, T.L. and Raymond, K.N. *J. Am. Chem. Soc.* **1978**, *100*, 5362.

(39) McBryde, W.A.E. *Can. J. Chem.,* **1964**, *42*, 1917.

(40) Jovanovic, S.V.; Simic, M.G.; Steenken, S. and Hara, Y. *J. Chem. Soc*., *Perkin Trans. 2* **1998**, 2365.

(41) Murata, A.; Tominaga, M.; Inoue, H. and Suzuki, T. *Jpn. Anal.* **1973**, *22*, 179.

(42) Escanda, G.M. and Sala, L.F. *Can. J. Chem.* **1991**, *69*, 1994.

(43) Tereza Fernandez, M.; Mira, L.; M.; Florencio, M.H. and Jennings, K.R. *J. Inorg. Biochem.* **2002**, *92*, 105.

(44) (a) Hynes, M.J. and O'Coinceanainn, M. *J. Inorg. Biochem.* **2001**, *85*, 131. (b) Hynes, M.J. and O'Coinceanainn, M. *J. Inorg. Biochem.* **2004**, *98*, 1457.

(45) Mentasti, E. and Pelizzetti, E. *Dalton Trans.* **1973**, 2605.

(46)   Cavasino, F.P. and Di Dio, E. *J. Chem. Soc. A*, **1970**, 1151.

(47)   (a) Zhang, Z. and Jordan, R.B. *Inorg. Chem*. **1996**, *35*, 1571. (b) Xu, J. and Jordan, R.B. *Inorg. Chem.* 1988, *27*, 1502.

(48)   Xu, J. and Jordan, R.B. *Inorg. Chem.* **1988**, *27*, 1502.

(49)   Gabricevic, M. and Crumbliss, A.L. *Inorg. Chem.* **2003**, *42*, 4098.

(50)   Birus, M.; Kujundzic, N. and Pribanic, M. *Inorg. Chim. Acta* **1981**, *55*, 65.

(51)   Grant, M. and Jordan, R.B. *Inorg. Chem.* **1981**, *20*, 55.

(52)   (a) Helm, L. and Merbach, A.E. *Chem. Rev.* **2005**, *105*, 1923. (b) Richens, D.T. *Chem. Rev.* **2005**, *105*, 1961.

(53)   Albrecht-Gary, A.M. and Crumbliss, A.L. in *Metal Ions in Biological Systems*, Ed. A. Sigel and H. Sigel, Marcel Dekker, Inc., New York, **1998**, *35*, 239.

(54)   Crumbliss, A.L. and Albrecht-Gary, A.M. in *Scientific Bridges for 2000 and Beyond*, Ed. Académie des Sciences, Institut de France, Paris, **1999**, 73-89.

(55)   (a) Eigen, M. and Wilkins, R.G. *Adv. Chem. Ser.* **1965**, *49*, 55. (b) Eigen, M. *Z. Electroche*m. **1960**, *64,* 115. (c) Eigen, M. *Pure. Appl. Chem.* **1963**, *6*, 97.

(56)   Biruš, M.; Bradič, Z.; Krznarić, G.; Kujundžic, N.; Pribanić, M.; Wilkins, P.C. and Wilkins, R.G. *Inorg. Chem.* **1987**, *26*, 1000.

(57)   Batinic-Haberle, I.; Birus; M. and Pribanic, M. *Inorg. Chem.* **1991**, *30*, 4882.

(58)   Palanché, T.; Blanc, S.; Hennard, C.; Abdallah, M.A. and Albrecht-Gary, A.M. *Inorg. Chem.* **2004**, *43*, 1137.

(59)   Tomišić, V.; Blanc, S.; Elhabiri, M.; Expert; D. and Albrecht-Gary, A.M. *Inorg. Chem.* **2008**, *47*, 9419.

(60)   Kakhlon, O. and Cabantchik, Z.I. *Free Rad. Biol. Med.* **2002**, *33*, 1037.

(61)   Bates, G.W.; Billups, C. and Saltman, P. *J. Biol. Chem.* **1967**, *242*, 2810.

(62)   Li, Y.; Harris, W.R.; Maxwell, A.; McGillivray, R.T.A. and Brown, T. *Biochemistry* **1998**, *37*, 14157.

(63)   El Hage Chahine, J.M. and Pakdaman, R. *J. Chim. Phys.* **1996**, *93*, 283.

(64)   Gabricevic, M.; Anderson, D.S.; Mietzner, T.A. and Crumbliss, A.L. *Biochemistry* **2004**, *43*, 5811.

(65)   Faller, B. and Nick, H.; *J. Am. Chem. Soc.* **1994**, *116*, 3860.

(66)   Gabricevic, M. and Crumbliss, A.L. *Inorg. Chem.* **2003**, *42*, 4098.

(67)   Nowack, B. *Environ. Sci. Technol.* **2002**, *36*, 4009.

(68)   Sanchiz, J.; Esparza, P.; Dominguez, S.; Brito, F. and Mederos, A*. Inorg. Chim. Acta* **1999**, *291*, 158.

(69)   (a) White, L.S.; Nilsson, P.V.; Pignolet, L.H. and Que Jr., L. *J. Am. Chem. Soc.* **1984**, *106*, 8312. (b) Que Jr, L.; Kolanczyk, R.C. and White, L.S. *J. Am. Chem. Soc.* **1987**, *109*, 5373.

(70)   Feng, Y.; Ong, S-L.; Hu, J. and Ng, W-J. *Acta Crystallogr., Sect. C: Cryst. Struct. Commun.* **2002**, *58*, m34.

(71)   Malfant, I.; Morgenstern-Badarau, I.; Philoche-Levisalles, M. and Lloret; F. *Chem. Commun.* **1990**, *19*, 1338.

(72)   Wallis, S.C.; Gahan, L.R.; Charles, B.G. and Hambley; T.W. *Polyhedron* **1995**, *14*, 2835.

(73)   Raymond, K.N. *Chem. Eng. News* **1983**, *61*, 4.

(74)   Bastian, R.; Weberling, R. and Palilla, F. *Anal. Chem.* **1956**, 28, 459.

(75)   (a) Bates, G.W.; Billups, C. and Saltman, P. *J. Biol. Chem.* **1967**, *242*, 2810. (b) Li, Y.; Harris, W.R; Maxwell, A.; MacGillivray, R.T.A. and Brown, T. *Biochemistry* **1998**, *37*, 14157. (c) El Hage Chahine, J.M. and Pakdaman, R. *J. Chim. Phys.* **1996**, *93*, 283. (d) Gabricevic, M.; Anderson, D.S.; Mietzner, T.A. and Crumbliss, A.L. *Biochemistry* **2004**, *43*, 5811.

(76)   (a) Gampp, H.; Maeder, M.; Meyer, C.J. and Zuberbühler, A.D. *Talanta* **1985**, *32*, 95. (b) Rossotti, F.J.C.; Rossotti, H.S. and Whewell, R.J. *J. Inorg. Nucl. Chem.* **1971**, *33*, 2051. (c) Gampp, H.; Maeder, M.; Meyer, C.J. and Zuberbühler, A.D. *Talanta* **1985**, *32*, 257. (d) Gampp, H.; Maeder, M.; Meyer, C.J. and Zuberbühler, A.D. *Talanta* **1986**, *33*, 943.

(77)   Marquardt, D.W. *J. Soc. Indust. Appl. Math.* **1963**, *11*, 431.

(78)   Maeder, M. and Zuberbühler, A.D. *Anal. Chem.* **1990**, *62*, 2220.

(79)   (a) Brandel, J.; Humbert, N.; Elhabiri, M.; Schalk, I.J.; Mislin, G.L.A. and Albrecht-Gary, A.M. *Dalton Trans.* **2012**, *41*, 2820. (b) Flynn Jr., C.M. *Chem. Rev.* **1984**, *84*, 31.

(80)   Bio-Logic Company In *Biokine V3.0 User's Manual*; Ed.; Bio-Logic Company; Echirolles, France, 1991.

(81)   Nelder, J.A. and Mead, R. *Comput. J.*, **1965**, *7*, 308.

(82)   Yeramian, E. and Claverie, P. *Nature*, **1987**, *326*, 169.

Chapter VI. Flavone-Mg(II) complexes and dual-drug assembly

In this chapter, the biological importance of Mg(II) will be described. The formation and stability of the flavone-Mg(II) complexes have been evaluated as well. The complexes have been characterized and quantified using UV-Vis absorption spectrophotometry, ESI-MS and cyclic voltammetry. The pharmacokinetic properties of one of the complexes have also been studied and will be discussed. Last, the additive activity of ladanein with chloroquine is explained as well as the first steps of the synthesis of a dual-drug containing both the chloroquine and the flavone pharmacophores.

5.1. Magnesium(II) Biology

Magnesium is a very important metal for the correct functioning of the body. Indeed, it is the second most abundant intracellular divalent cation. Furthermore, it plays an important role in more than 300 biological reactions.[1] For instance, it is involved in protein synthesis, reproduction and DNA and RNA synthesis among others. An adult human body has around 24 g of magnesium. It is mainly present in bones (60 %) and muscles (27%), but can be found in other cells or as extracellular magnesium.[2] It can be found in whole grains, spinach, nuts or potatoes.[3]

Magnesium deficiency has been linked to various diseases. For instance, it was found that magnesium concentrations were lower in Alzheimer's patients than in individuals of the same age not suffering the disease.[4] Low magnesium levels may also lead to hypocalcemia,[5] osteoporosis[6] or hypertension[7] among others.[8] In addition, magnesium intake has beneficial effects for conditions such as migraine (as magnesium citrate),[9] risk of stroke,[10] cardiovascular disease[11,12] or diabetes.[13]

Different magnesium complexes are used as nutritional complements or as magnesium sources for drugs. For instance, magnesium citrate (Figure 1) can be used in nephrolithiasis,[14] as a supplement because of its high bioavailability[15], to treat leg cramps, either chronic[16] or pregnancy-induced[17] or for colon cleansing before a colonoscopy.[18] Furthermore, it is also used as a food preservative and is known as E345. Magnesium pidolate (Figure 1) is used in patients suffering from sickle cell disease.[19] It is used as well in women with dysmenorrhea.[20] Magnesium chloride (Figure 1) is used as a coagulant in the field of waste water treatment[21] and to suppress dust and stabilize non-paved roads.[22] Magnesium sulfate (Figure 1) is another magnesium compound that is widely used. For example, it can be used as a laxative,[23] to prevent eclampsia,[24] pre-term labour,[25] torsade de pointes[26] or in the treatment of acute asthma.[27] Furthermore, it is known as well for its desiccant properties as well as in agriculture to correct magnesium or sulfur deficiency in soil. Finally, magnesium stearate (Figure 1) is used as an excipient and lubricant for medical tablets.[28] It is also used in aliments as a food additive and is known as E470b.
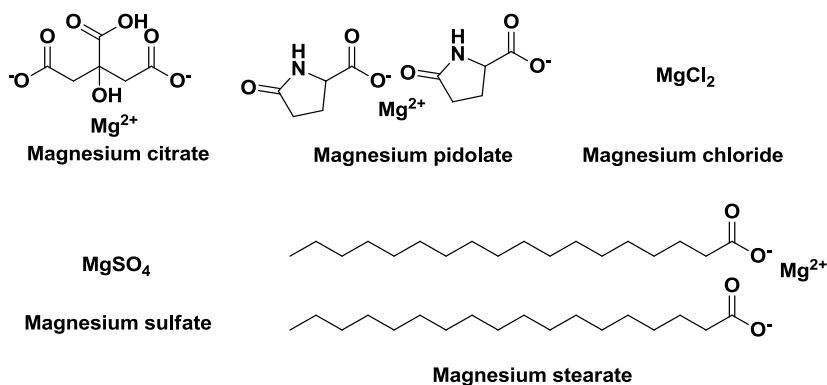
Figure 1. Various magnesium complexes.

One of the main drawbacks of ladanein is its rather low bioavailability and its short half-life. Even though it displays a potent pangenotypic activity, it is quickly metabolized in the body and hence its activity diminishes rapidly (see introduction). Bioavailability tests performed on ladanein by our team showed that the half-life time of the compound is of 7.3 minutes in mice serum.
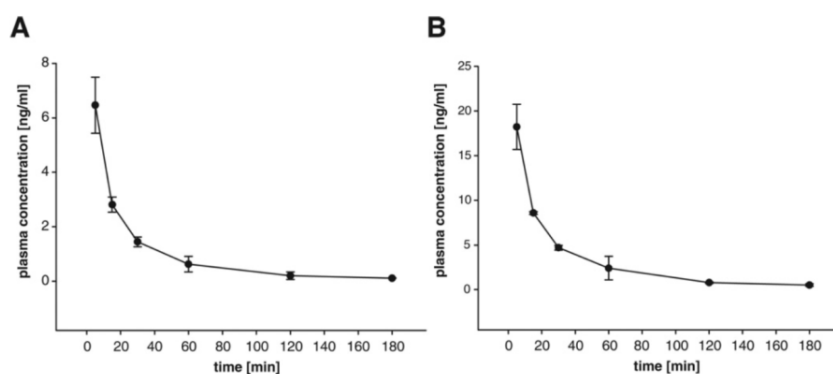

Figure 2. Oral bioavailability of ladanein in mice. A single dose of 0.25 mg/kg of ladanein was administered (A) orally or (B) intravenously. Plasma levels of ladanein were determined 5, 15, 30, 60, 120 and 180 minutes after administration. Mean values of 2 animals including the standard errors are given.

It is suggested that the low half-life time is due to degradation of the flavone *in vivo*, probably due to 2 e$^-$ oxidation (see the previous chapter related to the acido-basic properties of ladanein). To protect the flavone from this unspecific oxidation and increase its bioavailability, it was decided to undertake the formation of flavone-magnesium complexes. Mg(II) was chosen because it is biocompatible, biologically relevant and redox inert, so that it can protect the flavone from undesired oxidation. Magnesium compounds have already been used to treat different human conditions without toxicity problems.

The literature on flavonoid-magnesium complexes is scarce. Nonetheless, a few natural products have been described. For instance, commelinin is a blue pigment that can be isolated from flowers of *Commelina communis*.[29,30] It was shown that the pigment is not a single molecule but rather an assembly of malonylawobanin (reddish purple colored), flavocommelin (pale yellow) and Mg (Figure 3).[30] This type of molecule is known as metalloanthocyanin. The synthesis of commelinin has been performed and it has been shown that without magnesium no commelinin was obtained. Furthermore, if no Mg was present, the blue color did not appear.
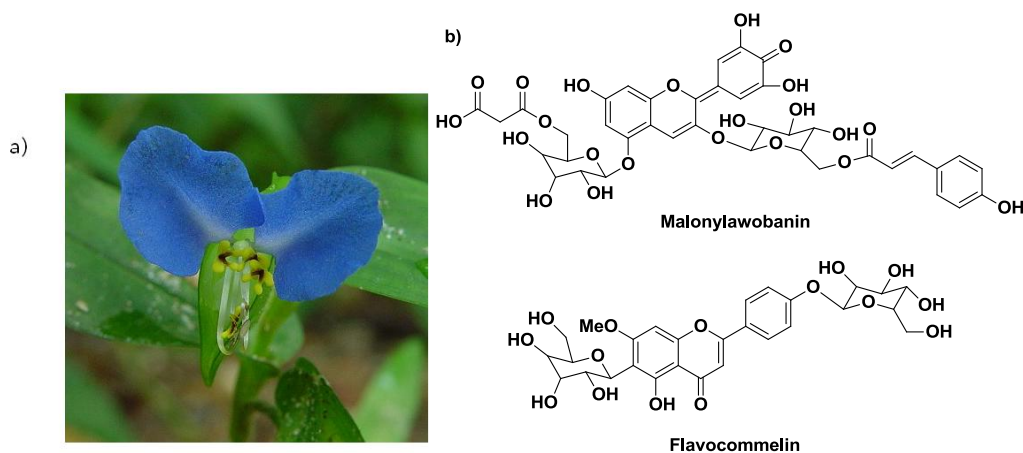

Figure 3. (a) Flower of *Commelina* communis. (b) Structures of two of the components of commelinin, malonylawobanin and flavocommelin.

Interestingly, the complex is very stable and the pigment does not change its color between pH 2 and pH 7. A crystal structure of commelinin has been obtained[31] and revealed that the molecule has a three-fold symmetry and four Mg^{2+} ions. The metals are coordinated to six malonylawobanin molecules and six flavocommelin molecules, forming an ellipsoidal shape. Malonylawobanin and flavocommelin are self-associated and form anthocyanin-anthocyanin and flavone-flavone pairs. The crystal structure is depicted in Figure 4.
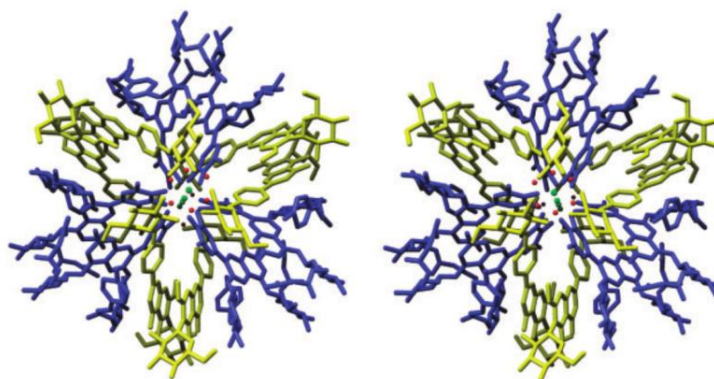
Figure 4. Crystal structure of commelinin. Depicted in blue are the malonylawobanin molecules, in yellow the flavocommelin molecules, in green the Mg^{2+} and in red the water molecules. Image taken from a publication by Takeda *et al.*[31]

There are other closely related metalloanthocyanins that exhibit similar structures such as protodelphin, which is isolated from flowers of *Salvia Patens*.[32] Protodelphin is composed of malonylawobanin (M), the flavone apigenin (F) and Mg^{2+} in a ($M_6F_6Mg_2$) supramolecule. Protocyanin, extracted from *Centaurea cyanus*, shares similar features as well, forming a supramolecular assembly composed of succinylcyanin, malonylflavone, a magnesium ion and a Fe(III) ion.[33] Finally, another metalloanthocyanin has been recently discovered in the petals of *S. uliginosa*, cyanosalvianin.[34] Cyanosalvianin is also formed by six molecules of an anthocyanin and six molecules of a flavone assembled around two Mg^{2+} atoms.

Magnesium complexation has also been reported as an important feature to enhance the antibacterial activity of certain quinolones such as pefloxacin and sparfloxacin (Figure 5).[35] Indeed, in the presence of magnesium, the activity of these antimicrobial compounds is increased up to 1024-fold. It has been shown that quinolones bind DNA effectively only in the presence of Mg^{2+}, forming DNA-quinolone-Mg adducts.[36] The quinolones have been proposed to bind Mg(II) in a 2/1 ratio.[37]
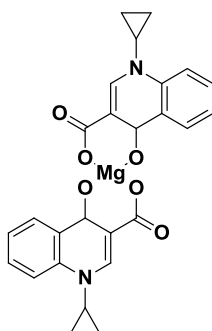

Figure 5. Proposed binding of a quinolone derivative to magnesium.

Finally, Uivarosi *et al.* showed that primuletin, an antagonist of the androgen receptor, formed complexes with magnesium and other metals such as Pb(II) or Fe(III).[38]

5.2. Flavone-Magnesium Complexes

A study of the formation of the flavone-magnesium complexes was therefore undertaken. As the last step of the improved synthetic route to ladanein involves deprotection of the 5-methoxyl group in final precursor **6** with the Lewis acid $MgBr_2$ etherate (see the section related to the improved synthesis of ladanein), we anticipated that the deprotection/complexation steps could be performed in a one-pot manner with $MgCl_2$, thus constituting a smart formulation approach.

Toward this objective, the coordination of the flavone and $MgCl_2$ was first studied using an absorption-spectrophotometric approach. Because of the low solubility of the magnesium salt at room temperature, a mixed solvent made of 50% CH_3CN (the solvent used for the demethylation reaction) and 50% water (by volume) was used to ensure the solubility of both the flavone and the magnesium complex. Statistical analysis of the spectral data (Figure 6) allowed us to calculate the stability constant of the **FOMe**.$MgCl_2$ complex (log $K^*_{FOMe.MgCl2}$ = 1.4(3)) as well as its electronic spectral properties. The flavone is characterized by two absorption maxima lying at 283 nm (band II) and 333 nm (band I), which have been assigned to the π-π^* transitions of the B and A aromatic systems, respectively (see the previous chapter related to the acido-basic properties of ladanein). Coordination of Mg(II) on the β-hydroxyketone bidentate site of **FOMe** induced a bathochromic shift of band II which tends to blend with band I. A new band with much lower intensity is also formed in the visible region (370 nm - 500 nm).

(a)   *(b)*

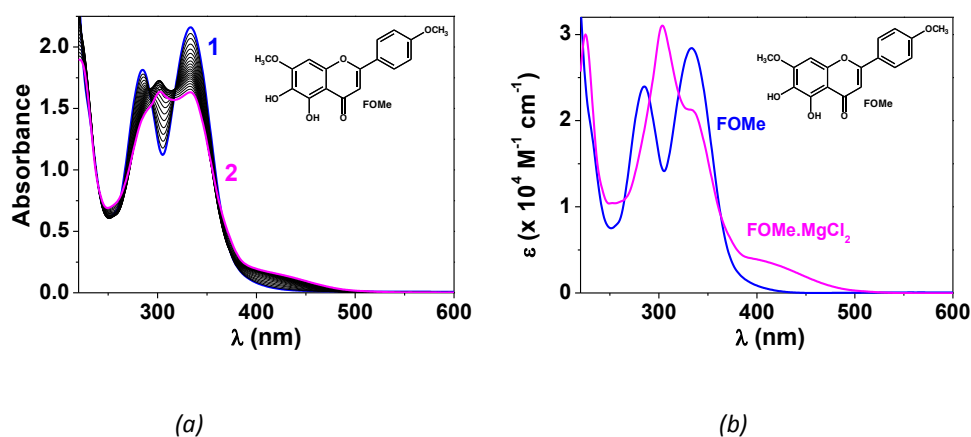**Figure 6.** (a) UV-visible absorption spectrophotometric titration of **FOMe** by $MgCl_2$ and (b) absorption electronic spectra of the flavone **FOMe** and its magnesium(II) complex **FOMe**.$MgCl_2$ Solvent: CH_3CN/H_2O (1:1 by volume); T = 25.0 °C; l = 1 cm; [**FOMe**]$_{tot}$ = 7.63 × 10^{-5} M; (1) [$MgCl_2$]$_{tot}$/[**FOMe**]$_{tot}$ = 0; (2) [$MgCl_2$]$_{tot}$/[**FOMe**]$_{tot}$ = 185.8.

The knowledge of the thermodynamic parameters of **FOMe**.$MgCl_2$ allowed us to simulate the experimental conditions required for a potential one-pot deprotection-complexation reaction of the final precursor with magnesium chloride. The relatively low stability of the **FOMe**.$MgCl_2$ complex indicated that a significant excess of $MgCl_2$ is required for the formation of more than 95% of the flavone-magnesium complex under the experimental conditions used for the demethylation reaction ([**FOMe**] = 0.016 M). As it can be seen from the distribution diagram depicted in Figure 7, around 6 equivalents of $MgCl_2$ are needed to obtain 95% of the flavone-magnesium complex.
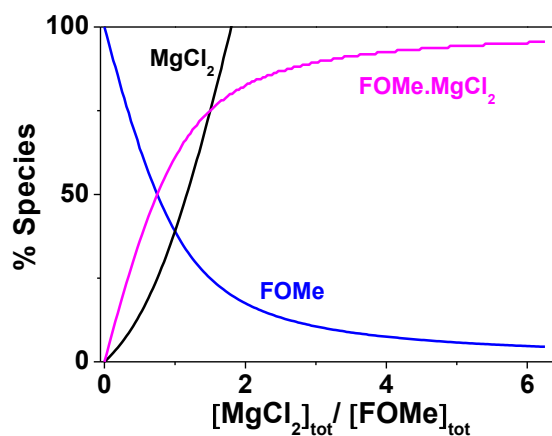

Figure 7. Distribution diagram of the Mg(II) complex formation with ladanein **FOMe** and $MgCl_2$. CH_3CN/H_2O (1/1 by volume); *T*=25.0°C. [**FOMe**]$_{tot}$= 0.016 M (*i.e.* equivalent to 40 mg of ladanein in 8 mL of CH_3CN).

The complex can be then formed and favored if all solvent is evaporated once the reaction is completed. Nevertheless, the main drawback is that $MgCl_2$ is by far less reactive than $MgBr_2$ and a longer reaction time is subsequently needed for the reaction to finish (*i.e.* 40 hours of reaction time instead of only 2 hours for all the starting material to be consumed). Furthermore, several equivalents of $MgCl_2$ are necessary for the complexation to occur, meaning that $MgCl_2$ will also be present with respect to the flavone.Mg complex. A test to monitor the development of the reaction by UV-Vis absorption spectrophotometry was performed. However, the maximum temperature that can be used with spectrophotometer is 40 °C and no significant change was observed during the reaction time that was used.
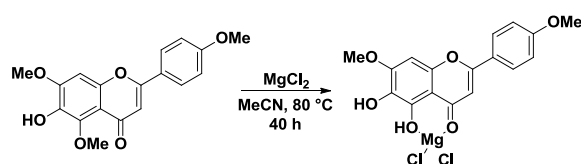
Scheme 1. Synthesis of the **FOMe**.$MgCl_2$ complex in one step, using $MgCl_2$ as the demethylating agent.

It was then decided to proceed through a two-step approach. First, the demethylation step using $MgBr_2$ etherate followed by recrystallization to obtain pure ladanein and then the complexation step in presence of a magnesium precursor. Among the numerous Mg(II) salts safely employed in pharmacological compositions, magnesium stearate was chosen as a proof of concept (Scheme 2). When ladanein was reacted with magnesium stearate, the color of the solution instantaneously changed from bright yellow (the color of the free flavone) to dark orange, probably indicating the preferential formation of the complex.

Scheme 2. Synthesis of **FOMe**.MgStearate complex from ladanein and MgStearate.
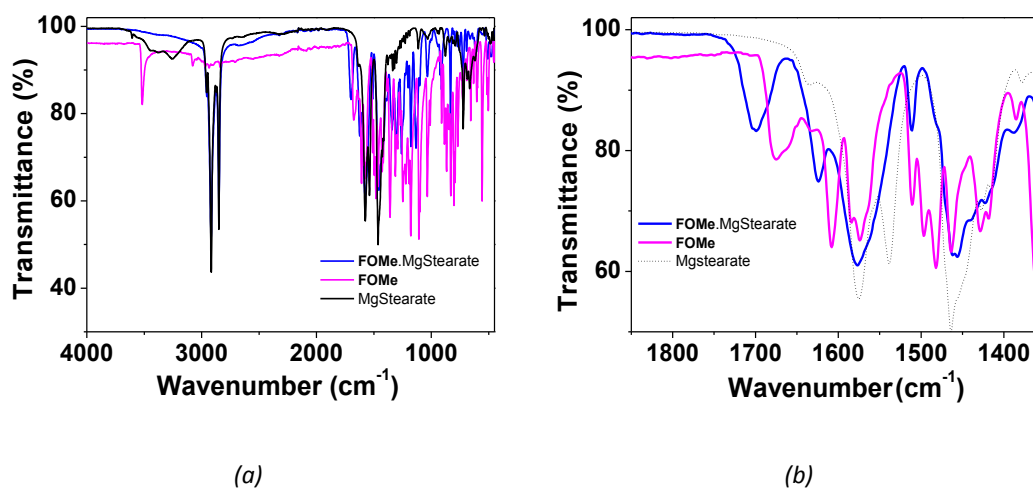

(a)   *(b)*

Figure 8. IR spectra of **FOMe** and **FOMe**.MgStearate. (a) Depiction of the whole spectra and (b) Zoom between 1850 and 1360 cm^{-1}.

To confirm the formation of the flavone.MgStearate complex, the infrared (IR) spectra of the free flavone, MgStearate and **FOMe**.MgStearate were recorded. The corresponding overlaid spectra are shown in Figure 8. It can be observed that the peak at around 3500 cm^{-1} from the **FOMe** spectra) disappears for **FOMe**.MgStearate. This peak is probably due to the presence of the OH group in position 5 in **FOMe** and disappears when the complex is formed (*i.e.* involved in a strong hydrogen bond with the adjacent carbonyl group).[39] Also, as it can be seen from graph B (Figure 8), the bands due to C=O stretching have a slight shift between the free flavone and the magnesium complex, most likely indicating complexation. Indeed, it has been shown that 5-hydroxy-flavonato complexes show

$v(CO)$ bands shifting towards a lower frequency by 14-35 cm^{-1}, indicating that the 5-hydroxyflavone is coordinated to the metal ion as a bidentate chelate.[40]

Indeed, it can be observed from the first C=O band that there is a $\Delta v(CO)$ of around 22 cm^{-1} while the second C=O band experienced a shift of 17 cm^{-1}, which correlates perfectly with a complexed flavone. Finally, it appears that no free stearic acid is present since it has a very characteristic band around 1700 cm-1, which is not present in the spectrum of the complexed flavone.

To further evaluate the stability of the **FOMe.**MgStearate complex, an absorption spectrophotometric titration was performed in pure dioxane. Nonetheless, Mg(II) stearate being poorly soluble in dioxane, a concentrated stock solution was refluxed in this solvent and aliquots were added to a **FOMe** solution in a quartz optical cell. As previously observed for **FOMe**.MgCl$_2$ (Figure 6), the formation of the complex can be monitored thanks to valuable significant spectral variations (Figure 9). Even though the experimental conditions were different, the stability of the **FOMe**.MgStearate complex (log $K^*_{\text{FOMe.Mgstearate}}$ = 4.1(6)) is three orders of magnitude higher with respect to that of **FOMe**.MgCl$_2$. This stabilization may be the result of the auxiliary stearate ligands.

(a)   *(b)*
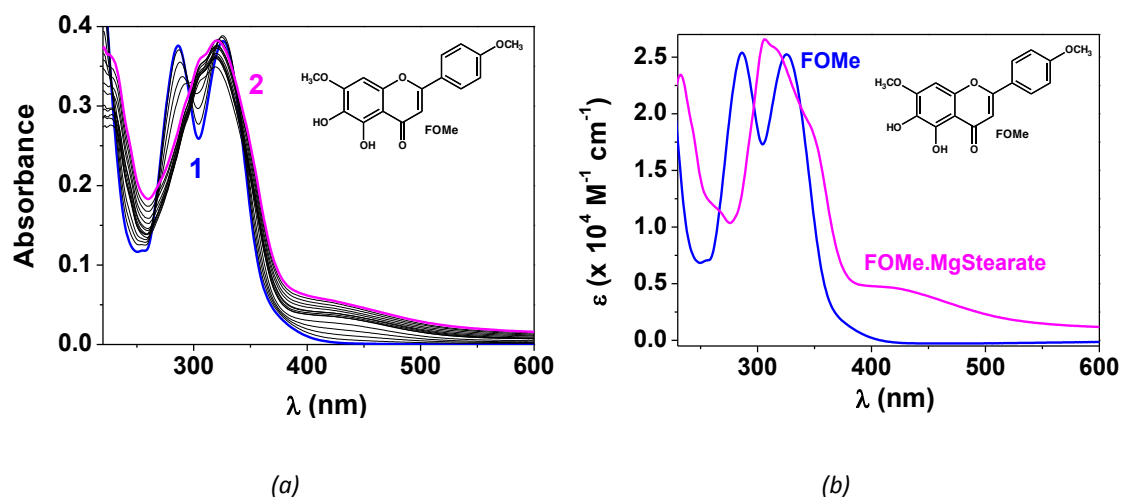
Figure 9. (a) UV-visible spectrophotometric titration of **FOMe** by Mg(stearate)$_2$ and (b) absorption electronic spectra of the flavone **FOMe** and its corresponding magnesium(II) complex **FOMe**.MgStearate. Solvent : dioxane; T = 25.0 °C; l = 1 cm; [**FOMe**] = 1.52 × 10^{-5} M; (1) [Mg(stearate)$_2$]$_{\text{tot}}$/[**FOMe**]$_{\text{tot}}$ = 0; (2) [Mg(stearate)$_2$]$_{\text{tot}}$/[**FOMe**]$_{\text{tot}}$ = 13.26.

The distribution diagram depicted in Figure 10 indicates that under the same reaction conditions as those used for MgCl$_2$ ([**FOMe**] = 0.016M), the addition of only one equivalent would lead to the formation of more than 93% of the targeted magnesium complex.

Figure 10. Distribution diagram of the Mg(II) complex formation with **FOMe** using stearate auxiliary anion. Solvent: dioxane; T=25.0 °C; [**FOMe**]$_{tot}$ = 0.016 M (*i.e.* equivalent to 40 mg of the starting flavone in 8 mL of dioxane.
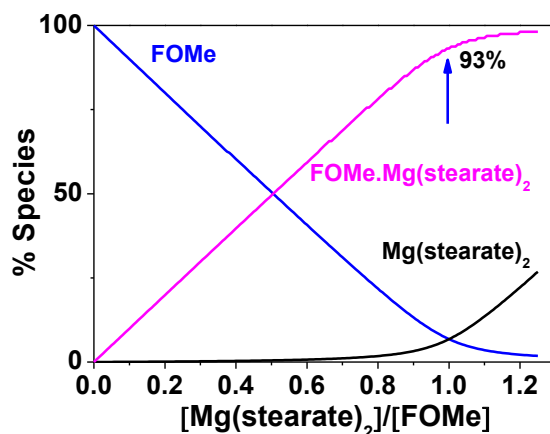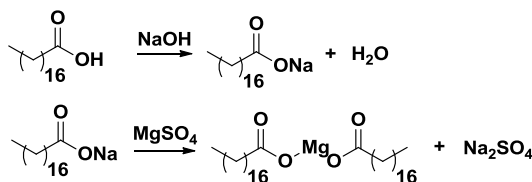
Following these observations, we decided to investigate the synthesis of new Mg complexes from commercial carboxylic acids. Magnesium stearate is prepared *via* a two-step pathway involving, first a deprotonation in presence of NaOH followed by a reaction in presence of MgSO$_4$ to yield the desired Mg(II) stearate (Scheme 3).

Scheme 3. Preparation of magnesium stearate from stearic acid and magnesium sulfate.

It was then thought that this sequence may be applied to other commercial carboxylic acids and could be used to form magnesium complexes containing the flavone and other functional molecules, such as biocompatible supports able to limit the degradation of the flavone, specific lipids, lipophilic or hydrophilic residues to modulate the solubility of the metal complexes, other bioactive molecules for synergistic or additive drug combination and efficient target delivery of the flavone.

As a proof of concept, this strategy was then applied to a commercial carboxylic (4-(trifluoromethyl)benzoic acid) acid available in the laboratory. Nonetheless, the two-step synthesis used for the formation of magnesium stearate did not function to form the desired magnesium complex. Instead, a shorter synthetic route (Scheme 4) was used involving the reaction between the desired carboxylic acid and magnesium hydroxide, which acts both as the magnesium source and the base necessary for the deprotonation of the carboxylic acid.
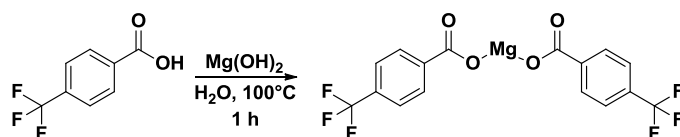
Scheme 4. Formation of the Mg(II) complex (noted Mg181) from a commercial carboxylic acid.

The fact that a molecule containing a carboxylic acid may be used to obtain Mg(II) complexes reflects a greater control over the stability, solubility and electronic and steric characteristics of the targeted magnesium species, which may then be translated on a greater control of the ternary flavone-Mg(II)-carboxylate complex, giving rise to more stable ternary complexes with the desired properties in terms of solubility and bioavailability.

At this point, a thorough physico-chemical investigation of the formation of Mg(II) complexes was undertaken for ladanein **FOMe** and its various synthetic analogues using as partners magnesium chloride, magnesium pidolate and the magnesium complex obtained from 4-(trifluoromethyl)benzoic acid, named Mg181. Magnesium stearate was discarded because of its extremely low solubility and the laborious procedure needed to perform the spectrophotometric titrations. Studies were performed using UV-Visible absorption spectrophotometry followed by statistical analysis of the spectral data (Figure 12) in order to evaluate the stability constants of the respective ternary complexes. The formation of these magnesium complexes was also studied using mass spectrometry (ESI-MS).

The corresponding stability constants measured for ladanein and its synthetic analogues in combination with the different magnesium precursors are gathered in Table 1.

Table 1. Stability constants of the different flavone-Mg(II) complexes (Solvent = CH_3OH; T = 25 °C; the errors are given as 3σ with σ = standard deviation).

	$\log K^*_{F.MgX}$ ($\pm 3\sigma$)		
	$MgCl_2$	MgPid	Mg181
FOMe	4.50(4)	4.92(7)	4.8(4)
FH	1.97(4)	4.38(5)	4.77(8)
FF	5.36(2)	5.09(3)	3.1(2)
FCF_3	4.4(2)	4.6(2)	<3
$FFCF_3$	4.93(2)	5.04(2)	<3
$FOCF_3$	5.47(4)	5.26(3)	4.1(2)

As can be observed, for the lead compound **FOMe**, the strongest complexes are formed with magnesium pidolate and Mg181 with log K^* of 4.92(7) and 4.8(4), respectively. It is likely that the additional groups borne by the Mg(II) cation help stabilizing the ternary complex compared to the ternary complex with $MgCl_2$. Furthermore, if the stability constant in CH_3CN and water (1:1 *v/v*, Figure 6) is compared that obtained in CH_3OH for $MgCl_2$, it can be clearly seen that the complexes are by far much more stable in CH_3OH, probably because the water molecules compete with the binding and decrease the stability of the complex. Interestingly, this effect is amplified for **FH**; which forms much more stable complexes with MgPid and Mg181 than $MgCl_2$ (Figure 11)
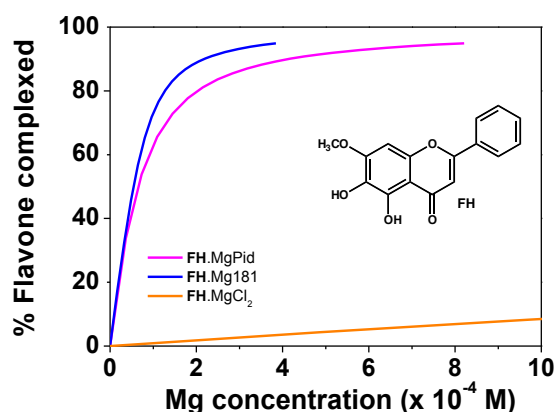
Figure 11. Percentage of complexed flavone negletein **FH** with three different Mg precursors.

Interestingly, for the fluorine-containing ladanein analogues (**FF**, **FCF₃**, **FFCF₃** and **FOCF₃**), better results are generally obtained with $MgCl_2$ and MgPid (*i.e.* both lacking F atoms) instead of Mg181. It is possible that this effect is due to the presence of six fluorine atoms on Mg181, which may destabilize the ternary complex with the F-containing flavones. For instance, **FOCF₃** and **FCF₃** form the most stable complexes with MgPid and $MgCl_2$.
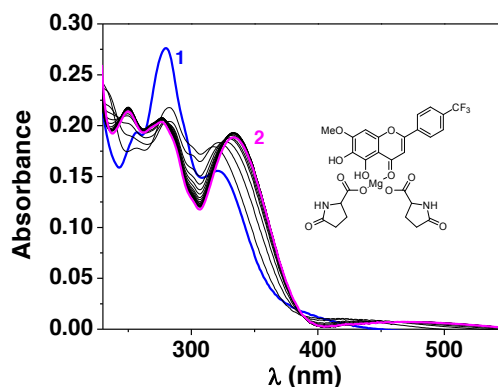
Figure 12. Spectrophotometric absorption titration of **FCF₃** with MgPid. Solvent: CH_3OH; T = 25 °C; l = 1 cm; $[FCF_3]_{tot}$ = 1.59 × 10^{-5} M; (1) $[Mg(pidolate)_2]_{tot}/[FCF_3]_{tot}$ = 0; (2) $[Mg(pidolate)_2]_{tot}/[FCF_3]_{tot}$ = 15.09.

(*a*)   (*b*)
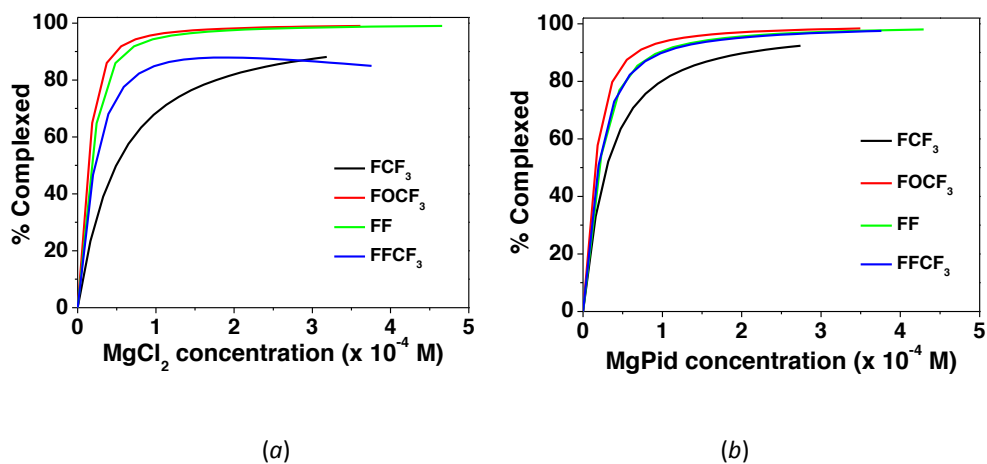
Figure 13. Percentage of complexed flavone with increasing concentration of (a) MgCl$_2$ or (b) MgPid.

As can be observed from Figure 13, in general, the use of MgPid as magnesium source to form the complex leads to higher formation percentage of the complex at the same metal concentration.
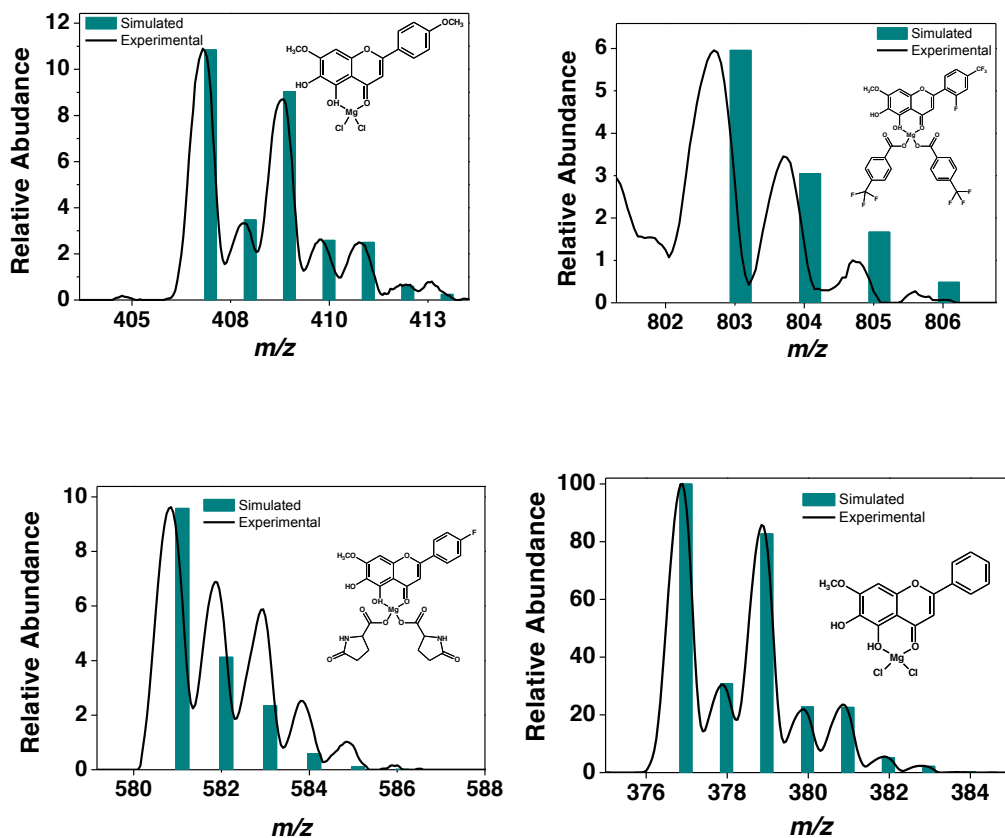
Figure 14. ESI-MS spectra of different flavone-Mg(II) complexes. Negative mode. Solvent CH$_3$OH/H$_2$O (80/20 by volume).

In order to corroborate the formation of the magnesium complexes, an ESI-MS study was undertaken. Solutions of the flavones and magnesium precursors at 10^{-4} M were mixed immediately before injection and the outcome was observed. All complexes were clearly characterized except for **FCF₃**.Mg181 and **FOCF₃**.Mg181. Their isotopic profiles showed an excellent agreement with the simulated ones thus substantiating our observations.

Figure 14 showcases some of the examples obtained. The formation of the **FOMe**.MgPid complex was also assessed by ^{1}H NMR spectroscopy. As it can be seen from Figure 15, the signals corresponding to the methoxy groups are shifted when compared to the free flavone. The same effect can be observed for the peaks corresponding to the aromatic proton at around 8 ppm.
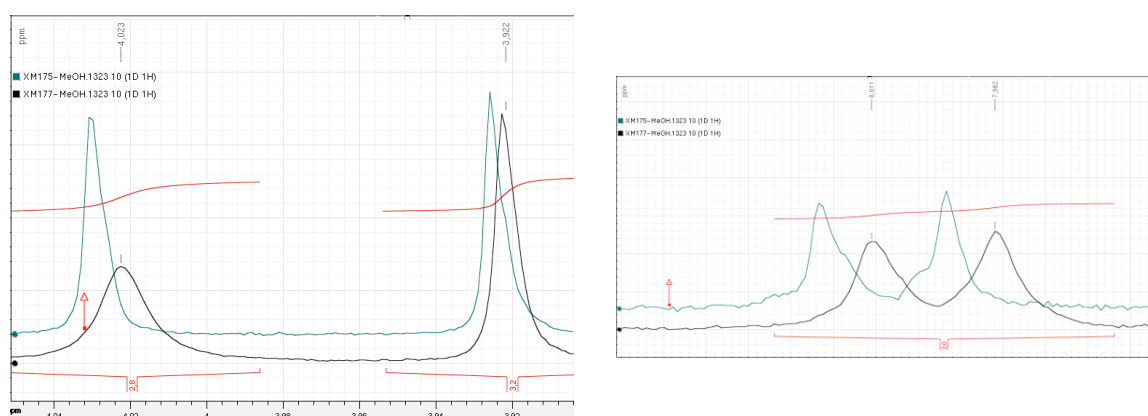
Figure 15. NMR spectra of **FOMe** (blue) compared to its magnesium ternary complex **FOMe**.MgPid (black).

Further proof that the flavones and Mg(II) precursors are held together through complexation was obtained when studying the electrochemical properties of the compounds (see previous chapter on the redox properties of the flavones). An excess of MgCl₂ (*i.e.* about 10 equiv.) was added to the solution of the flavone and, as it can be seen in Figure 16, the signals corresponding to oxidation/reduction processes centered on the A-ring (between -0.8 V and 1.2 V) were significantly shifted. Table 2 gathers the values of E_{pa} and E^{pc} for the free flavones and for the corresponding Mg(II) complexes. This feature indicates that the redox processes centered on the flavones are not markedly affected thus confirming that the 6-OH group (*i.e.* suggested not to be involved in Mg(II) complexation) is essential for triggering the oxidation/reduction.
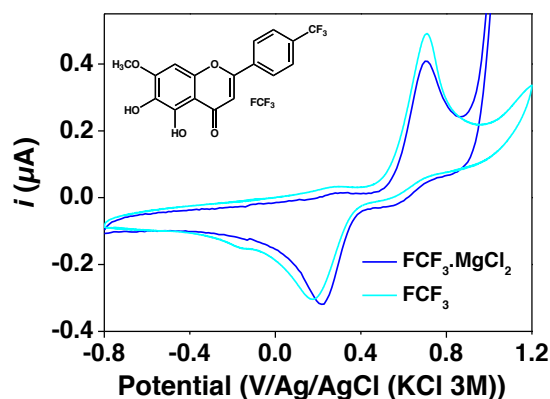
Figure 16. CV profile of **FCF$_3$** (light blue) and **FCF$_3$**.MgCl$_2$ (dark blue). [FCF$_3$]$_{tot}$ = 2.44 mM, [MgCl$_2$]$_{tot}$ = 23.7 mM. Measured in DMSO at a sweep rate of 200 mV s^{-1} with 0.1 M *n*-Bu$_4$NPF$_6$ electrolyte support at 25 °C. Reference electrode = KCl(3 M)/Ag/AgCl; working electrode = glassy carbon disk of 0.07 cm^2 area; counter-electrode = Pt wire.

Table 2. Summary of the values for E$_{pa}$ and E$_{pc}$ (in V, measured at 200 mV s^{-1}) with and without the presence of MgCl$_2$**.**

	Potential (V)	Free flavone	+ MgCl$_2$
FOMe	E$_{pa}$	0.720	0.736
	E$_{pc}$	0.181	0.160
FH	E$_{pa}$	0.71	0.698
	E$_{pc}$	0.201	0.223
FF	E$_{pa}$	0.72	0.705
	E$_{pc}$	0.200	0.202
FCF$_3$	E$_{pa}$	0.706	0.699
	E$_{pc}$	0.181	0.222
FFCF$_3$	E$_{pa}$	0.709	0.727
	E$_{pc}$	0.198	0.189
FOCF$_3$	E$_{pa}$	0.699	0.721
	E$_{pc}$	0.19	0.19

5.3. Antiviral Activity and Bioavailability

As discussed previously in this chapter, the formation of the flavone-magnesium complexes was studied in order to be able to improve their half-life times and pharmacokinetic properties, primarily its bioavailability. As the tests are time consuming and rather expensive, they were only performed with **FOMe**.MgPid, which was suggested to be the most interesting compound in terms of stability and solubility.

First, the antiviral activity of the complex was tested, so as to verify that the antiviral activity was retained with the formation of the magnesium complex. Interestingly, it was found that the magnesium pidolate complex of ladanein showed similar to slightly improved anti-HCV potency thus confirming our initial hypotheses and demonstrating that the antiviral activity is not inhibited when the flavones is complexed to an inert metal ion.
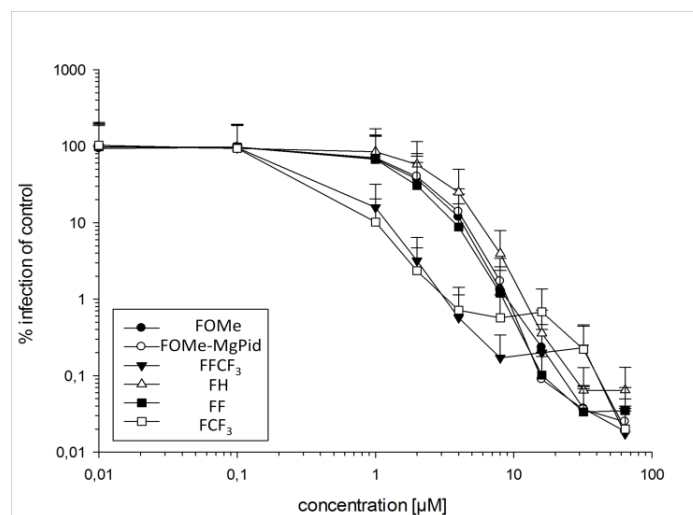
Figure 17. AntiHCV activites of ladanein, its analogues and its magnesium pidolate complex. Summary of four independent experiments. Jc-R2a reporter virus was preincubated with indicated concentration of inhibitors for 30 min at 37 °C prior to infection of Huh-7.5 cells. Cells were subsequently lysed for 72 h and luciferase activity was then measured.

As can be observed in Figure 17, both ladanein (**FOMe**, black circles) and its magnesium complex (**FOMe**.MgPid, white circles) displayed a very similar antiviral activity during the test. The EC_{50} was calculated for each compound and was found to be 1.6 µM for ladanein **FOMe** and 1.5 µM for **FOMe**.MgPid, respectively. It can be thus concluded that the formulation of a Mg(II) complex of ladanein has no effect whatsoever on the antiviral activity and potency of the flavone.

Subsequently, the bioavailability if the compound was tested as well. The tests were performed both orally and intravenously on CD-1 mice. Twelve of them had the compound administered orally whereas it was administered *via* an intravenous injection for the rest. The pharmacokinetic data obtained is summarized in Table 3.

Table 3. Pharmacokinetic properties of the **FOMe**.MgPid complex and **FOMe.**

	FOMe-MgPid	FOMe
$t_{1/2}$ (min)	8 ± 1	7 ± 1
Cl (mL/min/kg)	143 ± 20	442 ± 116
V_z (mL/kg)	1688 ± 445	4657 ± 2137
AUC last IV (min.ng/mL)	3295 ± 457	566 ± 134
AUC last PO (min.ng/mL)	575 ± 70	171 ± 27
Oral bioavailability (%)	17 % ± 5	30 ± 12

Pharmacokinetic studies describe the process by which a substance is absorbed, distributed, metabolized and eliminated. Pharmacokinetic processes can be divided into two different groups, input processes (liberation and absorption) and output processes (distribution, metabolism and excretion). The biological half-life time ($t_{1/2}$) of a substance is the time needed for the concentration of drug in plasma to decrease by half. Effectively, this parameter provides information on how long it takes to eliminate the drug and hence how often a drug should be administered. Cl stands for clearance and is the rate at which waste substances are cleared from the blood, either *via* metabolism or unchanged in the urine. V_z is the apparent volume of distribution and is an important indicator of the extent of drug distribution into body fluids and tissues. The bigger the V_z value is, the more likely the drug is found in the tissues. On the contrary, the smaller the number is, the more likely the drug stays in the circulatory system. The area under the curve (AUC) is generally calculated from the time of administration until the concentration of the drug is negligible. It represents the total exposure to the drug over time. In this case, IV means that the drug was administered intravenously whereas PO (*per os*) means that the administration was done orally. Finally, the bioavailability is defined by the fraction of the administered drug that stays unchanged when reaching the blood circulation. Bioavailability is always of 100% when administered intravenously, by definition. However, when administered *via* other routes, it generally decreases due to metabolism and excretion/elimination.

Even though, the biological half-life times for ladanein **FOMe** and **FOMe**.MgPid apparently seem relatively low, they are comparable to other compounds tested under the same conditions. For example, Midazolam, a drug used for the treatment of insomnia or seizures has an *in vivo* half-life time in the mouse of around 12 minutes. Other compounds such as Antipyrine or caffeine display higher half-life times of 28 and 30 minutes respectively. However, it is important to highlight that these three compounds show much higher half-life times when tested on humans. Indeed, Midazolam shows a half-life time of 4 hours in humans, while the half-life time of Antipyrine is 12

hours and that of caffeine 5 hours. Hence, it would be expected that the half-life time of both ladanein and its magnesium pidolate complexes to be improved if tested on humans. IFN-α is a clear example of a compound with low half-life time and high clearance that arrived into the market. When it was used for anti-HCV treatment, it had to be injected at least three times per week, causing discomfort in the patients receiving the therapy. Consequently, PEG IFN-α was developed, which has an improved pharmacokinetic profile. Boceprevir, also accepted by the FDA for anti-HCV therapy has a half-life time of 3.4 hours and hence a 3-times-per-day dosing is necessary. The half-life time of another approved NS3 inhibitor, Telaprevir, is of 4 hours. In contrast, the main metabolite formed when Sofosbuvir is administered has a half-life time of 27 hours, which allows for once-daily dosing. Lastly, Simeprevir, the last anti-HCV FDA-approved drug displays a half-life time of 10 hours. Other polyphenols that display anti-HCV activity such as EGCG, EGC and EC display half-life times of 3.4, 1.7 and 2.0 hours respectively.[41]

Even though the half-life time of the ternary magnesium compound is not significantly improved when compared to that of free **FOMe**, its solubility has been greatly enhanced, which makes it easier to perform the tests. Furthermore, it also displays an oral bioavailability. Bioavailability is always lower for orally administered drugs, because they must pass through the intestinal wall and circulate to the liver, during which first-pass metabolism may occur. Interestingly, many drugs display improved bioavailability when administered with food. Nonetheless, oral bioavailability of ladanein **FOMe** can be greatly improved by using galenic formulation. For example, Telaprevir has extremely poor water solubility and its oral bioavailability was between 2 and 4 % in crystalline form. Nonetheless, the bioavailability was improved when administered as a dispersion, with bioavailabilities of up to 40 % with that formulation.[42]

Moreover, the plasmatic concentration obtained is superior to the EC_{50} of the tested compound, which means that the compound can actually exert its activity while in the body. An important plasmatic concentration is necessary to achieve antiviral activity. For instance, curcumin displays a wide range of biological activities,[43–45] however its levels in serum are extremely low and negligible amounts of curcumin are found in plasma after oral administration. Other reasons for the low bioavailability of curcumin are its very low tissue distribution and rapid metabolisation.[46]

Even though 5,6,7-trihydroxylated flavonoids may undergo rapid metabolism either by sulfonation, methylation, glucuronidation or other mechanisms, their metabolites may still be active (see introduction). For example, baicalin, which is the glucuronidated metabolite of baicalein, is active against dengue virus[47] and HIV-1.[48]

5.4. Dual-Drug Approach

As discussed before, ladanein exerts a synergistic antiviral activity with cyclosporine A (CsA),[49] which is known to be an inhibitor of HCV replication both *in vitro* and *in vivo*. It is thought that CsA not only inhibits HCV replication by disrupting an NS5 complex necessary for replication[50] but also by restoring IFN-α expression.[51] By combining both ladanein **FOMe** and CsA, the infection was entirely eliminated, which does not happen when using CsA alone. Furthermore, the addition of 1 μmol/L of **FOMe** substantially decreased the EC_{50} of cyclosporin A and *vice versa*.
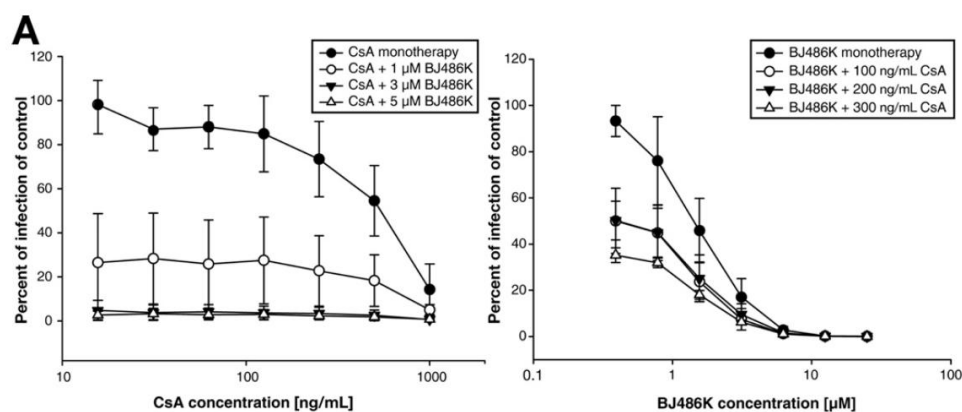

Figure 18. Synergistic antiviral activity of **FOMe** (here noted BJ486K from former synthesis) and CsA. Combined effects of CsA on **FOMe** and vice versa were analyzed by inoculation of Huh7-Lunet/CD81 cells with JcR-2a virus in the presence of given drugs and determination of luciferase activity 72 hours later. Mean values of 3 independent experiments each conducted in triplicate including the standard deviations are given. Data are normalized for values determined in mock-treated controls.

Chloroquine, a very well known antimalarial drug also exerts an important antiviral activity. It has been reported that it is active against influenza A,[52] SARS[53] or HIV[54,55] among others. It is thought that the mechanisms by which chloroquine exerts its antiviral activity are diverse. First, chloroquine inhibits endocytosis in viruses that require a pH-dependent step for entry. Second, it impedes post-translational modification of envelope glycoproteins, a process that often needs a low pH. Third, replication of members of the *Flaviviridae* family is also disrupted by chloroquine by blocking maturation of the prM protein. Finally, by inhibiting the glycosylation of the envelope proteins in some viruses of the Retrovirus family, it induces the production of non-infectious viral particles.[56]

Chloroquine has also been reported to exert an antiviral activity for HCV. One of the key steps in HCV virion entry involves the release of the genetic material when passing through an acidic vesicle. Chloroquine is a lysosomotropic agent, meaning that it is selectively taken up into lysosomes. Once inside, it accumulates and concentrates in a protonated form, effectively increasing the pH inside the

vesicle, which in turn impedes the liberation of the genetic material.[57] Other lysosomotropic agents such as NH_4Cl act in a similar manner. Chloroquine does not only affect HCV entry, it is active against viral replication as well. Indeed, HCV hijacks the autophagic machinery proteins of the host cell in order to initiate the translation or delivery the viral RNA to the translation apparatus and to establish a productive infection.[58] Interestingly, once the translation/replication is started, autophagic proteins are no longer needed. Chloroquine is believed to disrupt autophagic proteolysis inducing the accumulation of ineffective autophagosomes, inhibiting the pathway that the virus utilizes to initiate its replication.[59]

Interestingly, chloroquine analogues also display a potent activity. Ferroquine, a chloroquine analogue bearing a ferrocene is active against HCV by blocking viral entry at the fusion step.[60] This effect was shown to be pangenotypic. Nonetheless, the mechanism of action is thought to be different between chloroquine and ferroquine, since ferroquine is a weaker base and may not block acidic endocytosis. Furthermore, ferroquine can generate reactive oxygen species that may lead to lipid peroxidation. Since lipid metabolism is important for HCV entry, this could be important for the antiviral activity of ferroquine.
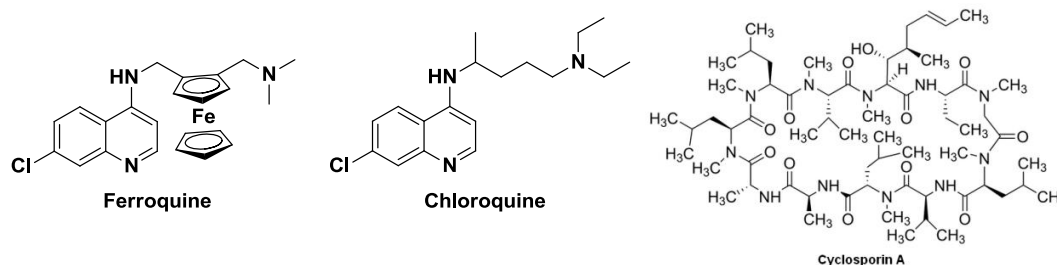
Figure 19. Chemical structures of ferroquine, chloroquine and cyclosporin A.

Our laboratory recently published a study with antimalarial chloroquine analogues displaying a different side-chains.[61] Interestingly, changes in the side chain were tolerated, hence retaining the antimalarial activity while lowering the molecular weight of the final compound. Moreover, thanks to these subtle structural changes, the compounds were active against chloroquine resistant strains.

An additive effect was observed when testing ladanein **FOMe** and chloroquine alongside. Results are depicted in Figure 20. Unlike the synergistic effect observed between cyclosporin A CsA and ladanein **FOMe**, chloroquine and ladanein display an additive activity.
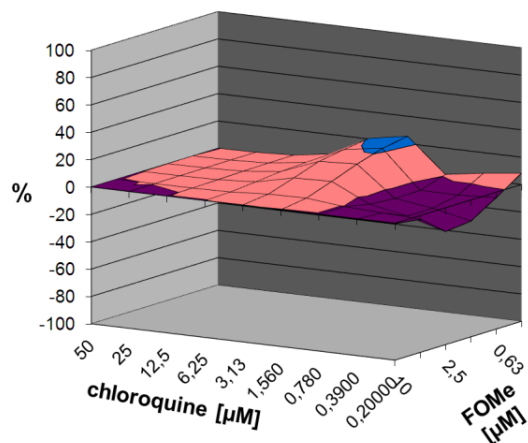
Figure 20. Combined effects of chloroquine on **FOMe** activity (and *vice versa*) were analyzed by inoculation of Huh7.5 F-Luc cells with JcR-2a virus in the presence of given drugs and determination of luciferase activity 72 h later.

Hence, it was decided to use the methodology allowing the transformation of a carboxylic acid into a Mg(II) complex developed during my PhD to build a dual drug bearing a flavone linked to a chloroquine analogue through a central biocompatible magnesium atom. The main goal was to develop a new complex with an improved antiviral activity taking advantage of the additive effect observed between ladanein and chloroquine.

Very few examples of similar approaches can be found in the literature. For example, Pt- and Rh-drug complexes were studied for their antitrypanosomal activities.[62] However, the approach is markedly different because in these complexes the metal has a primordial role in the biological activity of the molecule. Moreover, of all the complexes prepared, none presented two pharmacophores attached to the metallic centre. Other dual drug delivery systems have also been prepared but they rather involve supramolecular structures such as micelles,[63] nanoparticles[64] or dendrimers.[65]

My hosting laboratory has a long-term experience in synthesizing chloroquine analogues. The synthetic pathway starts from 4,7-dichloroquinoline **14** which is reacted with ethylenediamine to afford the desired product **15** with 44 % yield. This is a basic precursor for the synthesis of various analogues. Then, through a reductive amination with acetone, the corresponding secondary amine **16** is obtained with 92 % yield (Scheme 5).
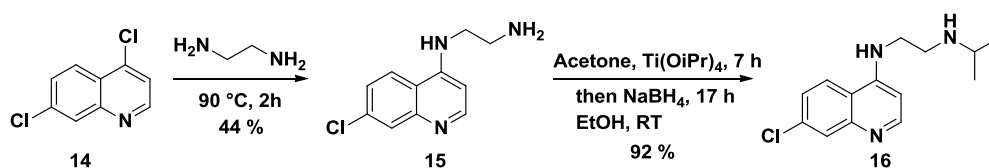
Scheme 5. Synthesis of the short chloroquine precursor **16** developed in the laboratory.

The goal was then to add another substituent to form a tertiary amine. This substituent should carry an ester or a carboxylic acid in order to be easily transformed into a suitable functional magnesium complex. Hence, several conditions were tested, which are summarized in Table 4.
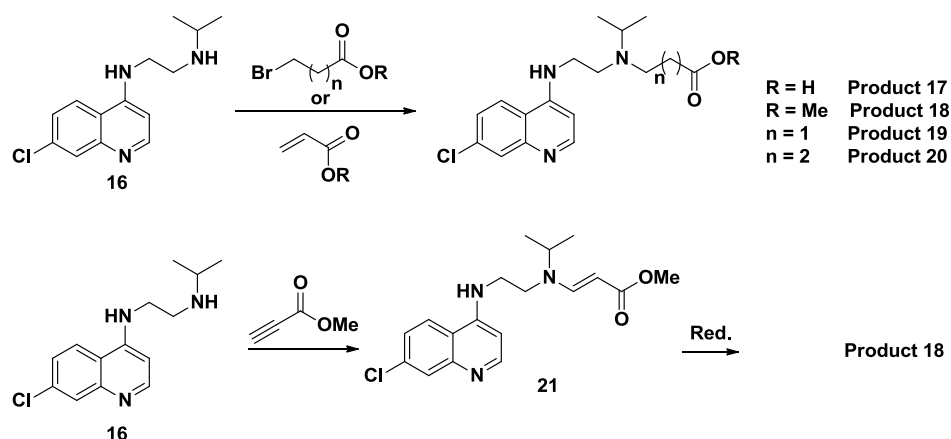
Scheme 6. Different conditions tested to form an ester or carboxylic acid.

Table 4. Summary of the conditions screened for the formation of the short chloroquine ester. RT = room temperature.

| Entry	Reagent	Solvent	Temperature	Reactants	Desired product
1		THF	70°C	-	No
		CH₃CN	RT	-	No
		DMF	150°C	-	No
		DMF	150°C	NBu₄I	No
2		CH₃OH	60°C	NBu₄I	No
		DCM	RT	AgNO₃	No
		DMF	50°C	Cs₂CO₃	No
3		DMF	120°C	-	No
4		CH₃OH	60°C	-	No
		DMF	150°C	-	No
5		CH₃OH	60°C	-	Yes
		CH₃OH	60°C	Amberlyst-15	Yes
		CH₃OH	RT	CAN	Yes
		CH₃OH	RT	CuOTf	Yes
6		DCM	RT	-	-

The first attempts involved the reaction with either 3-bromopropanoic acid or its corresponding methyl ester (entries 1 and 2 in Table 4). Nevertheless, the desired product was not obtained. It was then decided to perform the same reaction with 4-bromobutanoic methyl ester (entry 3 in Table 4),

in order to make sure that a decarboxylative elimination of the 3-bromopropanoic acid was not taking place. The desired product was not obtained using this butanoic acid either.

Subsequently, it was decided to test if the desired product could be obtained through an Aza-Michael reaction, using acrylic acid or methyl acrylate. Results obtained with acrylic acid were negative. However, when reacting methyl acrylate (entry 5 in Table 4) with quinoline **16** in methanol at 60 °C, the desired product was obtained. Indeed, an LC-MS analysis showed the presence of two products with identical mass, corresponding to the mass of the desired tertiary amine, probably product **18** and its isomer. Nonetheless, the reaction proceeded very slowly, and three days of reaction time were needed for all the starting material to be consumed. Furthermore, separation of both compounds was not possible through either silica gel column chromatography or recrystallization. To reduce the long reaction time, various catalysts were tested (Amberlyst-15,[66] CuOTf[67] and CAN[68]). Unfortunately, the reaction did not proceed any faster and three days were still needed to consume all the starting material.

Finally, a slightly different approach was undertaken. It was decided to test the reaction between methyl propiolate and quinoline **16** in methanol in order to obtain compound **21** (entry 6 in Table 4). After 60 hours, all the starting material had been consumed. However, the desired product could not be separated from the other by-products present in the crude by either column chromatography or recrystallization.

Since the secondary amine present in compound **16** seems not to be very reactive, probably because it is hindered by the presence of the isopropyl group, it was decided to test if by swapping the order of the reductive amination and aza-Michael reactions, the desired product could be obtained more easily. The aza-Michael reaction on the primary amine **15** allows us to obtain the desired product **22** in 71 % yield. However, the reductive amination step could not be performed under the conditions tested, using $NaBH_4$ and $NaBH(OAc)_3$.
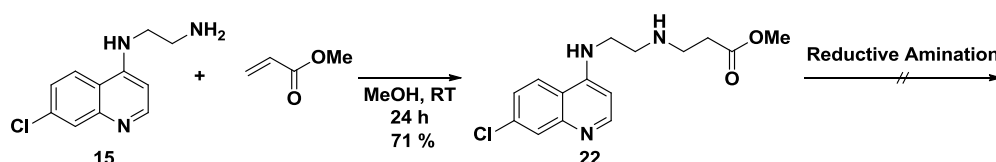
Scheme 7. Conditions for the synthesis of product **22.**

Interestingly, a secondary product is formed alongside compound **22**, and it is the molecule formed from two consecutive aza-Michael reactions (compound **23**, Scheme 8). In order to gain insight on

the selectivity of the reaction, three reactions were performed with 1, 2 and 4 equivalents of methyl acrylate respectively and the formation of compounds **22** and **23** was followed by ^{1}H NMR spectroscopy. Results are summarized in Table 5.
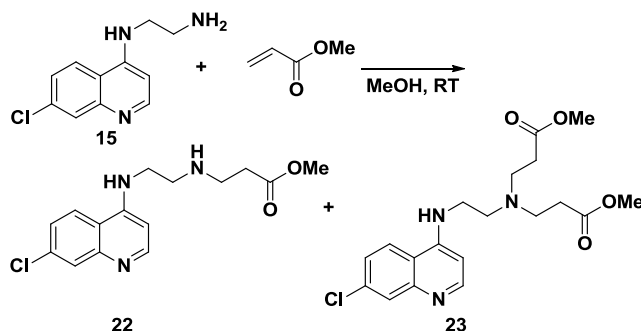
Scheme 8. Main product and by-product obtained when reacting chloroquine **15** with methyl acrylate.

Table 5. ^{1}H NMR screening at different times and methyl acrylate equivalents (SM = starting material, Mono and Di = mono and di-*N*-alkylation products).

	1 equivalent	2 equivalents	4 equivalents
1 h	SM: 72 % Mono: 28 % Di: 0 %	SM: 52 % Mono: 47 % Di: 1 %	SM: 30 % Mono: 65 % Di: 5 %
2 h	SM: 64 % Mono: 34 % Di: 2%	SM: 38 % Mono: 57 % Di: 5 %	SM: 12 % Mono: 78 % Di: 10 %
3 h	SM: 56 % Mono: 42 % Di: 2%	SM: 24 % Mono: 69 % Di: 7 %	SM: 5 % Mono: 80 % Di: 15 %
4 h	SM: 47 % Mono: 50 % Di: 3 %	SM: 20 % Mono: 71 % Di: 9 %	SM: 3 % Mono: 79 % Di: 18 %
5 h	SM: 43 % Mono: 53 % Di: 4 %	SM: 12 % Mono: 78 % Di: 10 %	SM: 2 % Mono: 75 % Di: 23 %
1 d	SM: 14 % Mono: 77 % Di: 9%	SM: 3 % Mono: 67 % Di: 30 %	SM: 1 % Mono: 40 % Di: 59 %
4 d	SM: 7 % Mono: 79 % Di: 4 %	SM: 1 % Mono: 37 % Di:62 %	SM: 1 % Mono: 11 % Di: 88 %

As it can be observed from the results, the starting material is much more rapidly consumed with increasing equivalents of methyl acrylate. Indeed, a reaction time of 4 days is needed to consume most of the starting material when the reaction is performed with 1 equivalent of reagent. This study also allowed us to gain insight on when the reaction should be stopped depending on the targeted product, the secondary or tertiary amine. In order to preferentially obtain the mono-alkylated product **22**, two conditions seem to be the most appropriate. Either adding two equivalents during five hours, or, if a shorter reaction time is desired, four equivalents with a three hour reaction time yield the product in approximately the same ratio. However, if the dialkylated product **23** is the desired one, it is better to use four equivalents over the course of four days to obtain it with the highest ratio.

This compound obtained after the dialkylation reaction is very interesting since it possesses two ester groups in its structure. Rather than forming a 2:1 complex with Mg(II) as shown for magnesium pidolate or Mg181, because it bears two esters, a monometallic monochelate 1:1 Mg(II) can be formed since the dialkylated compound bears two identical ester groups. Unfortunately, due to lack of time, the synthesis of the magnesium complex and the flavone-Mg-quinoline ternary complex could not be performed. The possible **FOMe**.MgSCQ complex is depicted in Figure 21.
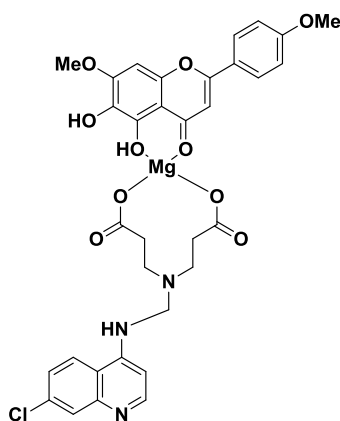
Figure 21. Chemical structure of the targeted flavone-Mg-Short chloroquine assembly**.**

In addition, compound **23** is structurally related to nitrilotriacetic acid (NTA) which was used to stabilize the flavone-Fe(III) complexes by forming a ternary complex (see previous chapter on Fe (III) coordination properties of ladanein and its analogues). Hence, it would be interesting to investigate the ferric ternary complexes between the flavones and product **23**, to know whether or not they are more stable.

5.5. Conclusion

In this chapter, it has been demonstrated that the synthesized flavones form 1:1 complexes with Mg(II). These complexes have been thoroughly studied studied (quantification and characterization) by UV-Vis absorption and IR spectrophotometries, ^{1}H NMR and ESI-MS. Furthermore, the stability of the ternary complexes can be tuned depending on the substituents of the ligands (flavone and carboxylate) bound to the magnesium cation. Also, a methodology allowing the straightforward transformation of a carboxylic acid into a magnesium complex that can be used to form Flavone-Mg entities has been developed as well.

The antiviral activity of **FOMe.**MgPid has been then tested and it was found to be similar to the activity displayed by ladanein, meaning that the formation of the complex does not alter the biological activity of the compound. In addition, the pharmacokinetic profile of **FOMe**.MgPid has been evaluated. Although the half-life time has not been significantly improved when compared to the free flavone, this new compound displays a much higher solubility. Moreover, the flavone-Mg(II) complex displays an oral bioavailability and a plasmatic concentration is superior to the EC_{50} of the drug.

Since chloroquine and ladanein were previously found to induce an additive effect when administered together, it was decided to build a dual-drug assembly bearing both drugs with a possible improved antiviral activity. The first steps of the synthesis were developed. However, due to lack of time, the project could not be finished. Product **18** was obtained after a long reaction time but purification was impossible to achieve. Product **22** bearing one ester group and compound **23** bearing two ester groups were synthesized and a ^{1}H NMR study was undertaken in order to find the best reaction conditions to obtain either the secondary or tertiary amine. This latter product could be an important precursor to synthesize the desired complex with enhanced antiviral activity.

EXPERIMENTAL SECTION

Starting Materials and Solvents

Magnesium(II) chloride ($MgCl_2$, anhydrous >98 %), magnesium(II) stearate ($Mg(C_{18}H_{35}O_2)_2$, puriss.) and magnesium pidolate ($Mg(C_5H_6NO_3)_2$ 98 %) were purchased from Sigma Aldrich and used without further purification. Distilled water was further purified by passing it through a mixed bed of ion-exchanger (Bioblock Scientific R3-83002, M3-83006) and activated carbon (Bioblock Scientific ORC-83005) and was de-oxygenated by CO_2- and O_2-free argon (Sigma Oxiclear cartridge) before use. Spectrophotometric grade methanol (Merck, p.a.) was de-oxygenated by CO_2- and O_2-free argon (Sigma Oxiclear cartridge). All the stock solutions were prepared by weighing solid products using an AG 245 Mettler Toledo analytical balance (precision 0.01 mg). All measurements were carried out at 25.0(2) °C.

Infrared Spectra

Infrared (IR) spectra were recorded neat on a Perkin-Elmer Spectrum One Spectrophotometer.

Spectrophotometric Titrations of the Flavones by Mg(II)

Stock solutions of flavone (from 3.069×10^{-3} M to 7.603×10^{-4} M) were prepared in methanol and then further diluted with methanol to obtain a ligand concentration ranging from 7.551×10^{-5} M to 1.630×10^{-5} M. The spectrophotometric titrations of the flavones by the various Mg(II) precursors were thus carried out in CH_3OH, dioxane or in a mixed solvent made of CH_3CN and water (*v/v*). Microvolumes of a concentrated solution of Mg(II) complexes (from 1.271×10^{-2} M to 6.167×10^{-3} M) were added to 2 mL of the ligand solutions in a 1 cm path length quartz optical cell (the $[Mg]_{tot}/[flavone]_{tot}$ ratio was varied from 0 to 20). Special care was taken to ensure that complete equilibration was attained. The corresponding UV-Vis. absorption spectra were recorded from 200 nm to 800 nm on a Cary 5000 (Agilent) or Cary 50 (Varian) spectrophotometer maintained at 25.0(2) °C by the flow of a Lauda E200 thermostat.

Analysis and Processing of the Spectroscopic Data

The spectrophotometric data were analyzed with Specfit program[69–72] which adjusts the absorptivities and the stability constants of the species formed at equilibrium. Specfit uses factor analysis to reduce the absorbance matrix and to extract the eigenvalues prior to the multiwavelength fit of the reduced data set according to the Marquardt algorithm.[73,74]

Electrospray Mass Spectrometric Measurements

Electrospray mass spectra of metal complexes with the different flavones were obtained with an AGILENT TECHNOLOGIES 6120 quadripole equipped with an electrospray (ESI) interface. Solutions ($\sim$10^{-4} M) of the magnesium(II) complexes with the flavones were prepared in a methanol:water (2:8 *v/v*). The sample solutions were continuously introduced into the spectrometer source with a syringe pump (KD SCIENTIFIC) at a flow rate of 800 µL/h. For electrospray ionization, the drying gas was heated at 250 °C and its flow was set at 6 L.min^{-1}. The quadrupole temperature was set to 100 °C. The capillary exit voltage was fixed at 5 kV and the skimmer voltage was varied from 100 to 250 V in negative mode in order to optimize the signal responses. Scanning was performed from m/z = 100 to 1000.

Bioavailability Studies

Bioavailability studies were performed by Patrick Gizzi at TechMed Strasbourg.

Synthesis of the Short Chloroquine Analogues

N1-(7-chloroquinolin-4-yl)ethane-1,2-diamine (15)
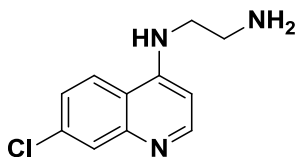
White powder
Chemical formula: $C_{11}H_{12}ClN_3$
Molecular Weight: 221.69 g/mol
Yield: 44 %

A mixture of 4,7-dichloroquinoline **14** (15 g, 75.74 mmol, 1 eq), and ethylenediamine (20.3 mL, 303 mmol, 4 eq) was stirred at 80-90°C for 3.5 hours under Argon and then cooled to room temperature. A solution of 1 N NaOH was added and the mixture was extracted with a solution of DCM/MeOH (8/2), dried over $MgSO_4$ and concentrated under vacuum. The crude was recrystallized from ethanol (7.47 g) Yield 44 %.

NMR ^{1}H (CD$_3$OD, 300 MHz) δ ppm 8.35 (d, *J* = 5.7 Hz, 1H), 8.11 (d, *J* = 9.1 Hz, 1H), 7.77 (d, *J* = 2.2 Hz, 1H), 7.39 (dd, *J* = 2.2, 9.1 Hz, 1H), 6.56 (d, *J* = 5.7 Hz, 1H), 3.44 (t, *J* = 6.4 Hz, 2H), 2.97 (t, *J* = 6.4 Hz, 2H)
NMR ^{13}C (CD$_3$OD, 100 MHz) δ ppm 152.9, 152.6, 149.8, 136.5, 127.7, 126.2, 124.5, 118.9, 99.8, 46.3, 40.9
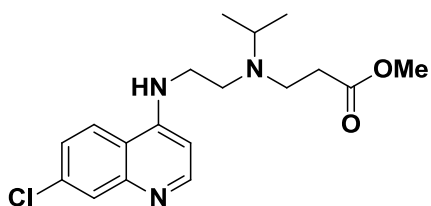
N^1-(7-chloroquinolin-4-yl)-N^2-isopropylethane-1,2-diamine (16)
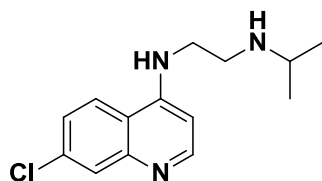
White powder
Chemical formula: $C_{14}H_{18}ClN_3$
Molecular Weight: 263.77 g/mol
Yield: 92 %

A mixture of acetone (0.796 mL, 10.8 mmol, 2.4 eq.), Titanium tetraisopropoxide (2.7 mL, 9.02 mmol, 2 eq) and molecule **15** (1 g, 4.51 mmol, 1 eq.) in absolute EtOH (7 mL) was stirred for 7 h at room temperature under argon. Then NaBH$_4$ (0.256 g, 6.77 mmol, 1.5 eq.) was added and the resulting mixture was stirred for 17 h. The mixture was slowly poured into of a 2M NH$_4$OH solution. The resulting white inorganic precipitate was filtered and washed with DCM. Phases were separated and the water layer was extracted with DCM. The combined organic layers were extracted with a 1 N HCl solution. The acidic layer was washed with DCM then treated with 2 N NaOH solution to reach pH 10-12 and extracted with DCM. The combined organic layers were dried over Na$_2$SO$_4$, filtered and concentrated under vacuum to afford the product 1.09 g. Yield 92 %.

NMR ^{1}H (CD$_3$OD, 300 MHz) δ ppm 8.37 (d, *J* = 5.6 Hz, 1H), 8.11 (d, *J* = 9.1 Hz, 1H), 7.78 (d, *J* = 2.2 Hz, 1H), 7.41 (dd, *J* = 2.2, 9.1 Hz, 1H), 6.58 (d, *J* = 5.6 Hz, 1H), 3.50 (t, *J* = 6.6 Hz, 2H), 2.89 (m, 3H), 1.11 (d, *J* = 6.3 Hz, 6H)
**NMR ^{13}C (CDCl$_3$, 100 MHz)** δ ppm 152.8, 152.6, 149.8, 136.5, 127.7, 126.2, 124.4, 118.9, 99.8, 48.9, 48.5, 43.7, 22.6

3-((2-((7-chloroquinolin-4-yl)amino)ethyl)(isopropyl)amino)propanoate (18)

Chemical Formula: $C_{18}H_{24}ClN_3O_2$
Molecular Weight: 307.78 g/mol

N^1-(7-chloroquinolin-4-yl)-N^2-isopropylethane-1,2-diamine (100 mg, 0.38 mmol, 1 eq.) was dissolved in 5 ml methanol, 1.7 eq. of methyl acrylate were added and the reaction mixture was heated at 60 °C under reflux for 3 days. Reaction advancement was monitored by TLC on silica gel 60 using $CHCl_3$:CH_3OH:NH_4OH 90:10:1. Afterwards, water and dichloromethane were added and the phases were separated. The organic phase was washed with water and brine, dried over $MgSO_4$ and concentrated under reduced pressure.

An LC-MS analysis was performed and a product of the correct mass was observed. However, it could not be isolated.

Methyl 3-((2-((7-chloroquinolin-4-yl)amino)ethyl)amino)propanoate (22)
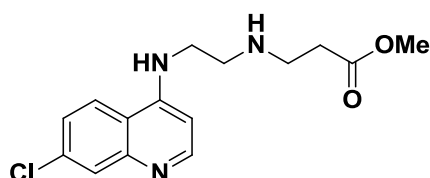
White solid
Chemical formula: $C_{15}H_{18}ClN_3O$
Molecular Weight: 307.78 g/mol
71 % yield

Quinoline **15** (160 mg, 0.722 mmol, 1 equiv.) was dissolved in 10 mL of MeOH and then methyl acrylate was added (0.13 mL, 1.46 mmol, 2 equiv.). The reaction was stirred at RT for 36 h. Once all the starting material had been consumed, solvent was evaporated and water was added. The aqueous phase was then extracted three times with DCM. The organic phase was then dried over $MgSO_4$ and solvent evaporated under reduced pressure to yield a yellow oil. Product was purified through a silica gel column chromatography (eluent DCM 3/1 EtOH) to yield 0.1434 g of an oil that crystallizes in the freezer. Yield 71%.

^{1}H NMR (CDCl$_3$; 300 MHz): δ (ppm) 8.54 (d, J=5.3 Hz, 1H), 7.97 (d, J=2.2 Hz, 1H), 7.78 (d, J=9.0 Hz, 1H), 7.38 (dd, J=9.0 Hz, J=2.2 Hz, 1H), 6.39 (d, J=5.3 Hz, 1H), 5.92 (br s, 1H), 3.70 (s, 3H), 3.34 (m, 2H), 3.06 (m, 2H), 2.98 (t, J=6.1 Hz, 2H), 2.57 (t, J=6.1 Hz, 2H)
Due to lack of time ^{13}C NMR could not be performed.

Methyl 4-((2-((7-chloroquin-4-yl)amino)ethyl)(3-methoxy-3-oxopropyl)amino)butanoate (23)
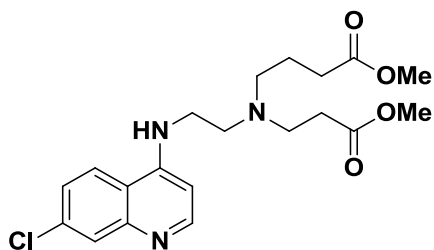
Yellow oil
Molecular Formula: $C_{20}H_{26}ClN_3O$
Molecular Weight: 407.89
Yield: 41 %

Quinoline **15** (1.02 g, 4.62 mmol, 1 equiv.) was dissolved in 50 mL of CH_3OH and then methyl acrylate was added (0.84 mL, 9.34 mmol, 2 equiv.). The reaction was stirred at RT for 60 h. Once all the starting material had been consumed, solvent was evaporated and water was added. The aqueous phase was then extracted three times with DCM, dried over $MgSO_4$ and solvent evaporated under reduced pressure to yield a yellow oil. Product was purified through a silica gel column chromatography (EtOAc 9/1 CH_3OH) to yield 0.738 g of a yellow oil that crystallizes in the freezer. Yield 41 %. Product **22** was also obtained in 57% yield

¹H NMR (CDCl₃; 300 MHz): δ (ppm) 8.54 (d, J=5.3 Hz, 1H), 7.96 (m, 2H), 7.38 (dd, J=9.0 Hz, J=2.2 Hz, 1H), 6.39 (d, J=5.3 Hz, 1H), 5.97 (br s, 1H), 3.58 (s, 6H), 3.36 (m, 2H), 3.06 (m, 2H), 2.84 (m, 6H), 2.50 (t, J=6.4 Hz, 4H)
Due to lack of time ¹³C NMR could not be performed.

References

(1)   Elin, R. *Am. J. Clin. Pathol.* **1994**, *102*, 616–622.

(2)   Vormann, J. *Mol. Aspects Med.* **2003**, *24*, 27–37.

(3)   Volpe, S. L. *Adv. Nutr.* **2013**, *4*, 378S – 383S.

(4)   Lemke, M. *Biol. Psychiatry* **1995**, *3223*, 341–343.

(5)   Rude, R. K.; Oldham, S. B.; Singer, F. R. *Clin. Endocrinol. (Oxf).* **1976**, *5*, 209–224.

(6)   Cohen, L. *Magnes. Res.* **1988**, *1*, 85–87.

(7)   Joffres, M.; Reed, D.; Yano, K. *Am. J. Clin. Nutr.* **1987**, *45*, 469–475.

(8)   Rude, R. K. *J. Bone Miner. Res.* **1998**, *13*, 749–758.

(9)   Peikert, A.; Wilimzig, C.; Köhne-Volland, R. *Cephalalgia* **1996**, *16*, 257–263.

(10)   Larsson, S. C.; Orsini, N.; Wolk, A. *Am. J. Clin. Nutr.* **2012**, *95*, 362–366.

(11)   Song, Y.; Manson, J. E.; Cook, N. R.; Albert, C. M.; Buring, J. E.; Liu, S. *Am. J. Cardiol.* **2005**, *96*, 1135–1141.

(12)   Chakraborti, S.; Chakraborti, T.; Mandal, M.; Mandal, A.; Das, S.; Ghosh, S. *Mol. Cell. Biochem.* **2002**, *238*, 163–179.

(13)   Mooren, F.; Krüger, K.; Völker, K.; Golf, S. W.; Wadepuhl, M.; Kraus, A. *Diabetes, Obes. Metab.* **2011**, *13*, 281–284.

(14)   Ettinger, B.; Pak, C.; Citron, J.; Thomas, C.; Adams-Huet, B.; Vangessel, A. *J. Urol.* **1997**, *158*, 2069–2073.

(15)   Lindberg, J.; Zobitz, M.; Poindexter, Z.; Pak, C. *J. Am. Coll. Nutr* **1990**, *9*, 48–55.

(16)   Roffe, C.; Sills, S.; Crome, P.; Jones, P. *Med. Sci. Monit.* **2002**, *8*, 326–331.

(17)   Dahle, L. O.; Berg, G.; Hammar, M.; Hurtig, M.; Larsson, L. *Am. J. Obstet. Gynecol.* **1995**, *173*, 175–180.

(18)   Berkelhammer, C.; Ekambaram, A.; Silva, R. G. *Gastrointest. Endosc.* **2002**, *56*, 89–94.

(19)   De Franceschi, L.; Bachir, D.; Galacteros, F.; Tchernia, G.; Cynober, T.; Neuberg, D.; Beuzard, Y.; Brugnara, C. *Br. J. Haematol.* **2000**, *108*, 284–289.

(20)   Benassi, L.; Barletta, F. P.; Baroncini, L.; Bertani, D.; Filippini, F.; Beski, L.; Nani, A.; Tesauri, P.; Tridenti, G. *Clin. Exp. Obstet. Gynecol.* **1992**, *19*, 176–179.

(21)   Tan, B.; Teng, T.; Omar, A. *Water Res.* **2000**, *34*, 597–601.

(22)   Goodrich, B. a.; Koski, R. D.; Jacobi, W. R. *Water. Air. Soil Pollut.* **2008**, *198*, 165–188.

(23)   Izzo, a a; Gaginella, T. S.; Mascolo, N.; Capasso, F. *Br. J. Pharmacol.* **1994**, *113*, 228–232.

(24)   Altman, D.; Carroli, G.; Duley, L.; Farrell, B.; Moodley, J.; Neilson, J.; Smith, D. *Lancet* **2002**, *359*, 1877–1890.

(25)   Kawagoe, Y.; Sameshima, H.; Ikenoue, T.; Yasuhi, I.; Kawarabayashi, T. *J. Pregnancy* **2011**, *2011*, 965060.

(26)   Tzivoni, D.; Banai, S.; Schuger, C.; Benhorin, J.; Keren, a.; Gottlieb, S.; Stern, S. *Circulation* **1988**, *77*, 392–397.

(27)   Bloch, H.; Silverman, R.; Mancherje, N.; Grant, S.; Jagminas, L.; Scharf, S. M. *Chest* **1995**, *107*, 1576–1581.

(28)   Ertel, K. D.; Carstensen, J. T. *J. Pharm. Sci.* **1988**, *77*, 625–629.

(29)   Takeda, K. S.; Fujii, T.; Iida, M. *Phytochemistry* **1984**, *23*, 879–881.

(30)   Tamura, H.; Kondo, T.; Goto, T. *Tetrahedron Lett.* **1986**, *27*, 1801–1804.

(31)   Shiono, M.; Matsugaki, N.; Takeda, K. *Proc. Jpn. Acad. Ser. B. Phys. Biol. Sci.* **2008**, *84*, 452–456.

(32)   Takeda, K.; Yanagisawa, M.; Kifune, T.; Kinoshita, T.; Timberlake, C. F. *Phytochemistry* **1994**, *35*, 1167–1169.

(33)   Kondo, T.; Ueda, M.; Tamura, H.; Yoshida, K.; Isobu, M.; Goto, T. *Angew. Chem. Int. Ed. Engl.* **1994**, *9*, 9–10.

(34)   Mori, M.; Kondo, T.; Yoshida, K. *Phytochemistry* **2008**, *69*, 3151–3158.

(35)   Lecomte, S.; Baron, M. H.; Chenon, M. T.; Coupry, C.; Moreau, N. J. *Antimicrob. Agents Chemother.* **1994**, *38*, 2810–2816.

(36)   Palù, G.; Valisena, S.; Ciarrocchi, G.; Gatto, B.; Palumbo, M. *Proc. Natl. Acad. Sci. U. S. A.* **1992**, *89*, 9671–9675.

(37)   Turel, I.; Šonc, A.; Zupančič, M.; Sepčić, K.; Turk, T. *Met. Based. Drugs* **2000**, *7*, 101–104.

(38)   Uivarosi, V.; Badea, M.; Olar, R.; Draghici, C.; Barbuceanu, S. F. *Molecules* **2013**, *18*, 7631–7645.

(39)   Jose, C.; Phadke, P.; Rao, A. *Spectrochim. Acta* **1974**, *30A*, 1199–1206.

(40)   Hiraki, K.; Onishi, M.; Ikeda, T.; Tomioka, K.; Obayashi, Y. *Bull. Chem. Soc. Jpn.* **1978**, *51*, 2425–2426.

(41) Lee, M.; Maliakal, P.; Chen, L.; Meng, X.; Bondoc, F. Y.; Prabhu, S.; Lambert, G.; Mohr, S.; Yang, C. S. *Cancer Epidemiol. Biomarkers Prev.* **2002**, *11*, 1025–1032.

(42) Kwong, A. D.; Kauffman, R. S.; Hurter, P.; Mueller, P. *Nat. Biotechnol.* **2011**, *29*, 993–1003.

(43) Anggakusuma; Colpitts, C. C.; Schang, L. M.; Rachmawati, H.; Frentzen, A.; Pfaender, S.; Behrendt, P.; Brown, R. J. P.; Bankwitz, D.; Steinmann, J.; Ott, M.; Meuleman, P.; Rice, C. M.; Ploss, A.; Pietschmann, T.; Steinmann, E. *Gut* **2013**, 1137–1149.

(44) Koide, T.; Nose, M.; Ogihara, Y.; Yabu, Y.; Ohta, N. *Biol. Pharm. Bull.* **2002**, *25*, 131–133.

(45) Khalil, M.; Al-Zahem, A.; Al-Qunaibit, M. *Bioinorg. Chem. Appl.* **2013**, *2013*, 1–6.

(46) Anand, P.; Kunnumakkara, A.; Newman, R.; Aggarwal, B. *Mol. Pharm.* **2007**, *4*, 807–818.

(47) Moghaddam, E.; Teoh, B.-T.; Sam, S.-S.; Lani, R.; Hassandarvish, P.; Chik, Z.; Yueh, A.; Abubakar, S.; Zandi, K. *Sci. Rep.* **2014**, *4*, 5452.

(48) Li, B. Q.; Fu, T.; Dongyan, Y.; Mikovits, J. A.; Ruscetti, F. W.; Wang, J. M. *Biochem. Biophys. Res. Commun.* **2000**, *276*, 534–538.

(49) Haid, S.; Novodomská, A.; Gentzsch, J.; Grethe, C.; Geuenich, S.; Bankwitz, D.; Chhatwal, P.; Jannack, B.; Hennebelle, T.; Bailleul, F.; Keppler, O. T.; Poenisch, M.; Bartenschlager, R.; Hernandez, C.; Lemasson, M.; Rosenberg, A. R.; Wong-Staal, F.; Davioud-Charvet, E.; Pietschmann, T. *Gastroenterology* **2012**, *143*, 213–222.e5.

(50) Puyang, X.; Poulin, D. L.; Mathy, J. E.; Anderson, L. J.; Ma, S.; Fang, Z.; Zhu, S.; Lin, K.; Fujimoto, R.; Compton, T.; Wiedmann, B. *Antimicrob. Agents Chemother.* **2010**, *54*, 1981–1987.

(51) Liu, J.-P.; Ye, L.; Wang, X.; Li, J.-L.; Ho, W.-Z. *Transpl. Infect. Dis.* **2011**, *13*, 24–32.

(52) Ooi, E. E.; Chew, J. S. W.; Loh, J. P.; Chua, R. C. S. *Virol. J.* **2006**, *3*, 39.

(53) Keyaerts, E.; Vijgen, L.; Maes, P.; Neyts, J.; Van Ranst, M. *Biochem. Biophys. Res. Commun.* **2004**, *323*, 264–268.

(54) Savarino, a.; Gennero, L.; Sperber, K.; Boelaert, J. R. *J. Clin. Virol.* **2001**, *20*, 131–135.

(55) Savarino, A.; Gennero, L.; Chen, H. C.; Serrano, D.; Malavasi, F.; Boelaert, J. R.; Sperber, K. *Aids* **2001**, *15*, 2221–2229.

(56) Savarino, A.; Boelaert, J. R.; Cassone, A.; Majori, G.; Cauda, R. *Lancet Infect. Dis.* **2003**, *3*, 722–727.

(57) Ashfaq, U. a; Javed, T.; Rehman, S.; Nawaz, Z.; Riazuddin, S. *Virol. J.* **2011**, *8*, 163.

(58) Dreux, M.; Gastaminza, P.; Wieland, S. F.; Chisari, F. V. *Proc. Natl. Acad. Sci. U. S. A.* **2009**, *106*, 14046–14051.

(59) Mizui, T.; Yamashina, S.; Tanida, I.; Takei, Y.; Ueno, T.; Sakamoto, N.; Ikejima, K.; Kitamura, T.; Enomoto, N.; Sakai, T.; Kominami, E.; Watanabe, S. *J. Gastroenterol.* **2010**, *45*, 195–203.

(60) Vausselin, T.; Calland, N.; Belouzard, S.; Descamps, V.; Douam, F.; Helle, F.; François, C.; Lavillette, D.; Duverlie, G.; Wahid, A.; Fénéant, L.; Cocquerel, L.; Guérardel, Y.; Wychowski, C.; Biot, C.; Dubuisson, J. *Hepatology* **2013**, *58*, 86–97.

(61) Friebolin, W.; Jannack, B.; Wenzel, N.; Furrer, J.; Oeser, T.; Sanchez, C. P.; Lanzer, M.; Yardley, V.; Becker, K.; Davioud-charvet, E. *J. Med. Chem.* **2008**, *51*, 1260–1277.

(62) Farrell, N. P.; Williamson, J.; McLaren, D. J. M. *Biochem. Pharmacol.* **1984**, *33*, 961–971.

(63) Wei, L.; Cai, C.; Lin, J.; Chen, T. *Biomaterials* **2009**, *30*, 2606–2613.

(64) Dilnawaz, F.; Singh, A.; Mohanty, C.; Sahoo, S. K. *Biomaterials* **2010**, *31*, 3694–3706.

(65) Tekade, R. K.; Dutta, T.; Gajbhiye, V.; Jain, N. K. *J. Microencapsul.* **2009**, *26*, 287–296.

(66) Das, B.; Damodar, K.; Chowdhury, N. *J. Mol. Catal. A Chem.* **2007**, *269*, 81–84.

(67) Xu, L.-W.; Li, J.-W.; Xia, C.-G.; Zhou, S.-L.; Hu, X.-X. *Synlett* **2003**, 2425–2427.

(68) Varala, R.; Sreelatha, N.; Adapa, S. *Synlett* **2006**, *2006*, 1549–1553.

(69) Gampp, H.; Maeder, M.; Meyer, J.; Zuberbühler, A. D. *Talanta* **1985**, *32*, 95–101.

(70) Rossotti, F. J. .; Rossotti, H. S.; Whewell, R. J. *J. Inorg. Nucl. Chem.* **1971**, *33*, 2051–2065.

(71) Gampp, H.; Maeder, M.; Meyer, C. J.; Zuberbühler, A. D. *Talanta* **1985**, *32*, 257–264.

(72) Gampp, H.; Maeder, M.; Meyer, C. J.; Zuberbühler, A. D. *Talanta* **1986**, *33*, 943–951.

(73) Marquardt, D. *J. Soc. Ind. Appl. Math.* **1963**, *11*, 431.

(74) Maeder, M.; Zuberbuhler, A. D. *Anal. Chem.* **1990**, 2220–2224.

General Conclusion

Hepatitis C Virus (HCV) is one of the most important and widespread viral diseases affecting nearly 200 million people worldwide, of whom around 80 % will suffer chronic hepatitis that may lead to hepatocellular carcinoma and ultimately to death. The scientific research in anti-HCV drugs has greatly increased during the last years, leading to the approval of four new drugs that importantly enhance the SVR rates when compared to the former established therapies. Even though the newly developed and promising drugs display great potency, some of them have a low barrier to HCV resistance. Furthermore, their prices are extremely high and most likely will not be accessible to people living in developing countries, where HCV is most widespread. Hence, the need for new cheap and efficient anti-HCV drugs is still very high and urgent. These compounds may be used in conjunction with other known drugs to achieve an all oral therapy or to treat problems arising from liver transplantation, for which current therapies are still not convenient.

A preparative bioactivity-guided fractionation approach, conducted by Dr E. Davioud-Charvet and her co-workers, and investigated in close collaboration with HIV (Dr O. Keppler) and HCV (Pr T. Pietschmann) virologists, allowed the identification of a novel antiviral lead structure, the flavone ladanein. Ladanein was synthesized (**BJ486K**) using a versatile and scalable synthetic route and its peculiar antiviral properties were further confirmed. Preliminary mechanistic studies showed that **BJ486K** exposure of free lipid-enveloped virions potently inhibited infection in a post-attachment entry step, while ladanein exposure of surface-bound virions or target cells had a reduced or virtually no antiviral effect, and no role on RNA replication or assembly. Kinetics of **BJ486K**-mediated blockade of HCV cell entry is comparable with CD81-specific antibodies (*i.e.* CD81 plays a critical role in HCV and *P. falciparum* attachment or cell entry) or with ITX5061, a clinical stage compound that is thought to interfere with HCV infection through inhibiting viral interaction with SR-BI receptor. In line with these observations, a virion-fusion assay demonstrated that HIV-1 entry was also impaired following treatment of viral particles with **BJ486K**. Last but not least, **BJ486K** is effective against all major HCV genotypes, including a variant that is resistant to a reference entry inhibitor.

However, the former synthesis had several drawbacks that were needed to be overcome to afford larger amounts for further mechanistic and physico-chemical studies. In addition, introduction of functional diversity on the B-ring of the flavone was hindered by the stability and the tedious purification steps. The former synthesis of flavones established in the laboratory was thus improved in the first part of this PhD work. The new synthesis starts from a much cheaper starting material and allows access to multigram quantities of final compound with a greatly improved yield (54 % compared to 16%).The overall time needed to obtain the final compounds was shortened from 3 weeks to only one. Furthermore, the chromatographic purifications and Sephadex LH-20 column were eliminated only purifying compounds by recrystallization. Six different analogues were synthesized, all of them displaying good antiviral activities with FCF$_3$, FOCF$_3$ and FFCF$_3$ arising from the rest with a better antiviral activity.

The acido-basic properties of this homogenous set of flavones were then studied. The pK_a values were determined using an absorption spectrophotometric *vs.* pH titration and were attributed to the 6-OH group since the 5-OH group forms a strong hydrogen bond with the adjacent carbonyl moiety. It was also found that the substitution on the B-ring does not exert a great influence on the acido-basic properties of the compounds. The stability of the flavones was studied as well and it was found that, while they are stable at acidic or neutral pH, the deprotonation of the 6-OH position triggers a

2-step slow oxidation/degradation process. The process was also studied by ESI-MS and oxidation/degradation products were identified.

The electrochemical behaviour of the compounds was then described. It was found that, within the 0.8 and 1.2 V potential range, any of the flavones undergo a 2 electrons irreversible oxidation and reduction limited by diffusion and with no adsorption observed. This electrochemical behavior could arise from an ECE process centered on the 5-OH and 6-OH groups on cycle A. Between -2.35 and -1.5 V, a 1 electron (quasi)reversible redox process takes place. This corresponds to the oxido-reduction process of the enone moiety present in cycle C. In this case, the substituents present in cycle B exert an important influence on the potential values. Side-reactions (dismutation, coupling) may occur within this potential range and lead to the formation of new species which are characterized by the emergence of new peaks when the flavones are examined between -2.35 and 1.2 V.

Since Fe(III) is believed to play a central role in the antiviral activity of the flavones (*i.e.* bioactivation), the ferric coordination properties of these synthetic flavonoids were then examined. Absorption spectrophotometry was used in order to characterize and evaluate the strength of the flavone.Fe(III) complexes. All of the flavones examined in this work bind Fe(III) through the 5-hydroxy-4-carbonyl binding site and form monoferric monochelates. The kinetics of the Fe(III) binding was studied as well and it was also observed that Fe(III) catalyzes the oxidation of ladanein. To investigate the complexes under physiological conditions and overcome Fe(III) insolubility at higher pH values, ternary complexes with NTA at pH 7.4 were evaluated by analytical methods (absorption spectrophotometry, ESI-MS, fast kinetics) in terms of speciation, stability and formation kinetics. Importantly, we demonstrated that the use of an exogenous ligand influences the metal-centered redox properties and prevents the degradation of the flavone.

The Mg(II) complexes of the flavones were then studied by UV-Vis absorption spectrophotometry and ESI-MS. The stability of these complexes is dependent on the substituents born by the Mg(II) atom of the precursors. One of the complexes, **FOMe**.MgPid, was synthesized and its antiviral activity and pharmacokinetic properties were evaluated. The compound displays the same antiviral activity as ladanein with a better solubility and oral bioavailability. Encouraged by these promising preliminary results, the first steps of the synthesis of a dual-drug assembly composed of a flavone and a short chloroquine analogue (*i.e.* chloroquine displays additive antiviral activity when combined with ladanein) linked by a Mg(II) atom were studied at the end of my PhD work. However, due to lack of time, the project could not be finished.

In the future, aside from improving the dual-drug assembly as a first strategy, novel formulations of these antiviral flavonoids will be investigated. For instance, formulation with functionalized Fe_2O_3 superparamagnetic nanoparticles, which could improve the pharmacokinetic properties of the compounds will be considered as another interesting strategy. Further studies on the mechanism of action by which ladanein and its analogues exert their antiviral activities will be undertaken. Furthermore, because HCV and *Plasmodium* parasites share factors for their entry into hepatocytes, the antimalarial properties of the flavones will be evaluated as well.

Xavier MARTIN BENLLOCH

Synthesis and physico-chemical study of a novel antiviral lead

Résumé

Le travail de recherche présenté dans ce mémoire de thèse a été centré sur une nouvelle famille de flavones aux propriétés antivirales. Mon travail de thèse avait pour premier objectif d'améliorer la synthèse de la ladanéine (tête de série) et permettre l'accès à d'autres analogues. Un développement méthodologique a permis de mettre au point une synthèse compatible avec les procédés industriels qui permette d'améliorer les rendements et de raccourcir significativement les délais d'obtention. De plus, aucune purification par colonne de silice n'est nécessaire.

Une étude physico-chimique détaillée a ensuite été menée. Les propriétés acido-basiques de la série de composés ont d'abord été évaluées avant l'étude des propriétés électrochimiques. Ces données sont déterminantes pour une meilleure compréhension du mécanisme d'action de ces flavones. La complexation au Fe(III) a été également démontrée comme essentielle pour l'activité antivirale de ces composés. Les propriétés de complexation de ce cation ont donc été étudiées et ont apporté des informations importantes. Finalement, dans le but d'améliorer les propriétés pharmacocinétiques de ces agents virucides, des formulations originales avec le Mg(II), cation biocompatible, ont été élaborées et étudiées.

Mots clés : Flavone, Ladanéine, Virus de l'hépatite C, Activité antivirale, Inhibiteurs d'entrée des virions, Coordination, Physico-chimie, Electrochimie, Formulation, Synthèse totale

Abstract

The research work presented in this manuscript was centered on a novel flavone series displaying potent antiviral activities toward enveloped viruses such as HCV. The first goal of my research work was to improve the synthesis of ladanein (the lead antiviral compound) and to allow an easy access to a broad range of analogues. A methodological approach allowed setting up a synthetic route compatible with industrial processes with high yields and significantly shortened preparation time. Furthermore, no silica gel column chromatography was needed throughout the synthetic route.

A thorough physico-chemical study was then undertaken. The acido-basic properties of this homogenous series of compounds were first evaluated prior to the investigation of their electrochemical parameters. These data are essential for a deeper understanding of the mechanism of action of these polyphenolic compounds. Fe(III) was shown to be essential for the antiviral activity of these compounds and, hence, the Fe(III) complexation properties of the flavones have been studied and provided important information. Last but not least, in order to improve the pharmacokinetic properties of the flavones, original formulation approaches using the biocompatible Mg(II) cation were undertaken and thoroughly investigated.

Keywords: Flavone, Ladanein, HCV, Antiviral activity, Entry inhibitors of virions, Coordination, Physico-chemistry, Electrochemistry, Formulation, Total Synthesis